

Characterization of cardiomyopathy causing mutation in Muscle Lim Protein (C58G)

A Thesis Submitted for the Degree of Doctor of Philosophy

Trinity Term, 2019

Mehroz Ehsan

Brasenose College

Department of Cardiovascular Medicine

University of Oxford

Supervisors:

Dr. Katja Gehmlich and Dr. Charles Redwood

Acknowledgements

The four years that I have spent at the Radcliffe Department of Medicine, Brasenose College and the University of Oxford have been the most memorable years of my life. I know I will always look back at them fondly and cherish all the relationships and experiences I have had.

I would like to first thank my primary supervisor, Dr. Katja Gehmlich, for her guidance, encouragement, and support during my time at Oxford. I am extremely grateful to her for providing me with the opportunity to come to Oxford. She taught me not only how to do science but also how to deal with disappointments and get excited about the positive results. Special thanks to my second supervisor, Dr. Charles Redwood, for being a great source of encouragement and invaluable feedback and suggestions. His calming presence helped me weather the inevitable lows of research work. I would not have been able to complete this work without their patient mentorship.

I am deeply grateful to my colleagues and friends in the Watkins research group. Dr. Charlotte Hooper for teaching me several laboratory techniques and guiding me in performing my experiments. Dr. Carin de Villiers for her support and discussions of research ideas. Dr. Paul Robinson for being a patient teacher and providing critical feedback on my work. Dr. Julia Beglov and Dr. Matthew Kelly for their support in animal work. Dr. Anuj Goel for his help in RNASeq computational work. They have all been a source of constant support throughout my journey at Oxford.

I would like to thank the Clarendon Fund and the Radcliffe Department of Medicine for providing me the scholarship for this degree and the British Heart Foundation for

funding my research. Thank you to Brasenose College as well for providing me with support scholarship for an enriching academic experience.

I would like to thank my friends and colleagues in the Cardiovascular Medicine department, Naveed, Jillian, Alex, Laurienne, and Akanksha, for their friendship, scientific discussions, and much needed emotional support. I would also like to thank Dr. Elspeth Garman for being a shoulder to lean on whenever things became overwhelming. I would also like to give a special thanks to Brasenose College for providing me the leadership opportunities to grow on a personal level.

None of this would have been possible without the support of my family. I am forever indebted to my parents, Nabeela and Ehsan, for always believing in me and, above all, the sacrifices they have made in their lives to allow me and my siblings to have a life we had never imagined growing. Thank you to my siblings Mehreen and Shahroz for always encouraging me to pursue my dreams and having more faith in me than myself. Last but not least, I am so grateful to my wife, Mehak Mumtaz, for being my rock and supporting me throughout the highs and lows of this journey and beyond. I wouldn't be who I am and where I am without her and my family's endless love and support.

Abstract

Muscle LIM Protein (MLP) is encoded by the gene Cysteine and glycine rich protein 3 (*CSRP3*), a well-established disease gene for Hypertrophic Cardiomyopathy (HCM). Unlike most HCM disease genes, which code for sarcomere related proteins, MLP is a non-sarcomeric protein that is critical for signalling within the cardiomyocyte. To better understand the mechanism underlying MLP associated HCM a knock-in (KI) mouse model carrying *CSRP3* mutation C58G was generated. *In vivo* phenotyping of homozygous KI/KI mice recapitulated aspects of human cardiomyopathy with diastolic and systolic left ventricular dysfunction. No differences were observed between heterozygous KI/+ and WT littermate controls. RNASeq based transcriptomic analysis revealed activation of pro-fibrotic signalling, induction of the fetal gene programme and activation of markers of hypertrophic signalling in hearts of homozygous animals at 3 months. C58G mutation led to increased degradation of MLP protein *in vitro* and *in vivo*. MLP protein expression was reduced by 80% in KI/KI and by 50% in KI/+ mice. The reduced expression was due to increased proteasome activity which was verified by a proteasome reporter mouse. To uncover phenotype in KI/+ mice they were crossed with knock-in mutant mouse for *MyBPC,* which has been associated with increase proteasome activity. The double mutant failed to show any differences compared to heterozygous knock-in mice. In conclusion, the *CSRP3* C58G mouse serves as a unique mouse model to study cardiomyopathy caused by mutations in the non-sarcomeric protein MLP. The results suggest that the lack of protein and proteasomal overload both contribute to the development of disease phenotype.

Acronyms and abbreviations

AC	Adenylate cyclase
ACh	Acetylcholine
ADP	Adenosine 5'-diphosphate
AMP	Adenosine 5'-monophosphate
AMPK	AMP-activated protein kinase
ANOVA	Analysis of variance
ATP Atg5	Adenosine 5'-triphosphate Autophagy related 5
BSA	Bovine serum albumin
CaMK	Calcium/calmodulin-dependent protein kinase
CaMKKβ	Ca_{2+}/calmodulin-dependent protein kinase kinase-β
cAMP	Cyclic adenosine monophosphate
CrP	Creatine phosphate
cTnI	Cardiac troponin I
cTnT	Cardiac troponin T
DAPI	4',6-diamidino-2-phenylindole
dATP	2-deoxy-ATP
DCM	Dilated cardiomyopathy
DTT	Dithiothreitol
ECM	Extracellular matrix
EDPVR	End-diastolic pressure volume relationship
EDV	End-diastolic volume
EF	Ejection fraction
ELC	Essential light chain
ESPVR	End-systolic pressure volume relationship
ESV	End-systolic volume
FS	Fractional Shortening
H&E	Haematoxylin and eosin
HCM	Hypertrophic cardiomyopathy
HEPES	4-(2-hydroxyethyl)-1-piperazineethanesulfonic acid
Het	Heterozygous
Homo	Homozygous
LA	Left atrium
LTCC	L-type Ca2+ channel
LV	Left ventricle
MAPK	Mitogen-activated protein kinase
MLP	Muscle Lim Protein
mTOR	Mammalian target of rapamycin
MyBPC	Myosin binding protein C
NFAT	Nuclear factor of activated T-cells
PAGE	Polyacrylamide gel electrophoresis
PBS	Phosphate buffered saline
PKA	Protein kinase A
PKC	Protein kinase C
PKG	cGMP-dependent protein kinase

PLN	Phospholamban
RA	Right atrium
RLC	Regulatory light chain
RV	Right ventricle
SAN	Sinoatrial node
SDS	Sodium dodecyl sulphate
SEM	Standard error of the mean
SERCA	Sarco/endoplasmic reticulum Ca2+-ATPase
SL	Sarcomere length
SR	Sarcoplasmic reticulum
SV	Stroke volume
TBST	Tris-buffered saline + Tween 20
Tm	Tropomyosin
Tn	Troponin
TnC	Troponin C
TnI	Troponin I
TnT	Troponin T
UPS WT	Ubiquitin proteasome System Wild type
β-AR	β-adrenergic receptor

Table of Contents

Abstract ..... **i**

Acronyms and abbreviations ii

Chapter 1- Introduction **0**

1.1 Cardiac Function and Dysfunction 0

1.1.1 Macroscopic Physiology of the Heart 0

1.1.2 Cardiac Cycle: 3

1.1.3 Pressure Volume Relationship in the heart 6

1.2 The cardiomyocyte 9

1.3 Sarcomere 9

1.4 Thin Filament Proteins: 11

1.4.2Tropomyosin (Tm) 13

1.4.3 Troponin (Tn) 15

1.5 Thick Filament 17

1.5.1. Myosin II Heavy Chain 18

1.5.2 Myosin Light Chains 19

1.5.3 Myosin binding protein C (MyBPC) 20

1.6 Non-Filamentous Proteins 22

1.6.1 Titin 22

1.7 Sliding Filament Model and Cross Bridge Cycling 24

1.8 Heart failure: 26

1.9 Inherited Cardiomyopathy: 27

1.10 Hypertrophic Cardiomyopathy (HCM) 28

1.10.1 Pathogenesis of HCM: 33

1.11 Dilated Cardiomyopathy 35

1.11.1 Diagnosis and Treatment 37

1.11.2 Molecular Genetics of DCM 38

1.11.3 DCM Causing Cytoskeletal Genes 39

1.11.4 Mutations in sarcomeric proteins 41

1.12 Muscle LIM Protein 46

1.12.1 MLP Protein Structure 46

1.12.2 MLP Interacting Partners 47

1.12.3 MLP in Human Disease 48

1.12.4 Mouse Models of MLP 50
1.13 Hypothesis and Specific Aims 54
1.13.1 Hypothesis 54
1.13.2 Specific Aims 55
Chapter 2 - Materials and Methods 56
2.1 Molecular Biology 56
2.1.1 Transformation 56
2.1.2 Plasmid Purification 56
2.1.2 Quality Control / Sequence Verification 56
2.2 Genotyping – DNA extraction and PCR 56
2.3 Western Blot 57
2.3.1 Sample preparation 57
2.3.2 Protein concentration 57
2.3.3 SDS-PAGE 58
2.3.4 Western blotting 58
2.4 Co-immunoprecipitation 59
2.5 Cell Culture 60
2.6 Cell Transfections 60
2.7 Neonatal Rat Cardiomyocyte Isolation 61
2.7.1 Inhibitor Treatment of NRCs 63
2.7.2Transfection of NRCs 63
2.7.3 Immunohistochemistry NRCs 64
2.8 Mouse Handling Ethics: 64
2.8 In vivo phenotyping 65
2.8.1 Transthoracic echocardiography (TTE) 65
2.8.2 In vivo haemodynamics 67
2.9 Ex vivo phenotyping 68
2.9.1 Tibial length Measurement 68
2.9.2 Tissue harvesting 68
2.9.4 Histology 68
2.9.5 Immunofluorescence 69
2.10 Statistical analyses 69
2.11 Solutions 70
2.12 Antibody List 73
2.13 Primer List 74
Chapter 3 – Characterisation of MLP C58G Cardiac Phenotype 75

3.1 Introduction 75
3.2 Previous Work Done on Mouse Model 75
3.2.2 Generation of *CSRP3* KI/KI mouse model 75
3.3 Results: 82
3.3.1 Assessment of Cardiac Function by Echocardiography 82
3.3.3 Changes in Morphometric Measurements 92
3.3.4 Molecular Characterization of Day 0 and Day 7 hearts 95
3.3.4 Absence of fibrotic phenotype in knock-in mice 96
3.4 Primary Conclusions of this Chapter: 96
3.5 Discussion 97
Chapter 4 – RNA Sequencing of MLP Mouse Models 103
4.1 Introduction 103
4.1.1 A typical RNAseq experiment 108
4.1.2 RNAseq and cardiomyopathies 114
4.2 Methods 118
4.2.1 RNA Extraction 118
4.2.2 RNA sequencing Differential Expression Pipeline 118
4.3 Results 120
4.3.1 Distribution Analysis for RNAseq data 120
4.3.2 Sample Distance Matrix and PCA Plot 122
4.3.3 Highlighting Significant genes in pairwise comparisons 125
4.3.4 Differentially Expressed Genes between KI/KI and WT animals 126
4.3.5 RNASeq Gene Ontology Analysis 129
4.3.6 Upstream Regulator analysis with IPA 133
4.3.7 KEGG Analysis of transcriptome 135
4.3.8 Sample Distance Matrix and PCA Plot for KO and WT animals 137
4.3.9 Highlighting Significant genes in pairwise comparisons 139
4.3.10 Differentially Expressed Genes between KO and WT animals 141
4.3.11 RNAseq Gene Ontology Analysis 143
4.3.12 Comparison of *CSRP3* KI/KI and KO transcriptomes 145
4.4 Primary Conclusions of this Chapter: 146
4.5 Discussion 146
Chapter 5 – Role of Protein Degradation in MLP KI mice 157
5.1 Introduction 157
5.1.1 Autophagy 157
5.1.2 Ubiquitin Proteasome System (UPS) 160

5.1.3 Myosin Binding Protein C 3 (MYBPC3) 163
5.2 Results 167
5.2.1 C58G MLP is destabilized *in vitro* 167
5.2.2 The UPS is responsible for the protein depletion of HCM-associated MLP mutants 167
5.2.3 Impairment of the ubiquitin-proteasome system In Csrp3 KI mice 169
5.2.4 Assessment of Cardiac Function by Echocardiography 171
5.2.5 Proteasomal Activities in Csrp3 KI/KI mice 174
5.2.6 Csrp3 KI/+ Mybpc3 KI/+ mice do not develop cardiomyopathy 175
5.2.7 Assessment of Cardiac Function by Left Ventricular Haemodynamics 178
5.2.8 Molecular Characterization of Csrp3 KI/+ Mybpc3 KI/+ mice 182
5.3 Primary Conclusions of this Chapter: 183
5.4 Discussion 184
Chapter 6. General Discussion 192
6.1 Further Studies and Therapeutic Implications: 198
References 203

Chapter 1- Introduction

1.1 Cardiac Function and Dysfunction

Humans rely on the circulatory system to perform the critical function of supplying nutrients and oxygen, removing waste and metabolites and to relay signals from one part of the body to another. The force required to maintain circulation is generated by the rhythmic contraction (systole) and relaxation (diastole) of the muscular heart tissue. The heart, located within the chest cavity between the lungs behind the sternum and above the diaphragm, beats approximately 100,000 times a day, pumping the five litres of blood throughout the blood vessels of the body (1).

1.1.1 Macroscopic Physiology of the Heart

Though the macroscopic workings of the heart are simple and well-studied, scientists' still lack the complete understanding of how the different components of cardiomyocytes, the unit cell of heart tissue, work synergistically to help perform its function. Since perturbations in the signalling within the cardiomyocyte, specifically those involved in the contractile mechanism, lead to a disease state and eventual heart failure, a better understanding of these mechanisms can help to reduce the burden of cardiovascular disease.

The mammalian heart consists of two halves, each composed of two chambers, the atrium and the ventricle, which are separated by unidirectional valves (Figure 1-1). Deoxygenated blood from the peripheral organs enters the right atrium (RA) via the superior and inferior vena cava. The RA contracts pushing the blood into the right ventricle (RV) through the atrioventricular tricuspid valve, which ensures unidirectional flow. The tricuspid valve remains open while the ventricles fill up, which marks the

diastole phase. This is followed by the ventricular contraction, which generates enough pressure to cause the AV valve to close and blood to push through the semilunar pulmonary valve into the pulmonary artery. The pulmonary artery takes the blood to the lungs where gas exchange takes place between the pulmonary capillaries and the alveoli. Carbon dioxide leaves the blood while oxygen diffuses in. Oxygenated blood returns to the left atrium via the pulmonary vein. Once filled the LA contracts pushing the blood to the left ventricle (LV) via another AV valve called the bicuspid valve. This is followed by the LV systole which pumps blood through the semilunar aortic valve into the aorta which takes blood to the rest of the body. The blood passes through arteries, arterioles reaching the capillaries within tissues where the exchange of gases, nutrients and wastes takes place before blood passes through venules, veins and reaches back to the RA. Similar to the right side, the bicuspid valve closes during ventricular systole, preventing any backflow of blood into the atrium. The atria of both halves contract together followed by the ventricles of both sides of the heart. The contraction of atria and ventricles together comprises of one heartbeat which, in a healthy individual, takes slightly less than 1 second to complete.

The time between each heartbeat is the duration for a complete cardiac cycle. The rhythmic contraction of the heat chambers is coordinated by electrical activity, that transmits between cardiac cells through attachments called the gap junctions. The synchronous contraction and relaxation of heart chambers is maintained by a network of specialized cells that not only generate but also propagate electrical signals responsible for the contraction of cardiomyocytes. The cycle starts with the spontaneous generation of electrical activity, the action potential, from a group of cells in the RA called the sinoatrial node (SAN). This action potential travels from the top of the atria to the atrioventricular node (AVN). As the impulse spreads, simultaneously

throughout both atria, it causes atria to contract and push blood into the ventricles. Conduction velocity is slow through the AVN, to allow the atria to finish contraction before ventricular depolarization occurs. From the AVN the electrical impulse travels in a network of fast-conducting fibres, which include the bundle of His, the bundle branches, and Purkinje fibre system, resulting in rapid ventricular depolarization. The depolarization leads to ventricular contraction which originates from the apex of the ventricles and proceed towards the semilunar valves, generating the pressure required for the maximum ejection of blood from the heart towards the rest of the body.

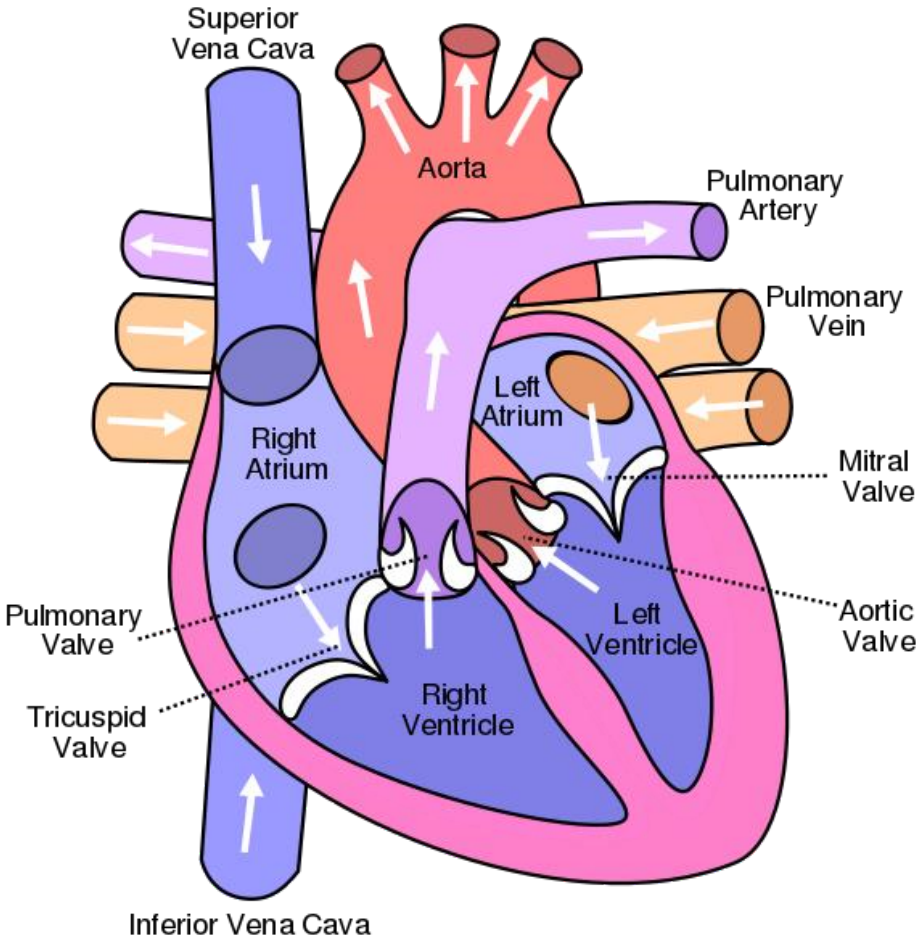


Figure 1-1. Cross Sectional Structure of the Heart – The heart is divided into two halves and four and has two valves separating the ventricles and the atria, bicuspid and tricuspid and has two semilunar (pulmonary and aortic) valves. The ventricular septum separates the two halves of the heart. The arrows indicate the direction of blood flow. The two vena cava bring deoxygenated blood to the heart. The pulmonary artery and vein take deoxygenated blood away and oxygenated blood back to the heart, respectively. Wikipedia Commons Accessed 10 April 2019.

1.1.2 Cardiac Cycle:

To analyse systole and diastole in more detail, the cardiac cycle (Figure 1-2) is usually divided into seven phases. The first phase begins with the P wave of the electrocardiogram, which represents atrial depolarization, and is the last phase of diastole. Phases 2-4 represent systole, and phases 5-7 represent early and middiastole. The last phase of the cardiac cycle ends with the appearance of the next P wave, which begins a new cycle.

Phase 1 - Atrial Contraction

The first phase begins with electrical depolarization of the atria, represented by the Pwave on the ECG. This leads to contraction of atria, which increases the pressure within the atria forcing the AV valve to open and blood to flow across into the ventricles. The contraction of the left atria only accounts for about 10% of the left ventricular filling. Most of the filling takes places before atrial contraction as blood passively flows from the pulmonary veins, into the LA, then into the LV via the open bicuspid (or mitral) valve. As atrial pressure drops, the AV valves to come back to the position before closure. At this time, the ventricular volumes are maximal, which is termed the enddiastolic volume (EDV). The left ventricular EDV (LVEDV) is typically about 120 ml.

Phase 2 - Isovolumetric Contraction

The next phase of cardiac cycle is marked by the initiation of QRS complex on the ECG, which represents ventricular depolarization. This sets off the excitationcontraction coupling, myocyte contraction and a sudden increase in

intraventricular pressure. The maximal change in rate of pressure development in the heart (max dP/dt) is achieved early in this phase. The increase in dP/dt is dependent on the rate of contraction of the muscle fibres, which in turn is affected the mechanisms driving excitation-contraction coupling.

The AV valves close as intraventricular pressure becomes greater than the pressure in atria. The closure of the AV valves results in the first heart sound (S1).

In between the closure of AV valves and the opening of aortic and pulmonary valves the ventricles undergo isovolumetric contraction, that is increase in pressure without any change in volume (ejection of blood). The "c-wave" on the pressure curve of left atrial pressure is attributed to the pressure generated by bulging of mitral valve leaflets back into left atrium.

Phase 3 - Rapid Ejection

This phase takes place as the aortic and pulmonic valves are open while the AV valves remain closed. The stage is characterized by the initial, rapid ejection of blood into the aorta and pulmonary arteries from the left and right ventricles, respectively. The ejection occurs as pressure within the ventricles exceeds that within the aortic and pulmonary artery forcing the aortic and pulmonary valves open.

Phase 4 - Reduced Ejection

Ventricle repolarisation starts after approximately 200 msec of the QRS complex. This leads to a decrease in pressure generation resulting in a reduction of the rate of ejection. The atrial pressure continues to rise as the atria fill up with venous blood from the pulmonary and systemic circulation.

Phase 5 - Isovolumetric Relaxation

The aortic and pulmonary valves close as the pressure within the ventricles falls below that in the arteries. This causes the second heart sound (S2) which also marks the start of isovolumetric relaxation. A small amount of blood flows back from the arteries into the ventricles as the AV valves close which is represented by a characteristic notch in the arterial pressure tracings.

The decline in pressure of the ventricles is determined by relaxation of muscle fibres after contraction. There is no change in ventricular volume as all valves are closed. Following ejection, the left ventricles has approximately 50 ml of blood left in the chamber which represents the end-systolic volume. The difference between the enddiastolic volume (EDV) which is usually about 120 ml and the end-systolic volume (ESV) is ~70 ml which represents the stroke volume (SV). The proportion of blood that is ejected from the heart during each contraction is called ejection fraction (EF). EF is calculated as SV/EDV. As the ventricles relax, left atrial pressure rises due to pulmonary venous return.

Phase 6 - Rapid Filling

The AV valves open as intraventricular pressure falls below atrial pressure leading to rapid rapidly open and passive ventricular filling. The ventricular pressure starts to rise as blood fills up in them following complete relaxation.

The opening of the bicuspid valve causes a sudden decrease in in left atrial pressure. There is no heart sound in healthy adult individuals during ventricular filling.

Phase 7 - Reduced Filling

As ventricular pressure increases, the pressure gradient across AV vales is reduced leading to a decrease in the rate of ventricular filling late in diastole. This precedes atrial contraction, by which time 90% of the ventricles have been filled.

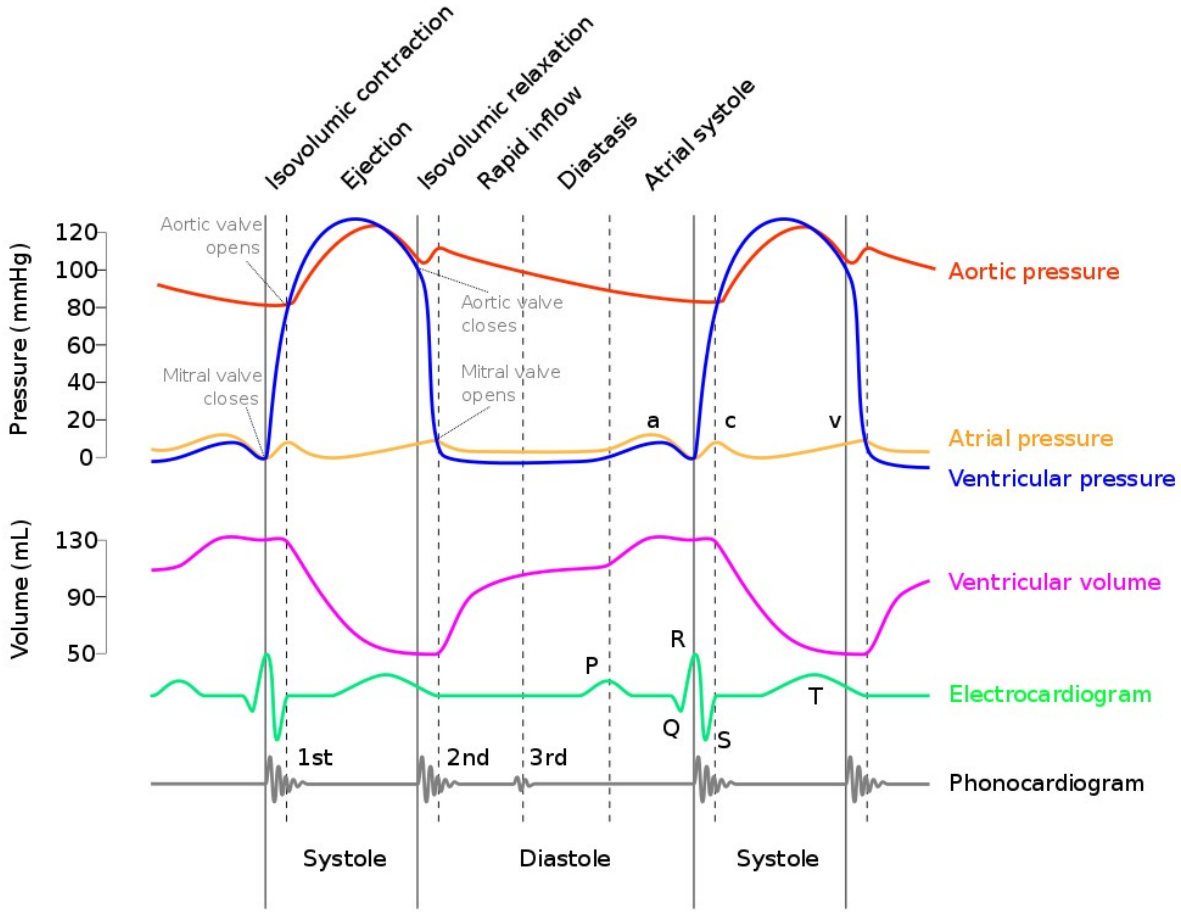


Figure 1-2. The Cardiac Cycle – Accessed Wikipedia Commons 12 April 2019

1.1.3 Pressure Volume Relationship in the heart

As illustrated in the cardiac cycle, the change in pressure within the heart chambers drives the flow of blood throughout the body. Increase in ventricular volume leads to a rise in pressure. As the mitral valve closes the ventricles undergo a rapid increase in pressure represented by isovolumetric contraction. The aortic valve opens reducing

the volume of ventricles and as the aortic valve closes there is a sudden decrease in pressure without any change, known as isovolumetric relaxation. The pressurevolume relation helps describe the cardiac output. The cardiac output represents the amount of blood ejected from the left or right ventricles in a given amount of time.

Usually cardiac output refers to the left ventricle. This is calculated as a product of the heart rate (HR), or number of beats and the stroke volume (SV). Figure 1-3 highlights the relationship between left ventricle pressure and volume. The area within the Pressure Volume loop represents the stroke work (SW), which is a product of the SV and pressure. SW represents the work exerted upon the blood during every cardiac cycle.

The pressure and volume parameters during the cardiac cycle help clinicians and researchers evaluate cardiac function. These parameters, however, can be affected by the cardiac preload and afterload. Cardiac preload represents the stretching of the myocardium prior to contraction. This is related to sarcomere length which is directly dependent upon venous return. Increase in venous return leads to increase in left ventricular end diastolic pressure and volume which stretches the sarcomeres, increasing their preload. The ventricular preload is directly related to the central venous pressure, ventricular compliance, force of contraction of atria and aortic pressure whereas it is indirectly related to heart rate. Ventricular preload has a direct effect on SV/CO by what is called the Frank-Starling mechanism. The Frank Starling mechanism states that the stroke volume increases with preload. The contractility of the ventricular muscle increases as the ventricle is stretched which explains the increase in force generated by the muscle.

Cardiac afterload represents the pressure that the heart must eject blood against, and it depends upon the blood (aortic) pressure. The afterload on individual cardiac muscle

fibres is expressed as ventricular wall stress which is directly dependant on ventricular pressure and radius and indirectly upon the ventricular wall thickness. Afterload is increased when aortic pressure and systemic vascular resistance are increased, by aortic valve stenosis, and by ventricular dilation. An increase in afterload causes an increase in end-systolic volume and a decrease in stroke volume. A hypertrophied ventricle has increased wall thickness and therefore lower wall stress and reduced afterload resulting in an increase in stroke volume.

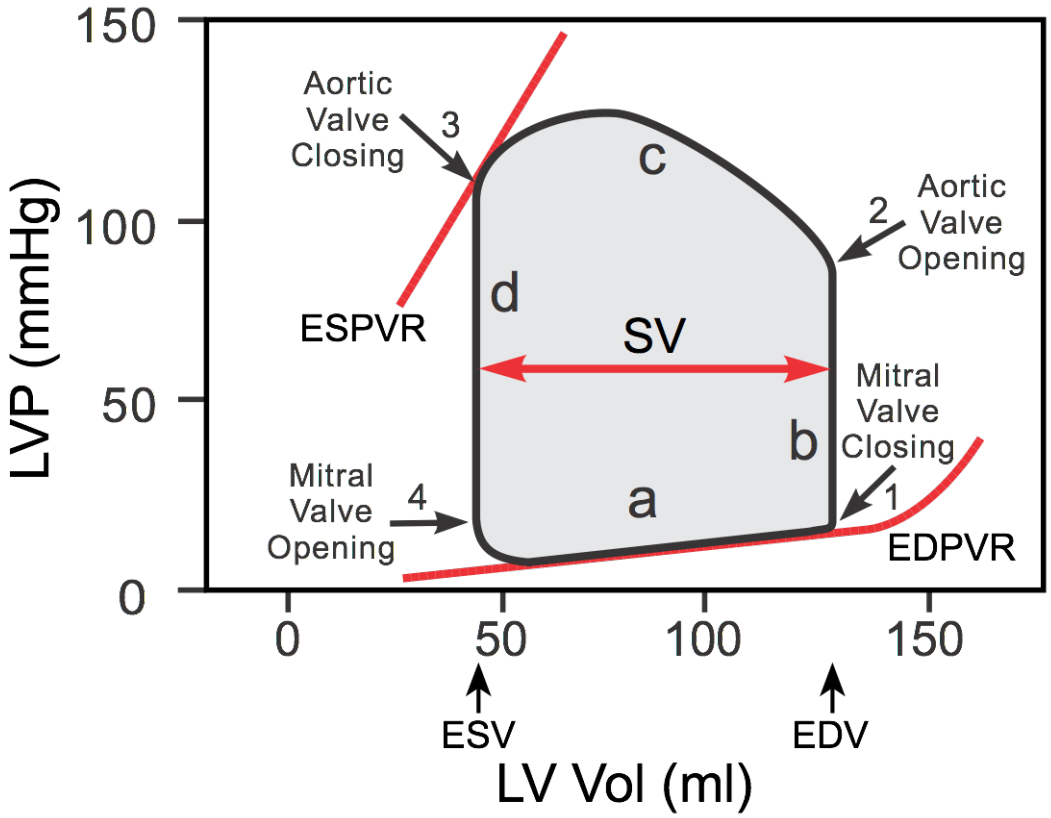


Figure 1-3. Pressure-volume relationship for a single cardiac cycle. the cycle can be divided into four basic phases: ventricular filling (phase a; diastole), isovolumetric contraction (phase b; systole), ejection (phase c; systole), and isovolumetric relaxation (phase d; diastole) Adapted from (2)

1.2 The cardiomyocyte

The myocardium is a highly organized tissue comprising of several cell types which include fibroblasts, myocytes, endothelial cells and vascular smooth muscle cells. Though the contraction of the heart is due to cardiomyocytes, the network of all these cells allow for coordinated metabolic, electrical and mechanical that maintain the continuous beating of the heart (3).

Cardiomyocytes occupy three quarters of the resting myocardial volume, yet only account for approximately one third of the cells, by number (4). Cardiomyocytes, which are cylindrical in shape, have well defined cross-striations and are arranged into layers of muscle fibres, which have different orientation. These cells are connected to each other by intercalated discs (IDs), which allows them to work as a syncytium. These IDs are comprised of three types of cells junctions; gap junctions, adherns junction and desmosomes (5). The desmosomes and adherens junctions are important for anchoring the myofibrils and facilitating the transmission of mechanical force from one cell to another. The gap junctions provided low resistance electrical pathways permitting ions can flow between cells, which allow for the propagation of action potentials that lead to depolarization and synchronized contraction to occur through excitation contraction coupling (6).

1.3 Sarcomere

Sarcomere makes up the basic contractile unit of the cardiomyocyte. Electron micrograph of the sarcomere highlight its structural features. Repeating units of thick and thin filaments form the backbone of sarcomere structure (Figure 1-4), and the

alignment and overlap of these thick and thin filaments gives the myocyte its striated appearance.

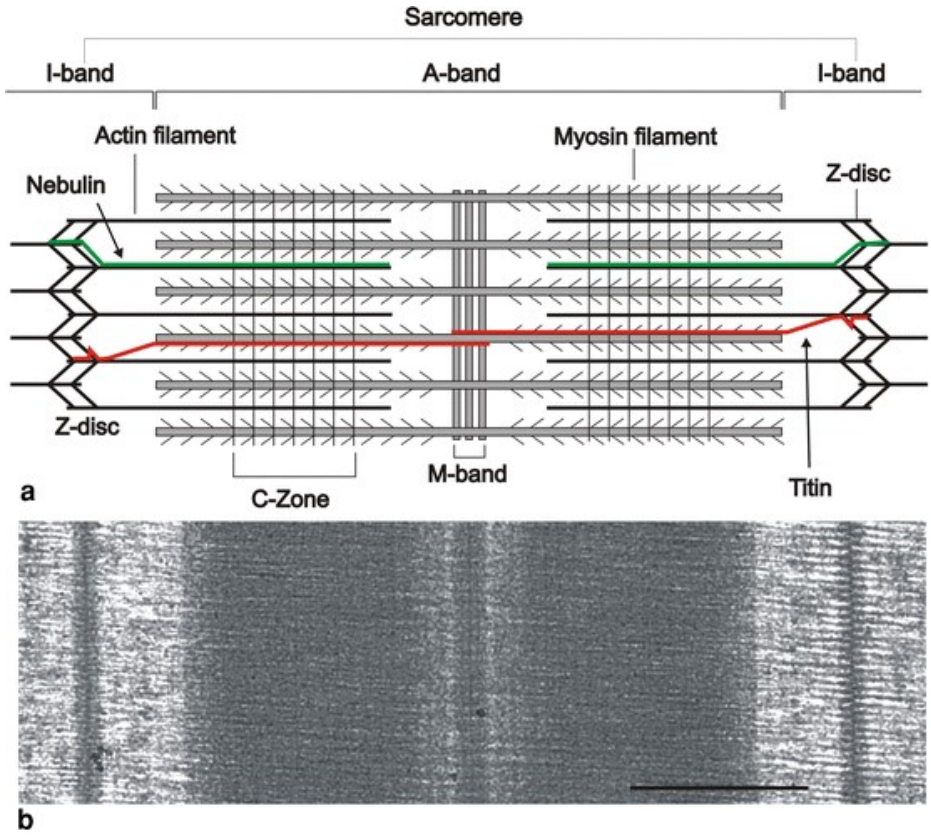


Figure 1-4. The structure of the straited muscle sarcomere (7)

The dense region in the electro micrograph is composed of thick filaments and is called the anisotropic or “A” band. The thick filament is composed of the myosin head and rod, the myosin light chains and Myosin binding protein C. The less dense region is composed of thin filaments only and is called the isotropic or “I” Band. the thin filaments are composed of a helical polymer of globular actin along with regulatory protein tropomysin and the troponin complex which consists of three protein troponin-C (TnC), troponin-T (TnT) and troponin-I (TnI). The M-line highlights the midpoint of the thick filament, and Z-line which is composed of actin cross-linking protein α-actinin is where the actin filaments are anchored.

1.4 Thin Filament Proteins:

The thin filament is composed of actin, tropomyosin (Tm), and the troponin (Tn) complex (including TnC, TnI, and TnT subunits) in a 7:1:1 ratio. The myosin head binds to actin in the thin filament to initiate contraction. An action potential triggers the influx of Ca^{2+} ions into the cytosol which acts as a primary signal for muscle contraction. Ca^{2+} binds to TnC causing a change in the conformation of the troponin complex, which moves Tm exposing the myosin binding sites on the actin filament. The interactions between actin and myosin, called actomyosin cross-bridges, produce force and shortens the sarcomere. During contraction thin filaments slide relative to the M-line to the thick filaments, resulting in shortening of the I band whereas the A-band's length stays constant. (8, 9). The force of contraction is dependent on the number of active actomyosin cross bridges which is regulated by a number of pathways acting on proteins in both the thick and thin filament. The structure and function of thin filament protein is discussed in detail in the sections below.

1.4.1 Actin

Actin is one of the most abundant proteins in the eukaryotic cells and its sequence is also highly conserved across species (10). It shares more protein-protein interactions than any other known protein. Initially described by Hailburton as a "ferment which brings about the coagulation of myosin" (11), actin is expressed at high levels in several cell types and in muscle tissue it makes up approximately one-fifth of the total protein mass (12). Actin is the most abundant component of the sarcomeric thin filament.

Actin occurs in an equilibrium between its globular and filamentous form *in vivo*. Gactin is a 42kDa protein that can polymerize in the presence of ATP and divalent ions such as Mg^{2+} or Ca^{2+} (13). The G-actin molecule is comprised of four subdomains with the

two smaller subdomains 1 and 2 involved in binding to myosin. The other two subdomains are surrounded by a nucleotide binding pocket where ADP/ATP and divalent ions can bind. Incorporation of actin into a filament activates the actin ATPase (14) which causes hydrolysis of ATP to ADP resulting in a conformational change that promotes polymerization (15). Actin filament length is maintained by a process called treadmilling, where one end of the filament is undergoing polymerization which is balanced by simultaneous depolymerization at the other end (16).

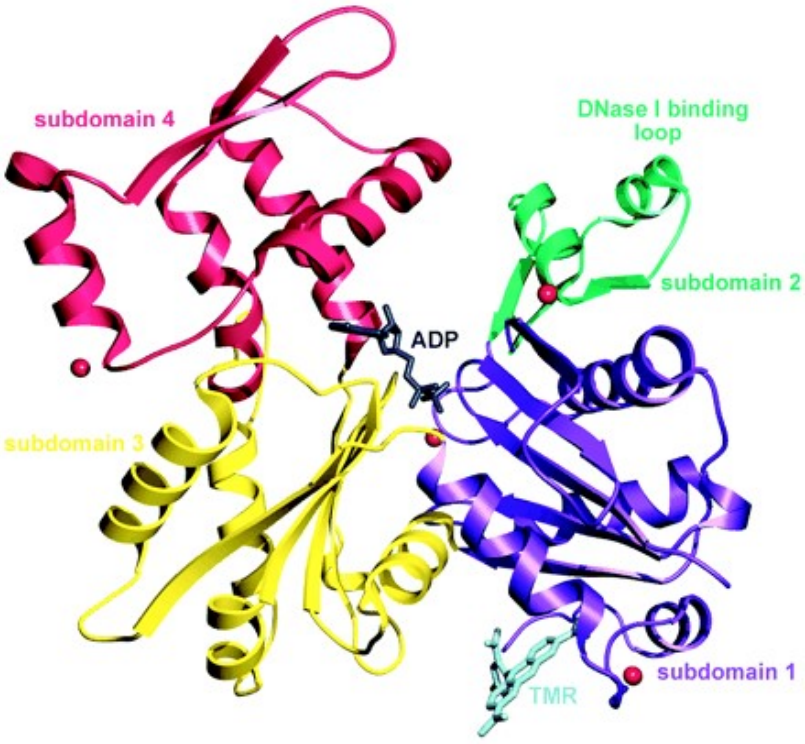


Figure 1-5: Structure of uncomplexed actin in the ADP state. From (15)

Monomeric actin polymerises under physiological conditions to form filamentous actin (F-actin) (17). F-actin has a number of functions in cells including muscle contraction, cell motility, morphological changes, cell division and intracellular movements. F-actin filaments form a double helical structure subdomain 1 and 2 are positioned on the outside, for interaction with myosin, whereas subdomains 3 and 4 are placed in the centre of the structure. The structure enables the actin molecules to interact with other

molecules within its strand and those in the adjacent strand. The assembly, length, and stability of actin filaments are controlled by specialized actin capping proteins which are themselves regulated by a number of different pathways (18).

In the sarcomere actin filaments are anchored to the Z-line by alpha-actinin. These filaments provide binding sites for myosin heads resulting in shortening of sarcomere and muscular contraction. The actomyosin interaction, however, is controlled by the protein tropomyosin (Tm).

1.4.2Tropomyosin (Tm)

Tropomyosin is a 32.5 kDa protein that is encoded by four genes. It has two different isoforms, α and β, which are expressed differentially depending on the type of muscle. Further, these isoforms form homodimers and heterodimers depending on the cell type and species. α-tropomyosin, which is encoded by the *TPM1* gene, is the predominant isoform in cardiomyocytes accounting for 97-99% of the total actin protein. β tropmopysoin, encoded by the *TPM2* gene, makes of 30-50% of the total tropomyosin in skeletal muscles.

The quaternary structure of Tm dimers is composed of two alpha helical peptides formed into a parallel coiled-coil structure. The hydrophobic interactions between side chains on each coil confer the structure stability. Each molecule has an approximate length of 42 nm and spans seven actin monomers. Tm binds to the groove of each side of double-helical actin filaments Electrostatic attraction between side chains of Tm and F-actin peripheral domains stabilize the interaction between the two proteins. Tm forms a polymer along the length of the actin in a head-to tail-fashion that repeats every 38nm. The head-to-tail overlap not only strengthens the binding but also allows

Tm dimers flexibility so that it is not strained along the length of the filament.
Though the conformation of Tm impedes the actomyosin interaction, its length, flexibility and weak interactions allow for a great deal of motion on the filament surface. This movement is regulating the activation of the filament. Tm is found in three states; blocked, closed and open, with each state representing increasing level of filament activation. During relaxation, while there is no calcium influx trigger, the Tn complex keeps Tm in blocked state where myosin head cannot bind actin. This state is maintained as TnI binds to two actin monomers while TnT subunit binds to Tm at the Tm-Tm overlap region (19). Leading upto muscular contraction Ca^{2+} binds to TnC causing a conformation change which leads to TnC interacting with TnI causing it to detach from the actin monomers (20). This allows Tm to move on the filament exposing the binding site for myosin (21). Even at saturating concertation of Ca^{2+} the majority (80%) of the Tm molecules are in a closed position. Myosin interactions with actin, shifts Tm further on the surface of the filament and into an open position.

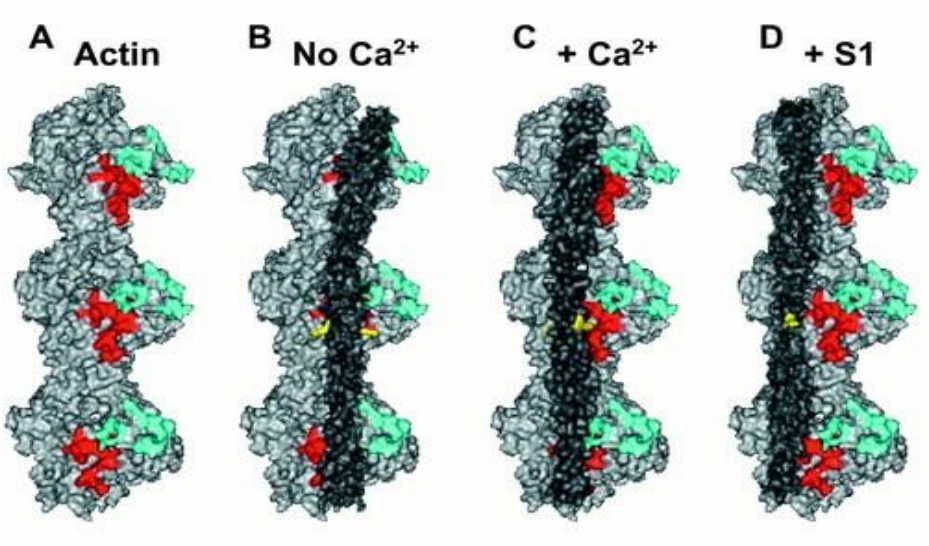


Figure1-6: Tm movement over the surface of the actin filament at various degrees of activation.Actin residues interacting with myosin are highlighted (green = weak interaction, red = strong interaction). Three adjacent actin molecules within one strand of the filament are shown in A. At rest, the Tm helix is shown to block both weak and strong interaction residues (B,"blocked"). Activation of the filament by Ca2+ (C, "closed") is shown to shift Tm, exposing weakly interacting actin residues. Upon myosin binding (D, "open"), Tm is further shifted to expose strongly interacting actin residues. Figure adapted from (19).

Upon strong actin-myosin cross bridge formation, the thin filament is activated in surrounding actin monomers, greater than that regulated by a single Tm section. The head-to-tail arrangement of Tm allows for this cooperativity in the system which leads propagation of activation signal along the filament. This decreases the amount of Ca^{2+} required to cause high yields of contraction, thus making the contraction more efficient by reducing the energy spent on influx of Ca^{2+}. This cooperation in the system also allows for a coordination of muscle contraction (19).

1.4.3 Troponin (Tn)

Though the interaction of myosin with actin is impeded by the presence of tropomyosin along the length of the thin filament, its movement along the filament is regulated by its interactions with the troponin complex (22). The troponin complex is made up of three proteins: troponin C (TnC), a 18 kDa protein that binds to Ca^{2+}, troponin I (TnI) a 25 kDa protein which interacts with Tm to prevents myosin attachment and troponin T (TnT) a 36 kDa protein that interacts directly with Tm to control actomyosin interactions (23).

TnC is the primary Ca^{2+} sensor within myocytes. TnC is a dumbbell shaped protein that has two metal binding globular EF hand motifs at both the N and C terminus, that are linked by a long central α helix (24, 25). C-terminal sites are insensitive to intracellular Ca^{2+} concertation and are occupied by Mg^{2+} ion under physiological conditions which strengthens the TnC- TnI interactions (26). On the other hand, the Nterminal EF-hand motifs act as the Ca^{2+} sensors, as they bind preferentially to Ca^{2+} over Mg^{2+} (27). Binding of Ca^{2+} to the N-terminus hand motifs results in conformational change of TnC. This exposes hydrophobic amino acids proximate to TnI. The resulting hydrophobic

interactions cause detachment of TnI from the actin filament (28). Even at saturated Ca^{2+} concentrations, not all cardiac TnC is activated (29).

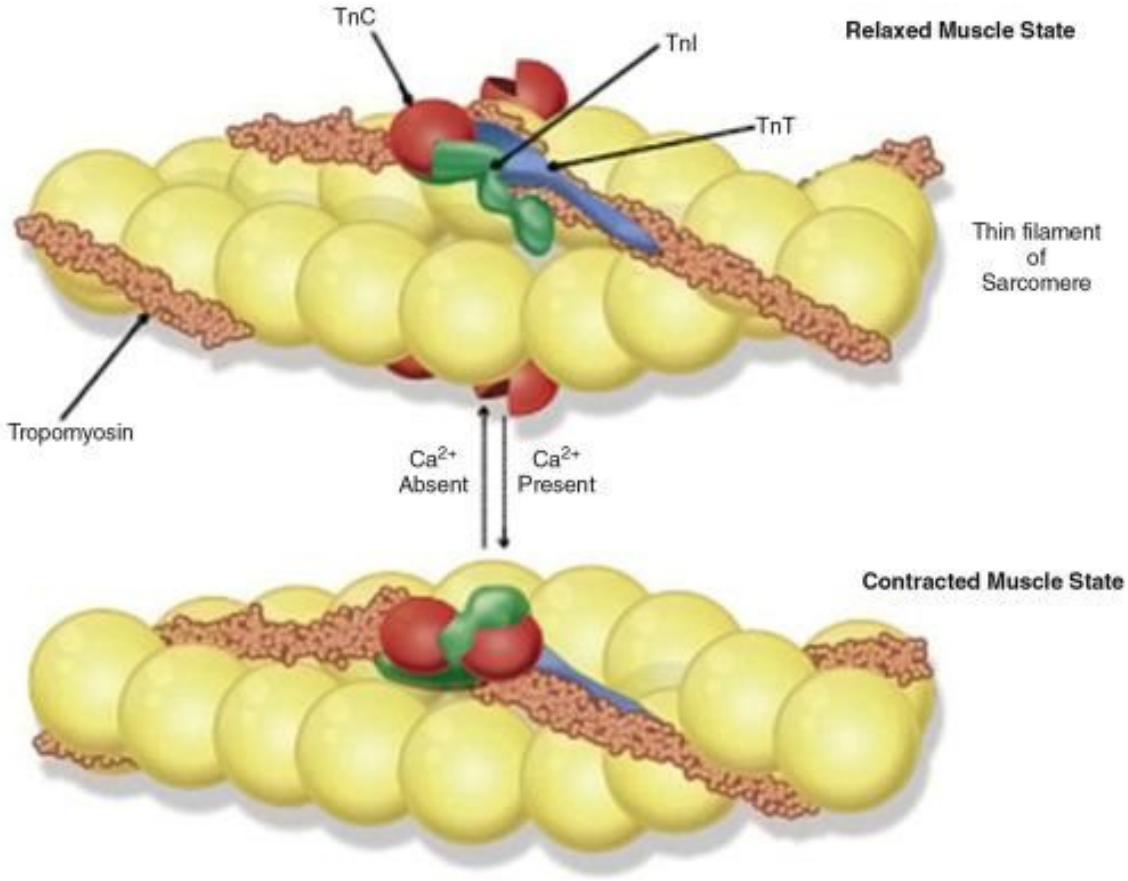


Fig 1-7. Cardiac muscle showing location of cardiac troponin I (TnI), cardiac troponin T (TnT), and troponin C (TnC) in relation to actin and tropomyosin. *Adapted from* (30)

TnI restricts the movement of Tm on the actin filament. TnI has three different isoforms: slow skeletal, fast skeletal and cardiac and all the primary protein sequence is highly conserved between the three isoforms. The cardiac isoform notably has 27-33 amino acid N-terminal extension which has been found to contain two phosphorylation sites important in the ß-adrenergic stimulation of the myocardium. Several phosphorylation sites within cardiac TnI are identified which regulate its function. The most important phosphorylation sites on cardiac TnI are located on the N-terminal extension as phosphorylation of Ser 23 and Ser24 by Protein Kinase A, Protein Kinase G and

Protein Kinase C reduces the strength of the cTnC-cTnI interaction (31). The phosphorylation state of TnI has implications on its function of regulating the amount of force generated within the sarcomere and therefore cardiac function (32-34). TnI phosphorylation can be regulated under physiological conditions to match the demand of the body however, under pathological conditions the dysregulation of phosphorylation sites of TnI may contribute to impaired cardiac function (35, 36).

TnT is a primarily structural protein that anchors TnC, TnI and Tm (37). It has a large number of isoforms and splice variants however, the primary isoform in cardiomyocytes is a 34 kDa protein encoded by the *TNNT3* gene (38). Cardiac TnT (cTnT) has a N-terminal alpha helical domain called T1 and a C-terminal globular head domain called T2. The globular head interacts with TnC, TnI, and Tm in calcium dependant manner whereas the T1 domain lies along the actin filament in an antiparallel binding arrangement to the Tm molecule (39). This position allows TnT to regulate the flexibility and motion of Tm while simultaneously influencing TnC-TnI interactions. Troponin T is thought to be responsible for the communication of conformational changes in TnC and TnI to Tm via its calcium dependant binding to actin at the T2 region and the interaction of the T1 region to the centre of the tropomyosin dimer (39).

1.5 Thick Filament

The thick filament is composed of myosin II and its two heavy motor chains, four regulator myosin light chains and the myosin binding protein C (MyBPC). Together these proteins are responsible for regulation and formation of force-producing crossbridges and regulating their activity.

1.5.1. Myosin II Heavy Chain

The striated muscle myosin protein is responsible for the generation contractile force. The protein forms a hexamer consisting of two myosin heavy chains (MHC), approximately 2000 amino acids long, two essential light chains and two regulatory light chains (Figure 1-8). The heavy chain makes up the catalytic head domain and the coiled-coil tail. Myosin heavy chain consists of two structurally and proteolytically defined domains. The head domain or sub fragment 1 (S1), which is a catalytic domain that forms the acto-myosin cross-bridges and contains the nucleotide binding sites responsible for acto-myosin ATPase activity. The second is the α-helical coiled coil tail domain that is responsible for polymerisation of myosin to form sarcomeric thick filament and also stabilizes the heads within its structures. The myosin molecules are oriented so that S1 heads point towards the end of the filament and the tails point towards the centre. This results in a bare or M-region with no myosin heads which ensures that filaments are pulled towards the centre of the sarcomere from both sides.

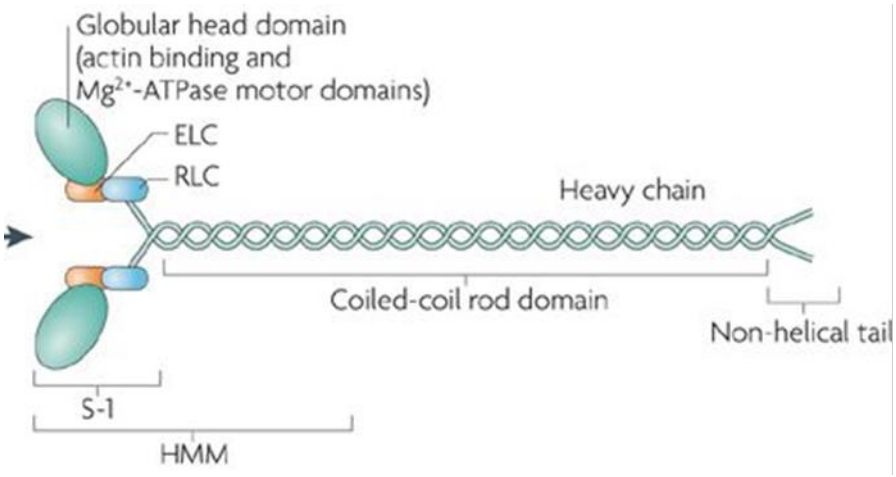


Figure 1-8 - Illustrative structure of myosin II and its component fragments. Figure adapted from (40)

The S1 domain contains binding sites for that binding actin and ATP. The head consists of a number of α-helices surrounding a 7-stranded β-sheet. Adjacent to the catalytic core of the S1 head are the converter and lever arm regions, which are the domains that undergo the conformational shifts that drive the myosin “power stroke” and muscle contraction. The power stroke by myosin head is the force-generating step of the cross bridge cycle.

1.5.2 Myosin Light Chains

Within a myosin molecule each heavy chain is associated with an essential light chain (ELC) and a regulatory light chain (RLC). These lights chains regulate the myosin cross-bridge activity (41). These chains are significantly smaller in size compared to the heavy chain with RLC being 20 kDa and ELC being 17 kDa. These chains attach non-covalently to the myosin lever arm, positioning them to have a role in regulation of cross-bridge formation (42). Though myosin is functional without these chains, *in vitro* analysis show that the lack the light chains results in significant decrease in velocity of sliding filaments suggesting that light chains tune myosin function allowing the generation of force to match the physiological demand (43). Mutations in these proteins are common causes of inherited cardiomyopathies, highlighting their role in cardiac function (44).

RLC and ELC are both Ca^{2+} binding EF-hand proteins that stabilize the myosin lever arm. Both of them have similar structure apart from an extra 30 amino acid extension on the N-terminal of ELC which allows it to interact with actin (45), slowing the kinetics of cross-bridge cycling (46, 47). The RLC function can be affected by its phosphorylation state. It can be phosphorylated by calmodulin-dependent myosin light chain kinase at its N-terminus, resulting in increased myosin ATPase rate(48) and

enhanced force development and cross-bridge cycling rates at sub-maximal Ca^{2+} concentrations (49). Animal studies have shown that partial or complete removal of RLC alone reduces the myosin ATPase rate (50) and disorders myosin head structure (51).

1.5.3 Myosin binding protein C (MyBPC)

The variants of MyBPC are expressed from three different genes, of which the cardiac specific isoform is encoded by *MYBPC3* (52). The importance of MyBPC in regulating cardiac function is highlighted by the fact that mutations in the gene *MYPBC3* account for 40–50% of all HCM mutations. Myosin binding protein C plays a part in regulation of contraction and relaxation and sarcomere maintenance. Cardiac MyBPC (cMyBPC) consists of eight immunoglobulin-like and three fibronectin-like domains. MyBPC also contains a unique ~100 AA domain containing key regulatory phosphorylation sites. MyBPC is not essential for sarcomere formation during embryogenesis as *Mybpc3*$^{-/-}$ are born in mendelian ratios. However, it is critical for sarcomere organization and maintenance of normal cardiac function as these mice develop severe cardiac hypertrophy (53).

At its C-terminal MyBPC interacts with members of the four-and-a-half-LIM-domain family, myosin rod and titin (54, 55). However, these interactions are thought to be necessary for controlling the location of protein rather than its function. The N-terminal interactions of MyBPC which include F-actin and the myosin-S2 domain are thought to likely drive its functional effect.

Regulation of MyBPC function and its structure is driven by phosphorylation at S273, S282, S302 by PKA and phosphorylation at S273 and S302 by PKC (56). These sites

are of importance as they are close to the location where MyBPC binds the S2 domain of myosin (57). Phosphorylation at these sites are predicted to promote formation of cross-bridges by inducing movement of myosin heads towards thin filaments (58). MyBPC phosphorylation is significantly decreased during the development of heart failure or pathologic hypertrophy. Further, mutant mice expressing nonphosphorylatable protein showed deterioration in cardiac hemodynamics when compared to littermate controls (56).

1.6 Non-Filamentous Proteins

1.6.1 Titin

Titin is a giant elastic protein weighing almost 3-3.4 MDa. It is the third most abundant protein within the myocardium, after actin and myosin(59). Titin is the largest known polypeptide in nature. It appears as long flexible filament and with a length of 1 μm one molecule spans half the sarcomere, from the Z-disk (N-terminal) to M-line (Cterminal) of the sarcomere. Titin, encoded by the gene *TTN*, has may different isoforms with the N2B (shorter, 2.97 MDa) and N2BA (longer, 3.3 MDa) being the most common isoforms expressed within the heart (60).

Titin is essential for sarcomere assembly (61-63) and an important determinant of sarcomere size and structure (64). Titin knockout mice exhibit defective thick filament formation and perturbed myofibrillogenesis (65). Beyond regulation of sarcomeric assemble, titin, in striated muscles, plays a key role in regulation of muscular contraction (review, (66)) as it limits the range of motion of the sarcomere under tension, thus contributing to the passive stiffness of muscle (67, 68). The different isoforms of titin, in skeletal and cardiac muscle, exhibit different stiffness, which has been correlated with the mechanical properties of these muscles (69).

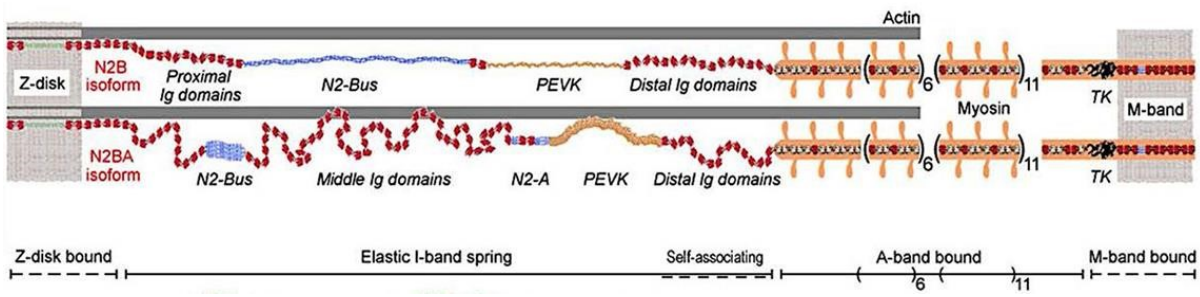


Figure 1-9 – Schematic illustration of titin N2B and N2Ba structures. Adapted from (70)

Spanning half the sarcomere, the titin molecule is composed of four distinct regions that interact with different protein partners which contribute to each region's mechanical properties. The N-terminal at the Z-line, which overlaps with N-terminal of titin from adjacent sarcomere, allows for binding with α-actinin (71). The region located in M-line binds to M-protein and myomesin that is thought to space out myosin thick filaments across the cross section of the sarcomere (72). This region also contains tyrosine kinase catalytic domain that senses mechanical load of the muscle. The kinase is predicted to activate the zinc-finger protein nbr1 which acts via p62 to cause nuclear localisation of MuRF2, a muscle-specific RING-B-box E3 ligase, to increase gene expression of muscle proteins and increase protein turn over, which prevents muscle atrophy and cell death at high workloads (72). The largest region of titin is situated in the A-band and is comprised of immunoglobulin and fibronectin domains that interact with myosin and MyBPC. The I-band region has three sub sections: a PEVK segment comprising of proline, glutamate, valine and lysine residues, a segment with variable number of Ig domains, and a section with alternating IgG domains and unique sequences in the N2 region. The I-band region acts as the elastic part of the molecule and it extends to begin generation of force during cardiac filling.
(73). This regulates the amount of cardiac filling during diastole and also contributes to contractile force developed in early systole. There are two alternative forms of the N2 region, N2A and N2B. Skeletal muscles are made up of N2A sequences whereas the cardiac muscle comprises of both N2A And N2B sequences(74). It is the relative ratio of these two sequences N2B/N2A that affect the stiffness of the cardiac muscle with increased amount of N2B causing a stiffer muscle (73).

Titin has also been found to contribute to stretch sensing within the myocardium. Titin is sensitive to variable levels of stretch in the myocyte as it contains elastic elements

that extend as the myocyte stretches (75). Further, titin has a number of interactions with protein complexes that are involved in force transmission and stretch sensing. Of particular importance are interactions with telethonin and muscle LIM protein (MLP), which have been associated with transcriptional signalling and pathophysiological responses (75).

1.7 Sliding Filament Model and Cross Bridge Cycling

The sliding filament theory of muscle contraction was first put forward in 1953 by Huxley & Hanson after observation of the sarcomeric structure under an electron microscope (76). Further studies observing the cross striations during contraction and relaxation suggested the movement of thick and thin filaments past one another (8, 9). These findings led to the proposal that the active sliding was due to the action of crossbridges between thick and thin filaments which was confirmed by the visualization of cross-bridges as projections of the myosin filaments (77) These findings led to the proposal of the swinging cross-bridge cycle by Huxley in 1969.

The filament sliding observed during muscle contraction is caused by the interaction of myosin heads with actin, a process regulated by Ca^{2+} and driven by the hydrolysis of adenosine triphosphate (ATP). Figure 1-10 details the specific steps in the process known as cross-bridge cycle. In the absence of ATP the myosin head binds tightly to actin producing a state known as rigor (A). ATP binds to myosin head resulting in a conformational change that irreversibly dissociates myosin from actin. (B) (78)

ATP, which is still bound to myosin head, is hydrolysed to adenosine diphosphate (ADP) and inorganic phosphate (Pi), by the myosin ATPase, resulting in the bending of the neck region (C)(78). The myosin-ADP-Pi complex can bind weakly to actin (D)

(79). Calcium regulated strong binding of myosin to actin (E) causes the two myosin subdomains to move towards each other. Pi is released from the ATP binding pocket resulting in a conformational change that moves the lever arm of myosin in a step called the “powerstroke” (E). The power stroke involves the release of ADP which causes the thin filaments to slide past the thick filaments, thus leading to sarcomere shortening and the generation of force.

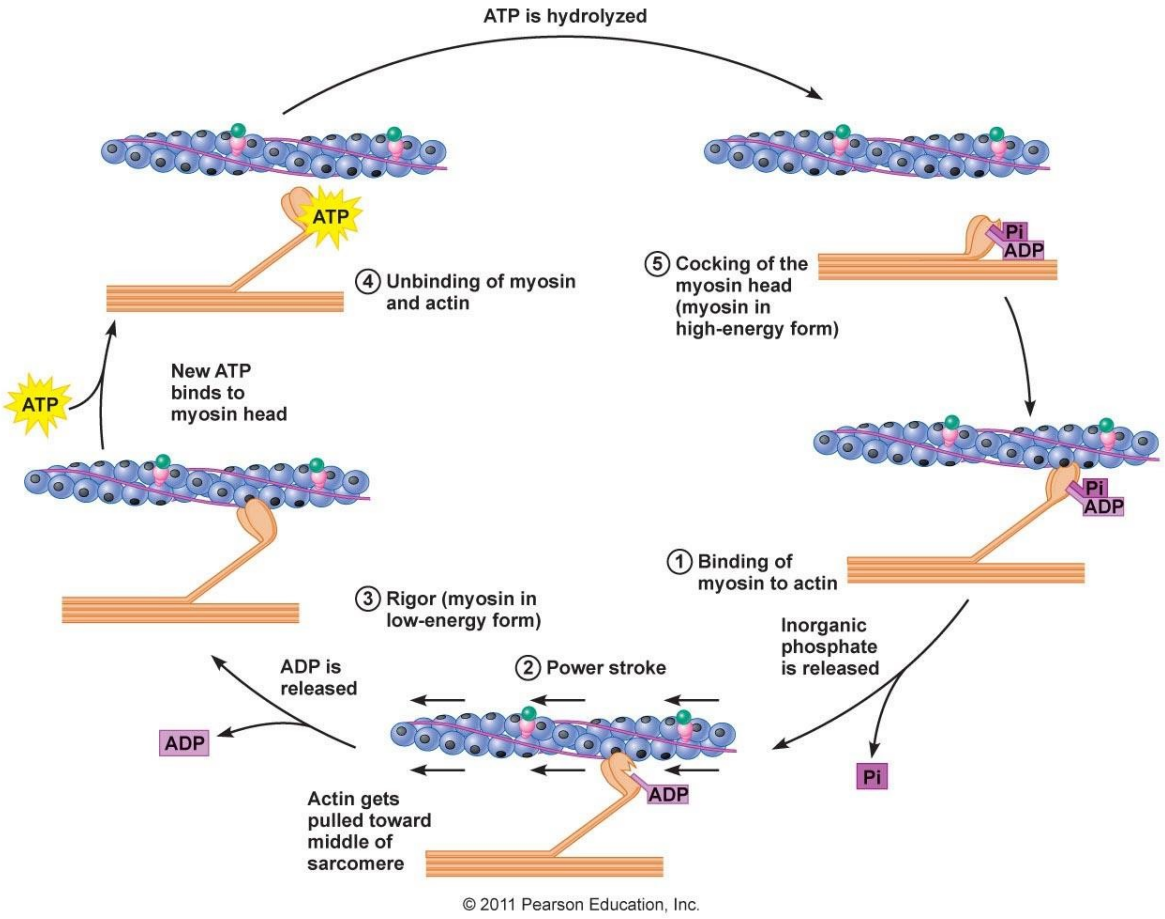


Figure 1-10 Cross-bridge cycle. The filament sliding observed during muscle contraction is caused by the interaction of myosin heads (orange) with actin (blue). ATP, adenosine triphosphate; ADP, adenosine diphosphate; Pi, inorganic phosphate. Figure from (80).

1.8 Heart failure:

There are a number of mechanisms that govern changes in the cardiac function to meet physiological needs. Disruptions in these coordinated efforts affects the heart's ability to meet the needs of the body and if these disruptions persist heart failure can result. Heart failure is the inability of the heart to supply adequate blood flow to the body. This reduces oxygen delivery to peripheral tissues and organs causing symptoms such as fatigue and shortness of breath and may result in organ failure in severe cases. It affects more than 26 million people worldwide and the numbers are increasing every year, especially due to the ageing population (81). Despite the improvement in treatment and care, the prognosis for heart failure still remains poor.

Around the world, 17-45% patients admitted to the hospital with heart failure die within 1 year of admission, while the majority die within 5 years of admission (82-85). The increasing burden of heart failure has huge economic consequences. In 2012, heart failure related total hospital costs were estimated to be US$20.9 billion and are projected to increase up to US$ 53.1 billion by 2030 (86).

Heart failure is caused by a number of factors, some of which are linked to the heart directly such as hypertrophic cardiomyopathy and dilated cardiomyopathy or by external factors such as long term hypertension, increased stroke volume and hormonal disorders (e.g. hyperthyroidism). Acute heart failure can develop rapidly, within hours to days, and can be life threatening as the heart does not have time to adapt. This may result from cardiopulmonary by-pass surgery, acute infection (sepsis), acute myocardial infarction, valve dysfunction or severe arrhythmias (87). Chronic heart failure last from months to years and is characterized by the heart having compensatory adaptations such as hypertrophy or dilation depending on the cause of

heart failure. These compensatory changes, however, can be deleterious in the longterm and lead to a worsening condition (87, 88).

Heart failure can be divided into a number of categories, but the broad categories are systolic and diastolic dysfunction. Systolic heart failure which is characterized by reduced ejection fraction and enlarged left ventricles and is generally caused by poor/reduced contractility. The muscle is not able to generate the force to eject the contents of the ventricle, to meet the demands of the body. This can be caused by myocardial disease or acute myocardial damage. Diastolic heart failure is characterized by the impaired ventricular filling, which is often caused by the inability of ventricles to relax completely owing to stiff ventricle walls (89). Reduced ventricular filling leads to reduced cardiac output via the Frank-Starling mechanism (2). The symptoms of heart failure include fatigue, shortness of breath, peripheral oedema. If not treated effectively, the worsening phenotype can lead to other complications and poor prognosis (87).

1.9 Inherited Cardiomyopathy:

One of the leading causes of heart failure is cardiomyopathy (90). Cardiomyopathies are a group of disorders affecting the myocardium resulting in varying degree of structural and functional abnormalities of the heart. The diseases present often in early adult life, despite mutations being present from birth. The two most common inherited cardiomyopathies, classified according to their structural and morphological features, are hypertrophic cardiomyopathy (HCM) and dilated cardiomyopathy (DCM) (90), though a number of additional overlapping disease also exist, as highlighted by Figure 1-11. Functional and morphological features are used to classify inherited

cardiomyopathies; additionally, molecular genetics can be used to establish exact disease (91). The identification of the type of cardiomyopathy can be difficult due to the disease heterogeneity, and unique phenotype presented by mutations within the same gene (92).

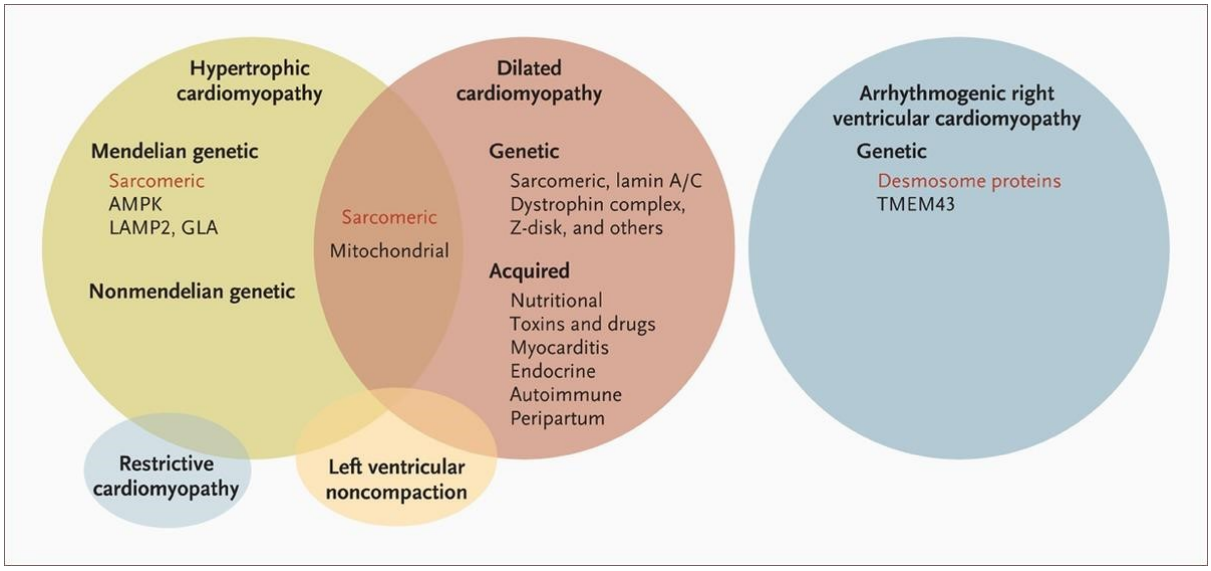


Figure 1-11. Clinical categories of inherited cardiomyopathies and their genetic causes (90)

1.10 Hypertrophic Cardiomyopathy (HCM)

HCM is the most common inherited heart disorder with a prevalence of 1 in 500 individuals (93). HCM is an autosomal dominant disease and is one of the most common causes of sudden cardiac death in individuals and the leading cause of death in athletes (94). It is characterized by asymmetric hypertrophy of the interventricular septum and the left ventricular wall. These changes manifest clinically as left ventricular outflow tract obstruction, diastolic dysfunction, ischemia, atrial fibrillation, and in some cases systolic impairment due to progression to a ‘burnt-out’ phase (95). In addition, on the microscopic level, there is myocyte disarray and development of

interstitial fibrosis. The presentation of these symptoms has been observed in a wide age range from infancy to individuals older than 80 years (93). Clinical diagnosis can be made by a positive family history, abnormal echocardiogram and/or apparent heart murmur. In adults, confirmation of disease diagnosis is made by the presence of left ventricular end diastolic wall thickness >13 mm by 2-D echocardiography (96). In patients with mild hypertrophy or where the onset has not yet occurred, an MRI might be required to confirm diagnosis. With technological advancements genetic screening of HCM causing mutations is also becoming common, especially to diagnose family members of affected patients (92, 97).

The prognosis of HCM is quite heterogeneous with variable age of onset of symptoms (98). Whereas some patients can be asymptomatic for their entire life others can suffer from sudden death during childhood. Cardiac hypertrophy in patients with underlying disease causing mutations is identified in older patients in majority of the cases, with half the case being identified after the age of 30 and 75% presenting with hypertrophy in their 60s(90). There is a wide array of symptoms that a patient can present with, including chest pain, dyspnoea, fatigue, breathlessness, palpitations and arrythmia (99). Sudden death is the most severe outcome, and though its most prevalent in children and young adults, it can happen at any age and without any preceding symptoms. The annual mortality for HCM is approximately 1% per annum (93). Some subsets of HCM, however, may have a higher risk of mortality. Risk stratification of HCM patients is quite complex and not completely understood. Ventricular wall thickness is directly correlated with the risk of sudden death and can therefore help clinicians assess risk of the patient (100). The genetic background, especially the mutation causing HCM, affects severity of disease and the risk of sudden death

considerably. For example, patients carrying mutations in the beta-myosin heavy chain and Troponin T proteins have a higher risk of sudden death than those carrying mutations in MyBPC or alpha-tropomyosin (101-103).

At present there is no cure for HCM. Physicians focus on managing the symptoms and minimizing complications. Patients with a high risk of sudden cardiac death are implanted with a cardiac defibrillator as a preventative measure (104). Patients who experience atrial fibrillation or have symptoms progressing towards heart failure are given a wide variety of drugs including β-adrenergic receptor blockers to control the heart rate and calcium channel blockers to reduce hypercontractility (105). In cases where the hypertrophy obstructs ejection of blood from the ventricles surgery is performed (106). This involves the removal of small amount of muscle from the septal wall. This can also be achieved by injecting alcohol septal ablation, a process by which alcohol is injected into the branch of the artery supplying a region of hypertrophied septum, creating an infarction and resulting in decreased wall thickness (106). Patients with nonobstructive hypertrophy and with severe symptoms are considered for heart transplantation. Prophylactic treatment or surgery is ill advised in asymptomatic patients due to the side effects of these treatments (106). Though current therapies make the disease more manageable, they are unable to reverse or stop the progression of disease. More research is required to understand the mechanics driving pathology of HCM to allow for discovery of novel therapies.

HCM is generally an autosomal dominant disease, meaning a single heterozygous mutation is usually sufficient to cause the disease (90). The mutations, however, have different penetrance and expression and the differences in phenotype are attributed partly to the fact that these mutations work in coordination with a number of genetic

and non-genetic factors. The first identified case of HCM caused by a mutation was found in the gene encoding β-myosin heavy chain in 1990 (107). Since then a number of mutations in different genes have been shown to cause the disease. The majority of the mutations implicated in HCM are in genes that encode contractile myofilament proteins components of the sarcomere, which led to HCM being identified as “disease of the sarcomere”. Approximately three-fifths of HCM cases have been attributed to have a disease causing mutation (96). Table 1-1 highlights some of the prominent disease causing genes and their relative risk. Mutations in β-myosin heavy chain and cMyBP-C, alone account for up to 50% of all cases (108). Mutations in *TNNT2*, *TNNI3* (cardiac troponin I), and *TPM1* (α-tropomyosin) are uncommon and account for less than one-tenth of the cases (108, 109). Other established yet uncommon genes with causal mutations include *ACTC1* (cardiac α-actin), *MYL2* (myosin light chain 2), *MYL3* (myosin light chain 3), and CSRP3 (cysteine and glycine-rich protein 3 or Muscle LIM Protein, (MLP)) with each of them accounting for less than 5% of cases identified (110). Most of the causal mutations are missense mutations, except for mutation in cMyBP-C which are mostly insertion/deletion and premature truncation mutations caused by frameshift leading to haploinsufficiency (111-113). The changes in amino acid brought upon by missense mutations result in altered protein conformations and protein-protein interactions. The frameshift mutations results in either nonsense mediated decay at mRNA level or degradation by the ubiquitin proteasome system, in the case of truncated/misfolded proteins (114, 115).

Gene	Protein	Function	Tolerance to Variation	
			Missense (*Z*Score)	LoF (pLI)
MYH7	β-Myosin heavy chain	ATPase activity, force generation	6.54	0.00
MYBPC3	Myosin-binding protein C	Cardiac contraction	0.69	0.00
TNNT2	Cardiac troponin T	Regulator of actomyosin interaction	1.54	0.01
TNNI3	Cardiac troponin I	Inhibitor of actomyosin interaction	1.88	0.17
ACTC1	Cardiac α-actin	Actomyosin interaction	5.25	0.95
CSRP3	Cysteine- and glycinerich protein 3	Muscle LIM protein (MLP), a Z disk protein	−0.66	0.00
Likely causal genes for HCM (small families)				
FHL1	Four-and-a-half LIM domains 1	Muscle development and hypertrophy	1.29	0.92
PLN	Phospholamban	Regulator of sarcoplasmic reticulum calcium	0.57	0.11
TCAP	Tcap (telethonin)	Titin capping protein	0.45	0.08
TTN	Titin	Sarcomere function	−5.48	0.00
Genes associated with HCM (small families and sporadic cases)				
ACTN2	Actinin, α2	Z disk protein	1.76	1.0
ANKRD1	Ankyrin repeat domain 1	A negative regulator of cardiac genes	−0.01	0.00
MYH6	Myosin heavy chain α	Sarcomere protein expressed at low levels in the adult human heart	2.87	0.00
TNNC1	Cardiac troponin C	Calcium-sensitive regulator of myofilament function	2.22	0.51

Table 1-1. Genes Implicated in HCM. From (108).
The Z score for each gene reflects deviation of the observed variants in the ExAC database from the expected number. A higher positive Z score indicates that the gene is intolerant to variation. Likewise, pLI indicates probability of intolerance to LoF variants with 1 indicating total intolerance. HCM indicates hypertrophic cardiomyopathy; and LoF, loss of function.

1.10.1 Pathogenesis of HCM:

Based on the specific causal mutation there are diverse mechanisms which drive the pathology of HCM. The mutation may change the conformation of protein and affect its interaction with other sarcomeric proteins, especially missense mutations, or, in the case of myosin, its enzymatic activity; alternatively, it may affect the expression of protein by changing the regulation of transcription rate and translation efficiency(116, 117). The direct effect on expression regulation depends upon the mutation, as mentioned above.

Missense mutations in sarcomeric genes that affect protein conformation may affect the efficiency of sarcomere assembly (118). The expression of mutant protein and its fraction relative to the wild type protein and its incorporation in sarcomere assembly determine the functional defects. The variability in expression and incorporation might also help explain the variable phenotypic expression of HCM.

Once part of the sarcomere assembly, the mutant proteins affect different functions of the sarcomere including actomyosin cross-bridge cycling, altered calcium sensitivity of troponin complex and ATPase activity.

HCM causing mutations initially act to increase contractility by increasing Ca^{2+} buffering and altering Ca^{2+} handling (119). The resulting perturbations in downstream signalling pathways may drive cellular changes at the microscopic level. The increased contractility may be due to heightened sensitivity of activation or increased myosin cycling speeds (120). As cross-bridge cycling accounts for two thirds of cardiomyocyte energy usage at baseline, excess cross-bridge activity or inefficient force generation could negatively impact the energetic state of the cells. Hypercontractility is unlikely to affect cardiac output as the hear ejects majority of its contents during each cycle (121).

The inefficient use of ATP impairs cardiomyocyte's ability to perform critical functions such as energy-requiring ionic homeostasis, especially Ca^{2+} reuptake by SERCA2 (122). The compromised energetics have been observed in murine models of HCM (123) as well as early-stage human patients (124). Collectively these findings present a mechanism of energy deficiency that may underlie disease pathogenesis in HCM. In addition to the direct effects of mutations there are a number of other molecular pathways that are affected including calcium sensitive and stress responsive molecular pathways. These signalling pathways which include activation of calcineurin pathways, mitogen-activated protein kinases, transforming growth factor β pathway in addition to others contribute to the development of morphological and histological changes that are attributed to a clinical HCM phenotype. These changes include myocyte and cardiac hypertrophy, disarray, and interstitial fibrosis among others (125127).

Though the causal mutation determines the phenotype, the resulting clinical phenotype is a result of an interaction between a number of different signalling pathways and the environmental factors. Genetic background of the patient also influences the phenotype as the presence of additional variants of genes, whether pathogenic or not, would affect pathways involved in development and progression of cardiac hypertrophy. For example, an insertion/deletion variant in the angiotensin-1 converting enzyme gene has been shown to modify expression of cardiac hypertrophy and the risk of sudden cardiac death in HCM (140–142). Therefore, the final HCM phenotype is a result of a number of small effects brought upon by factors such as genetic background, environment factors in addition to the effect caused by the mutation.

1.11 Dilated Cardiomyopathy

Initially described by Evans as cardiomegaly (128), dilated cardiomyopathy is a disease characterized by enlarged heart chambers especially left ventricle and poor contractility. Figure 1.12 compares a normal heart with a heart from a patient with dilated cardiomyopathy. On a histological level the cells in DCM diseased heart have a bigger nucleus, show myofibrillar loss within the myocyte, focal myocyte apoptosis, and interstitial fibrosis (120, 129).

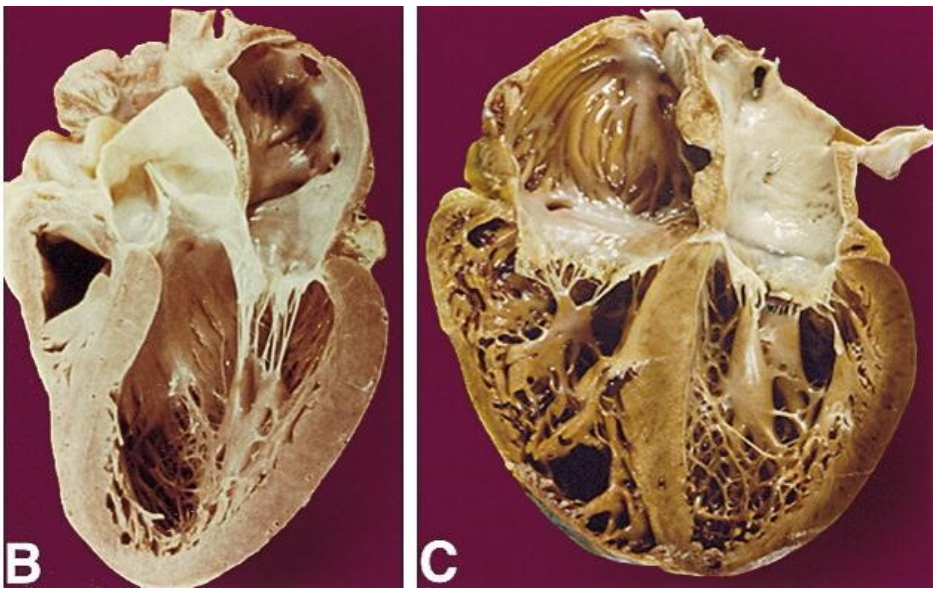


Figure 1-12: Comparison between normal and dilated cardiomyopathy heart (Adapted from (109))

Epidemiological studies using old imaging modalities estimated DCM to have a prevalence of 36.5/100,000 individuals globally, meaning a ratio of 1 in 2700 people (130). The prevalence values vary according to geographic region and ethnicities, as well as according to the methods used. A more recent study by Hershberger and colleagues estimated the prevalence to be much higher, in the range of 1:250. Their

model based this estimate on the known ratio of idiopathic DCM to HCM of approximately 2:1, estimated prevalence of heart failure, and prevalence estimates of left ventricle dysfunction as a proxy for DCM.

The majority (80%) of patients with DCM exhibit symptoms related to the onset of heart failure (131). These symptoms include excessive sweating, peripheral oedema, and fatigue after mild exertion. In extreme cases, circulatory collapse can occur as a result of advanced heart failure. Thromboembolic symptoms and sudden death are rare at early stage, especially in infants (132). LV dilatation is accompanied by remodelling which makes the LV assume a more spherical shape. Pathophysiological changes include a decrease in stroke volume and subsequently cardiac output, which causes not only diminished force generation but also impaired ventricular filling. The body tries to compensate to these changes by increasing systemic vascular resistance, reducing arterial compliance, and elevating venous pressure and circulating blood volume. Both cardiac preload and afterload are increased, with increased afterload resulting in elevated wall stress (133, 134).

DCM with diastolic dysfunction, brought upon by changes to both phases of diastole, active relaxation (early) and passive compliance (mid-to-late phase), can also have diminished systolic function at the same time. Impaired ventricular relaxation results in reduced rapid ventricular filling. The atypical morphology and cardiac physiology in

DCM leads to neurohormonal responses including increase in sympathetic adrenergic activity and reduction in vagal activity to the heart. These responses lead to increase circulating levels of catecholamines and vasopressin, increase in production of natriuretic peptide and activation of the renin–angiotensin–aldosterone system. This elevated catecholamine levels, along with increased cardiac afterload, fluid retention, and tachycardia result in further elevation of wall stress and myocardial oxygen

demand, as well as direct cardiotoxicity (51). These secondary adaptations lead to ongoing myocyte damage with further reduction in myocardial performance. Compensatory hypertrophy allows more muscle fibres to share in wall tension for any given ventricular pressure and radius. Patients at this stage also suffer from increased arrythmias and higher risk of acute myocardial infarction. The dilated ventricles are more prone to thrombus formation at the base of the ventricle due to a combination of enlarged cavities and slower movement of blood through the LV due to reduced contractility. The prognosis of DCM is poor with only half of the patients surviving after 5 years of the initial diagnosis.

1.11.1 Diagnosis and Treatment

Clinical diagnosis of DCM is made when (1) fractional shortening <25% (>2 SD) or ejection fraction <45% (>2 SD), and (2) LV end-diastolic diameter >117% (>2 SD of the predicted value of 112% corrected for age and body surface area), excluding any known cause of myocardial disease (135). LV dimension and function can be assessed using 2-D echocardiography or cardiac magnetic resonance. In some cases, an endomyocardial biopsy is performed, in addition to imaging, to confirm diagnosis. Similar to HCM, DCM has no cure and current treatments aim to manage symptoms and slow down progression towards heart failure and prevent arrythmias. Depending on severity and phenotype preventative treatment of thromboembolism is also carried out. There is no drug therapy that has shown to improve survival from acute heart failure. Angiotensin converting enzyme inhibitors and beta blockers are used as firstline of pharmacotherapy for chronic heart failure. Though non-pharmacological treatments such as limiting salt and fluid intake are recommended widely, there is limited evidence to support these recommendations (136-138). Patients with secondary DCM due to a

viral infection are treated with immunosuppression or interferon, however idiopathic DCM is more difficult to treat successfully (130).

Implantable cardiac defibrillators have been utilized in patients with non-ischemic DCM, however no improvement in overall survival has been observed, even though it reduces the risk of sudden cardiac death (139). Surgical interventions for DCM include heart transplantation and implantation of long-term mechanical circulatory support, either as a temporary treatment while patients wait for heart transplant or as a destination therapy. DCM patients make up the single largest group of patients on the transplant list. Median survival post-transplant is more than 10 years for adults and up to 20 years for infants (140, 141).

1.11.2 Molecular Genetics of DCM

Up to 35% cases of idiopathic DCM cases have a familial pattern and a genetic cause (142, 143). DCM is most commonly inherited in an autosomal dominant fashion, with half of the offspring at risk of inheriting the disease-causing gene mutation (144). Other modes of transmission such as autosomal recessive, X-linked, and mitochondrial inheritance patterns are less common (142, 145). Familial cases of DCM present at a younger age than other cases. Though there is not much difference in term of morphology and prognosis between the inherited and other cases, the familial DCM patients have a higher ejection fraction, have better exercise capacity and show some difference on ECG (143).

Linkage studies in large families and candidate gene screening have been used to delineate the occurrence of gene mutations which may cause familial DCM. DCM is genetically heterogeneous with DCM genes encoding proteins with diverse cellular

functions such as those coding for sarcomeric, cytoskeletal, nuclear envelope, desmosomal, and RNA binding proteins. As a result, the pathophysiological mechanisms leading to DCM are also diverse as well. From a clinical and functional perspective these genes can be divided into categories as those with genes that cause a predominant cardiac phenotype (include the sarcomere genes), those associated with neuromuscular disease, and those where DCM presents as part of a syndrome. Table 1-3 shows a list of DCM causing genes.

In addition to pathogenic mutations, DCM is also caused as a result of coronary artery disease, viral myocarditis, thyroid disease, immunologic processes, and toxins and drugs such as alcohol, cocaine and methamphetamines. However, in many cases the exact underlying cause of DCM is not yet discovered. These cases are referred to as 'idiopathic DCM'.

1.11.3 DCM Causing Cytoskeletal Genes

A number of the cytoskeletal proteins have been implicated in the development of DCM. Mutations in the cytoskeletal protein dystrophin were one of the first to be linked to X-linked DCM and familial cardiomyopathy phenotype in patients with Duchenne muscular dystrophy (DMD) (146-148). Further studies have highlighted that DMD patients, with X-linked DCM, have mutations within the dystrophin gene clustered in two positions. One region comprises of the promoter and first exon, which interacts with δ-sarcoglycan; and the second is the N-terminal 'hinge' region of dystrophin adjacent to the actin binding domains (149). This work was followed by identification of mutations in the δ-subunit of the sarcoglycan complex, which were usually associated with muscular dystrophy, to be a cause of DCM (150, 151). Under normal conditions these proteins play a critical role in maintaining sarcolemmal stability. The

sarcolemma becomes unstable in the case of mutant proteins leading to loss of cardiomyocytes and cardiac dysfunction. A number of therapies restoring dystrophin expression such as antisense oligonucleotides to produce truncated protein, and stop codon suppression compounds to promote run through premature stop codons, are being studied (152, 153). Mutations in Laminin α-2, another protein of the dystroglycan complex have been shown to cause DCM (150, 154, 155). Lamin A/C anchors into αsarcoglycan and protrudes out into the extracellular matrix. These mutations can cause recessive congenital muscular dystrophies, a disease which usually has some cardiac involvement, however the pathogenesis and morphological changes observed in the heart are mild (156).

Recent findings have highlighted mutations in *FLNC*, a gene encoding for filamin C protein, to be associated with DCM (157). Filamin C interacts with the dystrophin complex and the lack of filamin C in mice leads to skeletal myopathy (158). Filamin C truncating variants in humans lead to DCM phenotype with a high rate of ventricular arrythmias and sudden cardiac death (159). These findings suggest that filamin C has a role in cardiac conduction in addition to that in the cardiomyocyte.

Missense mutations in desmin, one of the earliest markers of myogenic development and a cytoskeletal protein of the intermediate filament, cause autosomal dominant DCM. Desmin plays a role in mechanotransduction within the myocyte and contributes to force transmission from the sarcomere and resistance to mechanical stress. Desmin knock out mice develops a DCM phenotype in addition to disruption of myofibril assembly (160) . Another cytoskeletal protein implicated in DCM is metavinculin, a protein part of the intercalated disc. Mutations in metavinculin alter the actin interactions, disrupting the force transmission at the thin-filament intercalated disc interface leading to DCM (161, 162).

The common disease mechanism underlying DCM in mutation of cytoskeletal proteins is the disruption of cellular assembly and the disruption of the sarcomere-cell membrane interaction. There is suggestion that in the presence of these mutations the cardiomyocytes are unable to resist changes in isometric force and stretch sensing during muscle contraction, which may lead to cell death and subsequently dilation of the heart chamber. However, mutations in nuclear envelope (lamin A/C) and calcium handling (phospholamban) proteins, as well as components of the sarcomere indicate that this impairment of force generation may be one of many factors contributing to DCM disease associated modelling.

1.11.4 Mutations in sarcomeric proteins

Encoding the largest protein in the heart titin, truncating mutations in the gene *TTN*, have been shown to be responsible for 12-25% of idiopathic DCM cases. Titin spans half the length of the sarcomere from the Z-disk to the M-band and it functions as a spring, providing passive force and regulating sarcomere contraction and signalling (163). Titin splicing varied throughout development and adapts to distinct pathophysiological states, including heart failure (164). It has a larger N2A and a smaller N2B form which are responsible for compliant ventricle and stiffer heart respectively. RNA sequencing of failing hearts highlights that *TTN* has highly variable exon usage that is consistent with even subtler defects in cardiac elasticity (165). Induced pluripotent stem cells derived cardiomyocytes demonstrate a paucity of sarcomeres, suggesting that force may be impaired directly through sarcomere loss in

TTN truncations (166). *TTN* has a high prevalence of missense variants, both rare and common (167). *TTN* missense variants have been reported in ARVC and other forms of cardiomyopathy (167-171) but majority of them are expected to be silent.

The DCM-causing mutations in cardiac alpha actin (ACTC) were among of the first to be reported in a sarcomeric gene. These missense mutations (Arg312His and Glu361Gly), were discovered following the discovery of mutations in actin binding region of dystrophin. (172). Further studies have highlighted several other mutations in the gene that are linked to DCM (161). Mutations in cardiac alpha actin are associated with both HCM and DCM. Though the exact basis for difference in phenotype of these mutations has not been established it is suggested that this depends on the distinct functional domain these mutations are present. Actin mutations causing HCM have been found in the regions of actomyosin interaction whereas the DCM mutations are located in the immobilized end of the actin molecule, a domain thought to be involved with the transmission of force to the cytoskeleton at the Z disk.

Mutations in myosin heavy chain along with MYBPC3 are one of the most frequent mutations causing HCM (92). Though the HCM may progress into a DCM phenotype there are other mutations in *MYH7* that lead to DCM phenotype directly. Kamisago and colleagues identified the DCM locus 14q12 corresponding to the β-myosin heavy chain (βMHC) (*MYH7*) by linkage analysis on a large multigeneration family with early onset DCM (92). This study identified two missense mutation S532P and F764L, which were studied by Schmitt and colleagues by engineering them into mouse with modified endogenous α-MHC. These mutations impaired contractile function of the cardiomyocyte as suggested by their location. The S532P mutation occurs within the actin-binding domain, and the F764L mutation occurs within the converter domain, which is one of the several flexible joints in myosin that undergo a conformational

change during the contraction cycle. Further studies have highlighted a number of other DCM associated mutations which are spread across all of the myosin subdomains from the catalytic head at the N-terminus to the helical rod at the C-terminus (173, 174).

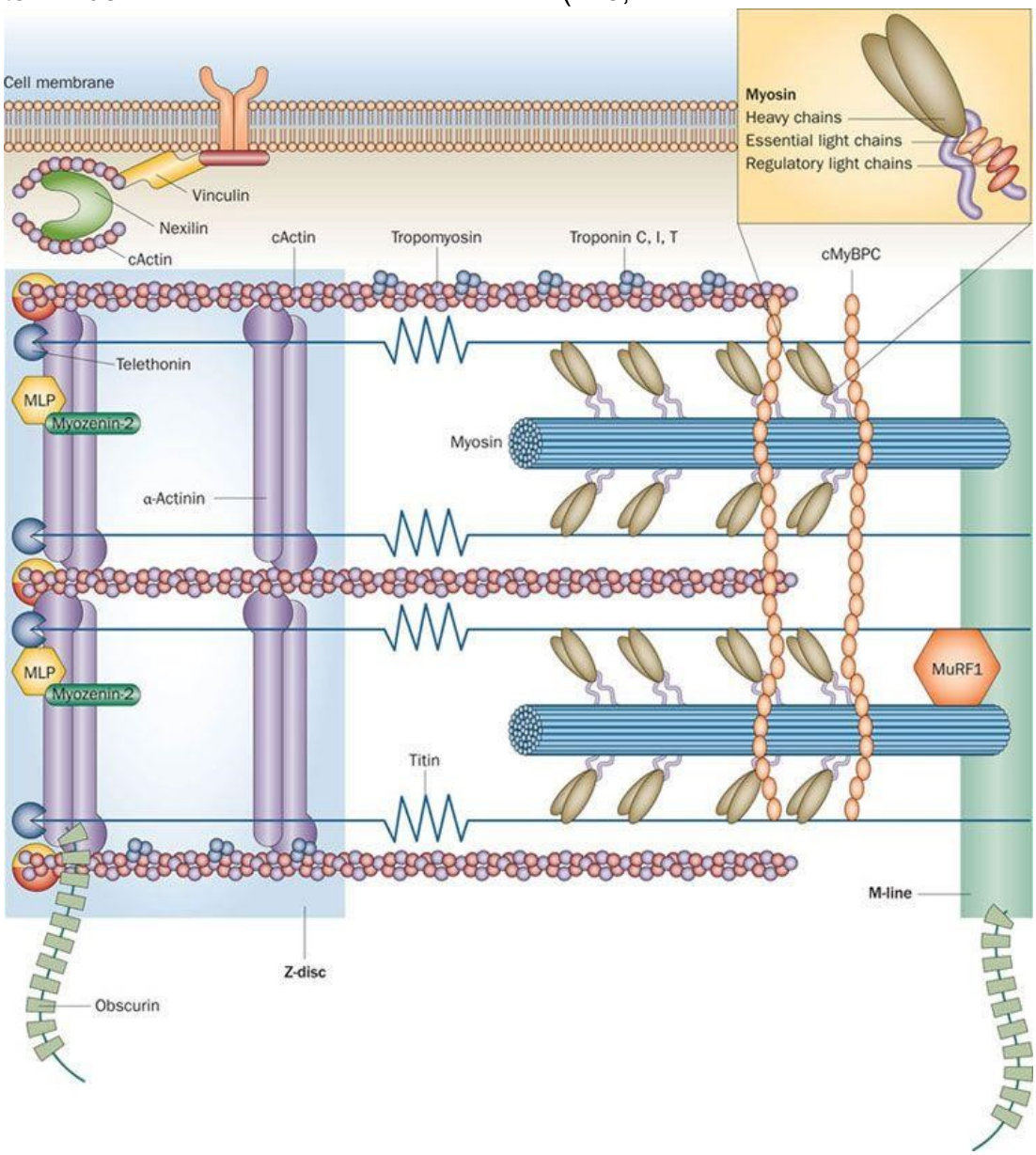


Figure 1-13. Components of the Sarcomere (175)

The extensive distribution of DCM mutations across the *MYH7* gene along with the distribution of about 200 HCM mutations in the *MYH7* gene, which are spread across various domains, suggest that the hypothesis that mutations can be categorized to be either HCM or DCM causing depending on the domain they are present in is too simplistic.

The study by Kamisago mentioned above also used candidate gene screening of genes encoding proteins thought to be functionally associated with myosin to characterise a third disease gene that encodes a sarcomeric protein. The remaining two families in the study had the same mutation in cardiac troponin T (*TNNT2*), a deletion of Lys210 in the T2 globular head which makes up part of the troponin core domain (176). This mutation was also found in a third family in a later report (177). Further mutations were then characterised in both the T1 tail (Arg141Trp) (178), Arg131Trp (179) and Ala172Ser (180) and T2 globular head region of troponin T (Arg205Leu and Asp270Asn (179). All the mutations appear to cause a severe and malignant form of DCM with a poor prognosis for affected patients. Troponin T also contains a large number of HCM causing mutations widely distributed across the protein therefore, as with the myosin mutations, conclusions on the mechanism of disease pathogenesis cannot be drawn.

Gene	Protein	Function	Percentage of DCM cases
Sarcomeric			
ACTC1	Actin	Force Generation	
MYH7	Beta Myosin Heavy Chain	Muscle Contraction	5%
TNNT2	Troponin T, cardiac muscle	Muscle contraction	3%
TTN	Titin	Extensible scaffold/	15–25%
MYBPC3	Myosin-binding protein C, cardiac type	Muscle contraction	2-4%
TNNC1	Troponin C, slow skeletal and cardiac muscles	Muscle contraction	
TNNI3	Troponin I, cardiac muscle	Muscle contraction	
Cytoskeleton			
DES	*Desmin*	*Contractile transduction force*	*<1%*
DMD	Dystrophin	Contractile transduction force	
Nuclear envelope			
LMNA	Prelamin-A/C	Nuclear structure membrane	4%
Spliceosomal			
RBM20	RNA-binding protein 20	Regulates splicing of cardiac genes	2%
Sarcoplasmic reticulum			
PLN	Cardiac phospholamban	Sarcoplasmic reticulum calcium regulator; inhibits SERCA2a pump	
Z-disc			
FLNC	Filamin-C	Structural integrity of cardiac myocyte; actin crosslinking protein	–
CSRP3	Cysteine and glycine-rich protein 3	Mechanical sensing stretch	–
TCAP	Telethonin	Mechanical sensing stretch	–
Other			
BAG3	BAG family molecular chaperone regulator 3	Inhibits apoptosis	–
ANKRD1	Ankyrin repeat domain-containing protein 1	Encodes CARP, a transcription co-inhibitor	<2%

Table 1-1 Frequency ad function of DCM causing genes. Adapted from (126)

1.12 Muscle LIM Protein

Muscle LIM Protein (MLP), is encoded by the gene Cysteine and Glycine-rich Protein 3 (*CSRP3*) located on chromosome 11p15.1 (181). MLP was initially identified by Arber and colleagues, as a regulator of myogenesis in straited muscles (Arber 1994). Since then a number of variants for the *CSRP3* gene have been directly implicated to cause DCM and HCM in an autosomal dominant fashion (182-186). Additional studies have highlighted MLP protein expression levels to be significantly altered in failing hearts and skeletal myopathies (187, 188).

1.12.1 MLP Protein Structure

MLP is a relatively small protein of 194 amino acids, which is expressed specifically in striated muscles (189, 190). It belongs to the LIM family of proteins which are characterized by the presences of one or more LIM domain. These LIM domains, which can be present throughout the length of the protein, have a consensus sequence of CX2CX16_23HX2CX2CX2CX16_21CX2(C/H/D), where X denotes any amino acid (191, 192). The LIM domains define a specific zinc binding structure with each LIM domain binding to two ions of zinc via the conserved sequence of cysteine and histidine residues in the consensus sequence (193-195). This coordination is required for proper folding of the LIM domain (194). The LIM domains are believed to be protein binding interfaces that allow diverse protein interactions and enable formation of macromolecular complexes (191, 192, 196).

MLP's two LIM domains, separated by 50 amino acids, are surrounded by glycine-rich repeat regions. This setup is characteristic of the cysteine-rich protein (CRP) family

(197). A study using nuclear magnetic resonance spectroscopy determined that MLP's LIM domains act independent of each other and are joined by a flexible linker region (198).

Recently, MLP has been shown to oligomerize, forming dimers, trimers and tetramers in myocytes (199, 200). This oligomerization potential of MLP is understood to play a fundamental role in its localization within the cell and its function.

Bioinformatic analyses predict MLP to have a number of phosphorylation sites. However, no MLP phosphorylation site has been published. Lange and colleagues have highlighted that MLP phosphorylation is significantly increased in heart samples of DCM patients compared to non-failing controls (201). The only other post translational modification of MLP to be published is the acetylation/deacetylation of MLP at a lysine residue at position 69 (K69), by acetyltransferase and histone deacetylase 4 (HDAC4), respectively (202). The study also observed that increased acetylation of MLP, by inhibition of HDAC4, increased calcium sensitivity of the heart (202). Since the K69 residue is within the predicted nuclear localization signal of MLP (203), it has been proposed that acetylation of K69 may control nuclear localisation of MLP. These findings together warrant the need to study post translational modifications on MLP as a means of regulating its function and localisation.

1.12.2 MLP Interacting Partners

A number of studies have highlighted MLP's interacting partners. MLP has been shown to interact with Z-disk proteins such as telethonin (T-cap) (204), α-actinin (205, 206), and others including cofilin-2 (207), calcineurin (208), HDAC4 (202) and MLP itself. (209). It has a number of interacting partners at the costamere including Zyxin, Integrin

Linked Kinase, and β1-Spectrin (209, 210) and interacts with the Nebulinrelated Anchoring Protein (N-RAP) at the intercalated disk (211).

Though MLP does not have a DNA binding region, it has been shown to interact with nuclear transcription factors MyoD, Myogenin, and Myogenic Regulatory Factor 4 (MRF4) (212) within the nucleus. These interactions and the presence of a nuclear signal led to the suggestion of nucleocytoplasmic shuttling of MLP. This hypothesis was supported by a study where mouse antibody raised against the C-terminus of MLP, detected both cytoplasmic and nuclear distribution of the protein (213). Boateng et al further showed that both pharmacological (phenylephrine) and mechanical (cyclic strain) stimuli caused an accumulation of MLP in the nucleus. Using cell permeable synthetic peptides, containing the nuclear localisation signal, in neonatal rat cardiomyocytes they were able to inhibit the translocation of MLP into the nucleus, even after phenylephrine stimulus. Further, the inhibition of MLP's translocation into the nucleus resulted in sarcomeric disarray, following cyclic strain. The inhibition of MLP into the nucleus prevented the increased protein synthesis and increased expression of brain natriuretic peptide that usually followed hypertrophic signalling induced by phenylephrine and cyclic strain. These findings not only give strong evidence of nuclear accumulation of MLP but also sheds light on the function of nuclear accumulation of MLP (200).

1.12.3 MLP in Human Disease

Mutations in MLP have been associated with development of both HCM and DCM (table 1-2). Interestingly, all of MLP's mutations are located within the first 100 amino acids, with nearly 50% of them located within the N-terminus. To date no disease causing mutation has been identified at the C-terminus (214). The increasing

availability of genetic databases has helped to validate previously published pathogenic variants. Reported to be one of the most common MLP mutations in cardiomyopathy patients, *CSRP3* p. W4R variant (187), has been re-classified as a benign polymorphism (182, 215). MLP C58G variant was identified by linkage analysis in a large German family with familial HCM (216). The mutant MLP showed reduced binding to both N-RAP and α-actinin *in vitro* (206). The MLP C58G mutant protein, was also more susceptible to degradation *in vitro*. This was supported by the findings that MLP expression in cardiac biopsy of patient with a heterozygous MLP C58G pathogenic variant was reduced by 40% (215). This led to the suggestion that the cause of hypertrophy in these patients was due to the lack of MLP rather than the presence of pathogenic variant (215). A recent report has also highlighted a case of homozygous *CSRP3* C58G mutation where the authors hypothesized that the *CSRP3* variant could result in HCM with an autosomal recessive inheritance rather than with an autosomal dominant transmission as usually reported on HCM (Janin et al 2018)

MLP Mutation	Phenotype	Reference	gnomAD (n, %)
L44P	HCM	[6, 23];	4, 0.0012%
S46R	HCM	[20]	8, (0.0024%)
S54R / E55G	HCM	[6]	0
C58G	HCM	[6]	0
R64C	HCM	[23]	10, (0.0028%)
Y66C	HCM	[23]	3, (0.00081%)
K69R	DCM	[24]	2, (0.000016%)
G72R	DCM	[25]	7, (0.0024%)
Q91L	HCM	[23]	4 (0. 00041%)

Table. 1-2: Mutations in Human MLP linked with cardiomyopathy

Another MLP variant that is functionally characterized is the K69R mutant, which has been identified as a mutation for DCM. This mutation lies within the nuclear localisation signal and has been shown to cause MLP to localise predominantly to the perinucleus

(185). It is also suggested that the mutation disrupts MLP's interaction with α-actinin as K69 MLP did not co-precipitate with α-actinin *in vitro* (185). Further, since MLP has been shown to be acetylated at K69R, the disease phenotype in these patients might be due to the lack of acetylation of MLP (217).

In addition to pathogenic variants, MLP protein expression changes have been shown to be associated with cardiac disease. MLP expression was significantly reduced in failing hearts of patients with dilated or ischemic cardiomyopathy (209). The reduced expression may have contributed to myofibril disarray in the failing myocardium (209). MLP mRNA levels remain unchanged in these patients suggesting that regulation of protein expression was either due to reduced protein production or increased turnover rather than due to regulation of transcription (209). Notably, MLP's expression was not consistent in hearts, meaning reduced expression could not be used as a marker for heart failure. Changes in MLP oligomerization have also been associated with cardiac disease. Oligomeric MLP was found to be significantly decreased in myocardium of patients with heart failure. This led to the suggestion that the lack of oligomerization of MLP may impair the mechanosensing function of MLP, contributing to the development and/or progression of heart disease (199).

1.12.4 Mouse Models of MLP

MLP KO mouse was one of the first characterized models of DCM. In addition to showing classic DCM phenotype, the hearts also showed induction of hypertrophic signalling pathways. Cardiomyocytes from these mice exhibited cytoarchitecture perturbations including disrupted myofibrillar assembly, abnormal alignment of Z-discs and marked fibrosis (190). There were aberrations at intercalated disc with upregulation of proteins including N-RAP, β-catenin, vinculin and plakoglobin, along

with upregulation of adherens junctions and downregulation of gap junction protein connexin-43 (211). This model of MLP KO was described to have two different phenotypes: an early postnatal phenotype characterized by fatigue, an enlarged heart and congestive heart failure leading to death at the age of postnatal day 6 (P6) and P12. Those mice that survived the first two weeks were viable till adult life but showed all the features of DCM, such as thinning of the left ventricular wall accompanied significantly increased chamber size. These mice also exhibited elevated hypertrophic markers natriuretic peptide A (Nppa) and cardiac ankyrin-repeated protein (Carp). Cardiac echocardiography confirmed the phenotype while also highlighting reduced LV function as measured by reduced fractional shortening and ejection fraction while haemodynamic analyses showed reduced contractility with impaired relaxation (189).

The functional and histological phenotype revealed that MLP regulates the cytoarchitecture of the cardiomyocytes.

MLP KO mice were found to have altered calcium handling along with defects in excitation–contraction coupling. (218-220). MLP KO mice were found to have significantly higher basal phosphorylation status of Phospholamban (PLN), at the sites Ser16 and the Thr17 (221). PLN, in its unphosphorylated state is an inhibitor of cardiac muscle sarcoplasmic reticulum Ca^{2+}-ATPase (SERCA2). However, its phosphorylation relieves the inhibition leading to faster Ca^{2+} uptake into the sarcoplasmic reticulum. Mutations in PLN have been shown to cause dilated cardiomyopathy (222). Its role in calcium handling was highlighted by the absence of an overt phenotype after the genetic ablation of sarcoplasmic reticulum regulator PLN in MLP KO (223). These mice lacking both MLP and PLN rescued the DCM phenotype.

They showed none of the morphological or ultrastructural defects observed in MLP KO mice including, myofibrillar disarray and fibrosis, and impaired cardiac function (224).

Calcium signalling is a major theme in pathological pathways of DCM induced by loss of MLP. Genetic ablation of β2-adrenergic receptor (β2-AR) was effective in rescuing MLP KO mice from cardiomyopathy while deletion of the β1-AR worsened cardiac phenotype in MLP KO mice. The lack of β2-AR enhanced myocyte shortening, improved Ca^{2+} availability, restoring cardiac function and survival (225). Ablation of calcineurin, a calcium/calmodulin dependent serine-threonine phosphatase, in MLP-/- resulted in resulted in increased apoptosis, decreased left ventricular function, enhanced fibrosis and cardiomyopathy. About 75% of these mice, lacking both Mlp and Carp, died within the first three month. Conversely, calcineurin overexpression in MLP KO mice improved cardiac function and adverse remodelling (226).

MLP has been shown to increase during stress such as aortic banding in mice (209, 215). Transgenic mouse overexpressing MLP showed normal contractile function and no overt phenotype, under baseline conditions. MLP overexpression failed to protect the heart from pathological hypertrophy induced by transverse aortic constriction or chronic infusion of angiotensin-II (227), suggesting that cardiac overexpression of MLP *in vivo* does not protect from maladaptive hypertrophy.

MLP KO mice are born in expected Mendelian ratios ruling out the possibility that it is essential for embryonic development. However, the protein is thought to be critical for adaptation of heart to increased hemodynamic stress post birth (217). MLP KO hearts are unusually soft at birth and have significantly reduced passive elasticity and cardiomyocytes from 2 week old MLP KO mice have also been shown to have a defect in muscle stiffness (228).

MLP heterozygous KO mice on the other hand develop normally and show no adverse phenotype under normal conditions. These mice, however, have significantly more left ventricular dilation and systolic dysfunction and decreased survival after myocardial infarction (MI), when compared to WT mice. This phenotype following MI is associated with a supressed pro-hypertrophic Calcineurin-Nuclear Factor of Activated T-cells (NFAT) signalling pathway (229). Calcineurin, which under normal condition colocalizes with MLP at the Z-disc, was displaced in MLP heterozygous mice, highlighting the importance of MLP in controlling calcineurin signalling. Further, MLP heterozygous cardiomyocytes *in vitro* showed reduced ability to activate the NFAT signalling pathway, underlining MLP's importance in hypertrophic signalling pathways (229). MLP expression was also shown to be significantly increased in animals subjected to aortic banding, suggesting a protective role (230). However, overexpression of MLP in mice was unable to inhibit pathological signalling following aortic banding or chronic infusion of angiotensin-II (230).

A recent study by Lange and colleagues highlighted a novel function of MLP as an endogenous inhibitor of Protein Kinase Cα in the heart. Aberrant PKCα signalling caused remodelling and pathological growth of the heart. In the absence of MLP the expression of adapter protein CARP was increased which led to recruitment of PKCα at the intercalated disc. The chronic activation of PKCα leads to aberrant downstream signalling regulating calcium handling and contraction. Mice lacking both MLP and CARP developed normally as PKCα signalling is inhibited at the intercalated disc. (201).

1.13 Hypothesis and Specific Aims

Mutations in the genes encoding sarcomeric proteins are the most common cause of familial cardiomyopathies. The mechanisms underlying these mutations and the genotype-phenotype correlations are more easily described as these mutations directly affect contractile function of the myocardium. However, mutations in nonsarcomeric proteins, such as MLP, are also associated with inherited cardiomyopathies. Unlike sarcomeric proteins, the relationship between these proteins and cardiac contractile function is not well understood making it challenging to determine the pathogenesis of disease.

MLP was identified over two decades ago by Arber and colleagues yet the exact function of MLP or the underlying pathomechanisms of *CSRP3* mutations remain unknown. It was initially suggested that MLP was part of a Z-disk complex that acted as a mechanical stretch sensor. However, recent findings have highlighted an alternative role of MLP, as an endogenous inhibitor of protein kinase C alpha (PKCα) activity in the myocardium [6].

1.13.1 Hypothesis

Given that patients carrying the CSRP3 p.C58G mutation showed a hypertrophic cardiomyopathy phenotype and showed a reduction in MLP expression level, I hypothesis that *CSRP3* p.C58G mutation affects the stability of the MLP, contributing to the development of a cardiomyopathy phenotype. To test this theory, a mouse model carrying the C58G mutation (Csrp3 C58G knock-in, KI) was generated. The component hypotheses were that the C58G MLP mutation causes:

I. impaired cardiac function and development of cardiac hypertrophy

II. reduced MLP stability, and reduced MLP expression

III. altered protein degradation, leading to increased proteotoxic stress on the cell

In accordance with these hypotheses, this thesis aims to characterize the phenotype and underlying regulatory pathways of the C58G MLP mouse.

1.13.2 Specific Aims

Aim 1 – To evaluate the phenotype of the knock-in mouse (KI) model, carrying the HCM-causing MLP mutation C58G (Chapter 3)

Aim 2 – To analyse the transcriptome of MLP C58G and MLP KO mice in order to find potential pathways and regulators driving pathogenesis of disease (Chapter 4)

Aim 3 – To determine whether protein stability and increased protein degradation and proteotoxic stress contributes to development of hypertrophy in C58G mice (Chapter 5)

Chapter 2 - Materials and Methods

2.1 Molecular Biology

2.1.1 Transformation

MLP plasmids were generated in the lab. To make copies of plasmid for transfection of cells, 5-10 ng of plasmid DNA was added to 100 µl of competent DH10β E.coli cells and left on ice for 30 minutes. This mixture was heat shocked for 30 minutes at 42°C and incubated in ice. 200 µl of LB medium was added to the cells and they were allowed to grow at 37 °C for 1 hour before being plated on L-agar plates containing antibiotics (ampicillin at 100 mg/ml). Plates were incubated at 37°C overnight.

2.1.2 Plasmid Purification

Successful colonies from the transformation were used to inoculate 5 ml of LB medium containing ampicillin which was grown at 37 °C, shaking at 220 rpm for ~1 hour. The clone that grew was used to inoculate 400 ml LB medium containing ampicillin, which was grown shaking overnight at 37 °C. This culture was used to extract a large amount of plasmid DNA, using the QIAprep Maxi Prep Kit (Qiagen (UK) Ltd), following the manufacture's protocol.

2.1.2 Quality Control / Sequence Verification

Sample of purified DNA was sent for sequencing to the DNA Sequencing Facility, Department of Biochemistry, University of Oxford. Results were compared to published sequence to ensure that the plasmid sequence was accurate.

2.2 Genotyping – DNA extraction and PCR

DNA Extraction and Genotyping was performed using REDExtract-N-Amp™ Tissue PCR Kit. For DNA extraction, ear notches were incubated 100µl extraction solution, and 25µl tissue preparation solution for 10 minutes at room temperature. The notches

were then incubated at 95°C for 3 minutes. 100µl neutralisation solution B was added to each sample. The samples were gently vortexed and centrifuged maximum speed for 1 minute. Samples were stored at 4°C before being used for PCR. Master mix for the PCR were made as following:

	Per 15µl reaction:
REDExtract-N-Amp PCR reaction mix	7.5µl
DNase-free water	3µl
Primer reverse	0.75µl
Primer forward	0.75µl

For each samples 12µl master mix and 3µl of the DNA extract was added to a centrifuge tube which as transferred to the thermal cycler and the appropriate program for the relevant primer (Section 2.13) was run. After completion of run the amplified PCR product was run on 1% Agarose gel along with gene ruler and positive control for identification of genotype.

2.3 Western Blot

2.3.1 Sample preparation

Cell pellets were washed with PBS and then mixed with 2x SDS loading buffer. The samples were then sonicated for 1 minute and then boiled at 95 °C for 5 minutes in a heat block.

2.3.2 Protein concentration

Protein concentration of TLB lysates was determined using the Bio-Rad protein assay. Briefly, protein standards (Thermo Scientific) were prepared using bovine serum

albumin and PBS. Diluted samples, 1:20 and 1:50 in PBS, and standards were combined with the Protein assay dye reagent (diluted 1:5 from concentrate) (Bio-Rad) and measured in triplicate using a FLUOstar Omega plate reader at 595nm. The buffer was diluted with PBS in the same concentration and was used as blank. A standard curve was created using Microsoft Excel to relate absorbance measurements with protein concentration. This calibration curve was used to assess protein concentration in the unknown samples.

2.3.3 SDS-PAGE

SDS-PAGE was performed using both pre-cast commercial gels (Mini-PROTEAN TGX Stain-free gels 4-15 % gradient, Bio-Rad) and self-made SDS-PAGE gels (recipe in appendix). Self-made gels contained varying acrylamide concentrations depending on the size of protein of interest. Most gels were made of 12% acrylamide. For PhosTag gels, to assess MLP phosphorylation, 100 µM PhosTag (Fujifilm Wako Chemicals) and 200 µM $MnCl_2$ was added to the resolving gel.
Gels were run using a standard tris-glycine SDS-PAGE running buffer at 110 V at room temperature until the dye front reached the resolving gel. Then, voltage was increased to 160 V until the dye reached the bottom of the gel.

2.3.4 Western blotting

Transfer of protein from SDS-PAGE gels to nitrocellulose/ polyvinylidene difluoride membrane (PVDF) membranes was accomplished using Invitrogen iBlot Dry Blotting System according to the manufacturer's protocols. Briefly, pre-run gels were placed on Anode Stack. The gels were covered with pre-soaked (in deionized water) iBlot® Filter Paper. Cathode stack was placed over the filter paper and bubbled were removed using a roller. A disposable sponge was placed on the top of iBlot device and the

protocol was started using the Standard P3 program for 7 minutes. Membranes were transferred to boxes and were continuously rocked on a bidirectional rotator during blocking and incubation. Blocking was performed with 5% dry milk or 5% BSA (see appendix) in TBST for 1 hour at room temperature. Blots were incubated with different blocking agents (BSA) and/or different concertation of blocking agents and antibodies, based on antibody used (see appendix). Primary antibodies were incubated overnight at 4 °C in blocking buffer. The membrane was then washed three times for 10 minutes followed by incubation with 1:4000 dilution of horseradish peroxidase-conjugated secondary antibodies (Section 2.12) for 1 hour at room temperature. Blots were washed with TBST four times for 10 minutes with TBST and developed using ThermoScientific SuperSignal™ West Dura/Pico according to manufacturer's protocol. Blots were washed with TBST with two different concentrations of Tween 20, 0.1% and 0.5% for blots developed with Pico and Dura chemiluminescent substrate, respectively. The blot was imaged using a BioRad

ChemiDoc XRS system, using high sensitivity setting.
In some experiments, a single membrane was probed with different antibodies. The membrane was washed with TBST for 10 minutes following imaging and then treated with with Restore ® Western Blot Stripping Buffer (ThermoScientific) for 10 minutes at room temperature before. The membrane was washed for another 10 minutes with TBST and then blocked ad incubated with different primary and appropriate secondary antibody. To ensure successful stripping of membrane it was treated with ECL reagent and imaged before proceeding with the next antibody.

2.4 Co-immunoprecipitation

Mouse heart tissue (20mg) was resuspended in 1 X TLB buffer (500µl) and incubated on ice for 20 minutes. Suspension was centrifuged at 13300 rpm at 4ºC for 15 minutes and supernatant containing proteins is removed. Bradford assay was performed to assess protein concentration. Protein (~1 mg) was incubated overnight with Primary antibody (0.75-2.5 µg) in 1 X TLB buffer (500µl) on a roller. Protein G Dynabeads (Invitrogen) were washed twice with 10x volume of immunoprecipitation (IP) buffer (1% BSA, 0.01% Triton-X , protease inhibitor cocktail in 10ml PBS) . Pre-washed beads (50µL) were incubated for 1 hour at room temperature with lysate-antibody mixture on a roller. The mixture was centrifuged at 1500 rpm for 1 minute and the beads were washed with IP buffer 5 times. The supernatant was removed after the last wash and 25ul 2x SDS-SB was added to the beads and the samples were incubated at 95°C for 3 minutes. Samples were centrifuged at 1500 rpm for 1 minute to removed the beads.

2.5 Cell Culture

HEK293 cells were cultured in Dulbecco's modified Eagle's medium (DMEM) media supplemented with 10% Fetal Calf Serum (FCS), L-Gluatmine (2mM) and 1% Penicillin/Streptomycin (P/S). Cells were grown in 75cm2 flasks and incubated at 37°C in a humidified atmosphere with 5% CO2. Cell detachment was performed using trypsin.

2.6 Cell Transfections

Cells, at 80% confluence, were transiently transfected with plasmids using ESCORT

IV transfection reagent using manufacturer's instructions. For silencing experiments ATG5 (siRNA ID s18158) and scrambled siRNAs (siRNA ID 4390843) were bought from ThermoScientific and were transfected onto HEK293 cells using Dharmafect IV (Cat. No. T-2004-02), according to manufacturer's guidelines.

2.7 Neonatal Rat Cardiomyocyte Isolation

Pups, aged 0-1 days, were sacrificed by cervical dislocation followed by cessation of circulation. Hearts were removed and put onto Petri dish on ice. The atria and aorta were trimmed off and the ventricles were cut a couple of times before being put into a Falcon tube containing ADS on ice. The hearts were rinsed a few times with sterile ADS, in tissue culture hood, until all the blood had been washed away. The ventricles were put on a cold petri dish on ice and chopped up into small pieces (~1mm^3). The pieces were transferred in ADS to the gentleMACS C tube carefully to avoid heart tissue sticking to the wall of the pipette tips. Heart tissue was left on ice to settle before ADS was removed. Usually tissue from 12 hearts was put in each gentleMACS C tube.

Fresh enzyme mixes were prepared for isolation of cells as follows:

Enzyme Mix A 5ml/C tube

Enzyme mix 1.A	
Enzyme P	125µl
Buffer X	4.6ml
Enzyme mix 2.A	
Buffer Y	50µl
Enzyme A	25µl
Enzyme D	200µl

Enzyme Mix B . 2.5ml/C tube

Enzyme mix 1.B	
Enzyme P	62.5µl

Buffer X	2.3ml
Enzyme mix 2.B	
Buffer Y	25µl
Enzyme A	12.5µl
Enzyme D	100µl

Enzyme mix A was prepared by heating enzyme mix 1.A for 5 minutes at 37°C mixing it with enzyme mix 2.A. Enzyme mix A was added to gentleMACS C tube containing heart tissue. The tube was inverted and incubated at at 37°C for 15 minutes. The tube was transferred to the gentleMACS dissociator and the relevant program was run. The gentleMACS C tube was turned into the upright position allowing any remaining tissue to settle to the bottom of the tube. Enzyme mix B was prepared by heating enzyme mix 1.B at 37°C water for 5 minutes and mixing it with enzyme mix 2.B. The complete Enzyme Mix B was added to the remaining tissue in the gentleMACS C tube. The tube containing heart tissue was inverted and incubated at 37°C for 10 minutes. The tube is transferred to the gentleMACS dissociator and the appropriate program is run. 5ml of M1 media was added to gentleMACS C tube and the following suspension was pipetted up and down a few times. The cell suspension was passed through the cell strainer filter, 70µm, into a 50ml Falcon tube containing the cell suspension from the first set of digest steps.

The cells were then centrifuged at 300xg for 5 minutes. The supernatant was removed, and the cell pellet was reuspend pellet in M1 media (~20ml media per 12 hearts). The cells were then pre-plated onto 10cm dishes (one dish per 5/6 hearts) and incubated at 37°C for 1 hour, to isolate cardiomyocytes from non-cardiomyocytes. The media, which contains cardiomyocytes, is removed after incubation. 10 ml M1 media was added 10cm dish with other cells and placed in 37°C incubator. Cardiomyocyte were

counted using haemocytometer and plated at desired density and kept in incubator overnight.

Commonly used cell densities for 1 well or dish:

6 well plate	500,000 cells/well
12 well plate	250,000 – 300,000 cells/well
35mm dish	350,000 – 500,000 cells/dish
60mm dish	1,000,000 cells/dish

The following day cells were washed twice with ADS. For inhibitor experiments cells were incubated with DMEM:M199 4:1 media (4ml/well). For transfections cells were put into TF media for at least 2 hours. before beginning transfection.

After transfection the cells can be maintained in M2 media.

2.7.1 Inhibitor Treatment of NRCs

For inhibitor experiments NRCs were incubated with DMEM:M199 media as stated above. Cells were washed and incubated with starving media on Day 2 and treated with inhibitor/activators, for the mentioned time and at specific concentration, before cells were scraped with PBS containing PhosStop, Protease inhibitors (Roche) and 100 mM N-Ethylmaleimide (NEM). Cells were spun down at 3000 rpm for 5 minutes at 4°C and the pellet was stored in -80°C.

2.7.2Transfection of NRCs

Before transfection magnefecto plate was incubated at 37°C. DNA (1µg) was mixed with neuronanofect (2.5 µL) and 400 µL Opti-MEM Media (Thermo) and incubated for 15 minutes at room temperature. NRCs were washed with DMEM twice and 800 µL Transfection medium was added to each well. 800 µL Transfection medium was added

to the DNA/nanofect mix and the mixture was added onto the well containing cardiomyocytes. The plate/dish was put on magnofect with the following settings: 30 minutes, 0.2 mm, 2 Hz. Following transfection, the cells are left in the incubator overnight. The media was replaced with M2 media the following day.

2.7.3 Immunohistochemistry NRCs

Cells were washed twice with PBS following removal of media. Cells were fixed in 4% PFA for 10 minutes at room temperature. The cells were washed with PBS twice and permeabilized with 0.2% Triton X for 10 minutes on a shaker. Cells were washed twice with PBS and the circumference was marked with Super Pap Pen (Invitrogen). Blocking was performed with 10% Neonatal goat serum (NGS) in PBS for 45 minutes at room temperature. Primary antibodies were incubated overnight at 4°C. Cells were washed twice with PBT (PBS + 0.002% Triton X) followed by 2 x5 minutes washes on shaker at room temperature. Secondary antibodies were diluted in 1% BSA Gold Buffer solution (GB; 20mM Tris-HCl, pH 7.5, 155mM NaCl, 2mM ethylene glycol tetraacetic acid, 2mM $MgCl_2$, 1% bovine serum albumin) and incubated for 1 hour at room temperature. Cells were washed again as mentioned previously. Excess PBT was removed using cotton bud and a drop of ProLong™ Diamond Antifade Mountant with DAPI was added onto the cells. A cover slip is placed over cells and fixed in position using nail polish. The cells were imaged using an Olympus Fluoview 1000 confocal microscope equipped with 40 × oil immersion lens.

2.8 Mouse Handling Ethics:

All experimental procedures were performed in accordance with the UK Home office guidelines (project licenses 30/2444 and 30/2977) and approved by respective institutional review boards. Mice (upto 5-6) were kept in each individually ventilated

cage (IVC) with free access to food and drinking water. The animal facility was subjected to a standard 12:12 h dark-light cycle. Mice were weighed and sacrificed through cervical dislocation, followed by confirmation of cessation of circulation, in accordance with UK Home Office regulations.

2.8 In vivo phenotyping

All echocardiography and left ventricular hemodynamic studies were performed on young adult mice (2-3 months old), unless stated otherwise. Age-matched and littermates male C57BL/6J (Charles River) served as controls for experiments.

2.8.1 Transthoracic echocardiography (TTE)

Echocardiographic imaging of left ventricular systolic and diastolic function was performed under light general anaesthesia using a 30 MHz linear transducer and the Vevo 2100 Imaging System (VisualSonics, Toronto, Canada). Prior to imaging the mouse anaesthesia was induced in mice in a chamber with 4 % isoflurane. After induction the mouse was placed on an adjustable heating pad set to 38 ˚C to avoid hypothermia. A steady state of sedation was maintained by putting a nose cone on the snout of the mouse throughout the procedure supplying 1.0% to 1.5% isoflurane mixed with 0.5 L/min 100% O2. To confirm sedation a toe pinch was performed. The mouse's thoracic area was shaved with a clipper. To monitor temperature throughout a rectal probe (after lubricating) was inserted. A layer of preheated (body temperature) ultrasound gel was applied to the chest, primarily the area overlying the heart. For evaluation of systolic function of heart recordings were performed at a heart rate above 450 beats per minute. The heart rate was modified by varying the concentration of isoflourane.

Two-dimensional (2D) imaging ('B-mode') was performed first to obtain a view along the parasternal short axis. This was followed by 1-dimensional (1D) view, the M-mode echocardiography, which allows for measurements of cardiac dimensions and contractility. Images are stored at stage for later evaluation of heart function. All acquisition and analysis was performed in a blinded fashion. The following systolic parameters were analysed: Left ventricular ejection fraction (LVEF), left ventricular end systolic dimension (LVESD), left ventricular end systolic volume (LVESV), left ventricular fractional shortening (FS). The following diastolic parameters were analysed: Left ventricular end diastolic dimension (LVEDD), end diastolic anterior and posterior LV wall thickness.

Analysis of echocardiography data was performed using Vevo 2100 Imaging System (VisualSonics, Toronto, Canada) in a blinded fashion. Several parameters were analysed in order to gauge cardiac function. First, M-mode images were analysed in order to gauge ventricular dimensions, by averaging 3-5 cardiac cycles. Left ventricular end-diastolic diameter (LVEDD); left ventricular end-systolic diameter (LVESD); were obtained from the parasternal short axis view at mid-papillary level.

These parameters were used to calculate left ventricular fractional shortening (FS), which represents systolic function.

$$\%FS = [(LVEDD - LVESD)/LVEDD] \times 100$$

Left ventricular systolic function is also demonstrated by the ejection fraction (EF) which was calculated from Left ventricular end systolic volume (LVESV), and left ventricular end diastolic volume (LVEDV) using the following formula:

LV EF= [(LVEDV – LVESV)/LVEDV] x 100

In addition, left ventricular mass to evaluate ventricular size and potential hypertrophy was calculated using the parameters epicardial area (EPI A), endocardial area (ENDO A), LV length in parasternal long-axis (L); LV wall thickness in diastole (t) with the following formula:

LV mass = 1.05 x ([5/6 x EPI A x (L + t)] – [5/6 x ENDO A x (L)])

2.8.2 In vivo haemodynamics

General anesthesia was induced in mice with 4% isoflourane. After induction the mouse was placed on a heating pad set at 38 °C to avoid hypothermia during the recording. Anaesthesia was maintained with isoflurane (1.25–1.5%) via a nose cone, which also supplied 0.5L 100% O_2. The right carotid artery was dissected and a 1.4 F Millar Mikro-tip catheter (Cat. No. SPR-671, ADInsturments UK) was inserted into the LV via the carotid artery to measure all haemodynamic indices. Echocardiography was used to ensure that the catheter is in the right place. After 15 min of baseline recordings, contractile reserve was assessed by infusion of dobutamine via the jugular vein (4–16 ng per g bodyweight per min). All data acquisition and analysis were performed using software LabChart Pro (ADInstruments, UK.). The following indices of left ventricular function were evaluated from the recordings: Central systolic and diastolic aortic pressure (SAP & DAP respectively), mean aortic pressure (MAP=(2 x diastolic)+systolic)/3), and left ventricle end diastolic and systolic pressure (LVEDP & LVESP respectively). Maximum pressure development rate during systole and diastole (+dP/dt & -dP/dt respectively) were derived from the pressure trace.

2.9 Ex vivo phenotyping

2.9.1 Tibial length Measurement

The legs were cut off above the knee and skin is stripped off. The legs were incubated with 5 ml 0.8 M KOH in a vial at room temperature overnight. The legs are incubated at 37 degrees for 1 hour for further digestion. The excess tissue and patella was removed and tibial length is measured with digital callipers.

2.9.2 Tissue harvesting

Chest cavity was opened, and the heart was harvested by cutting off the great vessels. All blood vessels were trimmed off the heart and it was flushed with cold PBS to flush out all the blood. The heart was blotted dry and for histology, whole heart was fixed in 4% PFA for 48 hours. The PFA was then removed and replaced with 70% alcohol until heart was embedded in paraffin. For Molecular Biology; the atria were cut off, hearts flushed with PBS and the heart was cut into cut into two pieces to have apex and upper part of ventricles. The tissue was then placed in a pre-chilled CRYO.S™ vial, snap frozen in liquid nitrogen and stored in -80°C until further use.

2.9.4 Histology

Tissue for histology was harvested as mentioned above. The cardiac tissues were dehydrated in a series of increasing alcohol concentrations and cleared in histoclear solution followed by embedding in paraffin wax. The hearts were placed in paraffin to facilitate sectioning in a transverse plane and cut into 7µm thick transverse (short axis) sections of the heart's apical, mid-ventricular and basal area using a Leica RM2155 microtome. Cardiac sections from each of these areas were then mounted onto glass slides and stained with a Sirius-red staining kit (Polysciences Inc.) according to manufacturer's instructions. The sections were then mounted with Neo-Mount® and

glass coverslips and imaged with a wide-field inverted Nikon TE2000U microscope under bright field and polarized light.

2.9.5 Immunofluorescence

Hearts were embedded in optimal cutting temperature (OCT) compound and sectioned into 10μm thick sections (Leica CM1850 cryostat) and mounted on glass slides. Immunofluorescence staining was conducted according to the following protocol. Frozen sections were removed from storage at -80°C and immediately fixed, either in -20°C acetone for 10 minutes or in 4% PFA for 15 minutes at room temperature. The slides were then washed in PBS and mounted onto coverplates (Thermo scientific). Blocking solution (PBS plus 5% goat serum) was added onto the slide and left on for one hour. Primary antibody solution (PBS plus 1% BSA, containing the primary antibody in a dilution of 1:100) was then added directly and left on at 4°C over night. Following overnight incubation, the slides were washed three times for five minutes with PBS. Consecutively, secondary antibody staining solution (PBS plus 1% BSA, containing fluorescently labelled secondary antibodies in a dilution of 1:400, and DAPI nuclear stain in a dilution of 1:1000) was added on the slides for one hour. The slides were then washed and mounted with glass coverslips overnight, using ProLong Gold mounting medium. The resulting slides were imaged using an Olympus Fluoview 1000 confocal microscope equipped with 40 × oil immersion lens

2.10 Statistical analyses

Statistical tests were conducted using GraphPad Prism 7.03. The type of test used for each measurement is indicated in figure legends. A one-way ANOVA test followed by Bonferroni post-hoc test was used to compare differences among multiple groups. Two-way ANOVA test was performed for invasive haemodynamic measurements.

Assessment of two unpaired samples groups was done by Student's t-test where $p < 0.05$ was considered to be significant. Statistical significance was reported at $p < 0.05$ (*), $p < 0.01$ (**), $p < 0.001$ (***), and $p < 0.0001$ (****).

2.11 Solutions

M1 (cardiomyocyte day 1 media)	**100ml**	**150ml**
DMEM 25mM Hepes	67ml	100.5ml
M199	17.5ml	26.25ml
Horse serum (HS)	10ml	15ml
Newborn calf serum (NCS)	5ml	7.5ml
Glutamine 200mM	1ml	1.5ml
Pen/Strep	100µl	150µl

M2 (cardiomyocyte day 2 media)	**100ml**	**150ml**
DMEM 25mM Hepes	75ml	112.5ml
M199	17ml	22.5ml
Horse serum (HS)	5ml	7.5ml
Newborn calf serum (NCS)	0.5ml	750µl
Glutamine 200mM	1ml	1.5ml
Pen/Strep	100µl	150µl
AraC 10mM (optional)	100µl	150µl
➔ Sterile filter		

TF (transfection media)	**100ml**	**150ml**
M199	21ml	31.5ml
DBSS-K	73ml	109.5ml
Horse serum (HS)	4ml	6ml
Glutamine 200mM	2ml	3ml
➔ Sterile filter		

DMEM:M199 4:1 (serum starvation media)

DMEM	500ml
M199	125ml
Glutamine 200mM	6.25ml
Pen/Strep	625µl

DMEM 10:1:1 (serum media)

DMEM	500ml
FBS	50ml
Glutamine 200mM	5ml
Pen/Strep	5ml

DBSS-K buffer	**500ml**	**1L**
116mM NaCl	3.4g	6.8g
1mM NaH_2PO_4 (anhydrous)	60mg	120mg
0.8mM $MgSO_4$ (anhydrous)	48mg	96mg
5.5mM Glucose	0.5g	1g
32.1mM $NaHCO_3$	1.35g	2.7g
* 1.8mM $CaCL_2.2H_2O$	132.5mg	265mg

Dissolve the first 5 ingredients in 250ml/500ml TC water. Add the $CaCl_2.2H_2O$ once it has been dissolved in 50-100ml TC water. Make up to 500ml/1L with TC water and sterile filter.

ADS 10X	**500ml**
1060mM NaCl	30.8g
200mM Hepes	23.8g
8mM NaH_2PO_4	0.568g
53mM KCl	1.976g
4mM $MgSO_4$	0.494g
50mM Glucose	4.506g
pH 7.4 with NaOH 1N and make up to 500ml with TC water and sterile filter.	

Stock: 2X TLB Buffer stored at -20ºC
40mM TrisHCl pH7.6
276mM NaCl
10x Glycerol
2% Triton X
10mM DTT

10ml 1X TLB buffer (4ºC):
5ml 2x TLB buffer
1ml OBG (Octyl-beta-glucopyranoside)
33ul 3M KCl
40ul 500mM ETDA
10% NP-40
1 Phos-stop tablet (Roche: 04906837001: Easy pack Phos-stop)
1 Protease inhibitor tablet (Roche: 04693159001; mini EDTA-free tablets)
3.127ml dH2O

2.12 Antibody List

Antibody	Dilution	ECL	Membrane	Blocking Agent	Company
LC3A/B	1:300	Dura	PVDF NC	5% BSA	Cell Signaling Technology, 4108
SQSTM1/p62	1:500	Dura	PVDF NC	Milk	Abcam, ab56416
GAPDH	1:3000	Pico	PVDF NC	Milk	Millipore, ABS16
MLP 79D2	1:1000	Dura	PVDF NC	Milk	(200)
FHL2	1:500	Dura	PVDF NC	Milk	MBL, K0055-3
FHL1	1:200	Dura	PVDF NC	Milk	Abcam, ab76912
Carp (Ankrd1)	1:500	Dura	PVDF NC	Milk	Abcam, ab88456
DSCR1 (Rcan1)	1:250	Dura	PVDF NC	Milk	Sigma, D6694
Calsequestrin	1:1000	Pico	PVDF NC	Milk	Thermo Scientific, PA1-913
HA	1:5000	Dura	PVDF NC	Milk	Roche, 11 583 816 001
Pan-Actin	1:1000	Pico	PVDF NC	Milk	Sigma, A2066
α-actinin		Pico	PVDF NC	Milk	Sigma, A7811
GAPDH	1:4000	Pico	PVDF NC	Milk	Millipore
MYBPC3	1:5000	Pico	PVDF NC	Milk	Gift by Elizabeth Ehler
Ubiquitin	1:1000	Dura	PVDF NC	Block: 5% Wash: TBST (0.1%Tween) 1°Ab: Dilute in TBST Continue as normal	DAKO

2.13 Primer List

Csrp3_KI_F	ATAGGAACTTCGTCGAGATAACTT
CSRP3_KI_R	GTGGGACTTTCAAGGAGGTAA
MCSRP3_1F	ATGCCAAACTGGGGTGGAGG
MCSRP3_194R	CTCCTTCTTTTCCACTTGCTGTG
pSh_IRES_F	CTCACGGGGATTTCCAAGTC
pSh_IRES_R	ATGCAGTCGTCGAGGAATTG
Ubi-GFP_R	TCGACCAAGCTTCCCCACCAC
Ubi-GFP_F	CCTACAGCTCCTGGGCAACGT

Chapter 3 – Characterisation of MLP C58G Cardiac Phenotype

3.1 Introduction

Mutations in the gene *CSRP3*, which encodes for the Muscle Lim Protein (MLP), have been shown to cause HCM and DCM. Linkage analysis in a large German family led to the identification of the C58G missense mutation in *CSRP3* as HCM causing (231). The study also highlighted that MLP is a cytosolic protein rather than a sarcomeric one. C58G mutant when compared to WT MLP was shown to be more susceptible to degradation *in vitro*. This supported the findings that MLP levels in a cardiac biopsy was significantly reduced, up to 40% in a patient with a heterozygous C58G MLP mutation (231). These findings led to the suggestion that HCM phenotype in humans with this mutation is due to the lack of functional MLP rather than a dominant-negative effect of the mutant copy of MLP.

To better understand the underlying pathogenesis of HCM caused by mutations in non-sarcomeric genes, a MLP knock-in mouse carrying the best characterized *CSRP3* mutation - C58G, was generated. The knock-in mouse model overcomes the disadvantages of transgenic mice where the gene of interest is integrated randomly into the genome. This random integration may result in the gene being regulated differently compared to its expression from the correct locus and under the correct promoter.

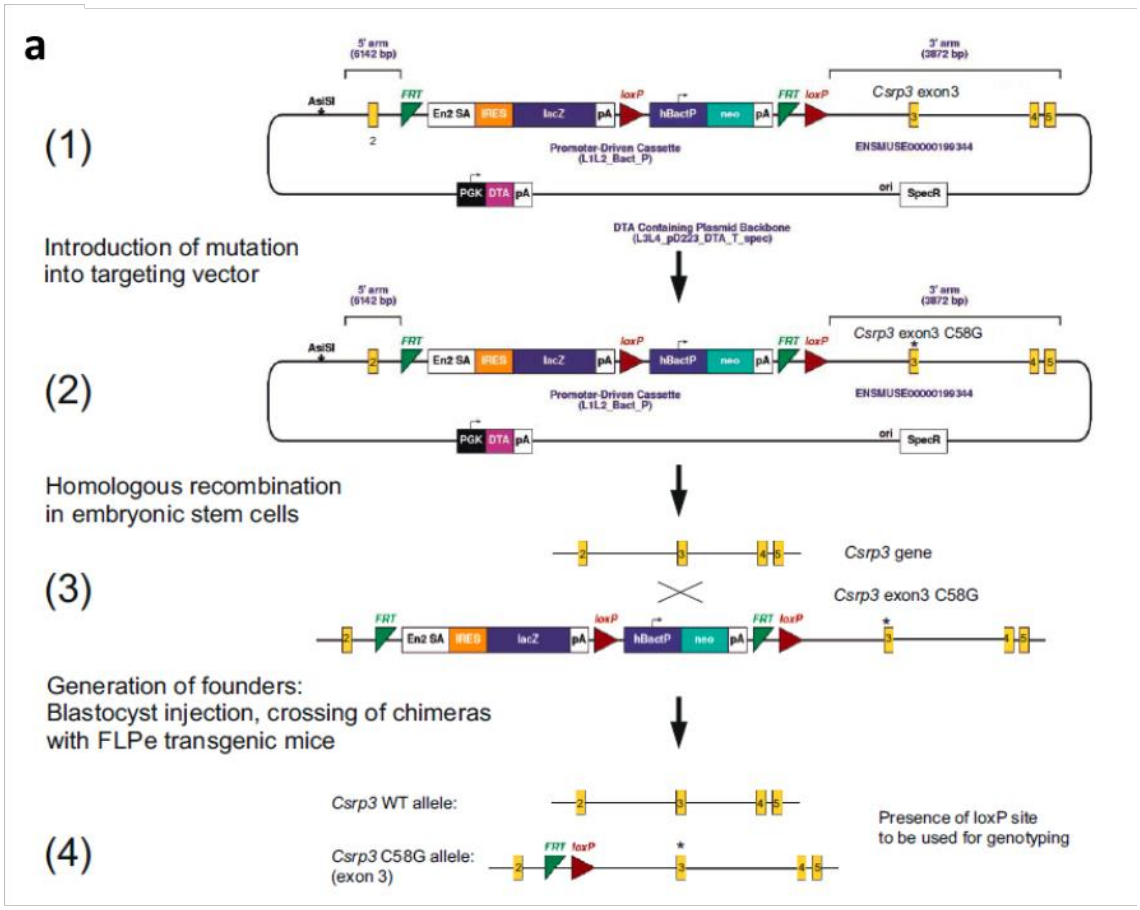
3.2 Previous Work Done on Mouse Model

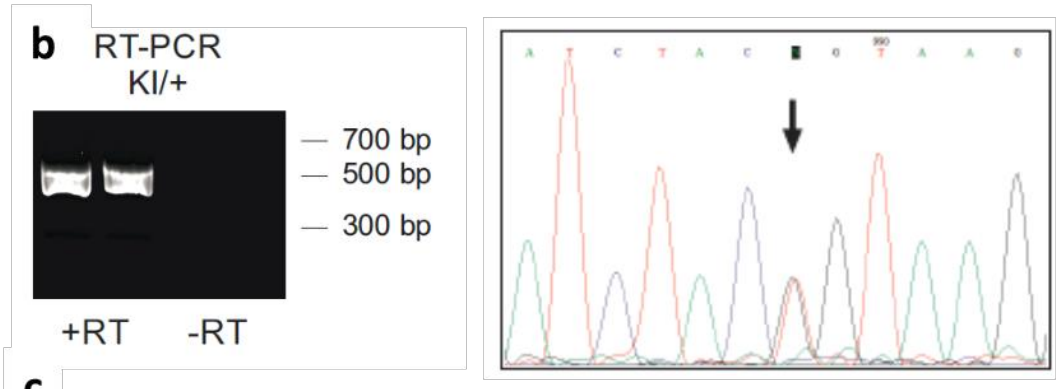
3.2.2 Generation of *CSRP3* KI/KI mouse model

Briefly, the model was generated by Dr. Gehmlich by introducing the mutation in exon 3 of *CSRP3* gene, in a targeting vector integrated with neomycin selection cassette

(neo) flanked by Flp recombinase recognition target (FRT) domains and loxP sites. Following successful recombination in C57BL/6N JM8F6 embryonic stem cells, the ES cells with the clones were injected into albino C57BL/6J blastocysts and the resulting chimeras were mated with albino C57BL/6J females. Founder mice were bred with C57BL/6J mice expressing Flp recombinase to remove the neomycin cassette and produce C58G heterozygous mice. The mutant heterozygous (Het), homozygous (Homo), and wild type (WT) mice that were generated were viable, fertile and had a normal lifespan. The presence of the mutation was confirmed at mRNA level, by RTPCR (Fig 3-1b) and by mass spectrometry at the protein level (Fig 3-1c).

Biochemical analysis of mouse ventricular protein highlighted that *Csrp3* mRNA levels (Fig. 3-2a) were increased markedly (~2.5 times) and significantly ($p < 0.0001$) in KI/KI animals compared to WT and KI/+ animals, when measured by RT-PCR. No differences were observed between WT and KI/+ animals. Western blot was performed to assess protein levels. MLP was reduced by 50% in KI/+ animals ($p < 0.001$) and by 80% in KI/KI animals compared to WT animals (Fig. 3-2b). These findings were supported by immuno-fluorescence staining of adult cardiomyocytes from these animals. MLP signal in KI/+ cardiomyocytes was lower than WT cells, and the reduction in signal was even greater in cardiomyocytes from KI/KI animals (Fig. 3-2c).


a
(1)
5' arm (6142 bp)
3' arm (3872 bp)
AsiSI
FRT
En2 SA
IRES
lacZ
pA
loxP
hBactP
neo
pA
FRT
loxP
Csrp3 exon3
Promoter-Driven Cassette (L1L2_Bact_P)
ENSMUSE00000199344
PGK
DTA
pA
ori
SpecR
DTA Containing Plasmid Backbone (L3L4_pD223_DTA_T_spec)
Introduction of mutation into targeting vector
(2)
Csrp3 exon3 C58G
Homologous recombination in embryonic stem cells
(3)
Csrp3 gene
Csrp3 exon3 C58G
Generation of founders: Blastocyst injection, crossing of chimeras with FLPe transgenic mice
(4)
Csrp3 WT allele:
Csrp3 C58G allele: (exon 3)
Presence of loxP site to be used for genotyping


b
RT-PCR
KI/+
700 bp
500 bp
300 bp
+RT
-RT

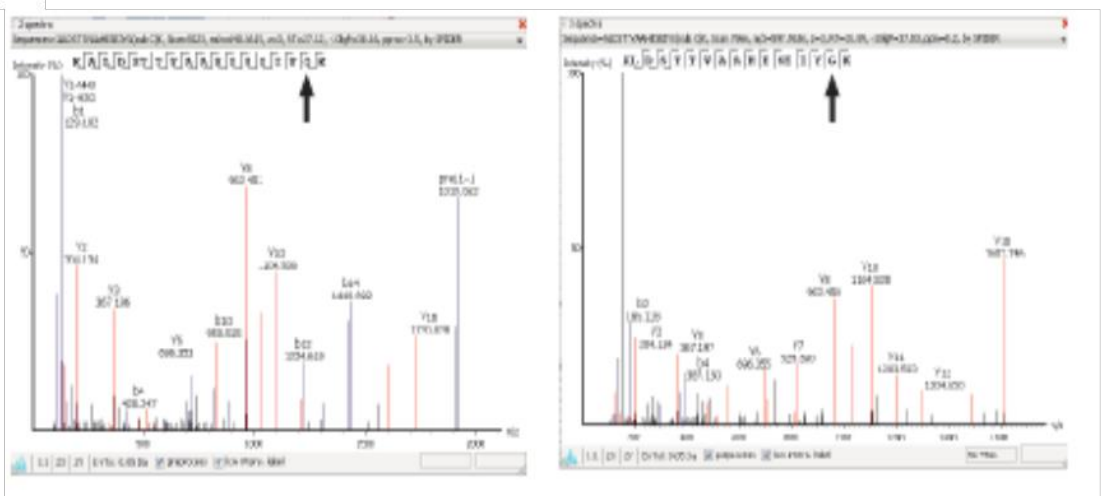

c

Figure 3-1**.** Gene targeting Strategy to generate the KI mouse model and validation. **(a)** Targeting vector with neomycin cassette flanked by Flp recombinase recognition target (FRT) domains and loxP sites was modified by introducing the C58G mutation into exon 3. The vector was used for homologous recombination in ES cells. Mice with the targeted allele, obtained after blastocyst injection of the targeted ES cells, were crossed with transgenic mice expressing Flp recombinase removing neomycin cassette to produce C58G heterozygous floxed mice. **(b)** Left panel-Confirmation of mutant expression at mRNA level by RT-PCR. Right panel - Right – Sanger sequencing trace of this PCR product shows the presence of both WT and mutant allele (arrow). **(c)** Identification of MLP C58G protein in KI/+ hearts by mass spectrometry: peptides containing WT sequence as well as peptides containing the C58G mutation (arrow) were identified based on their molecular weight. C – Direct sequencing of peptides by MS/MS shows the presence of the C58G mutation in two peptides (arrows). Figure from (208)

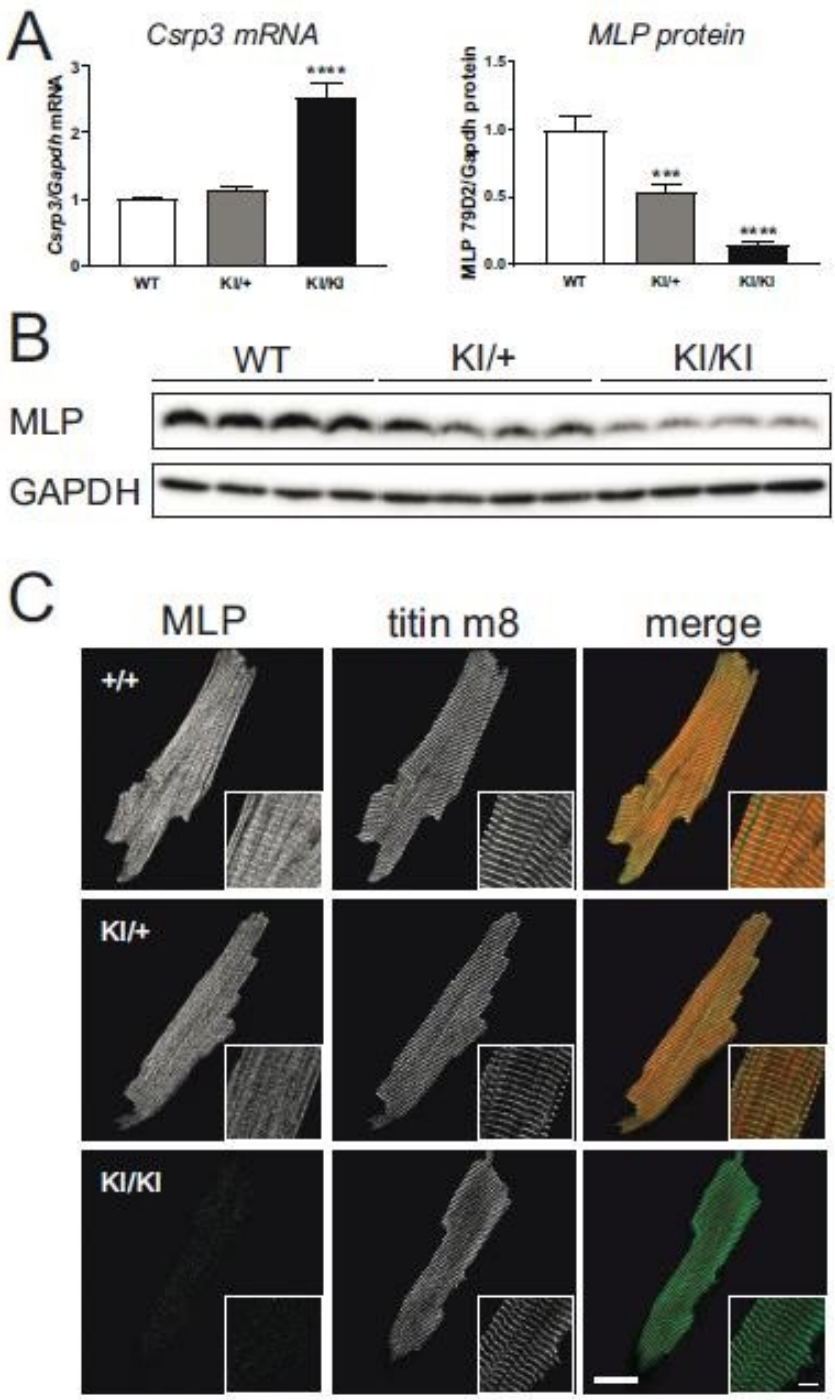


Figure 3-2. Molecular Characterization *CSRP3* KI mice. MLP mRNA (a) and protein (b) expression levels analysed by quantitative RT-PCR and Western blot respectively.KI/KI mice showed a 250% increase in MLP mRNA expression compared to WT. Compared to WT, MLP levels, normalized to GAPDH, were downregulated by 50% in KI/+ mice and 80% in KI/KI mice. *** $p < 0.001$, **** $p < 0.0001$ heterozygous (KI/+) or homozygous (KI/KI) animals vs WT littermates versus WT, n = 6 per group 0.05. Immuno-fluorescence (c) on isolated adult cardiomyocytes from mutant and WT animals. Left-hand panel show MLP staining, Middle panels show titin M-band epitope m8 staining and the right-hand panel illustrates the merged image of MLP (red) and titin m8 (green) Scale bar: 20 microns (normal), 5 microns (magnified). Figure from (208)

KI/KI animals exhibited increase in HW/BW ratio. To evaluate activation of hypertrophic pathway key markers of HCM were assessed in the mouse model. In line with morphometric analysis KI/KI hearts showed a significant increase in expression of *Nppa*, the gene for Atrial natriuretic Peptide (ANP) and *Nppb*, gene for Brain natriuretic Peptide (BNP) (Fig. 3-3a) which are key markers of HCM and heart failure. No significant difference was observed in KI/+ when compared to WT mice. These findings were supported by Western blot analyses of hypertrophic signalling proteins (Fig. 3-3b). KI/KI animals had a marked increase in expression of four and a half lim domains protein (Fhl1), cardiac ankyrin repeat protein (Carp)/Ankrd1 and calcineurin responsive Rcan1.4 when compared to KI/+ and WT animals. There was no difference between KI/+ and WT animals.

Sections of cardiac tissue from all three genotypes stained with haematoxylin and eosin (H&E) were unremarkable (Fig. 3-4). Staining of sections Sirius red staining, which highlights presence of collagen and myocardial fibrosis, revealed mild interstitial fibrosis in KI/KI hearts. No such difference was observed in KI/+ animals.

The findings from molecular and histological analysis suggest the induction of hypertrophic pathways within KI/KI animals. KI/+ animals were unremarkable compared to WT.

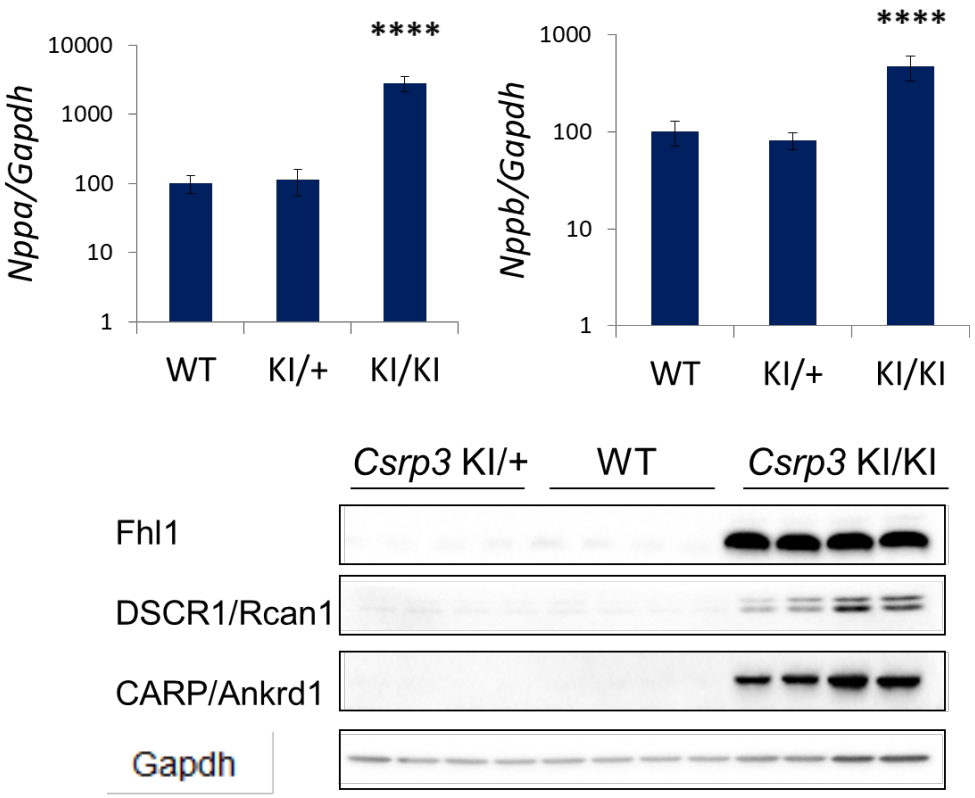


Figure 3-3. Molecular phenotype of KI/+ and KI/KI hearts. (**a**)– Assessment of transcriptional changes by qPCR for Nppa and Nppb showed significant upregulation of expression in KI/KI compared to WT and KI/+ animals. All measurements are normalised to *Gapdh*; **** $p < 0.0001$ versus WT, n = 6 per group. (**b**) Western blot analysis of hypertrophic signalling proteins assessed: Fhl1, CARP (Ankrd1) and DSCR1 (Rcan1) have elevated expression in KI/KI hearts, suggesting activation of Gapdh serves as loading control. Figure from (232)

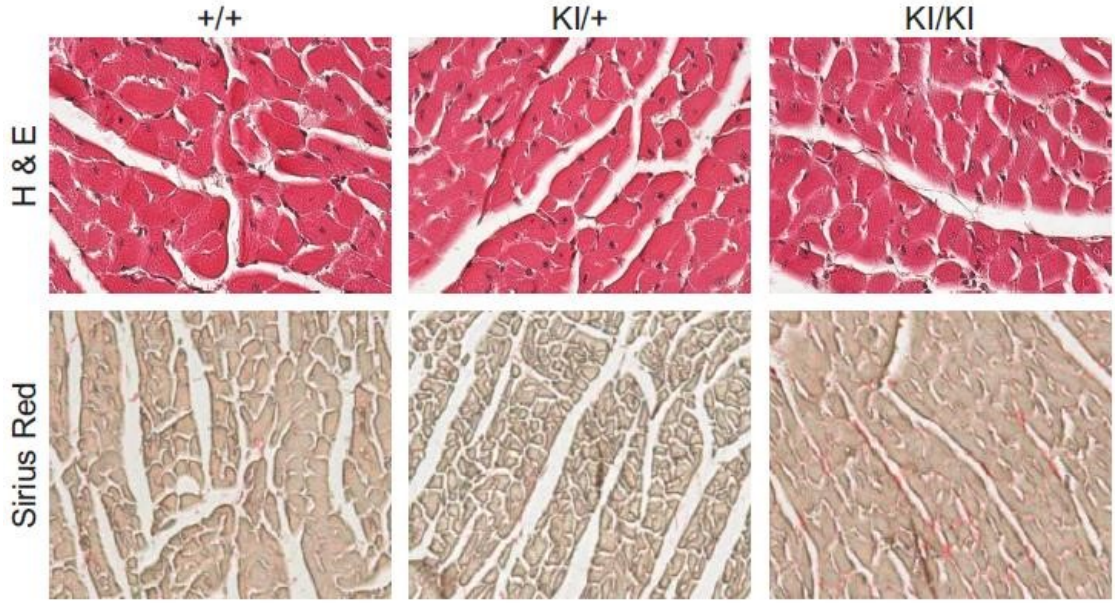


Figure 3-4. Characteristic histological staining of cardiac tissue from and WT mice at 2 months of age. Top row panels illustrate H&E staining (40x), lower row illustrates Sirius red staining (40x). No apparent differences between KI/+ or KI/KI and WT panels were observed

in H&E staining. Mild increase in fibrosis was observed in KI/KI heart compared to WT. No changes observed in KI/+ hearts. Figure from (232).

3.3 Results:

3.3.1 Assessment of Cardiac Function by Echocardiography

To evaluate the effect of C58G mutation on cardiac function and dimensions echocardiographic studies were performed on 10-week-old knock-in mice.

End diastolic anterior (Fig. 3-5a) and posterior wall thickness (Fig. 3-5b) measurements revealed a small decrease in end diastolic anterior wall thickness of the LV, in the KI/KI mice compared to WT and KI/+ mice. No difference was observed between KI/+ and WT mice.

LV end diastolic dimension (LVEDD) (Fig. 3- 5c) and end systolic dimensions (LVESD) (Fig. 3-5d) were significantly increased in KI/KI mice in comparison to WT and KI/+mice, whereas no statistically significant changes were observed between WT and KI/+ mice. The increased LVEDD and LVESD highlights increased ventricular dilation.

KI/KI animals developed significant ventricular dilatation, evidenced by a significant increase in (Fig. 3-6d) diastolic left ventricular volume. These animals also had elevated LV systolic volume (Fig. 3-6e). KI/KI animals also had decreased heart rate compared to WT animals under general anaesthesia, whereas no such differences were observed in KI/+ mice. Heart rate is maintained by isoflourane during echocardiography. The lower heart rate in KI/KI can be attributed to a difference response to isoflourane exposure.

Upon calculation of left ventricular mass from echocardiographic images, KI/KI showed significant increase in LV mass compared WT (Fig, 3-5c). These findings recapitulated

the results from absolute *ex vivo* morphometric heart weight measurements (Fig 3-8c, 3-8e).

Systolic function was assessed by calculating ejection fraction (EF) (Fig. 3-6a) and Fractional Shortening (FS) (Fig. 3-6b) of the LV. There was no statistical difference observed between KI/+ and WT mice, however both parameters were significantly ($p<0.0001$) reduced in KI/KI mice at 2 months (Table 3-1). These findings represent impaired systolic function in homozygous knock-in mice.

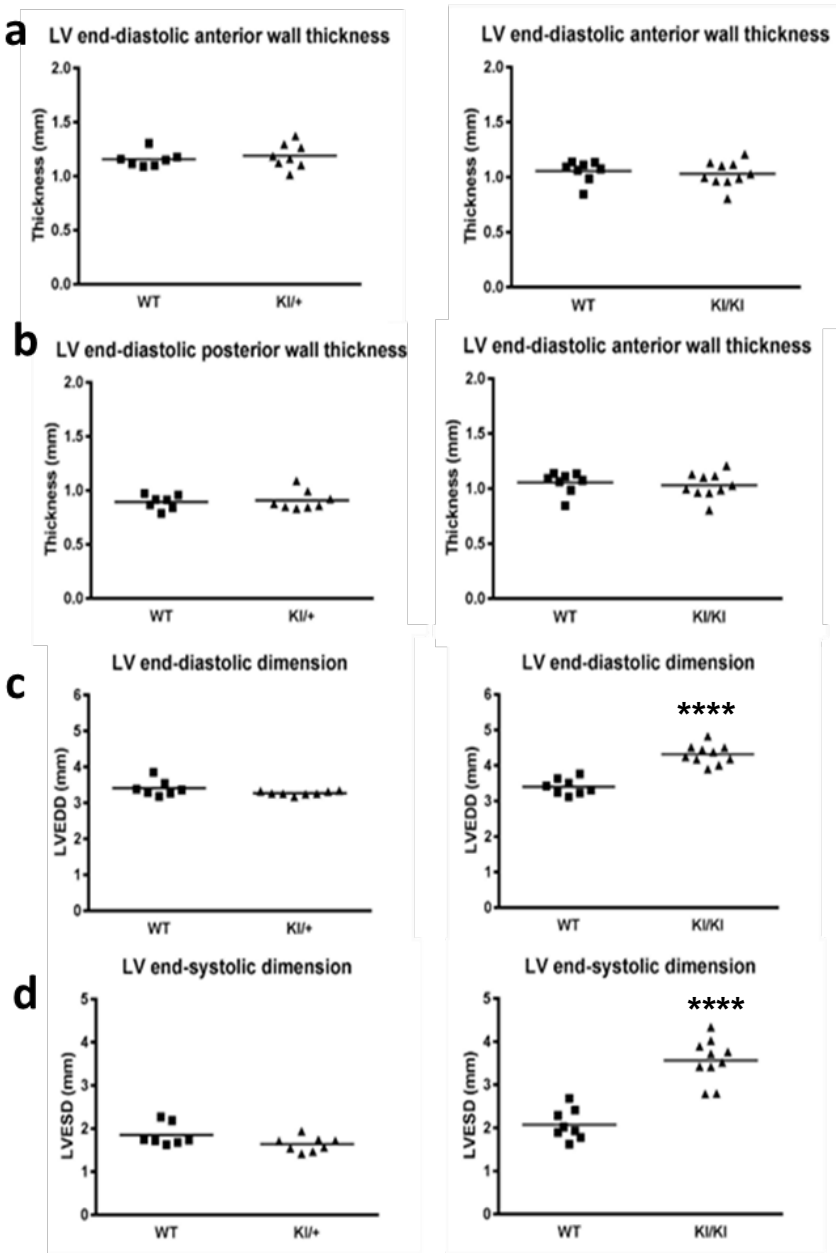


Figure 3-5.: Echocardiographic assessment to delineating the functional phenotype of MLP C58G mouse model. KI/+ animals showed no difference in phenotype when compared to WT animals in all parameters. KI/KI animals showed a slight increase in (**a**) anterior wall thickness (**b)** while no change in posterior wall thickness was observed. KI/KI animals had higher (**c**) LV end-systolic and (**d**)LV end-diastolic dimension. KI/KI animals had reduced heart rate when compared to WT animals. **** $p<0.0001$ versus WT

2 months	**WT**	**KI/+**	**KI/KI**

Body weight	g	24.5 ± 0.9	24.1 ± 0.8	25.3 ± 0.6
		7	8	7
FS	%	46.0 ± 1.7	50.0 ± 1.6	13.6 ± 1.32****
LVEDD	mm	3.41 ± 0.09	3.27 ± 0.02	4.39 ± 0.10****
LVESD	mm	1.85 ± 0.01	1.64 ± 0.06	3.80 ± 0.12****
LVAWD	mm	1.16 ± 0.03	1.19 ± 0.04	0.98 ± 0.04*
LVPWD	mm	0.89 ± 0.02	0.91 ± 0.03	0.88 ± 0.03
HR	bpm	486 ± 2	485 ± 3	455 ± 5****

Table 3-1. Echocardiographic parameters of WT, KI/+ and KI/KI hearts (mean ± SEM_ at 2 months. * p<0.05, ** p<0.001, **** p<0.0001 versus WT

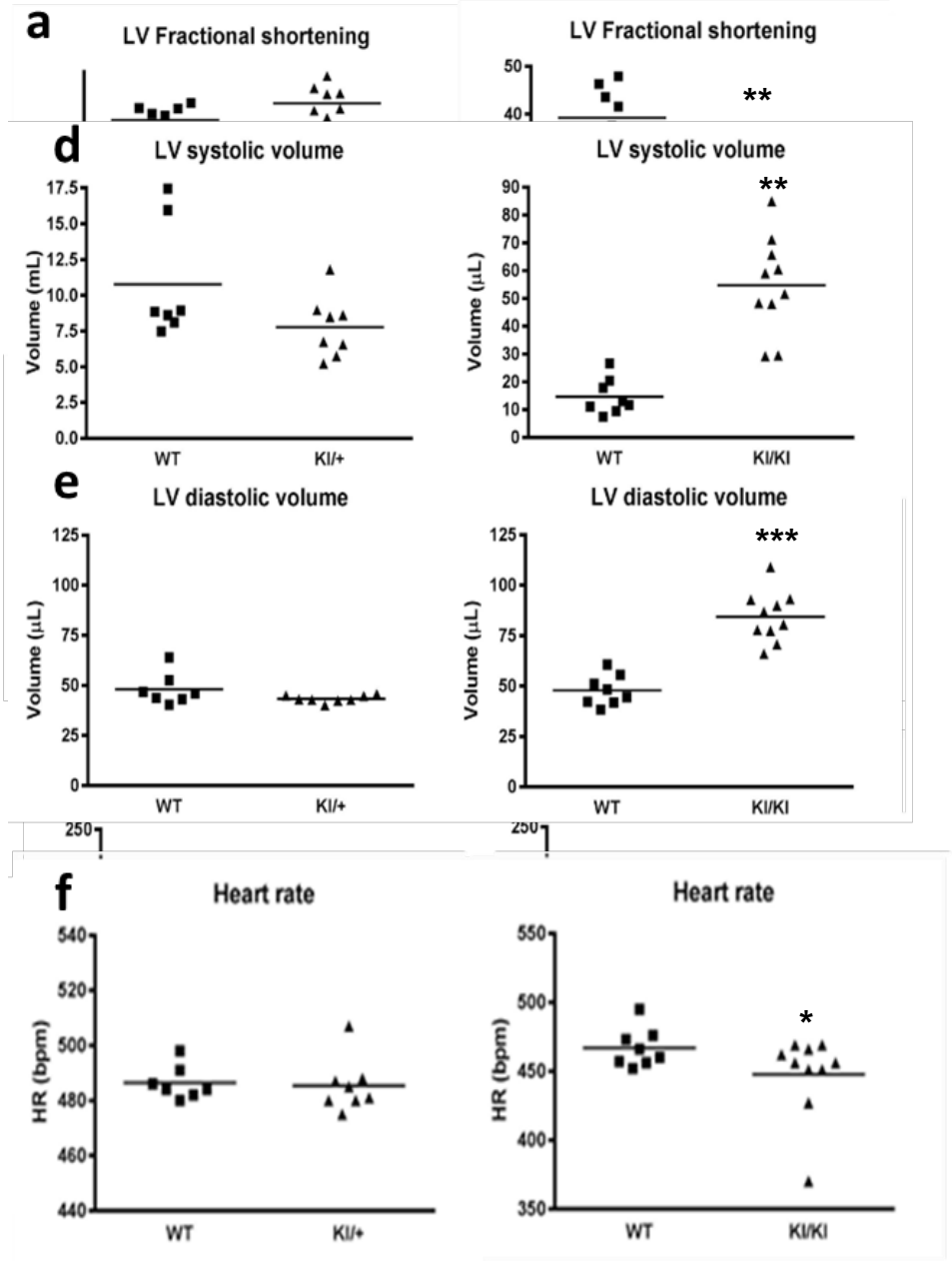


Figure 3-6: Echocardiographic assessment to delineating the functional phenotype of MLP C58G mouse model. KI/+ animals showed no difference in phenotype when compared to WT animals in all parameters. MLP C58G KI/KI animals demonstrated diminished systolic function as seen by (***a***), fractional shortening (***b***) and ejection fraction. KI/KI animals developed significant ventricular dilatation, evidenced by a significant increase in (**d**) diastolic left ventricular volume. KI/KI animals have increase in LV size (**c**) at 2 months while no change in (**f**) heart rate was observed. * $p<0.05$, ** $p<0.001$, **** $p<0.0001$ versus WT

3.3.2 Assessment of Cardiac Function by Left ventricular Haemodynamics

To further evaluate the effect of the C58G mutation on myocardial function, haemodynamic measurements of left ventricular pressures were conducted *in vivo*.

Left ventricular pressures were measured using a Millar catheter inserted into the left ventricle through the aortic valve. Pressure measurements were conducted at baseline and - to investigate cardiac reserve - during two increasing dosages (4 and 16 ng/g body weight/minute) of continuous dobutamine infusion.

No significant differences were observed between WT and KI/+ under baseline conditions or after dobutamine infusion in any of the parameters.

The maximal rate of pressure increase during systolic contraction (dP/dt max) was significantly reduced in KI/KI mice compared to WT and KI/+ mice (Fig. 3-7a), indicating impaired systolic function. This was also highlighted by the significantly reduced End Systolic Pressure (ESP) in the KI/KI group compared to the other two.

End Diastolic Pressure(EDP) was significantly increased in KI/KI (Fig. 3-7b) compared to the KI/+ and WT groups highlighting impaired diastolic relaxation. The difference was reduced after infusion of dobutamine.

Tau, the time constant of left ventricular relaxation, was significantly ($p<0.0001$) increased in KI/KI mice compared to WT and KI/+ mice (Fig, 3-7c), highlighting diminished diastolic function.

In addition to dP/dt max, systolic duration (Fig. 3-7f) was significantly increased while diastolic duration was significantly reduced (Fig. 3-7j) in KI/KI mice compared to both WT and KI/+, whereas no difference was observed between KI/+ and WT mice. This resulted in unchanged total cycle duration within the three different groups (Fig. 3-7e) There was no difference in the average heart rates (HR) between the groups (Fig. 37g),

however all groups showed increase in HR following infusion of dobutamine. Similarly, no significant differences were observed in mean Pressure within all three groups.

Further, the chronotropic (heart rate) and inotropic (contractility) responses to βagonist dobutamine were preserved in these animals. KI/KI animals, when compared to both WT and KI/+ animals, showed significant changes in heart rate, left ventricular developed pressure, end-diastolic pressure, and contractility (+dP/dtmax) under both unchallenged conditions and after administration of dobutamine.

These data from *in vivo* haemodynamic measurements suggests that the presence of C58G mutation in a homozygous state leads to impaired diastolic and systolic function.

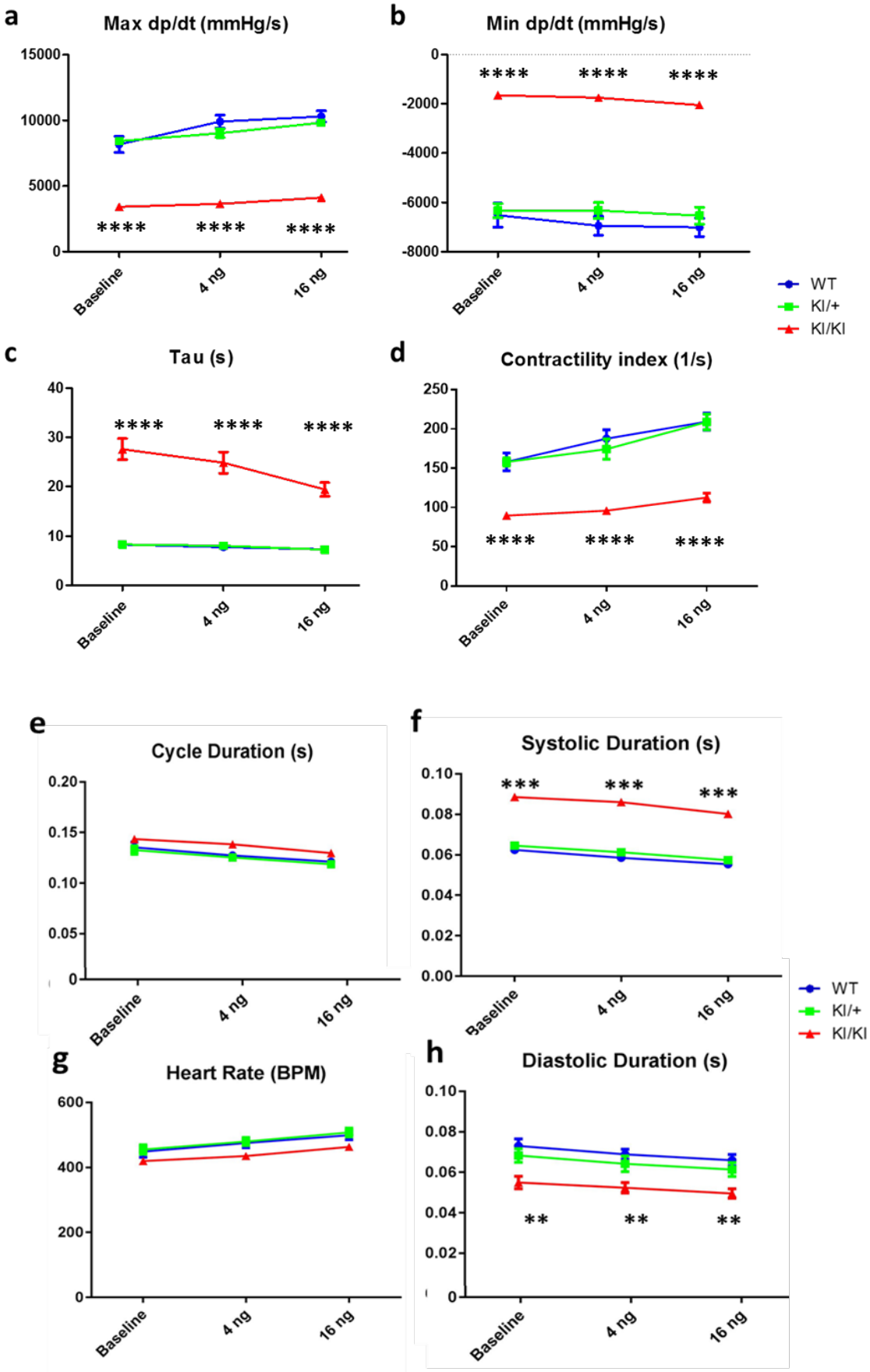

a
Max dp/dt (mmHg/s)
15000
10000
5000
0
****
****
****
Baseline
4 ng
16 ng
b
Min dp/dt (mmHg/s)
0
-2000
-4000
-6000
-8000
****
****
****
Baseline
4 ng
16 ng
WT
KI/+
KI/KI
c
Tau (s)
40
30
20
10
0
****
****
****
Baseline
4 ng
16 ng
d
Contractility index (1/s)
250
200
150
100
50
0
****
****
****
Baseline
4 ng
16 ng
e
Cycle Duration (s)
0.20
0.15
0.10
0.05
0
Baseline
4 ng
16 ng
f
Systolic Duration (s)
0.10
0.08
0.06
0.04
0.02
0.00
***
***
***
Baseline
4 ng
16 ng
WT
KI/+
KI/KI
g
Heart Rate (BPM)
600
400
200
0
Baseline
4 ng
16 ng
h
Diastolic Duration (s)
0.10
0.08
0.06
0.04
0.02
0
**
**
**
Baseline
4 ng
16 ng

Figure 3-7: Haemodynamic measurements in 3 month old WT, KI/+ and KI/KI mice. KI/+ were unremarkable from WT mice. KI/KI had significantly diminished (a) Systolic function (dP/dtmax) (**b**) Diastolic function (dP/dtmin). LV relaxation constant (**c**) Tau was increased while (**d**) contractility was reduced. No significant difference in (**e**)cycle duration was observed as the increase in (**f**) systolic duration was compensated by decrease in (**h**) diastolic duration. There was no difference in (**g**) heart rate Values are mean±s.e.m. ****P<0.0001 versus WT, **P<0.001 versus WT

Table 3-2 Haemodynamic parameter +/+, *Csrp3* KI/+ and *Csrp3* KI/KI (mean ± SEM)

		+/+	*Csrp3* KI/+	*Csrp3* KI/KI
n baseline		9	6	7
Heart rate	(bpm)	449 ± 18	455 ± 15	420 ± 11
dP/dTmax	(mmHg/s)	8168 ± 617	8415 ± 212	3417 ± 135****
dP/dTmin	(mmHg/s)	-6516 ± 486	-6329 ± 286	-1650 ± 134****'
Tau	(ms)	8.28 ± 0.45	8.27 ± 0.19	27.63 ± 2.16****'
LVESP	(mmHg)	91.23 ± 3.59	99.50 ± 7.18	75.48 ± 1.30**
LVEDP	(mmHg)	4.43 ± 1.11	6.06 ± 1.11	14.30 ± 1.54**
Mean AP	(mmHg)	39.65 ± 3.12	43.90 ± 2.89	48.02 ± 1.35*
Dobutamine (low dose; 4 ng g-1 BW min-1)				
Heart rate	(bpm)	475 ± 14	480 ± 13	435 ± 11
dP/dTmax	(mmHg/s)	9908 ± 490	9024 ± 333	3638 ± 141****
dP/dTmin	(mmHg/s)	-6846 ± 382	-6325 ± 326	-1750 ± 142****'
Tau	(ms)	7.75 ± 0.46	8.02 ± 0.22	24.87 ± 2.16****'
ΔdP/dTmax	(mmHg/s)	1740 ± 529	609 ± 517	221 ± 47*
Dobutamine (high dose; 16 ng g-1 BW min-1)				
Heart rate	(bpm)	499 ± 14	508 ± 14	463 ± 7
dP/dTmax	(mmHg/s)	10295 ± 432	9816 ± 256	4115 ± 146****
dP/dTmin	(mmHg/s)	-7013 ± 370	-6539 ± 342	-2049 ± 142****'
Tau	(ms)	7.32 ± 0.32	7.24 ± 0.29	19.44 ± 1.40****'
ΔdP/dTmax	(mmHg/s)	2128 ± 400	1402 ± 383	698 ± 111*

* $p < 0.05$ versus WT

** $p < 0.01$ versus WT

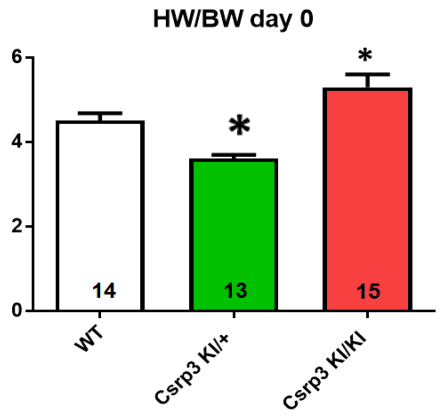
**** $p < 0.0001$ versus WT

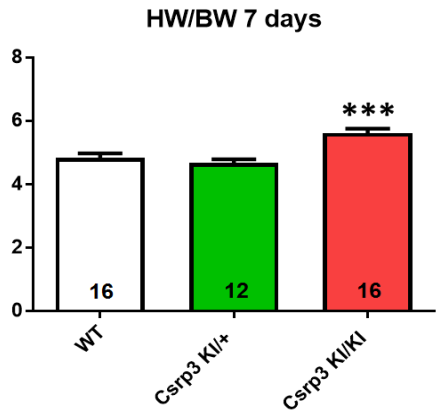
Table 3-2 Haemodynamic parameters of WT, KI/+ and KI/KI hearts

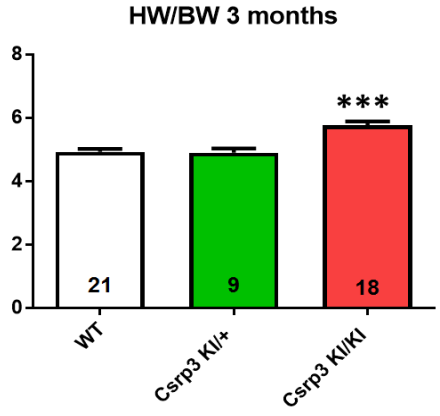
3.3.3 Changes in Morphometric Measurements

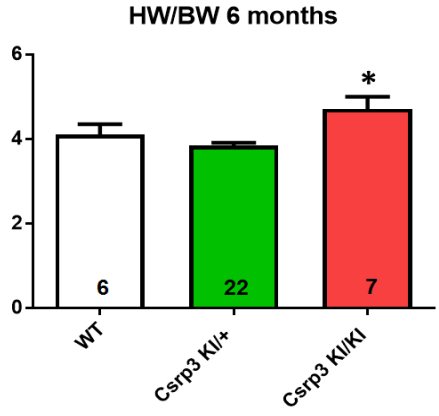
Morphometric analysis was performed on animals (Figure 3-8), from different genotypes at different ages, to check for any aberrant changes. Among day 0 pups, KI/+ animals had a significantly lower heart weight (HW) to body weight (BW) ratio (HW/BW) when compared to WT animals (Fig. 3-8a). KI/KI animals had significantly higher HW/BW when compared to both WT and KI/+ pups. At day 7 (Fig. 3-8b) KI/KI animals had increased HW/BW when compared to WT and KI/+ animals. No difference was seen between WT and KI/+ animals. At 6 months (Fig. 3-8c), like 3 months old mice KI/KI had significantly increased HW/BW while no difference was observed between WT and KI/+ animals at this age. Morphometric analysis of mice at different ages shows that KI/KI animals are born with a higher HW/BW compared to WT and KI/+ animals

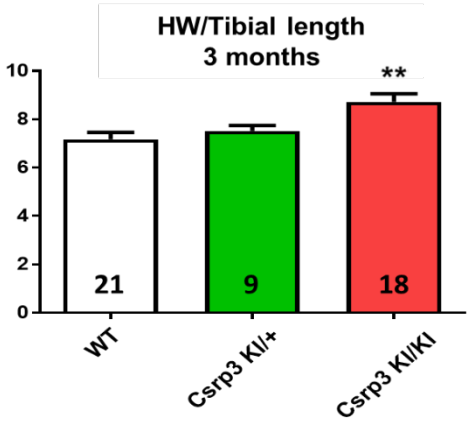
Normalization of organ weights to tibia length produced similar results to HW/BW at 3 months (Fig. 3-8e) and 6 months (Fig. 3-8f). This was important as fluctuations in body weight can occur as mice age making it unreliable reference for normalizing heart weight, especially in cases where the gene in question affects metabolism. BW/TL ratio for mice showed no difference between groups at 3 months (Fig. 3-8g) and 6 months (Fig. 3-8h) except for KI/+ mice at 6 months have a significant difference from KI/KI mice.

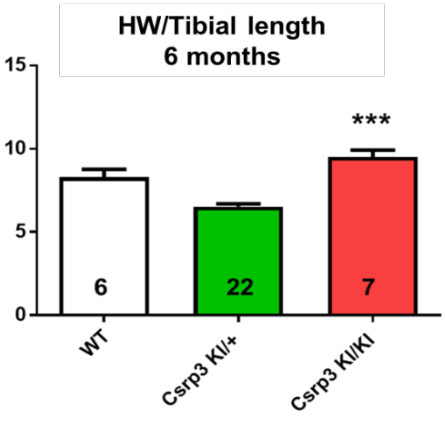

HW/BW day 0
6
4
2
0
*
*
14
13
15
WT
Csrp3 KI/+
Csrp3 KI/KI

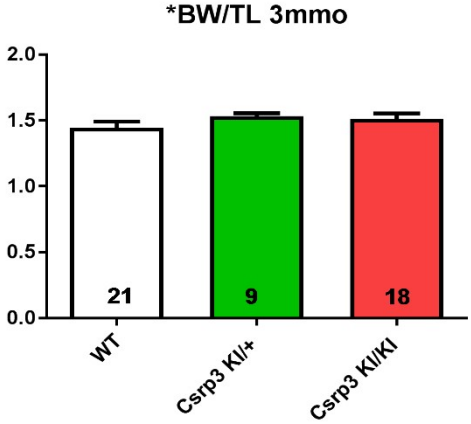

HW/BW 7 days
8
6
4
2
0
***
16
12
16
WT
Csrp3 KI/+
Csrp3 KI/KI


HW/BW 3 months
8
6
4
2
0
***
21
9
18
WT
Csrp3 KI/+
Csrp3 KI/KI


HW/BW 6 months
6
4
2
0
*
6
22
7
WT
Csrp3 KI/+
Csrp3 KI/KI


HW/Tibial length
3 months
10
8
6
4
2
0
**
21
9
18
WT
Csrp3 KI/+
Csrp3 KI/KI


HW/Tibial length
6 months
15
10
5
0
***
6
22
7
WT
Csrp3 KI/+
Csrp3 KI/KI


*BW/TL 3mmo
2.0
1.5
1.0
0.5
0.0
21
9
18
WT
Csrp3 KI/+
Csrp3 KI/KI

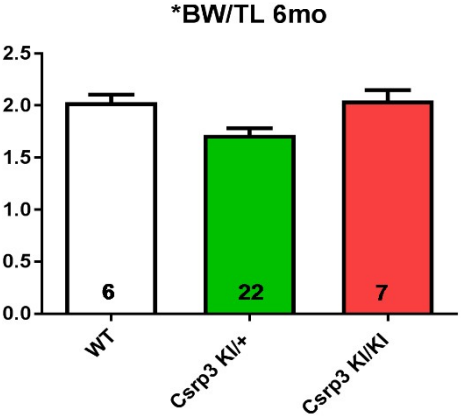

*BW/TL 6mo
2.5
2.0
1.5
1.0
0.5
0.0
6
22
7
WT
Csrp3 KI/+
Csrp3 KI/KI

Figure 3-8**.** Morphometric analysis of knock-in mice at different ages. Graphs represent the heart weight (HW) to Body Weight (BW) ratio (mg/g) for mice at **a)** Day 0 **b)** Day 7 **c)** 3 months **d)** 6 months. HW to Tibial Length (g/mm) for mice at **e)** 3 months **f)** 6 months.BW/TL ratio for mice **g)** 3months and **h)** 6 months. Data are expressed as mean ± SEM with *P<0.05 ***P < 0.0001, two-way ANOVA

3.3.4 Molecular Characterization of Day 0 and Day 7 hearts

Morphometric analysis highlighted increased HW/BW ratio in Day 0 and Day 7 animals suggesting an early onset induction of hypertrophy in these animals (Fig 3-4). Expression levels of key hypertrophic markers were assessed by Western Blot analysis (Fig. 3-9). Similar to expression of MLP at 2 months, knock-in mice showed reduced levels of MLP with KI/KI showing the greatest reduction. Contrary to findings at 2 months, key hypertrophic markers Rcan1, Capr, Fhl1 showed no changes in KI/KI compared to WT. KI/+, similar to hearts from 2-month-old mice showed no difference when compared to WT. Anti-hypertrophic protein Fhl2 showed no significant changes either. Further studies need to be performed to evaluate whether the change in morphometrics is independent of these key hypertrophic signalling proteins or not.

One Csrp3 KI/KIsample presented as an outlier and showed the presence of Rcan1, Carp.

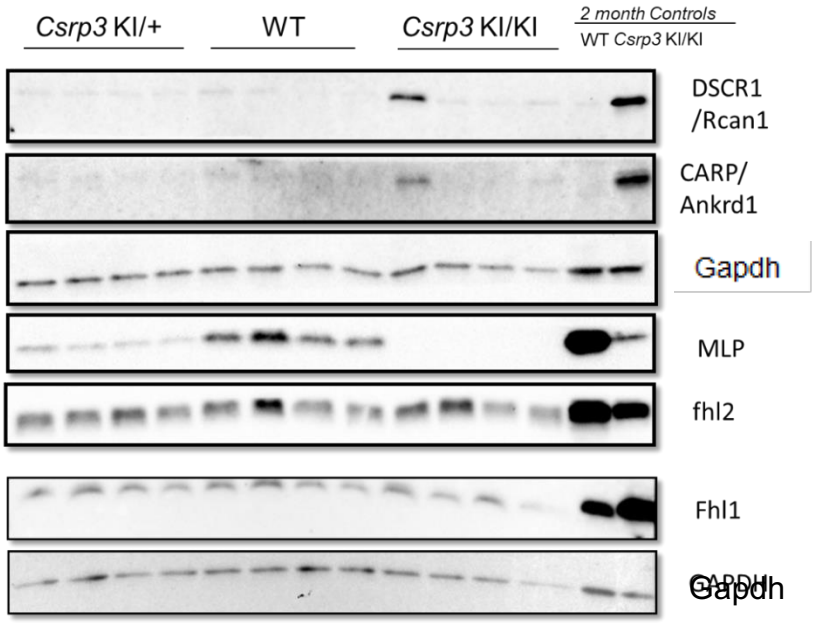


Figure 3-9. Western Blot Analysis of key hypertrophic pathway markers in cardiac tissue from 7-day old mice. Both KI/+ and KI/KI showed reduced expression of MLP compared to WT. No significant difference was observed between the groups in expression of Rcan1, CARP, Fhl1 and Fhl2

3.3.4 Absence of fibrotic phenotype in knock-in mice

In previous work from the lab, histological analysis using Sirius stain showed mild interstitial fibrosis in KI/KI mice. To assess for differences in fibrosis total collagen content per mg of heart ventricular tissue was assessed using a hydroxyproline assay (Fig. 3-10a). There was no significant change within any of the groups (n=4-6, 10week-old mice). The KI/+ group showed a trend towards higher collagen content, but this effect was not significant due to high standard deviation of data.

Col1a1 was assessed by Western blots (Fig. 3-10b) and no difference was observed between any of the groups.

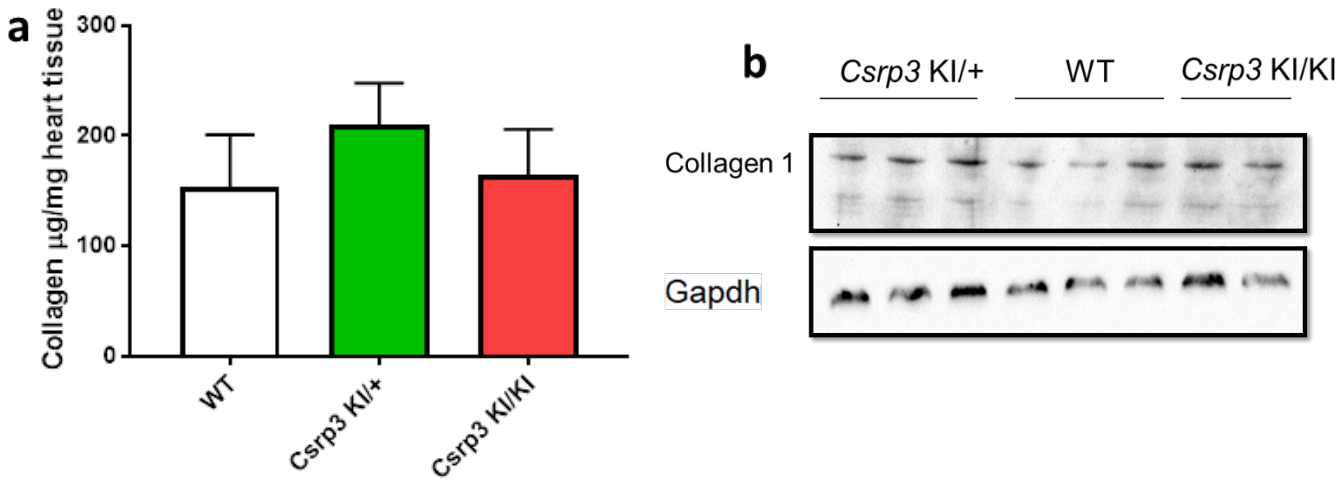


Figure 3-10: Absence of a fibrotic phenotype in Csrp3 KI mice a) There was no significant difference in the amount of total collagen content normalised to heart weight within any of the groups. Two-way ANOVA was performed to evaluate significance (n=4-6). **b)**. Representative Western blot for expression levels of collagen 1 in ventricular tissue lysates of KI and WT animals. Gapdh was used as loading control

3.4 Primary Conclusions of this Chapter:

1. KI/KI showed characteristics of dilated cardiomyopathy with compensatory hypertrophy
    - Significant reduction in EF/FS

- Increased LV chamber dimensions and volume
- Increased calculated mass, but no increase in anterior or posterior wall thickness

2. KI/+ showed no overt hypertrophy and the phenotype was not different to WT mice.
3. KI/KI showed increase in HW/BW ratio independent of age. No differences were observed in KI/+ mice.
4. Hearts from 7-day old animals showed no changes in protein expression of hypertrophic markers, even though the morphometric analysis show increase HW/BW ratio.

3.5 Discussion

Results presented in this chapter focus on characterization of the MLP C58G knockin mouse model. Mutations in the gene *CSRP3*, encoding for the protein Muscle Lim Protein (MLP) have been associated with dilated and hypertrophic cardiomyopathy (185, 216, 233, 234). Linkage analysis in a large German family led to identification of C58G missense mutation in *CSRP3* as HCM causing (231). The study also highlighted that MLP was a cytosolic protein rather than a sarcomeric one, making the C58G mutation one of the best recorded cases of HCM caused by non-sarcomeric proteins [15].

The homozygous C58G knock-in mouse recapitulates the phenotype of dilated cardiomyopathy. Morphometric results show increased HW/BW ratio for KI/KI from birth till the age of 6 months. Though KI/+ have decreased HW/BW ratio in Day 0 pups

they are otherwise unremarkable from WT mice. HW/BW was used as a measure of comparison as its difficult to measure the tibial length in mice at an early age. Normalization of heart weight to tibial length is a better measure as it relates HW to the physical development of the individual mice (235). HW to tibial length ratio revealed similar results in both 3-month-old and 6 month-old mice. These results indicate that the C58G KI/KI mice have significant cardiac hypertrophy compared to WT and KI/+ mice. The initial findings that there was no difference between KI/+ and WT animals suggests the absence the hypertrophy.

In vivo characterization by transthoracic echocardiography and left ventricular haemodynamic highlights that KI/KI mice develop cardiomyopathy with diastolic and systolic impairment. This supports morphometric analysis showing that KI/KI animals had increased LV mass per tibial length. I*n vivo* findings showed a significant change in the wall thickness, which is often thinner in cases of dilated cardiomyopathy, suggesting compensatory activation of hypertrophic pathways. These findings were supported by earlier work in the lab which showed upregulation of *Nppa* and *Nppb* mRNA in KI/KI mice. Plasma ANP (236, 237), encoded by gene *Nppa*, and BNP (238, 239), encoded by gene *Nppb*, have been shown to be elevated in HCM patients in various studies. The levels of these peptides vary directly with cardiac filling pressures, making them great markers for the presence of LV dysfunction and abnormal LV wall stress (240, 241) Similarly, human studies have highlighted that Fhl1 upregulation and Fhl2 downregulation correlated with development of HCM and mutations in genes lead to development of HCM (242-244). Carp (Cardiac-specific ankyrin repeat protein, CARP1/Ankrd1), is a stress marker which is shown to be increased in cases of heart failure (245). Though, the aberrations in expression of these molecules in KI/KI confirm activation of hypertrophic pathways, it remains yet to be investigated whether they play

a causative role in development of the DCM phenotype in these mice. One of the ways in which this could be studies is by making mouse models lacking these proteins in addition to mutation in MLP.

Previous work in the lab, as mentioned earlier, revealed mild interstitial fibrosis in KI/KI. Fibrosis is a hallmark of HCM and is thought to contribute to sudden cardiac death, left ventricular dysfunction, and heart failure (104, 246-249). Histological analysis of patients with HCM display significant increase in interstitial and focal myocardial fibrosis (249). It is unclear what the exact cause for this increased fibrosis in HCM is, however, it has been shown to lead to cardiomyocyte death due to stress induced by sarcomeric mutations and their pathological disease manifestations (250-253). Transcriptional profiling in animal models of HCM shows activation of profibrotic and collagen deposition pathways in young mice in which hypertrophy has not yet developed (254, 255) These findings highlight that the profibrotic pathways are active in early heart of HCM even when the histological findings appear normal (Figure 3-4). To get a measure of total collagen content a hydroxyproline assay was performed on ventricular tissue (235, 256). Hydroxyproline residues are essential for the intracellular assembly of stable collagen triple helices, and their absence results in the immediate intracellular degradation of the defective pro-α chains. The abundance of hydroxyproline in collagen, compared to negligible incorporation in other proteins can be utilised to measure the amount of collagen content in tissues (257). The hydroxyproline assay failed to show any significant differences between the groups. Similarly, procollagen-1 levels, which is pro-fibrotic, were unremarkable between different groups. These findings are different than those observed in MLP KO mice which showed significant fibrosis, as measured by Masson's Trichrome staining and pro-collagen1 levels, when compared to WT mice (189, 229, 258). The difference might

be attributed to the genetic background of the mice. Studies have highlighted that C57BL/6J mice, used in this study, are resistant to hepatic, renal and cardiac fibrosis but are susceptible to pulmonary and intestinal fibrosis (259-261). Another possible explanation for the difference is that our investigation was carried when mice were 10 weeks old whereas mice used in earlier studies performed evaluation at an age between 4 to 8 months (Lange et al 2016).

KI/+ mice showed no signs of developing hypertrophy and in most observations were unremarkable from the WT littermate controls. This was similar to heterozygous MLP knock out mice, which express significantly less MLP protein than WT littermates, yet do not develop any spontaneous phenotype. The KI/+ mice, when compared to WT animals, did not show any observable changes in phenotype upon aging (up to 12 months) or after transaortic constriction (Ehsan et al 2018). The lack of overt phenotype in these mice might be attributed to the differences in cardiac physiology of humans and mice. To highlight, despite being the most commonly used animal model of cardiac disease, the mouse heart rate and electrical conduction pathways are significantly different from humans. Mice have a heart rate of approximately 800 beats/min while the resting heart rate for humans in about 70 beats/min. This means that the cardiac action potential (AP) is much shorter in mice. The repolarisation phase of the cardiac AP, which is driven by the outward K^+ currents, is also much shorter in mice. This is due to the difference in expression of K^+ channel signalling genes within the mouse heart when compared to humans (262). Moreover, there are differences in sarcomere protein composition between humans and mice. For example, the primary myosin isoform expressed in murine hearts is the Myh6 or α-myosin heavy chain (263, 264). In order to study the human *MYH6* mutation, which is the most affected isoform in humans, it had to be transposed into *MYH6* in the mouse models. There are major

differences between the proteins in terms of their ATPase activity and actomyosin kinetics, with the Myh6 protein having a greater ATPase activity and greater velocity of actin displacement (264-266). It should also be noted that HCM caused by mutations in the *CSRP3* gene are often late-onset in humans, suggesting the stress over the years induces a phenotype. These mice, though in cage, however, lead a sedentary lifestyle. Further, there are quite a few other examples of well characterized HCM mutations such as myosin binding protein C mutations (114) and myosin heavy chain mutations (254, 267) which do not present similar phenotypes in a mouse model in the heterozygous setting.

Morphometric analysis of mice at different ages shows that KI/KI animals are born with a higher HW/BW compared to WT and KI/+ animals. This suggests there the development of hypertrophy in these mice does not progress with age. Further, the HW/BW ratio does not exhibit a higher ratio with age, unlike some other models of HCM (268). This led to studies on mice at Day 0 and Day 7. Protein levels at Day 7 showed that there were no changes in expression of Carp, RCAN, Fhl2, Fhl1 compared to WT controls, even though the HW is still increased. Lange and colleagues described that MLP and Carp double knock-out remains healthy. The authors showed evidence that MLP inhibits the activity of PKCα and in the absence of

MLP or end-stage DCM PKCα is concentrated at the intercalated disc of

cardiomyocytes with the help of adaptor protein Carp. The absence of Carp in double KO model impairs this concentrated localisation of PKCα at the intercalated disc, preventing an overt phenotype (258). Csrp3 KI/KI at an early age do not show any differences in expression of Carp while having an increased HW/BW ratio, whereas adult knock-in mice (2-months) show increased expression of Carp. These results

suggest that that Carp upregulation downstream of MLP may be due to maladaptive or compensatory hypertrophy.

Increased calcineurin activation has been associated with HCM and DCM (269-271). Genetic ablation of calcineurin Aβ protects the heart from hypertrophy in mice subjected to transverse aortic constriction (272). Calcineurin overexpression has been described to have protective effects in MLP KO mice. Almost three-quarters of MLP and calcineurin Aβ double knock-out died in the first 20 days after birth and mice that survived until adulthood had reduced left ventricular function, enhanced apoptotic and necrotic cardiomyocyte death and increased fibrosis (226). The human regulator of calcineurin 1 (RCAN1) gene, also termed Down syndrome candidate region (DSCR), is an endogenous regulator of calcineurin, has been shown to be associated with cardiac valve development and hypertrophy (273). RCAN1 binds to the catalytic subunit of calcineurin and inhibits its function (274). Further, induction of RCAN transcription is driven by the expression of nuclear factor of activated T cells (NFATc) and calcineurin activity within the endocardium during heart development (275). *Csrp3* KI/KI 2-month-old mice have an increased expression of Rcan1, which suggests its upregulated in response to the calcineurin pathways activation.

These findings suggest a role of hypertrophic markers in the development of DCM in the case in Csrp3 KI mice, is not as straight forward as previously thought. The lack of protein expression of these markers at birth in KI/KI hearts is unexpected and warrants further study.

Chapter 4 – RNA Sequencing of MLP Mouse Models

4.1 Introduction

DNA encodes genetic information that is primarily transcribed into messenger RNA (mRNA) and translated into proteins that perform cellular functions. Thus, genetic expression of genes plays a pivotal role in determining cellular phenotype. The complete set of these transcripts, which represent the genetic expression of the cell, is called the transcriptome. The transcriptome, including the type and the abundance of transcripts is essential for us, not only to interpret the phenotype but also understand how gene expressions affects development and disease. The study of the transcriptome, transcriptomics, aims to identify all types of transcripts (mRNAs, noncoding RNAs, and small RNAs), determine the structure of gene with regards to their start and end sites, splicing patterns and other post-transcriptional modifications such as phosphorylation, glycosylation and quantify the expressions levels of each transcript.

A number of different technologies have been used to study the transcriptome, among them hybridization or sequenced based approaches (276). The former was the basis of microarrays, where fluorescently labelled cDNA was incubated with predetermined probes. Microarrays were one of the most commonly used tools used by scientists in the recent past as it allowed them to probe for thousands of genes at the same time (277, 278). Microarray based methods are responsible for a great amount of our understanding of physiology and disease mechanisms. These could also be used for splicing variants by designing probes for the exonal junction sequence(276). Further, to get a high resolution mapping of the transcribed area, researchers could perform genome tiling microarrays, where probes with overlapping oligonucleotides were

designed (279-281). Apart from tiling microarrays, these hybridizations based approaches were high-throughput and relatively inexpensive (Table 4-1). These methods, however, have some limitations such as high background counts due to cross hybridization of probes with similar sequences, dependence on knowledge of existing genome sequences, and a restricted range of detection due to high background and saturation of signals (282, 283). Further comparison of expressions profiles between different experiments is usually challenging and usually requires complicated normalization methods(284).

The recent advancements in Next Generation Sequencing (NGS), have allowed the development of a new method, RNA-sequencing (RNAseq), to both quantify and map transcriptomes (285-289). This method has already been applied to assess transcriptomes of a number of species including yeast, mouse and human cells (286, 288-292).

Usually RNAseq experiments follow a similar protocol. Briefly, RNA (total or fractionated mRNA/miRNA) is isolated from the sample and converted into a library of cDNA fragments with adaptors attached to one or both ends. These fragments are then sequenced in a high-throughput manner to obtain short sequences, typically 30 to 400 bp in length, depending on the technology used. The sequencing can be singleended, meaning from one end, or pair-end, from both ends of the fragment. These short reads are then aligned and mapped onto a reference genome or assembled *de novo*. This results in the production of a genome-scale map of the transcriptome where expressions level of a gene or a noncoding region can be determined by counting the number of reads that are aligned to the respective regions (287).

Criterion	Expression arrays	Tiling arrays	RNA-Seq
Resolution of data	N/A	Dependent on genome size but ⩾35 bp for human/mouse	1 bp, at sufficient sequencing depth
Cost per sample (excluding equipment)	Low	Low–high, depending on arrays needed to cover genome	High
Linear dynamic range of expression values	<4 orders of magnitude	<2 orders of magnitude	Limited only by sequencing depth and biological expression levels
Sensitivity (Signal:Noise)	Moderate	Low	High
Discovery of novel transcribed regions	No	Yes	Yes
Monitor splice site usage	No	Limited	Yes
Identification alternative promoters/UTRs	No	Yes	Yes
Detection of antisense transcripts	Not standard	Not standard	Requires strand specific preparation
Detection of SNPs mutations, allelic differences	Limited	Limited	Yes
Size of raw data files per experiment	0.01–0.05 Gb	0.1–1 Gb	1–15 Tb
Downstream Bioinformatic requirements	Low	High	Very high

Table 4-1. Comparison of different methods for transcriptomics. Adapted from (293)

Compared to microarrays, RNAseq has a number of advantages. RNAseq does not require a sequenced genome, which is necessary for the hybridization-based approach of microarrays (Table 4-1). This makes it particularly attractive for transcriptomics of organisms whose sequences have not been confirmed. Further, RNA-Seq allows the resolution of the transcriptome to a single nucleotide which allows detailed analysis including precise identification of transcription boundaries, alternative splicing events, sequence variations e.g. Single Nucleotide Polymorphisms (SNPs) and post-transcriptional RNA editing events (294). The length of reads shows how two coding regions might be connected, in the case of 30bp reads, and how multiple exons are connected, in the case of longer (up to 200bp) or pair-end reads. These advantages make RNAseq a really useful tool for studying complex
transcriptomes (290, 292).

RNAseq has very low background compared to microarrays as cDNA sequences can be mapped onto the genome without requiring fluorescent probes. These probes limit the quantification range of microarrays. RNA-Seq has no upper limit for quantification and the large dynamic range correlates with the number of sequences obtained. RNAseq studies in mouse samples have been shown to have a difference of five orders of magnitude (287). This is in sharp contrast to microarrays, which are not sensitive for genes expressed at low or very high levels. Their range varies and can go up to a few hundred fold. In addition to being highly reliable, among both biological and technical replicates, the quantification of transcripts by RNAseq has been shown to be accurate, as confirmed by studies comparing results with quantitative PCR (qPCR) and spike-in RNA controls of known concentration (287, 288). Further, due to absence of cloning steps, RNAseq requires less RNA sample making it an invaluable tool for clinical studies (276).

Though RNAseq has a number of advantages over traditional microarrays it suffers from a number of biases: Before RNA can be sequenced, after ligation of adaptors, they need to be fragmented into smaller pieces (200-500 nucleotides) to be compatible with sequencing. This is carried out either by RNA fragmentation (RNase III enzymatic digestion) or cDNA fragmentation (DNase I treatment or sonication). RNA fragmentation has little bias over the main transcript body, however it has diminished levels of transcript ends when compared to other techniques (287). On the other hand, cDNA fragmentation is strongly biased towards the identification of sequences from the 3′ ends of transcripts. This however, is very useful in identifying the exact identity of these ends (288). Further, library preparations can introduce errors in counts. For example, many short reads that are identical to each other can be obtained from cDNA libraries that have been amplified. These sequences could be present as they are more abundant than others or could be the result of PCR artefacts. Comparison between biological replicates helps distinguish whether they are artefacts or not. PCR can also introduce bias based upon GC content and length due to non-linear amplification (295, 296). A number of tools have been developed to overcome these biases with varying success (297-299). During analysis there is a bias towards larger transcripts. Since the total number of reads per transcript is proportional to the product of level of a transcript and its length, for equal levels of expression, a long transcript will be more likely to be sequenced than a short transcript. And given statistical power is closely linked to sample size, a longer transcript will have a higher chance of being found differentially expressed when compared to a short transcript (300). To overcome this bias, expression levels are expressed by calculating the number of reads or fragments per kilobase per million reads (RPKM and FPKM, respectively) (287). The FPKM transformation also allows direct comparison of transcript expression between two

libraries with different sequencing depth as well as an indication of relative expression levels between two or more transcripts in a single library.

4.1.1 A typical RNAseq experiment

The library preparation, nucleotide detection protocol vary according to the platform used, however, a typical RNAseq experiment (illustrated in Figure 1) is comprised of the following main steps:

Preparation of total RNA: RNA extraction is performed on sample, and ribosomal RNA (rRNA), which typically constitutes of upto 90% of the cellular RNA, is removed. For eukaryotes, this is either performed by enrichment of mRNA using poly(A) selection or by depletion of rRNA. Poly(A) enrichment requires a relatively high proportion of mRNA with minimal degradation. Many biological samples, however, do not meet the quality control and therefore have to rely on rRNA depletion. Further enrichment can be carried out depending on class of RNA to be sequenced (i.e. mRNA, lincRNA, microRNA etc), Good quality total RNA is critical, although alternative protocols for degraded RNA exist (301).

Library preparation.

Library preparation consists of:

RNA fragmentation: mRNAs are fragmented to smaller pieces of RNA to enable sequencing.

Reverse transcription: First and second strand cDNA is reverse transcribed from fragmented RNA using random hexamers or oligo(dT) primers.

Adapter ligation: The 5’ and/or 3’ ends of cDNA have adapters of same and fixed length ligated to them. These sequences that allow the fragmented RNA to bind to the flow cell of sequencer

Library clean-up and amplification: Libraries are enriched for correctly ligated cDNA fragments and amplified by PCR

Library quantification, quality control and sequencing. Library concentration is assessed using qRT-PCR and/or Bioanalyzer and is ready for sequencing.

Sequencing: The most common next generation sequencing platform used for RNAseq is the Illumina HiSeq which uses a “sequencing by synthesis” (SBS) approach, whereby incorporation of dNTPs is detected simultaneously at millions of fixed positions on a flow cell.

For Illumina, once libraries have been prepared they are hybridized to a flow cell containing bound oligonucleotides with sequences complementary to the adapters. Following that the oligonucleotide primes DNA polymerase extension activity resulting in a covalently bound complimentary copy of the cDNA fragment, which is amplified by PCR. Fluorescently labelled reversibly terminatable dNTPs are introduced in the flow cell as the same time as extension step. These dNTPs are in equal quantity and the fact that they can be terminated reversibly helps ensure only one nucleotide is incorporated per cycle. After a nucleotide is incorporated and detected by fluorescence, the fluorophore is removed resulting in regeneration of a 3’ hydroxyl group which allows incorporation of the next dNTP in the subsequent cycle. Importantly, this reversible terminator chemistry allows sequencing of homopolymeric regions, such as “AAAAAA,” with high confidence. Error rate (incorporation of the

incorrect nucleotide) progressively mounts with increasing number of cycles; currently up to 150 cycles are supported with an overall error rate of 0.2% [32].

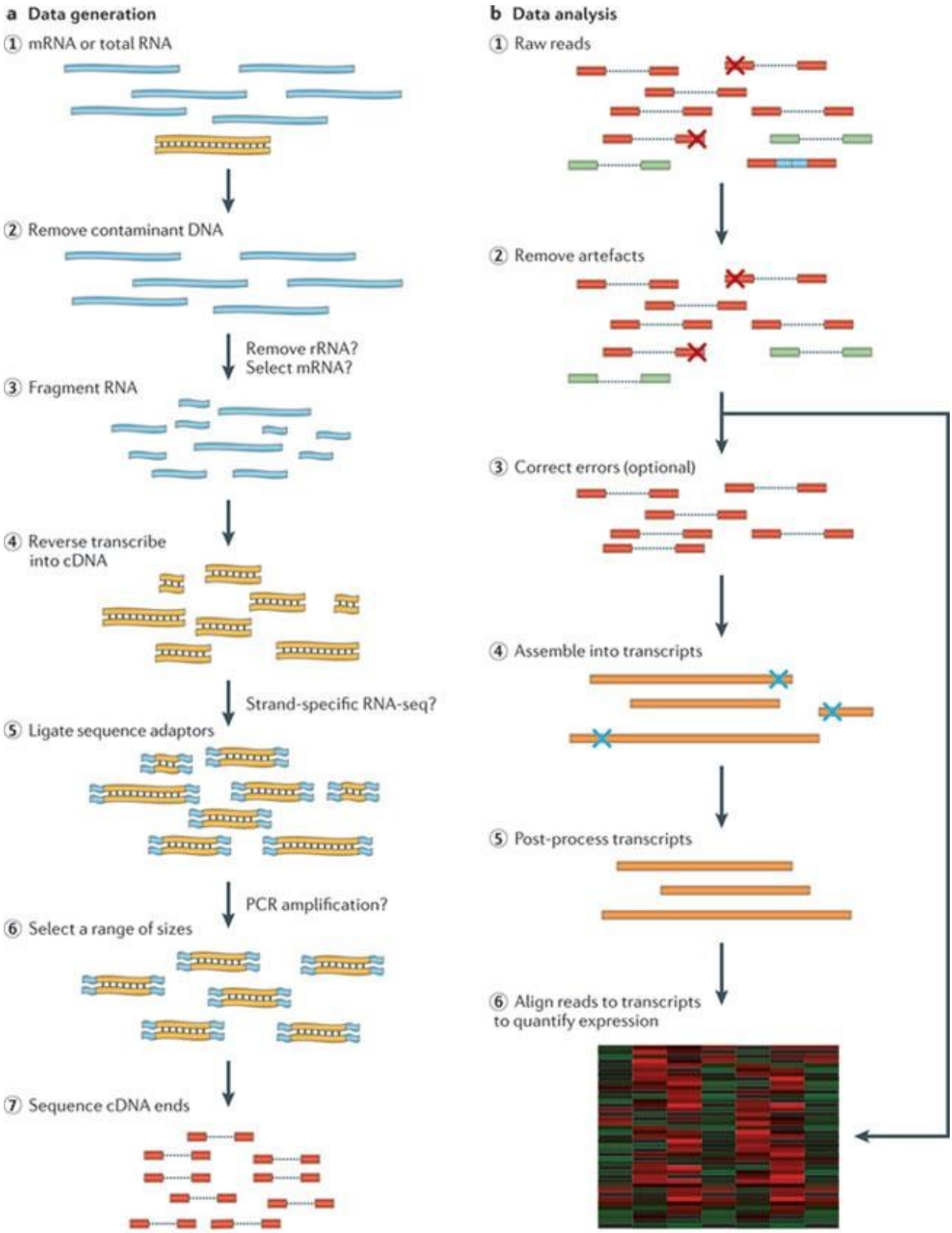


Figure 4-1: Outline for a typical RNAseq experiment. Adapted from (302) *Analysis of RNAseq data:*

There are a number of software packages and scripts that allow the quantification of these short reads leading to analysis of differential expression. However, the principle pipeline for analysis is typically the same. As an output, the sequencers gives out millions of short reads. The first step is to trim off the sequencing adapters from the reads. Following that quality control is performed on the raw data, to remove poor quality reads, which is routinely conducted by quality control (QC) software. The quality is assessed by a number of parameters provided by the QC software which include, percentage of GC content, per base sequence quality score (represents the of confidence in correct base calling), per base sequence content (a representation of each nucleotide at each base position to visualize position/sequence bias), per base N content (a plot of uncalled nucleotides (N's) at each base position), duplicate reads (typically a result of PCR over-amplification during library preparation) and overrepresented sequences.

The next step is to align the reads to a reference genome or in the absence of a genome map construct a transcriptome assembly. Alignment to a reference genome allows quantification of known genes and transcripts and allows for efficient computing and removal of any contaminating reads. The alignment is then summarized and aggregated over a genome map, often exons/genes/transcript names. Generally, the number of reads overlapping the exons in gene are counted. It should be noted that a significant amount of reads map to genome outside the annotated exon region. These can be included in assessment by including the sequences along the whole length of the gene. The disadvantage of this approach is that it might capture sequences that overlap different genes.

The data is then normalized to allow for accurate comparisons of expression levels between and within samples (287, 291, 303). Normalization is critical for the analysis of differential expression from RNAseq data (304-307). As mentioned earlier, longer transcripts will lead to higher read counts for the same expression. To overcome this bias, a ratio between the summarized counts and the length is taken. This is represented as reads per kilobase of exon per million mapped reads (RPKM), which accounts for both library size and gene length effects. This approach has been validated by the introduction or 'spike-ins' of foreign RNAs. The limitation of this methods is that read coverage along expressed transcripts can be non-uniform because of sequence content (308) and RNA preparation methods, such as random hexamer priming (297). The comparison can be improved by using RNA standards and using extra information such as total number of cells from which RNA was isolated and the RNA isolation yield (287).

Following normalization, statistical testing for differential expressions is performed using negative binomial distribution. In the most popular computing package Deseq2 and EdgeR, counts table (number of reads corresponding to each gene) with biological replicates are utilized to calculate variation and test for statistically significant differential expression (305, 309, 310). Both methods use ANOVA-like generalized linear models (GLMs) to analyze complex experimental designs which allows control for any known batch effects introduced during library preparation and the BenjaminiHochberg procedure to control the false discovery rate (FDR) associated with multiple hypothesis testing (305, 310).

Following differential gene expression analysis, visualization and pathway analyses can be performed in a similar way to microarrays. One of the analyses is to test for

enrichment of Gene Ontology (GO) terms associated with a list of significantly over- or under-expressed genes (311). GO consists of three organized and hierarchical vocabulary or ontology sets that area associated with biological processes, molecular function and cellular component. One of the most commonly used GO analysis application is *GOrilla*, which allows for identification of GO terms from all three ontologies that are significantly overrepresented in a given data set. *GOrilla* allows to attribute ontologies without the requirement of a background set of data and by using a statistical model that is able to discover GO terms based on a ranked list of differential gene expression(312). GOrilla and other packages currently used are able to control the length and selection bias introduced by longer transcripts, since there is greater statistical power to call strongly expressed genes as differentially expressed. There are a few other analyses that are routinely used for RNASeq. Hierarchical clustering allows to assess similarity between samples. Heatmaps allow for visualization for differential gene expression. Principle component analysis (PCA) allow visualization of variation and patterns within the data set and network analysis to see which pathways, affected by the conditions, are connected with each other (313).

4.1.2 RNAseq and cardiomyopathies

RNAseq provides a snapshot of the transcriptome at a time point, giving the information about the changes in activation or inhibition of various pathways in different pathophysiological states in an unbiased manner (276, 314). There are a number of studies that have used RNAseq to investigate the underlying genetic architecture underlying complex diseases such as cardiomyopathies.

Henig and colleagues have performed one of the most comprehensive transcriptomic analysis using RNA-sequencing of left ventricular samples from 97 patients with dilated

cardiomyopathy and 108 non-diseased controls (315). Extensive differences in gene expression and splicing patterns were observed between DCM patients and controls. These differences were present in known DCM genes such as *NPPA* (Natriuretic peptide A), *NPPB* (Natriuretic peptide B), *TBX20* (T-box 20) and some genes that were not implicated in DCM before such as *MYLK3* (Myosin light chain kinase 3), *CLIC5* (Chloride intracellular channel 5), *TRIM44* (Tripartite motif containing 44), *MAVS* (Mitochondrial antiviral signalling protein) among others. Further a diverse effect of genetic variation was observed on the regulation of transcription, isoform usage, and allele-specific expression. The findings from this study are a great resource linking genetic variants causing DCM and their effects on transcription regulation and genetic expression in humans (315).

The above mentioned study highlight the changes in transcriptome a time point. It is important to understand the changes in transcriptome over time, before and after the development of disease. Burke and colleagues assessed transcriptomes at different stages of DCM using a genetic mouse model of DCM (phospholamban missense mutation, $PLN^{R9C/+}$) (316). RNAseq was performed on hearts before development of DCM, during DCM and hearts with overt heart failure (HF). Further, these studies were performed using cardiomyocytes from left ventricle and on the non-cardioomyocyte fraction. Pre-DCM hearts were phenotypically normal yet displayed proliferation of nonmyocytes and activation of proinflammatory signalling. These changes were more significant as the DCM developed, and the mice exhibited heart failure. As disease progressed cardiomyocytes highlighted a marked shift in metabolic gene transcription: downregulation of aerobic respiration and subsequent upregulation of glucose utilization, changes coincident with attenuated expression of PPARα and PPARγ coactivators -1α (PGC1α) and -1β, and increased expression of the metabolic regulator

T-box transcription factor 15 (*Tbx15*). The study also compared the DCM model with a mouse model of HCM (MHC^{R403Q}) which revealed similar and distinct molecular mechanisms. The longitudinal and comparative transcription analysis shed light on the various mechanisms that may cause or lead to progression of disease (316). Further studies are required to enhance our understanding of mechanisms governing these diseases.

Christodoulou and colleagues developed a new methodology for acquiring 5′RNA-Seq gene expression profiles to detect and quantify start-site usage in WT and $MHC403^{/+}$HCM model (Arg403Gln, in the myosin heavy chain gene) (317). Significant changes in start-site usage response to mutation was observed in 92 genes. In addition to increased expressions of Fhl1, myocyte-specific induction of iFhl1 was observed. iFHL1 uses an alternative start-site and incorporates 16 additional amino acids and was not described in the literature before. These findings were also observed in 5′RNA-Seq analyses of human patients undergoing either myectomy heart surgery, cardiac transplant surgery, or valve replacement surgery. Further experiments with genetic ablation of Fhl1 in mice showed significantly worse HCM phenotype, suggesting that Fhl1 had protective role in development of this specific mouse model of HCM (317).

There are a number of other studies that have used RNAseq giving us insights into cardiomyopathies. Table 4-2 lists some of the key studies which have used a mouse model of cardiomyopathy or have performed studies on human heart samples from cardiomyopathy patients.

Paper	Year	Species	Disease and sample size
Song et al (318)	2012	mouse	C57BL/6J mice subjected to swim-training pressure overload by TAC
Yang et al (319)	2014	human	human failing LV samples: nonischemic (NICM; n=8) and ischemic (ICM; n=8) nonfailing human LV (n=8)
Christodoulou et al (317)	2014	mouse	MHC403/+, MHC403/+/*Fhl1*-null, and WT mice

Liu et al (320)	2015	human	3 healthy controls, 1 ICM, 2 DCM
Ren et al (321)	2016	human	6 healthy controls vs 6 HCM patients
Li et al (322)	2016	human	15 ICM patients vs 15 healthy controls
Ortega et al (323)	2016	human	13 ICM patients vs 10 control
Prunotto et al (324)	2016	mouse	Isoprotenol treated mice as model of hypertrophy vs WT littermate controls
Burke et al (316)	2016	mouse	PLNR9C/+ knock-in mice for DCM model MHC R403Q/+ knock-in mice as a HCM model
Heinig et al (315)	2017	human	97 DCM patients vs 108 healthy control
Schiano et al (325)	2017	human	2 DCM vs 2 RCM
Rindler et al (326)	2017	human	6 RCM vs 5 healthy controls
Gil-Cayuela et al (327)	2018	human	13 DCM patients with end-stage heart failure vs 10 health controls

Table 4-2: Literature on RNAseq used in cardiomyopathy patients or experimental models. Abbreviations: DCM (Dilated Cardiomyopathy), HCM (Hypertrophic Cardiomyopathy), TAC (transaortic constriction), LV (Left Ventricle), ICM (ischemic cardiomyopathy), RCM (Restrictive Cardiomyopathy)

4.2 Methods

4.2.1 RNA Extraction

Mouse ventricular samples were powdered by freezing with liquid nitrogen and smashing in a Biopulveriser. Powdered tissues samples were incubated with 1 ml Trizol Reagent at room temperature for 2-3 min. Chloroform was added in a 1:5 ratio (200 µl). The mixture was mixed manually for 20s and then centrifuged for 4 min at RT at 15,000 g. Following that the aqueous phase was transferred to a fresh centrifuge tube and 500 µl of a 1:1 mixture of acid phenol chloroform were added, mixed for 20 sec and centrifuged at for 4 min at RT at 15,000 g. The aqueous phase was again transferred to a fresh tube and 500 µl Isopropanol was added and mixed. Samples were incubated for 20 min at -20°C and centrifuged at 4°C for 10 min at maximum speed in a table top centrifuge. Supernatant was removed, and 1 ml of 70% ethanol was added to the mixture which was then centrifuged for 1 min at 15,000 g. Ethanol was removed and the tube was airdried before adding RNase-free water to dissolve the pellet. Samples were purified and treated with DNase according to the manufacturer's protocol for the PureLink RNA Mini Kit (Ambion by life technologies).

4.2.2 RNA sequencing Differential Expression Pipeline

Raw data was acquired with single-end read sequencing using HiSeq 50 cycle on Illumina HiSeq 2500 instrument using RNA isolated from ventricles from 9 weeks old WT and KI/KI mice. Sequencing was performed by the Huntsman Cancer Institute (University of Utah, US) and 30 million reads per sample per performed.

Sequenced libraries were aligned to the mouse reference genome *Mus musculus* (GRCm38; accessible at http://www.ensembl.org/Mus_musculus/Info/Annotation)

using HISAT2 package, in python (328). Following alignment the aligned files were sorted and indexed according to chromosomes and genes using SAMtools, on pyhton (329). After evaluating the counts for different genes, these counts were used to analyse differential expression using DESeq2 package in R, using standard protocol in DESeq2 manual (309).

Genes were defined to be differentially expressed if they met the following 3 criteria: (i) normalized read count > 2 copies/million reads in the RNA-seq library, (ii) log2 foldchange > 1 (upregulated) or < –1 (downregulated), and (iii) P < 0.001 for the comparison of normalized read counts between KI/KI and control animals. The differential gene list meeting these criteria was then used for pathway analysis using Gorilla, Gene Set Enrichment Analysis (GSEA) and ingenuity pathway analysis.

Gene Ontology (GO) analysis were performed using Gorilla (http://cbl-gorilla.cs.technion.ac.il) to find enriched GO terms on the differentially expressed genes (311). This analysis considers the total number of genes, the number of genes assigned to a GO term, and number of statistically significant genes overall to evaluate whether a differentially expressed gene belongs to a GO term, rather than it being a chance event. The Gorilla analyses were run on list ranked by p-value. GO categories with p-values <0.001 were considered significant.

Gene set enrichment analysis (GSEA) were performed based on software provided by the Broad Institute of MIT and Harvard using the 171 gene sets that represented Kyoto Encyclopaedia of Genes and Genomes pathways (330). GSEA determines whether a predefined set of genes show statistically significant and consistent differences between two biological states or phenotypes. The pathways were obtained from the MSigDB v.4.0 database (http://www.broadinstitute.org/gsea/msigdb/index.jsp). All default parameters were retained including keeping phenotype permutation for 1000

times and using the weighted signal to noise statistical approach to rank genes. Only the pathways with false discovery rate < 0.001 are reported.

The IPA (Ingenuity Pathway Analysis) (http://www.ingenuity.com/products/ipa) upstream regulator was used to predict the functional status of molecules (upstream regulators) such as transcription factors, kinases, and growth factors based on known downstream targets identified in the input gene set. Two different measures of significance were used to evaluate the regulators. The overlap P value (< 0.01 as significant) represents the significance in the overlap between the identified differentially expressed genes and all genes associated with a particular upstream regulator in the Ingenuity database. The Z-score accounts for the direction of activation of the differentially expressed genes in relation to published literature with respect to a particular upstream regulator, thereby allowing a prediction of whether the upstream regulator is activated or inhibited. A Z-score ≥ 2 (activated) or ≤ –2 (inhibited) was considered significant. The activation z-score is used to infer likely activation states of upstream regulators based on comparison with a model that assigns random regulation directions (319) Additional details can be found on (331).

4.3 Results

4.3.1 Distribution Analysis for RNAseq data

To compare the general characteristics of the dataset i.e. compare the distribution of gene expression between the two groups (KI/KI and WT) and individual animals, box plots for gene expression were created (Figure 4-2).

Though there were slight variations in median comparable distributions were found as indicated by box sizes and box plot whiskers. Although all arrays are scanned with the same scanner the distributions of signal intensities between arrays is not the same.

The comparability of intensities is achieved by normalization. This is achieved by aligning the distribution of intensities of all arrays by cantering medians and adjusting scale to the same value.

The results after normalization show no difference between the groups. Furthermore, whiskers sizes (+/−1.5 of the interquartile values representing more than 95% of the data in our distributions) were similar between the groups. These results indicate that the knock-in mutation did not have a profound effect at the genome-wide expression level.

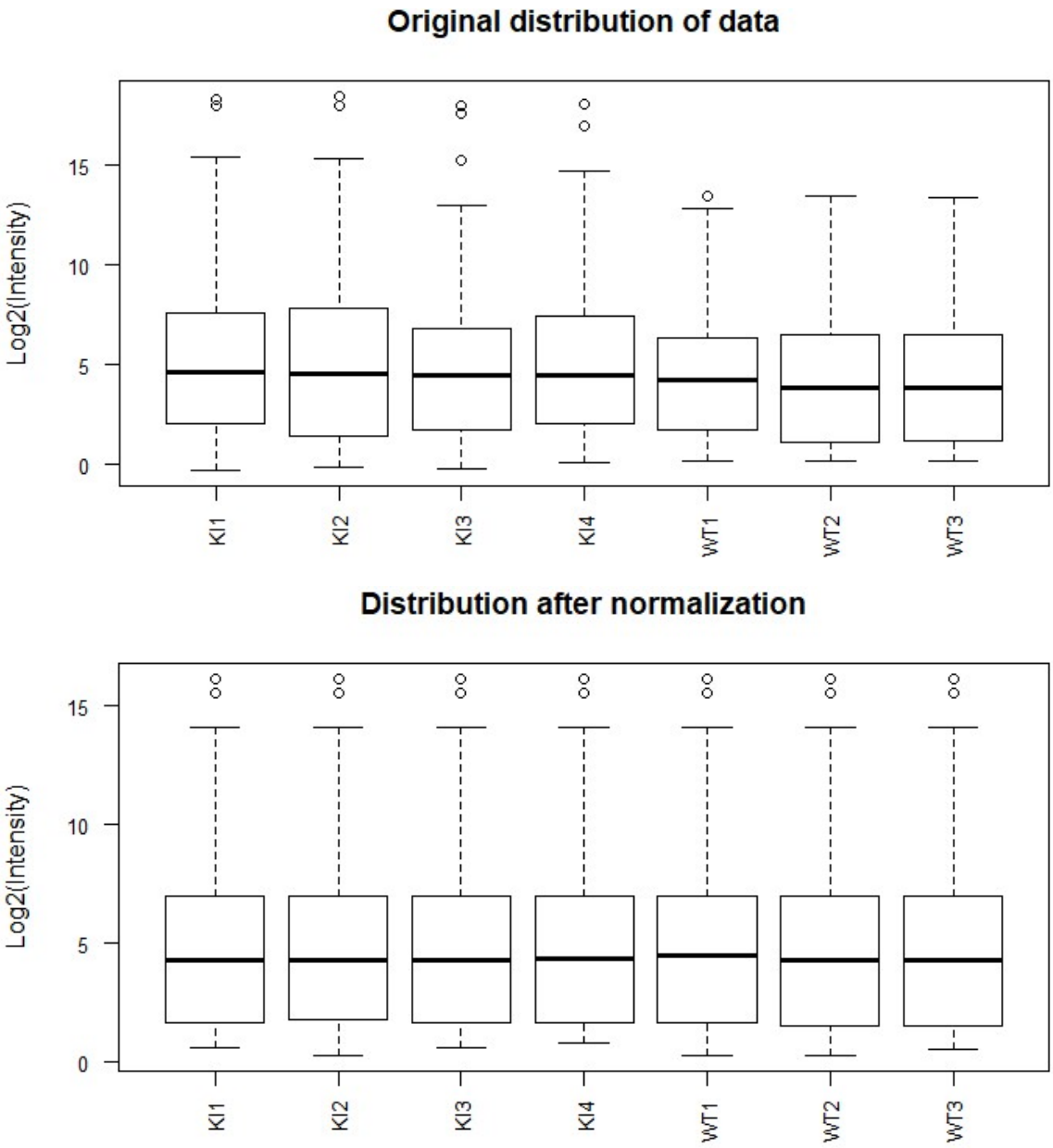


Figure 4-2. Distributions of the RNAseq datasets using Box plot representations. Box plot representing expression level distributions **a)** before normalization **b)** after normalization of log2 fold changes of intensity of reads for all animals in the KI/KI and WT groups. The box plot representation defines 25th to 75th percentiles (boxes), 50th percentile (lines in boxes) and ranges (whiskers, 1.5 times the interquartile range extended from both ends of the box or the maximal/minimal value). The outliers are represented by empty circles.

4.3.2 Sample Distance Matrix and PCA Plot

To assess the similarity between samples of a group, which samples are similar, and which are different a sample distance matrix is used. Euclidean distance between

samples is calculated and to ensure equal contribution from all genes the values used are from rlog-transformed data and hierarchical clustering is performed. Fig 4-3a highlights that transcripts from KI/KI and WT animals were similar within their groups but distinct from each other. The clusters are further divided by gender, highlighting potential differences in transcriptome as a result of gender difference.

Another way to visualize sample-to-sample distances is a principal component analysis (PCA). In PCA samples are represented on a 2D plan such that they spread out in the two directions that highlight most of the variance across samples. The xaxis, labelled as PC1, is the direction that the samples are separated by the most. Fig 3b shows that separation at PC1 is the difference between KI/KI and WT animals. This highlights that genes that contribute to the separation in PC1 are the ones in which the KI/KI and WT samples show strong differences in their transformed counts. The yaxis is the direction that separates the data the second most. The coordinates of the samples in this direction are written PC2. In the current dataset the second direction separates samples by gender. The percent of the total variance in each PC is expressed in the axis. Note that these percentages do not add to 100%, because there are more directions that contain the remaining variance. Since PC1 and PC2 combined form 91% variance the remaining dimension will explain the difference less than the two that observed.

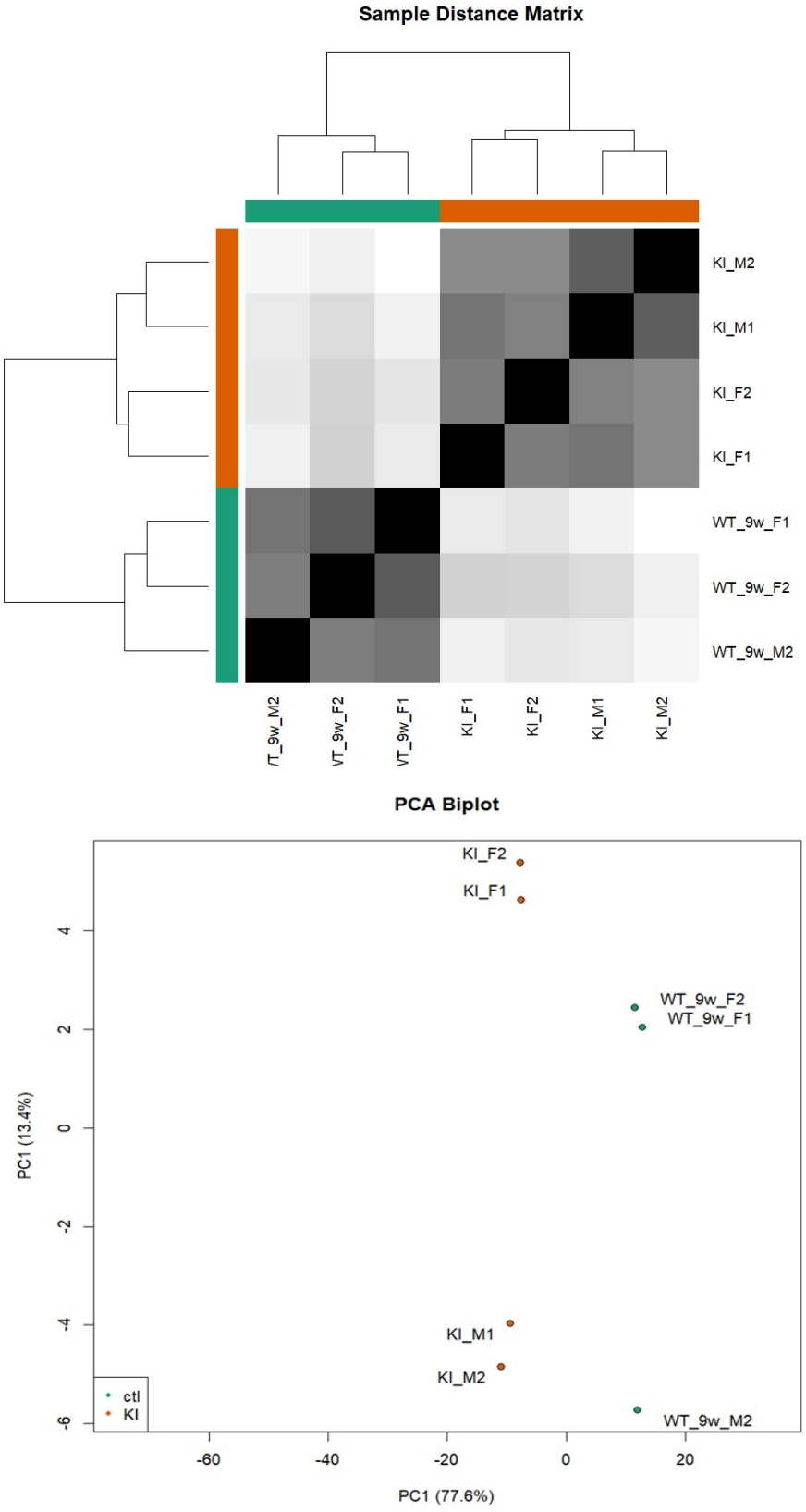


Figure 4-3. Comparison of RNA transcriptome profiles between KI/KI and WT mice **a)** Relationship of transcriptome profiles among KI/KI and WT samples. Sample-to-sample Euclidean distance matrix with hierarchical clustering using rlog-transformed read counts of all detected transcripts **b)** PCA plot clearly demonstrates clustering of animal transcriptomes reflective of their genetic origin and sex.

4.3.3 Highlighting Significant genes in pairwise comparisons

The MA-plot visualizes the differences between measurements taken between two samples and therefore is useful to visualize the reproducibility between samples. The differences are highlighted by plotting the log-fold change (M-values, i.e. the log of the ratio of level counts for each gene between two samples) against the log-average (Avalues, i.e. the average level counts for each gene across the two samples). The MAplot for comparison between KI/KI and WT (Fig. 4-4a) samples indicate that the genes in both groups show similar expression as they appear around the horizontal line y = 0. The outlier genes i.e. the differentially expressed genes are highlighted in red with those having a positive log-fold change having a higher expression in KI/KI animals and similarly those exhibiting negative log fold change having reduced expression in knock-in animals.

To assess the most meaningful changes in expression between groups a volcano plot can be utilized (Fig. 4-4b). The y axis represents the negative log of the p value. This means that data with low p-value (highly significant) appear at the top of the plot. The x axis is the log of the fold change between the two conditions. The genes with a positive log fold change have increased expression in KI/KI animals and those with negative value have reduced expression in KI/KI, compared with WT animals. The red dots highlight genes with a p-value of less than 0.05 which is the value set for false discovery rate. The yellow dots represent genes with a log 2 fold change of greater than 1 or less than -1. The green dot represent the genes with both a p-value less than 0.05 and a log 2 fold change greater than 1 or lesser than -1.

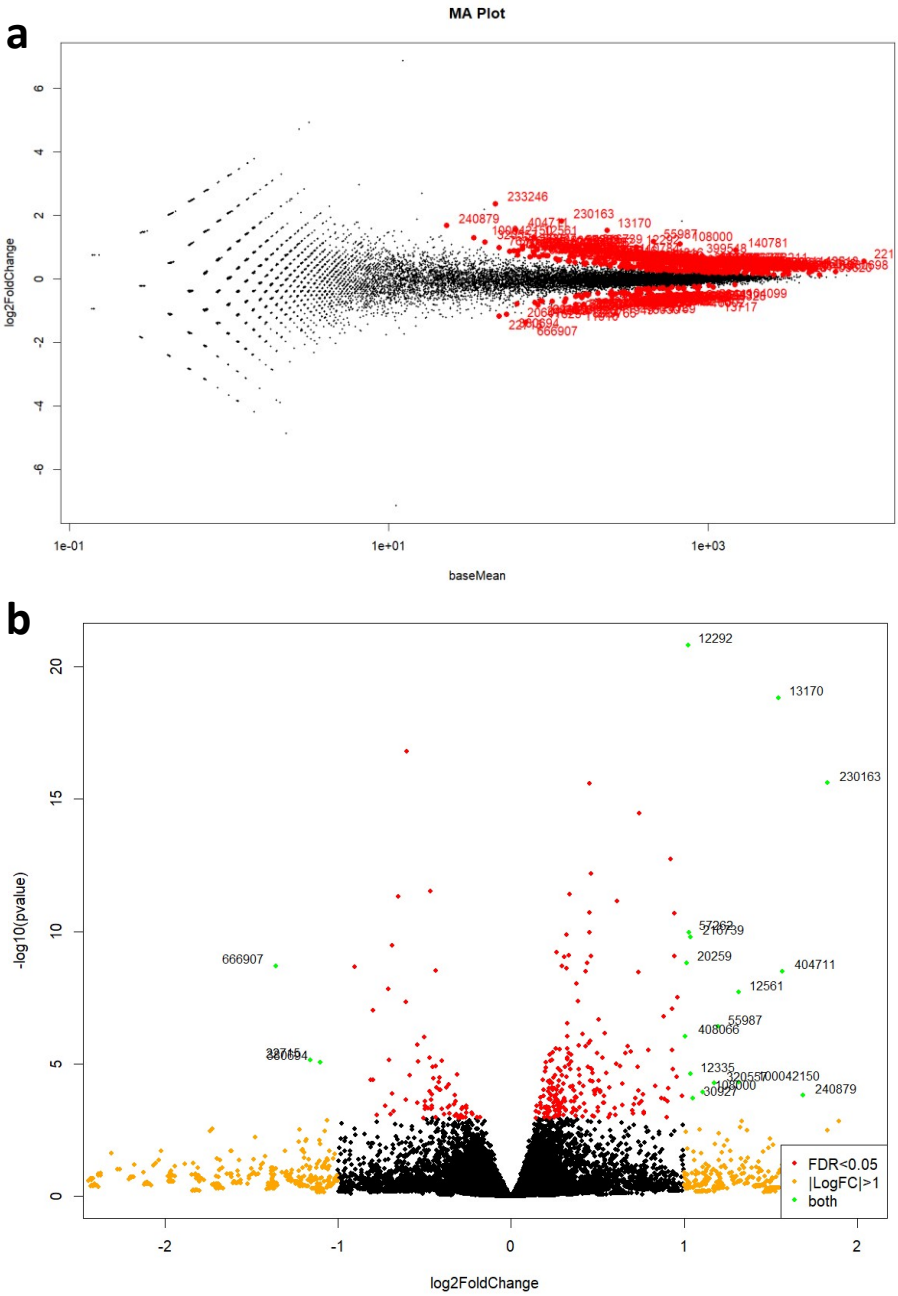


Figure 4-4. Comparisons of all genes assessed in RNAseq analysis of RNA extracted from mouse heart left ventricles of WT (n=3) and KI/KI (n=4). **A)** MA-plot represents an overview of the differentially regulated genes. Y-axis represent log-fold change or M-values which is the log of the ratio of level counts for each gene between two samples. X-axis represents the log-average or Avalues which is the average level counts for each gene across the two samples. **B)** The volcano plot displays the relationship between fold-change and significance between the two groups using a scatter plot view. The y-axis is the negative log10 of P values (a higher value indicates greater significance) and the x-axis is the difference in expression between two experimental groups. Significant genes are labelled green on the plot having a FDR t test < 0.05 and log 2 FC of greater or less than 1.

4.3.4 Differentially Expressed Genes between KI/KI and WT animals

RNAseq analysis were performed using the pipeline mentioned in methods and differential gene expression was analysed. The expression of genes was compared between WT and KI/KI animals and a total of 624 genes were found to be significantly different (both up and down regulated) in KI/KI animals when compared to WT animals (appendix). A heat map was constructed to highlight the 50 most differentially expressed genes between the groups (Figure 4-5). Table 4-3 provides detailed data for these genes.

Upregulated			**Downregualted**		
Gene	**logFC**	**p-value**	**Gene**	**logFC**	**p-value**
Syndig1	7.243	3.24E-27	Scd4	-3.952	2.52 E-50
Ankrd2	6.400	2.01E-14	Rtn4r	-3.422	1.95 E-11
Chodl	5.698	2.94E-32	Pfkfb1	-3.133	1.01 E-37
Col9a2	5.047	9.85E-75	Acot1	-2.939	1.08 E-51
Nppa	4.857	6.02E-67	Urah	-2.752	3.96 E-07
Acta1	4.823	0	Igfals	-2.736	1.82 E-29
Frem1	4.785	1.54E-96	Tg	-2.655	3.02 E-15
Serpinb1c	4.628	2.26E-82	Pdzrn4	-2.599	4.57 E-10
Fgf6	4.619	2.82E-09	Shisa6	-2.503	1.55 E-07
Thbs4	4.587	5.26E-164	Mylk4	-2.445	1.81 E-19
Tmem200a	4.368	3.15E-22	Epn3	-2.388	1.59 E-11
Myh7	4.214	2.03E-64	Retnla	-2.346	5.76 E-20
Gcnt4	4.083	5.67E-20	Fbp2	-2.338	2.08 E-50
Crlf1	4.058	4.53E-57	Lypd2	-2.258	4.26 E-09
Edn3	4.007	5.62E-22	Lgi1	-2.198	2.25 E-08
Lrp8	3.938	3.43E-55	Whrn	-2.171	8.29 E-35
Cilp	3.930	1.27E-154	Clcn1	-2.120	1.44 E-04
Tbx15	3.929	1.00E-19	Gabrr2	-2.046	1.12 E-08
Myom3	3.832	1.97E-29	Pla2g5	-2.045	3.64 E-37
Ptx4	3.758	1.39E-12	Ano10	-2.037	1.49 E-48
Lman1l	3.706	2.43E-49	Sord	-1.985	4.09 E-54
Lamc3	3.650	2.20E-38	Agt	-1.965	2.54 E-09
Tnmd	3.602	6.74E-22	Dbh	-1.964	6.33 E-15
Rbp4	3.555	3.50E-28	Fam222a	-1.963	4.57 E-10
Kcnc1	3.511	1.37E-08	Kcnv2	-1.962	1.30 E-29

Table 4-3. Differential gene expression in KI/KI compared to WT animals. Top 25 most upregulated and downregulated genes present in KI/KI animals using criteria i) normalized read count > 2 copies/million reads in the RNA-seq library, (ii) log2 fold-change > 1 (upregulated) or < –1 (downregulated), and (iii) P < 0.001

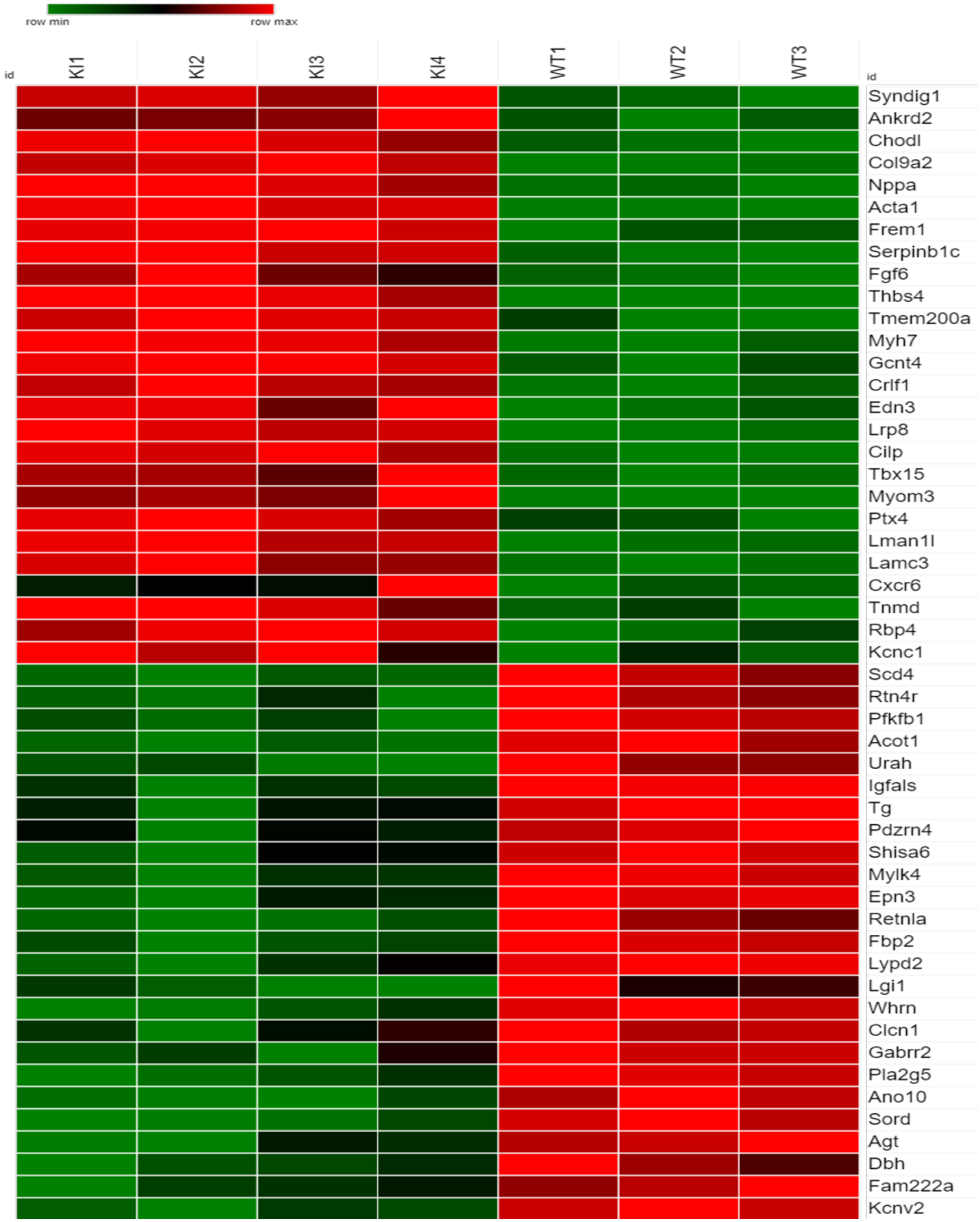
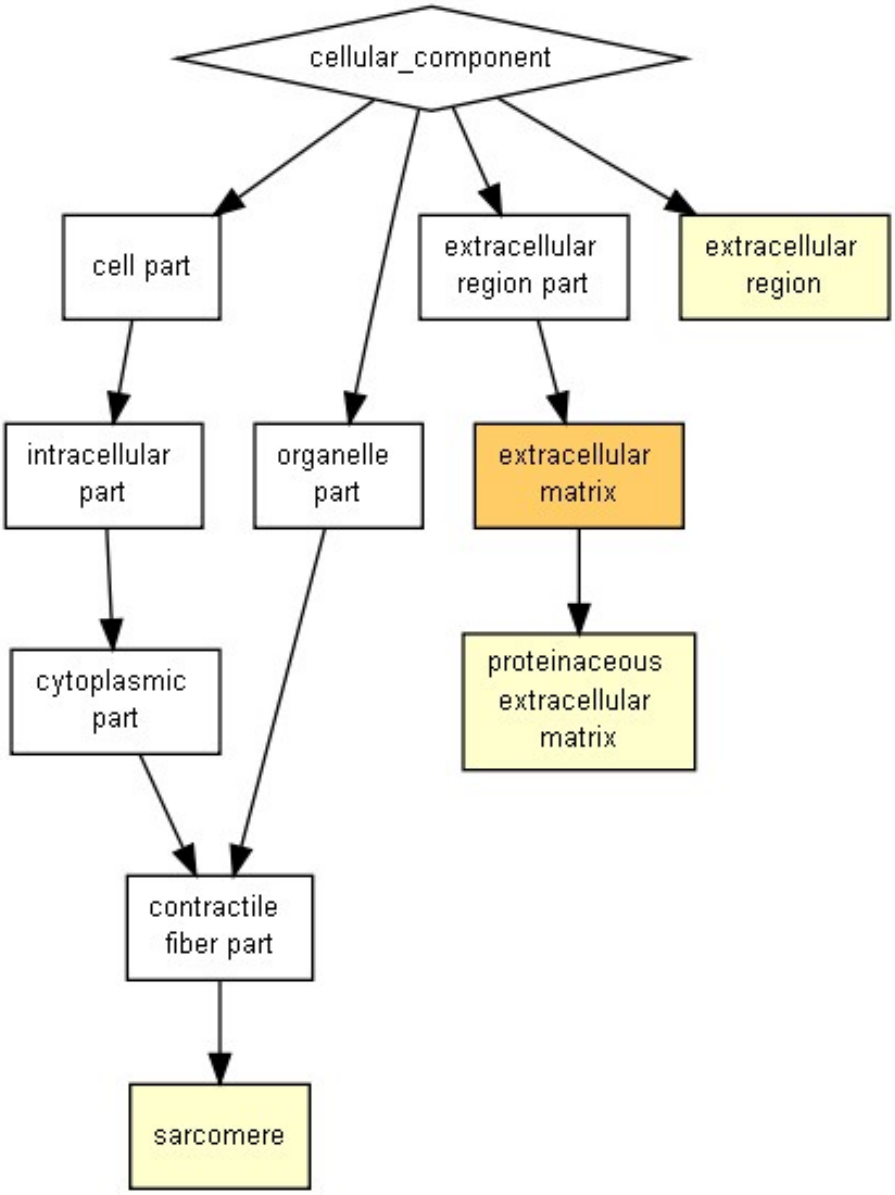


Figure 4-5. Heatmap of top 50 differentially expressed genes. Heatmap to represent the genes that are most upregulated and downregulated. Relative levels of gene expression are represented using a colour scale: Green represents downregulated genes and red represents upregulated gene levels.

4.3.5 RNASeq Gene Ontology Analysis

To determine the biological coherence of the set of genes found to be significant GO enrichment analysis using *GOrilla* was performed. Single Rank List method was used in which only significantly differentially expressed genes ($p>0.001$, l2fc >1 or <-1) were used. The degree of enrichment = (b/n)/(B/N), with (N, B, n, b) defined as follows: N is the total number of genes, B is the total number of genes associated with a specific GO term, n is the number of genes in the target set, b is the number of genes in the intersection.

The most enriched GO cellular components was the sarcomere with an enrichment score of 37 (Fig. 4-6a, 4-6c). Other significant ($p<0.01$, FDR<0.10) cellular components were extracellular matrix, proteinaceous extra cellular region and extracellular region. The most enriched GO biological process was regulation of heart rate (Fig. 4-6b, 4-6d). Other significant processes included regulation of cell proliferation, development process, anatomical structure development and negative regulation of biological process.

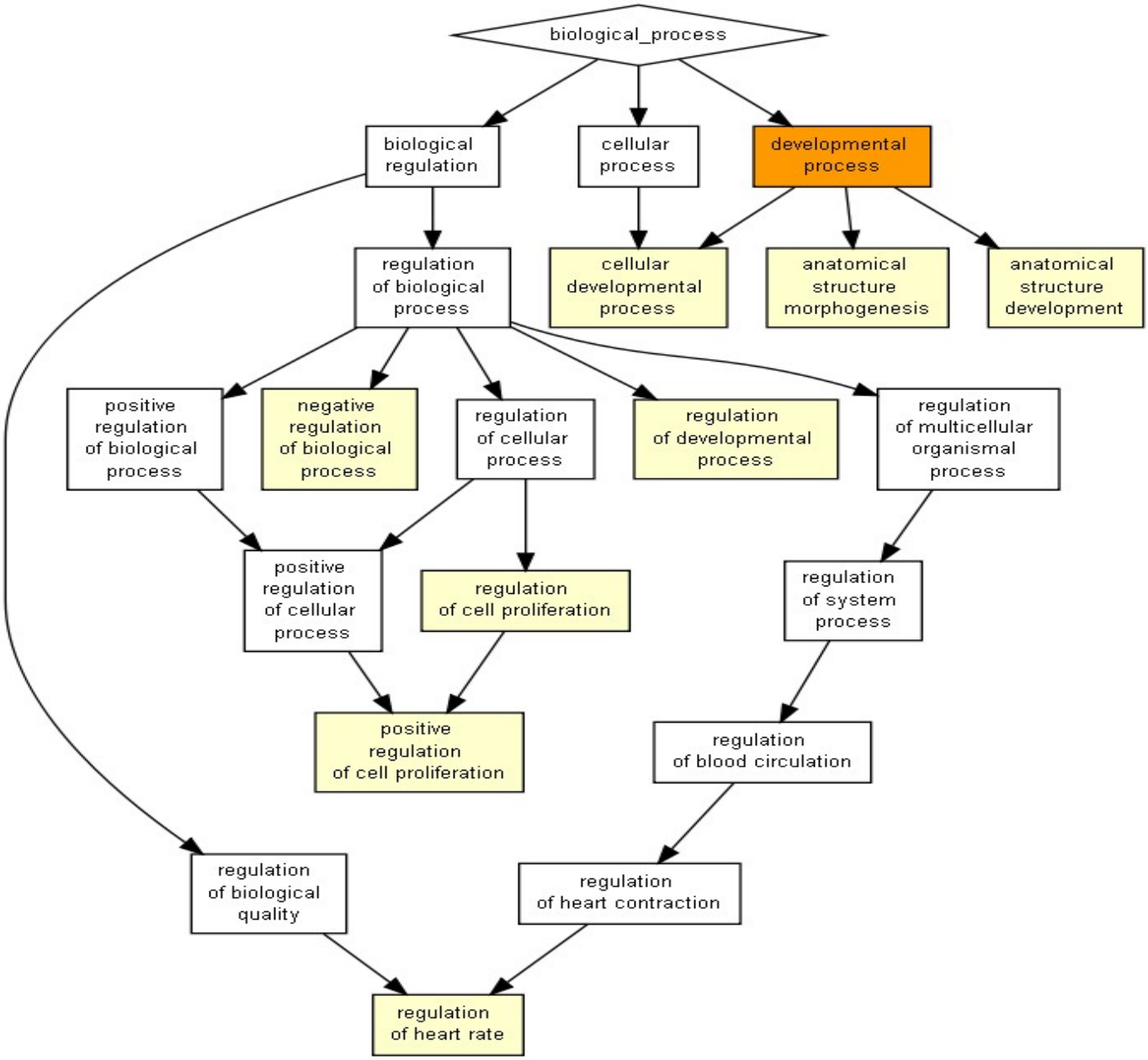


a

P-value colour scale

$>10^{-3}$	10^{-3} to 10^{-5}	10^{-5} to 10^{-7}	10^{-7} to 10^{-9}	$< 10^{-9}$

b



P-value colour scale

$>10^{-3}$	10^{-3} to 10^{-5}	10^{-5} to 10^{-7}	10^{-7} to 10^{-9}	$< 10^{-9}$

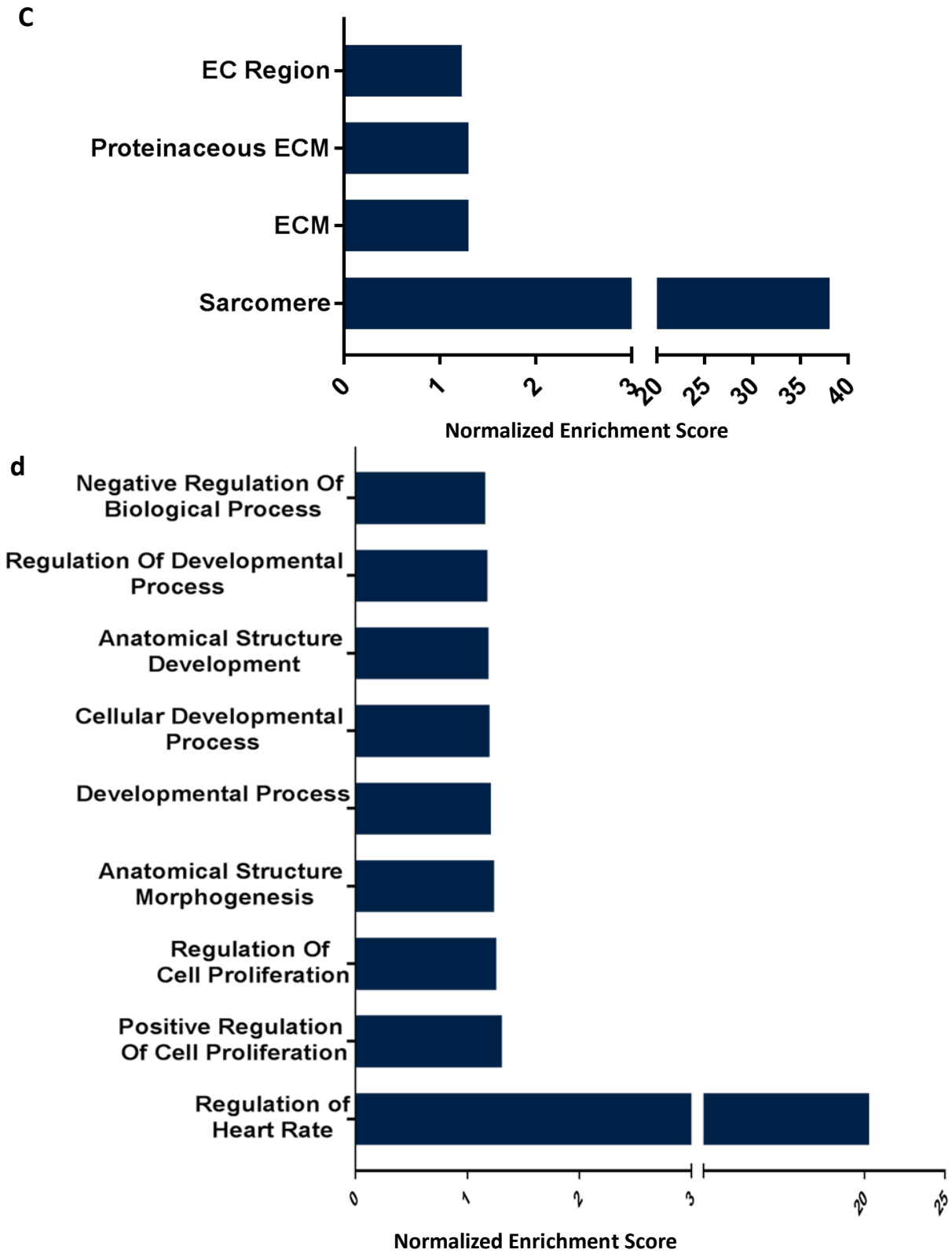


Figure 4-6. GO term enrichment analysis of genes with significant abundance changes. Significant differentially regulated genes ($p<0.001$, log 2 fold change >1 or <-1, >2 RPKM) were taken as input for the GOrilla web-server. Top panel shows functional enrichment map for **(a)** GO Component and **(b)** GO Process. The colour of each box represents associated p-value. **(c)** and **(d)** Highlights the enrichment scores of statistically significant GO terms for (a) and (b) respectively.

4.3.6 Upstream Regulator analysis with IPA

The upstream regulator analysis (URA) tool is a novel function in IPA which can, by analysing linkage to differentially expressed genes through coordinated expression, identify potential upstream regulators including transcription factors (TFs), kinases or any gene or small molecule that has been observed experimentally to affect gene expression. To identify significant upstream regulators only molecules with expression fold change greater to or lesser than 2, confirmed activation status (activated/inhibited) and a p-value less than 0.01 were selected. Sorting by p-value the five upstream transcription factor regulators were *TWIST1, RUNX2, ETV5, GLI2* and *PITX2* (Table 4). The top upstream kinase regulators included *CTGF, AGT, DIO2, CXCR3, BCL2, CNR1, AGER* (Table 5).

Upstream Regulator	Expr Fold Change	Predicted Activation State	Activation z-score	p-value of overlap	Target molecules in dataset
TWIST1	2.339	Activated	3.176	1.71E-18	ACTA2, ALDH1A1, APOD, BCL2, C3, CHI3L1, COL1A1, DCN, DKK3, DNM1, EMILIN1, FIBIN, FMOD, FN1, IL6, ITGB5, MME, MMP2, MRC2, MXRA8, OLFML3, PAM, PAMR1, PCOLCE, DGFRA, PRRX2, RUNX2, SPHK1, SPP1, TGFBI, UNC5B, VCAN
RUNX2	3.607	Activated	2.624	4.55E-07	ACTA2, BCL2, COL11A1, COL1A1, COL1A2, FN1, ITGBL1, LUM, MMP14, MMP2, RUNX2, SOST, SPP1, TG, TIMP1, TNFRSF11B
ETV5	2.158	Activated	2	2.67E-03	CLDN1, ETV5, FN1, MMP2, SPP1, TWIST1
GLI2	2.555	Activated	2.392	9.17E-03	BCL2, BMP4, GLI2, IL6, MEOX1, RUNX2, SOX9, SPP1
PITX2	-2.565	Inhibited	-2.165	1.09E-02	COL1A2, FGF16, FZD2, FZD9, KCNK2, NDUFB4, NPPA, SHOX2, TBX15

Table 4-4; Upstream regulators transcription factors and their target. TWIST1 (Twist Family BHLH Transcription Factor 1), RUNX2 (Runt Related Transcription Factor 2),

ETV5 (ETS Variant 5), GLI2 (GLI Family Zinc Finger 2), PITX2 (Paired Like Homeodomain 2).

Upstream Regulator	Expr Fold Change	Molecule Type	Predicted Activation State	Activation z-score	p-value of overlap	Target molecules in dataset
TGFB2	3.485	Growth Factor	Activated	2.747	2.18E-13	ACTA2, ASPN, BMP4, CNN1, COL1A1, COL1A2, CTGF, EGR2, FMOD, FN1, HBEGF, ID4, ITGB5, PDK4, SCD, SPHK1, SPP1, TGFB2, THBS1, TIMP1, TNFRSF11B, VCAN
CTGF	7.474	Growth Factor	Activated	2.782	4.19E-07	BCL2, COL1A1, COL8A1, CTGF, DCN, EMILIN1, FN1, FZD2, IL6, LOX, LTBP3, MMP14, MMP2, SFRP4, TIMP1
AGT	-3.892	Growth Factor	Activated	3.318	4.56E-07	ACE, ACTA1, ACTA2, AGT, ANGPT1, BCL2, BGN, CGREF1, COL1A1, COL1A2, COL4A6, CTGF, EREG, FN1, HBEGF, IL6, ITGB5, LDLR, MGST1, MMP2, MYH7, NOS1, NOVA1, NOX4, NPPA, Nppb, POSTN, SLC1A1, SPP1, SRGAP3, STAR, TGFB2, TGFB3, TIMP1
DIO2	6.569	Enzyme	Inhibited	-2.186	4.14E-04	HCN2, MYH7, NPPA, SLC1A3, SLN, TG
CXCR3	2.112	GPCR	Inhibited	-2	1.01E-03	BCL2, COL1A1, FN1, TNC
BCL2	2.232	transporter	Activated	2.155	1.20E-03	BCL2, CKM, IGFBP6, IL6, MMP2, SCG3, SOX9, SPHK1, TGFB2, TIMP1
CNR1	5.893	GPCR	Activated	2.332	8.74E-03	APBB1, BMP4, BMP7, CA9, IL6, MDK, MSX1, PDGFRA, PENK, TIMP1
AGER	2.027	Trans-membrane receptor	Activated	2.111	1.89E-02	BCL2, CKM, CTSK, IL6, MMP2, TNC

Table 4-5; Other Upstream regulators and their targets. TGFB2 (Transforming Growth Factor Beta 2), CTGF (Connective Tissue Growth Factor), AGT (Angiotensin II), DIO2 (Iodothyronine Deiodinase 2), CXCR3 (CXC chemokine receptor family 3), BCL2 (Bcell lymphoma 2), CNR1 (Cannabinoid Receptor 1), AGER (Advanced Glycosylation End-Product Specific Receptor), GPCR (G- Protein Coupled Receptor).

4.3.7 KEGG Analysis of transcriptome

RNAseq data was analysed using GSEA software to identify significant gene sets. Using a cutoff value of p<0.01, and The False Discovery Rate (FDR) of <0.10 six significant pathways were found. The pathways along with NES (Normalized Enrichment Score) which computes the density of modified genes in the dataset with the random expectancies, normalized by the number of genes found in a given gene cluster, to consider the size of the cluster, are presented in Figure 4-7**.** The most enriched KEGG pathways were extracellular matrix receptor interaction, cell and focal adhesion molecules, transforming growth factor (TGF) beta signalling, glycosaminoglycan biosynthesis and hypertrophic cardiomyopathy.

Enrichment pathways of significant enriched pathways as generated by GSEA are shown in Figure 4-8.

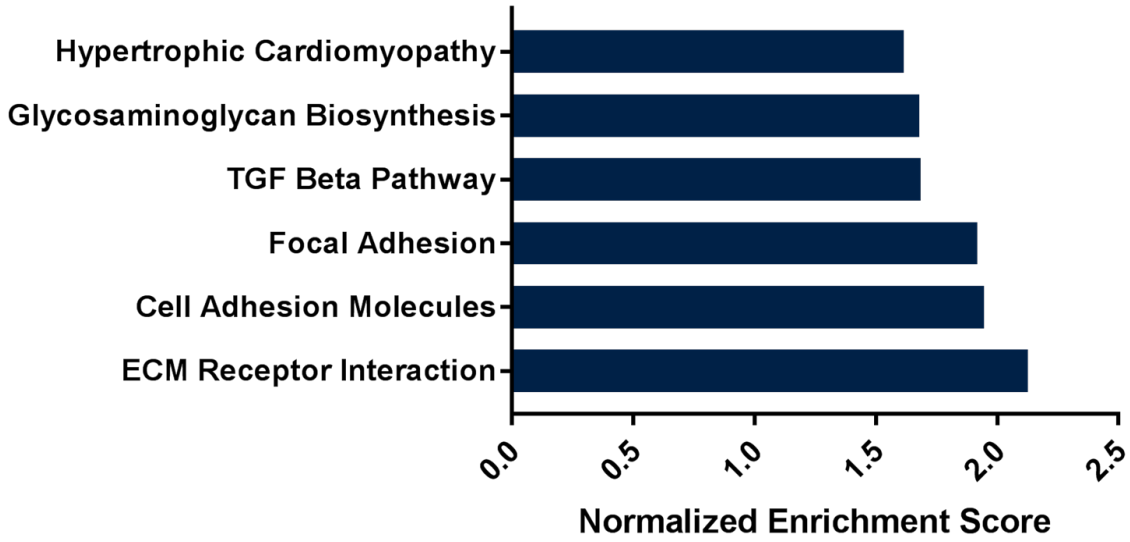


Figure 4-7: KEGG enriched pathways among differentially expressed genes in KI/KI compared to WT. Graph shows Normalized Enrichment Score for KEGG pathways as determine by GSEA.

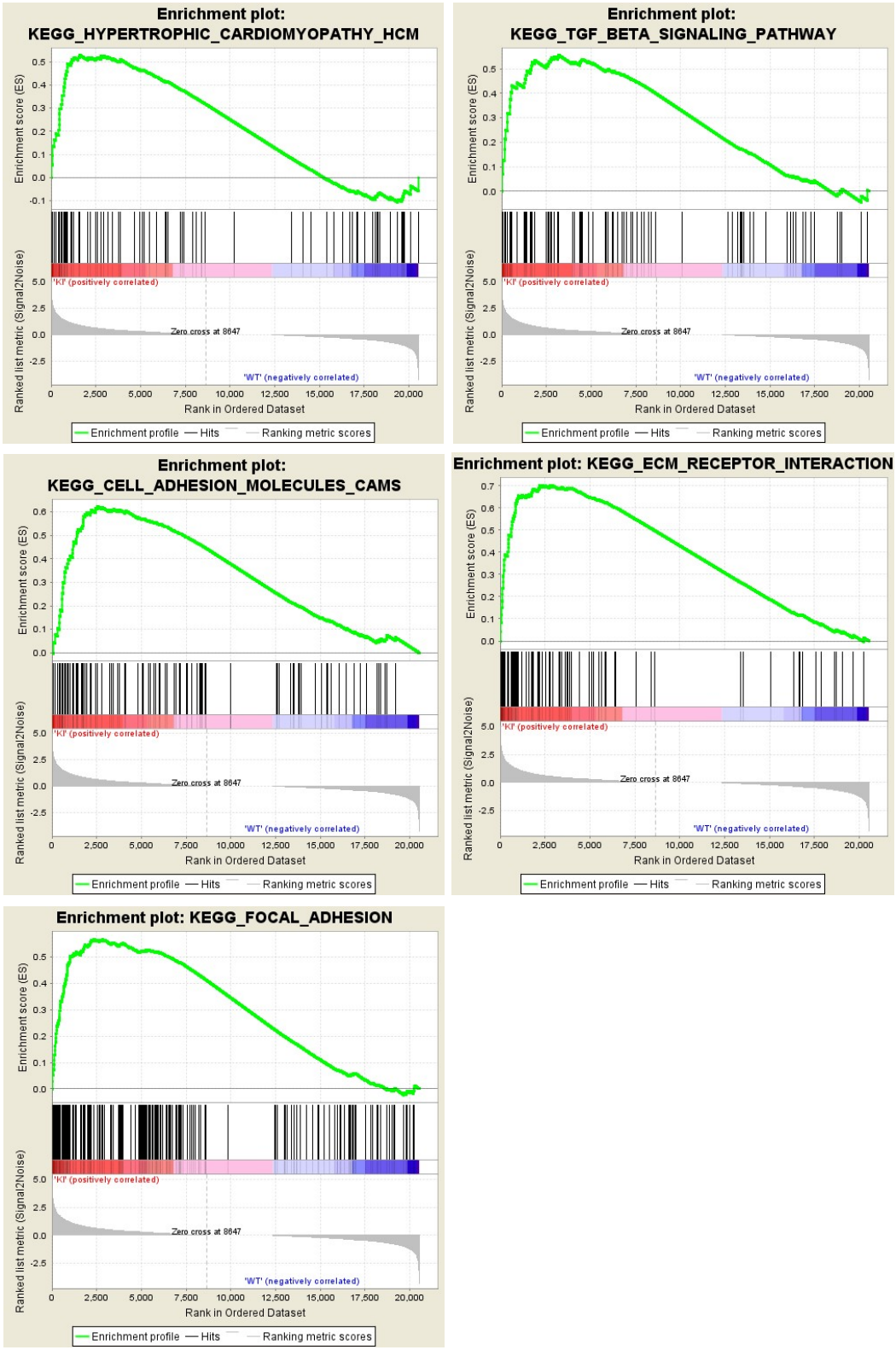


Figure 4-8. Enriched pathways identified by GESA analysis. GSEA of KEGG pathways enriched with genes that are differentially regulated in KI/KI hearts (n=4) compared to WT (n=3) hearts. The bars represent genes included in the pathway, which are sorted by their differential expression from the most up-regulated in KI/KI hearts (left) to the most down-regulated ones (right). The green curve corresponds to the GSEA enrichment score.

4.3.8 Sample Distance Matrix and PCA Plot for KO and WT animals

Similarity distance matrix for KO and WT transcripts (Fig 4-9a) highlighted that transcripts from KO and WT animals were similar within their groups but different from each other. Similar to KI/KI dataset the samples are further divided by gender.

PCA plot (Fig 4-9b) highlights the biggest separation between samples to be because of knockout of gene i.e. the difference between KO and WT animals. Similar to KI/KI data set the y-axis is the direction that separates the data the based on sex of the animal. The percent of the total variance adds up to 93% in this case.

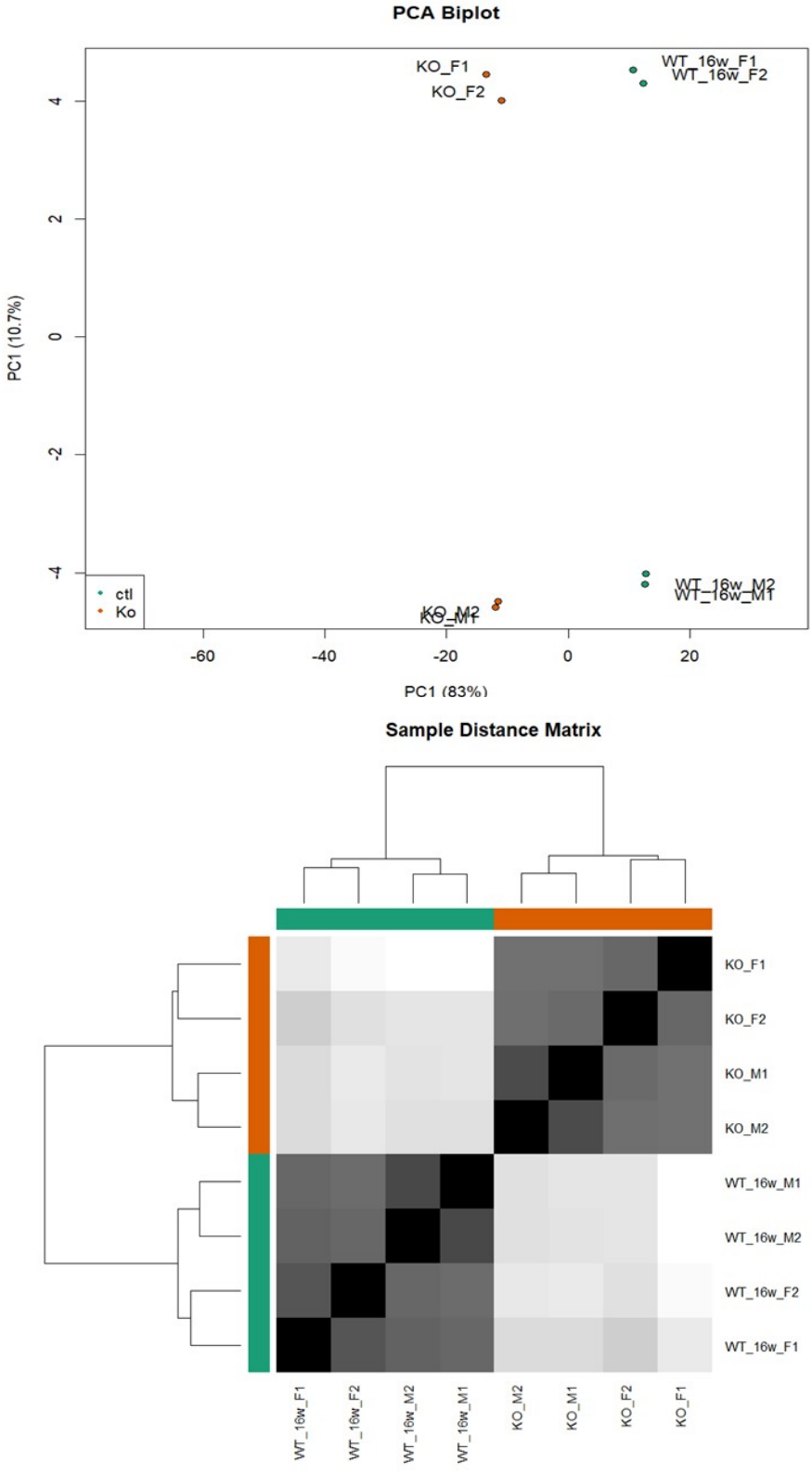


Figure 4-9. Comparison of RNA transcriptome profiles between KO and WT mice **a)** Relationship of transcriptome profiles among KO and WT samples. Sample-to-sample Euclidean distance matrix with hierarchical clustering using rlog-transformed read counts of all detected transcripts **b)** PCA plot clearly demonstrates clustering of animal transcriptomes reflective of their genetic origin and sex.

4.3.9 Highlighting Significant genes in pairwise comparisons

The MA-plot for comparison between KO and WT (Fig. 4-10a) samples indicate that the number of genes differentially regulated, and the degree of change is far greater than that observed in comparison of KI/KI to WT transcriptome. Using the criteria for differentially expressed genes there are 835 genes that are differentially expressed in KO mice when compared to WT mice as opposed to 622 genes in the comparison with KI/KI mice. Genes that show similar expression between KO and WT animals appear around the horizontal line y = 0 and the outlier genes i.e. the differentially expressed genes are highlighted in red with those having a positive log-fold change having a higher expression in KO animals and similarly those exhibiting negative log fold change having reduced expression in KO animals. The numbers represent Gene ID numbers.

To assess the gene expression changes in terms of significance a volcano plot is made (Fig. 4-10b) where gene log fold change is plotted against the negative log of the p value. The red dots highlight genes with a p-value of less than 0.05 which is the value set for false discovery rate. The orange dots represent genes with a log 2 fold change of greater than 1 or less than -1. The green dot represent the genes with both a p-value less than 0.05 and a log 2 fold change greater than 1 or lesser than 1. As highlighted before this plot helps visualize the significant differentially expressed genes which are far greater in the comparison of KO mice to WT mice when compared with the results of KI/KI animals.

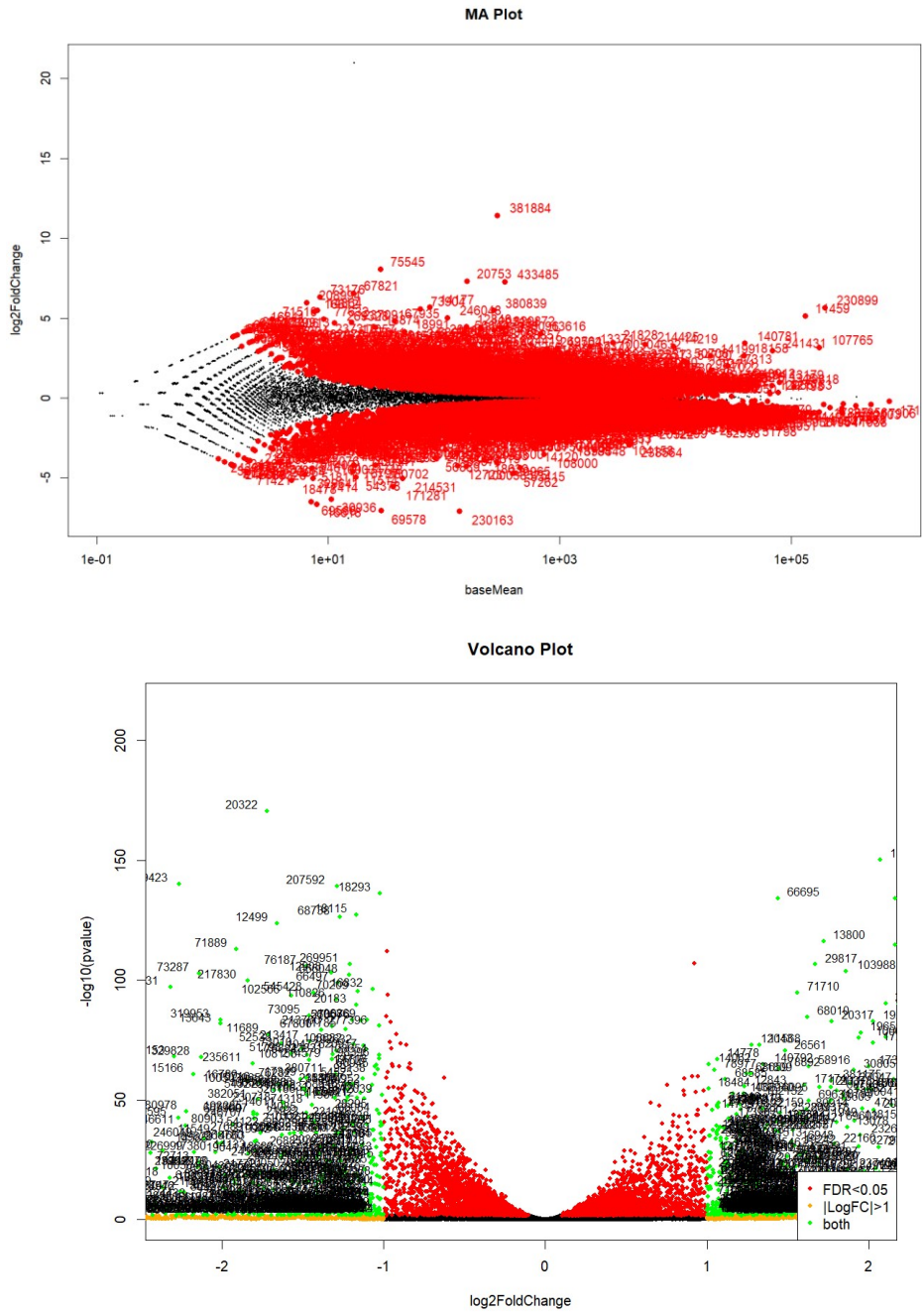


Figure 4-10. Comparisons of all genes assessed in RNAseq analysis of RNA extracted from mouse heart left ventricles of WT (n=4) and MLP KO (n=4). **A)** MA-plot represents an overview of the differentially regulated genes. Y-axis represent log-fold change or M-values which is the log of the ratio of level counts for each gene between two samples. X-axis represents the log-average or Avalues which is the average level counts for each gene across the two samples. **B)** The volcano plot displays the relationship between fold-change and significance between the two groups using a scatter plot view. The y-axis is the negative log10 of P values (a higher value indicates greater significance) and the x-axis is the difference in expression between two experimental groups. Significant genes are labelled green on the plot having a FDR t test < 0.05 and log 2 FC of greater or less than 1.

4.3.10 Differentially Expressed Genes between KO and WT animals

RNAseq analysis were performed using the pipeline mentioned in methods and differential gene expression was analysed. The expression of genes was compared between WT and KO animals at the age of 16 weeks and a total of 835 genes were found to be significantly different (both up and down regulated) in KO animals when compared to WT animals (appendix). A heat map was constructed to highlight the 50 most differentially expressed genes between the groups (Figure 4-11). Table 6 provides detailed data for these genes.

Upregulated Genes			Downregualted Genes		
Gene	**Log2FC**	**p-value**	**Gene**	**Log2FC**	**p-value**
Syndig1	7.286	2.98E-76	Retnla	-4.704	2.59E-153
Nppa	5.645	2.85E-171	Htatip2	-4.343	1.18E-189
Serpinb1c	5.479	1.11E-105	Clcn1	-4.225	1.22E-73
Acta1	5.161	5.00E-199	Scd4	-4.027	4.27E-26
Col9a2	4.489	2.82E-70	Pfkfb1	-3.876	2.09E-77
Frem1	4.359	5.07E-110	Lgi1	-3.760	7.58E-40
Crlf1	4.301	1.47E-29	Cenpf	-3.514	4.40E-212
Tbx15	4.250	7.65E-117	Rtn4r	-3.422	7.10E-36
Pou3f1	4.161	1.82E-21	Slc22a3	-3.260	9.59E-66
Ankrd2	4.081	5.16E-53	Gm11992	-3.223	1.83E-12
Edn3	4.032	3.37E-55	Igfals	-3.206	7.54E-55
Shisa3	4.023	2.19E-156	Acsm5	-3.120	5.18E-18
Lrp8	3.963	1.07E-88	Fbp2	-3.118	7.82E-79
St8sia1	3.839	3.24E-39	Helt	-3.117	3.68E-15
Lman1l	3.798	6.41E-88	Tmem150c	-3.042	9.04E-35
Rbp4	3.751	1.66E-47	Ccl11	-3.018	1.92E-09
Adamts20	3.698	3.13E-45	Sun3	-3.017	3.30E-10
Adamts8	3.691	5.78E-79	Tg	-2.969	5.21E-21
Ngef	3.629	2.93E-29	Mylk4	-2.873	3.37E-43
Fam180a	3.559	3.52E-60	Acot1	-2.856	8.49E-34
Gcnt4	3.547	3.26E-23	Poln	-2.852	9.46E-38
Nlrc3	3.507	4.39E-133	Pla2g5	-2.779	1.32E-91

Thbs4	3.469	7.89E-31	Scn4b	-2.770	5.49E-97
Rab33a	3.459	7.67E-10	Aqp4	-2.762	3.51E-38
Myh7	3.427	6.31E-28	Lrrc52	-2.760	1.67E-11

Table 4-6 Differential gene expression in KO compared to WT animals. Top 25 most upregulated and downregulated genes present in KI/KI animals using criteria i) normalized read count > 2 copies/million reads in the RNA-seq library, (ii) log2 fold-change > 1 (upregulated) or < –1 (downregulated), and (iii) P < 0.001

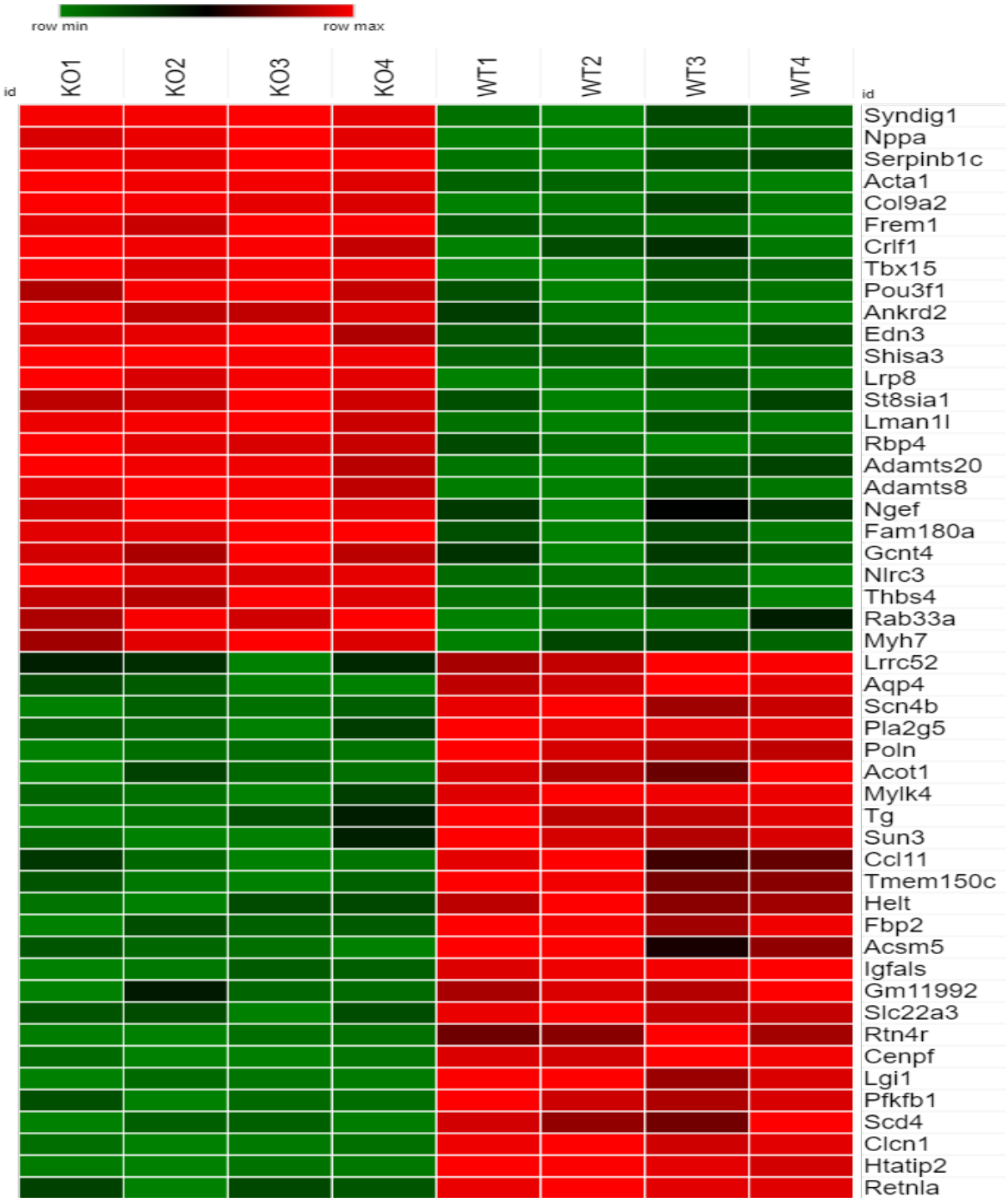
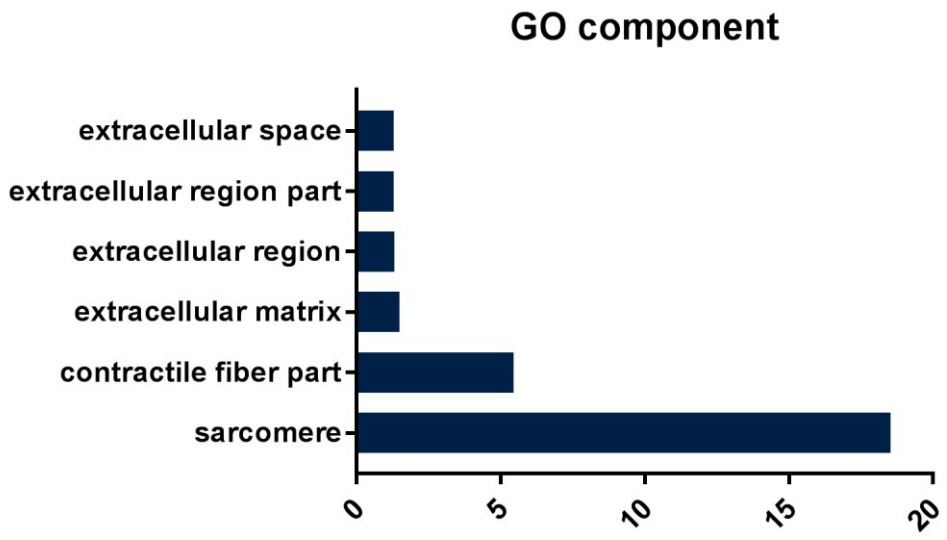


Figure 4-11. Heatmap of top 50 differentially expressed genes. Heatmap to represent the genes that are most upregulated and downregulated. Relative levels of gene expression are represented using a colour scale: Green represents downregulated genes and red represents upregulated gene levels.

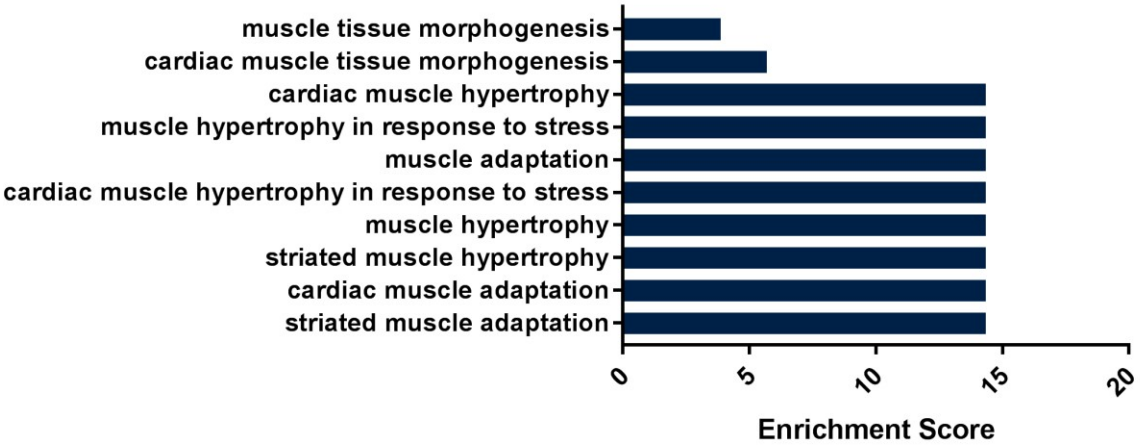
4.3.11 RNAseq Gene Ontology Analysis

To determine the biological coherence of the set of genes found to be significant GO enrichment analysis using the GOrilla program (was performed. Single Rank List method was used in which only significantly differentially expressed genes (p>0.001, l2fc >1 or <-1) were used.

The most enriched GO cellular components, similar to KI/KI, was the sarcomere with an enrichment score of 18.53. Other significant (p<0.01, FDR<0.10) are highlighted in the Figure 4-12a. Unlike KI/KI, there was no outright leading GO function. All significant functions are highlighted in the graph and table (Fig 4-12c). In contrast to GO analysis with KI/KI animals there was a significant GO function that was enriched in KO mice. This was cytoskeletal protein binding with an enrichment score of 1.29 (pvalue 6.89E-05 and FDR q-value of 9.09E-02)



Description	P-value	FDR q-value	Enrichment
sarcomere	9.19E-04	9.13E-02	18.53
contractile fibre part	3.24E-04	3.86E-02	5.45
extracellular matrix	1.53E-04	3.04E-02	1.49
extracellular region	3.16E-05	1.88E-02	1.32
extracellular region part	1.38E-04	4.12E-02	1.29
extracellular space	2.80E-04	4.17E-02	1.28



Description	P-value	FDR q-value	Enrichment
striated muscle adaptation	5.49E-04	1.35E-01	14.34
cardiac muscle adaptation	5.49E-04	1.29E-01	14.34
striated muscle hypertrophy	5.49E-04	1.25E-01	14.34
muscle hypertrophy	5.49E-04	1.20E-01	14.34
cardiac muscle hypertrophy in response to stress	5.49E-04	1.16E-01	14.34
muscle adaptation	5.49E-04	1.12E-01	14.34
muscle hypertrophy in response to stress	5.49E-04	1.08E-01	14.34
cardiac muscle hypertrophy	5.49E-04	1.05E-01	14.34
cardiac muscle tissue morphogenesis	5.59E-05	3.81E-02	5.71
muscle tissue morphogenesis	8.62E-04	1.23E-01	3.87

Figure 4-12. GO term enrichment analysis of genes with significant abundance changes. Significant differentially regulated genes ($p<0.001$, log 2 fold change >1 or <-1, >2 RPKM) were taken as input for the GOrilla web-server. Figure shows functional enrichment for (**a)** GO Component and **(b)** GO Function. The table associated highlights the P-value and False discovery rate (FDR) q-value in addition to the enrichment score.

4.3.12 Comparison of *CSRP3* KI/KI and KO transcriptomes

Two sets of RNA Sequencing analysis were performed, one on 16 week old KO (n=4) and 16 week old WT mice (n=4) and second on 9 week old KI/KI (n=4) and WT mice (n=3). Analysis in KI/KI compared to age matched WT controls and KO compared to age matched controls highlighted 622 and 835 differentially expressed genes respectively. To assess the overlap of genes and pathways contributing to underlying pathophysiology the difference in differentially expressed genes was visualized with Venn diagram (Fig 4-13). In comparison of upregulated genes there were 335 genes that were similar between KI/KI and KO animals with 185 and 119 genes that are upregulated only in KO and KI/KI animals, respectively. In the case of downregulated genes there were fewer genes (137) that were similar with KI/KI and KO animals having 31 and 249 genes that were downregulated differently, respectively.

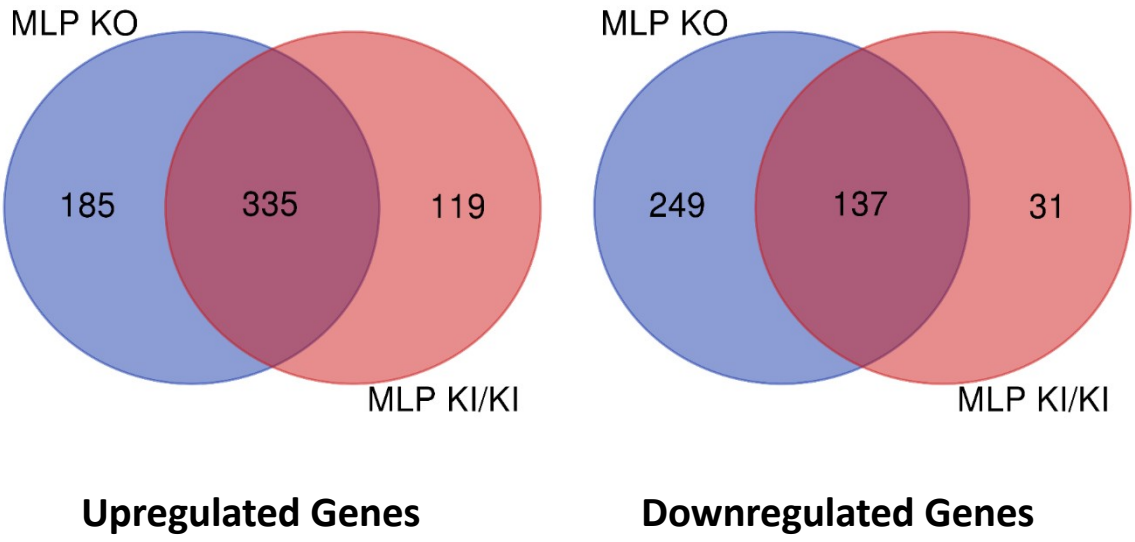


Fig. 4-13 Venn diagram to highlight the differences between KO and KI/KI datasets in terms of upregulated and downregulated genes.

4.4 Primary Conclusions of this Chapter:

1. KI/KI and KO have 622 and 835 differentially expressed genes when compared to age matched WT controls.
2. There is overlap and differences in the genes that are differentially expressed in KI/KI and KO animals.
3. Similarity distance matrix highlights that transcriptomes vary because of genetic background and sex of the animals.
4. GO pathways analysis highlight sarcomere and extracellular regions to be the regions which most differentially expressed genes are associate with, in both KI/KI and KO animals. There are similarities in GO Processes between the two datasets, however KO animals have enrichment of far more processes.
5. Ingenuity pathway analysis highlight novel transcription factors that are associated with the differential gene expression in KI/KI animals when compared to age matched WT controls.

4.5 Discussion

In this study RNAseq was used along with extensive bioinformatics analysis to characterize the transcriptome of Csrp3 C58G knock-in mice in an attempt to understand the underlying mechanisms driving the DCM phenotype. RNA was extracted from hearts of WT and KI/KI mice aged 9 weeks and 16 week old MLP KO mice and age matched WT controls. Sequencing was performed with Illumina HiSeq 2500 technology using single strand sequencing and sequencing depth of 50 million

reads. The results of differential gene expression and pathway analysis highlight the key genes in development of disease phenotype.

Initial quality control analysis showed a difference in transcript levels among the different individual animals. These differences can be attributed to biological differences but can also be caused due to different quantity of mRNA and minor differences in slightly different sample handling, even in a well standardized process (306, 307). The data was normalized to account for the differences between the groups. For normalization within conditions the results are normalized to replicated samples, in this case with data of other mice of same genotype. Normalization across groups was carried out, while preserving biological variability. After normalization the mean expression of all transcripts in KI/KI was not significantly different than WT animals highlighting no genome wide expression changes in left ventricles due to knock-in mutation.

The box plot representations (Fig. 4-3) showed that the distributions of the data were quantitatively comparable between groups and individual mice within groups. However, these representations do not allow to test if read numbers affect differential expression variance, especially for genes that are lowly transcribed. In order to visualize and estimate data dispersion according to read count levels, dispersion plots and MA plots were produced comparing KI/KI to WT animals.

The MA-plot serves as a useful overview for the differences between the two groups. The plot highlights that significant genes need to have a large average normalized count. The plot in figure 4-2b also highlights that there are more significant upregulated genes than down-regulated genes in KI/KI animals compared to WT animals. Similarly, the volcano plots helps visualize the genes with the most meaningful changes i.e.

significant and greater than the cut off of log2fold change. Similar results were observed for KO animals when compared with age matched WT controls. The number of differentially expressed genes and their mean fold change was greater than that observed in KI/KI animals suggesting a far greater dysregulation in signalling pathways within the KO animals.

		Et al					KI/KI vs WT data set		
Gene symbol	Description	Adjusted *P* value	Log fold change	DCM associated	CMP associated		Adjusted *P* value	Log fold change	Fold Change (KI/WT)
NPPA	Natriuretic peptide A	2.38E-08	0.58	Yes	Yes		2.95E-64	1.46	28.97
NPPB	Natriuretic peptide B	5.57E-06	0.57	Yes	Yes		8.75E-4	0.54	3.46
TBX20	T-box 20	3.01E-23	0.49	Yes	Yes		1.81E-12	0.20	1.60
MYLK3	Myosin light chain kinase 3	3.15E-20	0.42	Yes	Yes		0.14	-0.05	0.89
CLIC5	Chloride intracellular channel 5	5.40E-24	0.38	No	No		9.87E-07	0.19	1.56
TRIM44	Tripartite motif containing 44	3.73E-25	0.38	No	No		0.85	-0.01	0.99
MAVS	Mitochondrial antiviral signaling protein	4.67E-23	0.36	No	No		3.61E-07	-0.16	0.69
NPR3	Natriuretic peptide receptor 3	1.68E-21	0.36	No	Yes		0.06	0.10	1.26
SMCR8	Smith-Magenis syndrome chromosome region, candidate 8	3.46E-25	0.34	No	No		0.30	-0.04	0.91
JAK2	Janus kinase 2	8.67E-21	0.32	No	Yes		0.31	0.04	1.09
TUBA3D	Tubulin alpha 3d	6.63E-08	-0.26	No	No		NS	NS	
GADD45B	Growth arrest and DNA damage inducible beta	5.75E-08	-0.27	No	Yes		0.56	0.047	1.12
DLK1	Delta like non-canonical Notch ligand 1	4.03E-08	-0.28	No	No		0.81	-0.12	0.75
TUBA3E	Tubulin alpha 3e	6.04E-10	-0.30	No	No		Ns	NS	
GADD45G	Growth arrest and DNA damage inducible gamma	1.58E-10	-0.31	No	Yes		0.56	-0.04	0.92
RASD1	Ras related dexamethasone induced 1	1.14E-06	-0.32	No	No		0.13	0.18	1.50
MYL7	Myosin light chain 7	3.89E-09	-0.33	No	No		2.58E-3	0.80	6.24
FOS	Fos proto-oncogene, AP-1 transcription factor subunit	2.09E-07	-0.33	No	Yes		0.86	-0.03	1.08
MYH6	Myosin heavy chain 6	9.50E-09	-0.34	Yes	Yes		0.07	-0.09	0.81
DHRS7C	Dehydrogenase/reductase 7C	1.45E-08	-0.39	No	Yes		8.75E-05	-0.18	0.66

Table 4-7: Differentially expressed genes with greatest absolute log fold changes in (315). compared with study comparing KI/KI and WT animals. Rows highlighted orange have results similar to study by Heinig et al but do not reach significant p-value. The RNASeq values which do not reach significance are in red.

Differential gene expression highlighted over 600 genes that were significantly upregulated (log2fold>1) or down-regulated (log2fold<-1) in KI/KI animals compared to WT mice. The results highlighted genes attributed to cardiomyopathies such as *Ankrd2, Col9A2. Nppa, Acta1, Fgf6, Thbs4 and Myh7.* and those generally not related to heart disease such as *Syndig1, Chodl, Frem1, and Tmem200a* among others. In

addition to identifying underlying pathophysiological pathways the differentially expressed genes also help identify potential markers of disease. Hening and colleagues published a data set where they performed pair-end sequencing on 97 patients with SCM and 108 non-diseased controls (315). They identified several markers for DCM, some of which had been linked with disease while others were novel. The expression of markers identified by Henig and colleagues was checked in this data set of KI/KI and WT animals and presented in the table below (Table 7): Of all the biomarkers only *Nppa, Nppb, Tbc20, Clic5, Mavs, Myl7 and Dhr57c* had similar changes in expression (significant and regulated in the same direction) in both the findings of human study and the differences between KI/KI and WT animals (315). *Mylk3, Trim44, Npr3, Jak3, Dlk1, Gadd45g, Fos, and Myh6* exhibited changes in expression in similar direction however the changes were not significant ($p<0.01$) in the KI/KI mice. This may be due to differences in expression of these genes under basal conditions in mice and humans, due to the different physiology of these organisms but it may also be due to the small sample size used in the animal study (n=4 KI/KI vs n=3 WT) compared to the human study (n=107 DCM vs n=97 normal).

KO animals had over 800 genes differentially expressed when compared to their WT controls. These also included some of the genes associated with cardiomyopathies including *Nppa, Acta1, Col9a2, Ankrd2, Adamts20, Myh7* and shared some of the unique genes highlighted by analysis of KI/KI animals including *Syndig1, Chodl, and Frem1.*

Further studies in different mouse models of cardiomyopathy have been performed to evaluate the role of these genes in development of disease. One such study by Burke and colleagues analysed transcriptomes of the phospholamban ($PLN^{R9C/+}$) DCM

mouse model and the myosin heavy chain (MHC^{R403Q}) HCM mouse model (316). Both models have been well characterized in previous studies (254, 332). The study compared both myocyte and non-myocyte fraction of the heart between the HCM and DCM models. Myocytes from HCM mice had substantial changes in genes associated with metabolism pathway similar to myocytes from DCM myocytes. Despite these similarities, the majority of differentially expressed genes were unique to one or the other cardiomyopathy, with only 28% of differentially genes being shared by the two mouse models. Most genes (72% were) were unique to either DCM or HCM mice. Detailed analysis highlighted differences in signalling pathways between the two models. Several genes associated with PPAR signalling were differentially expressed between HCM and DCM. A subset of genes corresponding to aerobic metabolism were found to be unperturbed in HCM, however these genes, related to regulation of peroxisomal metabolism were differentially expressed in DCM, highlighting difference in peroxisome function between DCM and HCM at baseline. Most genes relating to glucose metabolism were found to be consistent, with the exception being *Tbx15*, which was not expressed in HCM. Analysis of unique genes that were differentially expressed in either model failed to highlight pathways or upstream regulators that were specifically enriched in the HCM model. The DCM model, however, showed enrichment in dopamine receptor and β-adrenergic signalling.

The Gene ontology project is a collaborative initiative with the purpose of developing a controlled vocabulary to describe gene product attributes in all organisms. GO consists of three structured ontologies that describe gene products in terms of their associated biological processes, cellular components and molecular functions (299, 333, 334). GO terms were assessed using Gorilla software platform. For KI/KI animals the GO enrichment score for cellular component highlighted a significant involvement of the

sarcomere, suggesting most of the differentially expressed genes underlying the phenotype belong to signalling within the sarcomere. Other components included the extracellular region which has been associated with changes in DCM. Collagen gene expression was markedly upregulated in the dataset, which has been associated with progression to DCM and HF, and along with other genes such as fibroblast growth factor can cause significant extracellular matrix remodelling that may ultimately result in fibrosis (316, 335, 336). These findings supported qPCR data in Figure 3-4 where markers of fibrosis are upregulated however these changes don't translate into changes in level of fibrosis between the different genotypes. GO biological processes showed significant enrichment of genes involved in heart rate regulation and cell proliferation, processes that are often associated with heart failure. These findings are supported by Gene set enrichment analysis (GSEA). The key pathways that were found to be significantly ($p<0.01$, False Discovery Rate <0.1) enriched were extracellular matrix receptor interaction, cell and focal adhesion molecules, transforming growth factor (TGF) beta signalling, glycosaminoglycan biosynthesis and hypertrophic cardiomyopathy. These pathways have been implicated in cardiomyopathies and development of heart failure in previous studies (337, 338).

KO animals shared similar results to KI/KI animals with sarcomere and extracellular regions being the most enriched GO components. Among GO processes the enriched signalling pathways for KO animals were all related to muscular and hypertrophic signalling, suggesting a less diverse underlying signalling disruptions within the KO animals in comparison to KI/KI animals.

Ingenuity Pathway Analysis's (IPA) upstream regulator analysis assesses molecules based on existing knowledge of expected effects between transcriptional regulators

and their target genes stored in its Knowledge Base. The analysis reviews the target of every transcription regulator present in the dataset, and also compares whether they are up-regulated/down-regulated compared to what is expected from the literature. If the observed direction of change is mostly consistent with a particular activation state of the transcriptional regulator, then a prediction is made about that activation state.

Of all the transcription factors significantly activated only some of them have been implicated in heart disease. Twist1 is an oncogenic transcription factor that has been shown to regulates genes such as *Tbx20, Cdh11, Sema3c, Rab39b and Gadd45a* that promote cell proliferation and migration in developing heart valves (339). Contrary to these findings TWIST1 has been observed to be down-regulated in DCM patients and its downregulation was associated with increased activity of the UPS (340). Further, cardiomyocytes transfected with Twist1 siRNA, compared to scrambled siRNA controls, showed decreased cell size, following stimulation with PE/isoprenaline, leading to the suggestion that it may be involved in the loss of cardiac mass during dilatation of the heart (341). *Runx2* is up-regulated in the $PLN^{R9C/+}$The dilated cardiomyopathy mouse model and is also a known regulator of collagen type-1 gene expression and a key mediator of aortic fibrosis (316, 342). *Pitx2* has been implicated in cardiac development and disease and null mutants displayed right atrial isomerism with impaired venous return (343). Though *Etv5* is one of the most abundant transcription factors in embryonic heart, *Etv5*null mice develop normally (344). GLI family zinc finger protein 2 (GLI2) promotes tumour progression (345). ETV5 and GLI2 have not been implicated in cardiac diseases, however, based on their target genes they seem to play a role in cardiac fibrosis (346).

IPA identified other transcription regulators which have been involved in cardiac development, disease and fibrosis including TGFB2 (Transforming Growth Factor Beta 2), CTGF (Connective Tissue Growth Factor), and AGT (Angiotensin II). DIO2

(Iodothyronine Deiodinase 2), which is an enzyme responsible for conversion of Serum tri-iodothyronine from thyroxin in hearts, has been to be up-regulated in a DCM mouse model, where 3 base pairs coding for K210 in cardiac troponin T were deleted (347). CXCR3 (CXC chemokine receptor family 3) is a chemokine receptor which has been implicated in cardiac inflammation (348). BCL2 (B-cell lymphoma 2) is known to inhibit apoptosis within the heart and is upregulated in end stage heart failure (349). CNR1 (Cannabinoid Receptor 1) is a G-protein coupled receptor which has not been involved with cardiac pathophysiology, but its target genes suggest involvement with cardiac fibrosis. AGER (Advanced Glycosylation End-Product Specific Receptor), also called RAGE, plays a key role in the development of diabetic cardiomyopathy and is a potential target for heart failure therapy (350, 351). These upstream regulators and their role in disease mechanisms such as cardiomyopathy, fibrosis, and apoptosis support the phenotype described in the previous chapters and making the knock-in mouse model a great tool to study dilated cardiomyopathy.

Though the transcriptome analysis and further analysis has been able to identify a few molecules and pathways that are excellent candidates for further research into understanding the mechanisms driving cardiomyopathy, this study has several limitations. RNA levels do not necessarily correlate with protein levels or their activity and therefore are an indirect measure of activation of signalling pathways. Further studies, evaluating protein expression and activity would be required to assess and validate the activity of these pathways before we can draw conclusive mechanistic

links. This study used RNA from whole heart which allows us to see the effect on all the cellular components as a whole. There was a significant upregulation of molecules and pathways associated with fibrosis and those associated with the extracellular region. These changes are often observed in the nonmyocyte component of the heart. To study the direct effects of mutation or gene knockout on cardiomyocytes, the myocytes need to be isolated and RNASeq needs to be performed on the isolated fraction. Though this might help narrow down the underlying signalling mechanisms and remove confounding results, the process of isolating cardiomyocytes has a low yield, especially in DCM models, and the harsh conditions of isolations may itself cause transient expression changes within the cells (352, 353).

Sequencing can be single-end or pair-end, the latter being preferred for discovery of novel transcripts or splicing patterns to evaluate isoform expression analysis (354, 355). Number of reads per sample also affect evaluation of expression. Some publications claim that 5 million reads are sufficient to assess differential expression of genes while others sequence upto 100 million reads to assess transcripts with low expression (356). Longer reads improve the ability to map and identify the transcripts (355, 357). The decision to perform the type of sequencing depends on the biological question of interest, which in this case differential gene expression. The choice of sequencing is also influenced by the increase in cost with the number of reads and pair-end being more expensive than single-end.

The bioinformatics tools used for analysis have their limitations as well. The pathway analysis with GOrilla, GSEA and IPA are based on previously reported findings in the literature and therefore might not be relevant for cardiomyopathies due to a lack of cardiomyopathy specific studies. There is a far greater representation of cancer related pathways compared to cardiovascular pathophysiology. Since GSEA identifies

pathways and sets of genes based on already published knowledge these analysis might fail to highlight all relevant pathways and may even deliver false positive results if proper quality controls are not used (358). More work needs to be done in the field of cardiomyopathies to compile specific databases to identify pathways and mechanisms involved in disease. Experimental design could be improved to include a greater number of animals which will help to highlight genes that might not have reached significant values, such as those compared in Table 4-7. Further, comparing KI/KI and KO animals at the same age would have strengthened the comparison made between the two datasets. It is hard to decipher whether the changes are causal or as a result of other changes within the heart. Comparison between hearts of 9 week and 16 week old WT animals yielded no apparent changes in gene expression, contradicting the previous theory. A study which evaluates transcriptome at various stages, such as that used by Burke et al. where they assessed transcriptome before development of DCM, after DCM and after development of end stage heart failure would be ideal (316).

With these limitation under consideration, the RNAseq analysis for KI/KI MLP C58G knock-in mice compared with WT littermate controls highlighted pathways usually implicated with heart failure and cardiac fibrosis. At the same time other genes were differentially expressed which have not been associated with cardiomyopathies or heart failure. GSEA/KEGG pathway analysis highlighted commonly associated pathway and provided new mechanistic insights to development of DCM. Further work to evaluate the role of these unique genes and pathways identified, needs to be performed to improve our understanding of pathophysiological mechanism and phenotypes that characterize development and progression of an overt cardiac phenotype in dilated cardiomyopathy.

Chapter 5 – Role of Protein Degradation in MLP KI mice

5.1 Introduction

As described in the previous chapter 3 (Figure 3-2), Csrp3 KI mice show MLP have reduced protein expression in both heterozygous, by 50% and in homozygous setting, by up to 80%. Previous work in the lab has shown that this is due to protein destabilization and resulting degradation within the cell. There are two major pathways of protein degradation within cells, the autophagy pathway and the ubiquitinproteasome system (UPS) (359, 360): The autophagy pathway degrades long-lived protein, and cytoplasmic organelles with the help of lysosomes (359). In addition to its role in degradation, recent findings have highlighted autophagy to play a part in processes such as cell growth, tissue homeostasis and intracellular clearance of mutated and misfolded proteins as well as damaged organelles (359). Excessive autophagy has also been shown as a mechanism for self-digestion, degradation and ultimately cell death (359). Though autophagy and UPS have been considered to be working independent of each other, with UPS being responsible for selective degradation and autophagy for non-selective degradation, there is evidence to suggest that autophagy pathway degrades ubiquitinated proteins (361, 362).

5.1.1 Autophagy

The process of autophagy is highly conserved across various species (359). There are three different types of autophagy, (i) macroautophagy, which involves enclosing organelles in a double membrane structure, the autophagosome, which fuses with lysosome to degrade proteins (363) (ii) microautophagy, in which small volumes of cytoplasm are directly engulfed by lysosomes, and (iii) chaperone assisted selective

autophagy (CASA), in which soluble substrates containing KFERQ-like motifs are recognized by a cytosolic chaperone Hsc70 and co-chaperones (359, 364, 365). These chaperone complexes are then translocated to the lysosome for degradation by lysosomal receptor, Lamp2a.

Of the three processes, macroautophagy is the best studied process (364). The molecular signalling pathways regulating macroautophagy are quite complex (366) (Figure 5-1). Briefly, the process can be divided into the following steps: initiation, autophagosome formation, fusion and degradation. Starvation/stress signalling leads to inhibition of mechanistic target of rapamycin (mTOR) inducing the formation of the ATG1/Ulk1 protein kinase autophagy regulatory complex, initiating the formation of a double-membranous phagophore (367). The phagophore is expanded by two ubiquitin-like conjugation pathways (367), both of which involve the E1 ubiquitinactivating enzyme autophagy-related 7 (ATG7) (368). In one of the pathways, ATG7 and the E2 ubiquitin-conjugating enzyme ATG10 form a complex between ATG12 and ATG5. In the second, a microtubule-associated protein light chain 3 (LC3) is synthesized and immediately cleaved by ATG4 to produce an active cytosolic form, LC3-I. ATG7 and E2-conjugating enzyme ATG3 subsequently conjugate phosphatidylethanolamine to LC3-I to yield LC3-II, a critical step in autophagosome formation. The fusion of autophagosomes with lysosomes causes the inner membranes to lyse, releasing lysosomal hydrolases that degrade the substrates enclosed within the autophagosome (367).

The conversion of LC3-I to LC3-II is achieved by the conjugation of the lipophilic phosphatidylethanolamine group which facilitates the insertion of LC3-II into the membranes of autophagosomes, and its subsequent degradation after the fusion of

autophagosome with lysosomes. The ratio of LC3-I to LC3-II also allows us to evaluate the relative autophagic flux, the dynamic process of autophagosome generation, their fusion with lysosomes, and the degradation of autophagic substrates in autolysosomes. Inhibitors of autophagy such as Bafilomycin inhibit the degradation of the of LC3-II-positive autophagosomes by inhibition of the Na+/H+ pump at the lysosome, increasing lysosomal pH and inhibiting acidic lysosomal proteases (369, 370).

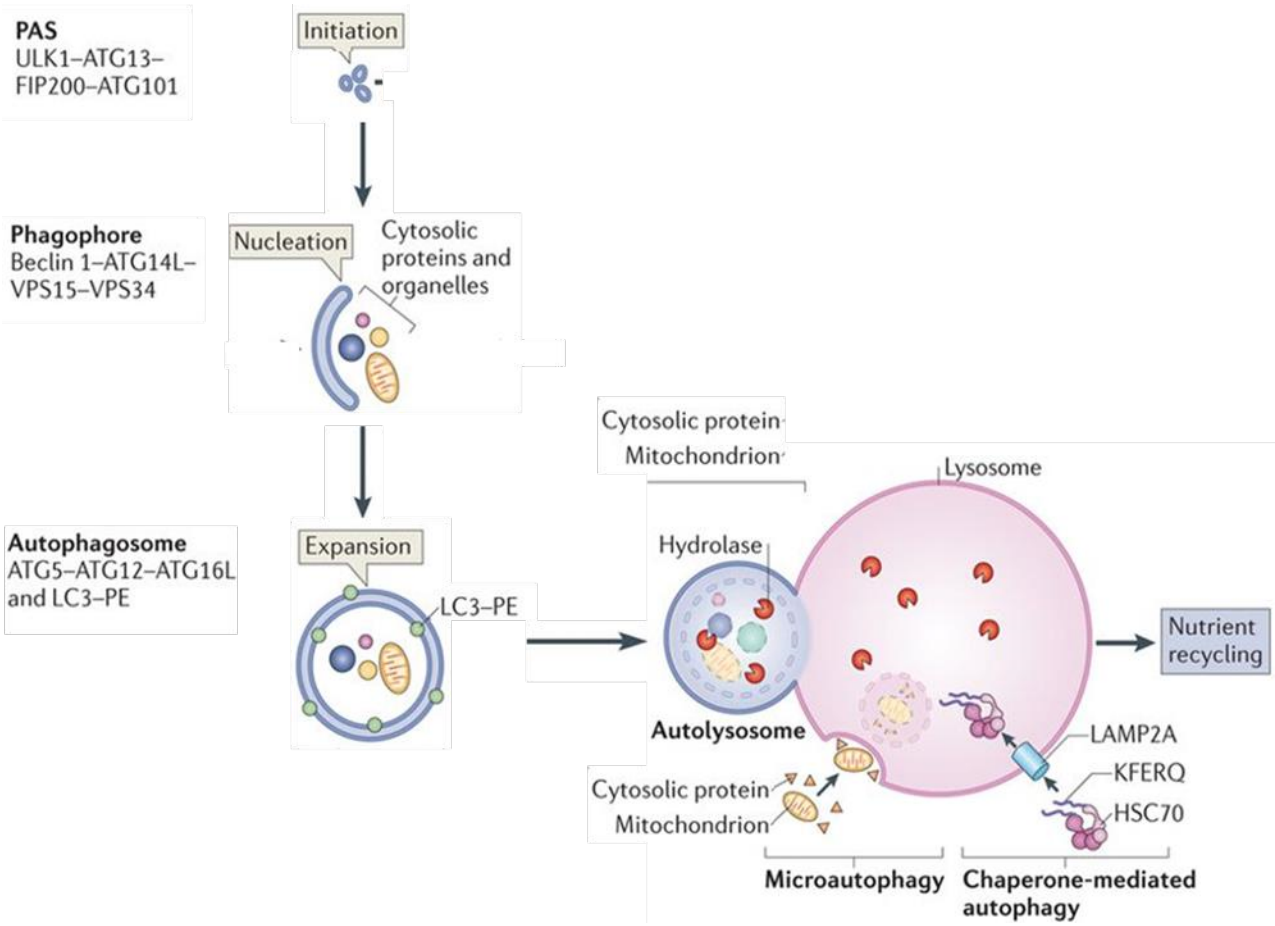


Figure 5-1. The following steps take place in macroautophagy; 1) Initiation: Phagophoreassembly site (PAS) is formed by the UNC51-like kinase (ULK) complex, which consists of ULK1 (or ULK2), autophagy-related protein 13 (ATG13), FAK family kinase interacting protein of 200 kDa (FIP200) and ATG101. 2. Nucleation: A phagophore is formed with vacuolar protein sorting 34 (VPS34) PI3K (class III), along with its regulatory subunits ATG14L, VPS15 and beclin 1. 3. Autophagosome formation: Autophagosome is formed with the aid of two ubiquitin-like conjugation pathways. The first generates a multimeric complex of ATG5–ATG12 and ATG16L, whereas the second forms a conjugate of phosphatidylethanolamine (PE) and LC3 (the microtubule-associated protein 1 light chain 3). LC3–PE is essential for the expansion of autophagic membranes, their ability to recognize autophagic cargoes and the fusion of autophagosomes with lysosomes. 4. Autolysosome Formation: Autophagosome fuses

with endocytic and lysosomal compartments to form the autolysosome where the cargo packaged within the autophagosome is degraded via lysosomal hydrolases. Figure from (371)

5.1.2 Ubiquitin Proteasome System (UPS)

The UPS is a quality control system within eukaryotic cells that is responsible for degradation of 80-90% of intracellular proteins (372). Present in both the nucleus and cytoplasm it is known to be a highly specific proteolytic pathway for short-lived cytosolic, nuclear and myofibrillar proteins (360) and its major function is to degrade damaged, misfolded and mutant proteins. The UPS has a crucial role in many fundamental biological processes such as cell proliferation, adaptation to stress and cell death (360). In addition to being indirectly involved in a number of pathways, as it controls the levels of key signalling proteins and degradation of short-lived proteins, the UPS is also involved in stress response signalling, antigen processing, DNA repair, apoptosis and transcriptional regulation (360, 373). The UPS is involved in pathogenesis of several genetic diseases, in immune surveillance or viral pathogenesis and pathology of neurodegenerative disorders such as Alzheimer's or Parkinson's (374).

Protein degradation by UPS is ATP-dependent and is carried out in two discrete steps (Figure 5-2). First, the target proteins are tagged with multiple ubiquitin molecules and second, the marked proteins are degraded by the 26S proteasome complex, releasing ubiquitin molecule to be reused again (375, 376). The conjugation of ubiquitin molecules to the protein targeted for degradation is a multistep enzymatic process. The initial activation step is driven by the ubiquitin-activating enzyme (E1) which activates ubiquitin in an ATP-dependent reaction. One out of several tissue specific ubiquitin-conjugating enzymes (E2) then conjugates the activated ubiquitin molecule from E1 to

the protein targeted for degradation. The protein targeted for degradation at this stage is bound to ubiquitin ligase enzymes (E3) which acts as a bridge in this step and helps catalyse the covalent linkage of ubiquitin to the substrate. Polyubiquitin chains are assembled by adding activated ubiquitin moieties to internal lysine residues on the previous ubiquitin. These polyubiquitin chains are then recognized by the 19S cap of the 26S proteasome complex, which degrades the polyubiquitinated proteins to small peptides. During this last process the polyubiquitin chain is hydrolysed into single ubiquitin moieties, which can then be recycled for the next round of protein degradation (377-379).

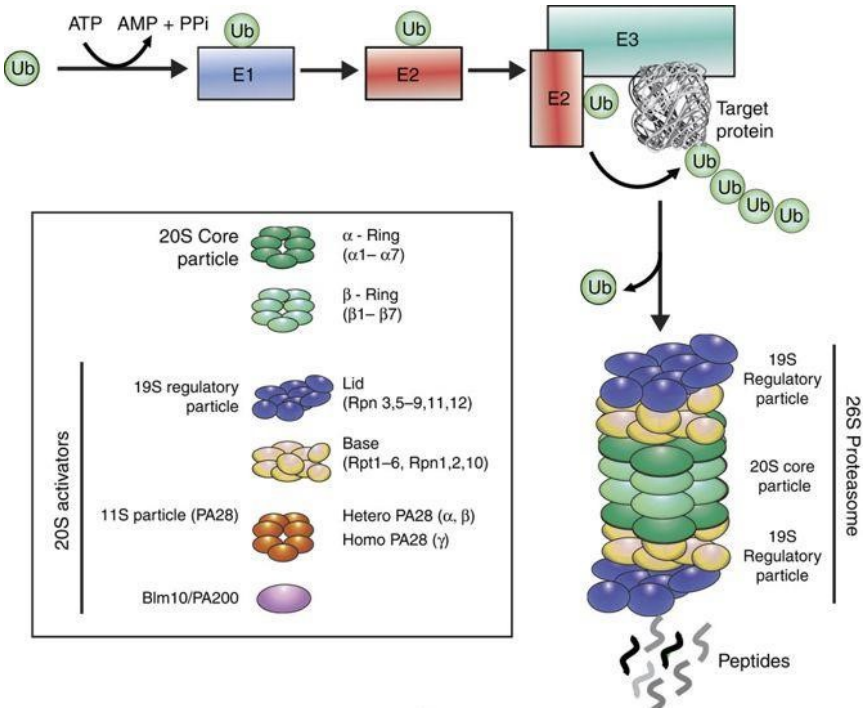


Figure 5-2. Schematic illustration of proteasome assemble. Adapted from (380)

The 26S proteasome is composed of one 20S particle structure and two 19S regulatory caps. These regulatory caps identify, de-ubiquitinate and unfold targeted proteins before they reach the hollow core of the 20S catalytic centre (381). The 20S particle

features four layered heptameric ring structures, which consist themselves of two different types of subunits (α and β) (382). The α-subunit has structural functions while the β-subunit is responsible for the proteolytic functions. The unfolded protein is degraded by three major peptidase activities; the caspase-like, the trypsin-like and the chymotrypsin-like activities which are carried out by the major catalytic subunits β1, β2 and β5 respectively. Each of these subunits prefers to cleave after specific amino acid residues. The caspase-like activity cleaves amino acids after hydrophobic residues, trypsin-like activity cleaves after alkaline residues whereas the chymotrypsin-like activity cleaves after acidic amino acid residues (369, 383). Theses proteolytic activities can be measured *ex-vivo* using synthetic fluorogenic substrates, which once cleaved at specific residues release a fluorescent reporter, whose fluorescence can be measured. These activities can also be inhibited with reversible or irreversible proteasome inhibitors to evaluate which activity is responsible for the degradation of a target protein.

To maintain the protein balance within the cell, both autophagy and UPS are tightly controlled. The relative contribution of each degradation pathway is different between cell types. In general, short-lived proteins are specifically degraded by the UPS (384), whereas long-lived proteins are preferential degraded by autophagy (385). These two pathways were considered independent for a long time, but recent findings suggest that ubiquitination can target substrates for degradation via both pathways. In addition, several proteins, such as α-synuclein (386, 387), aggregate-prone proteins (388, 389), are known to be degraded by both pathways. One of the signals deciding which pathway is used is the type of ubiquitin ligases and where ubiquitination occurs on the substrate (e.g., monoubiquitination, polyubiquitination at Lysine 48 (K48) residue of the ubiquitin protein, or polyubiquitination at Lysine 63 (K63) residue of the ubiquitin

protein (390). In general, K48-linked polyubiquitinated chains are a target substrate for the proteasome (391), while K63-linked polyubiquitinated chains or monoubiquitinated substrates favour autophagic degradation (392, 393).

To study the ubiquitin proteasome *in vivo* a mouse model expressing a mutant ubiquitin UbG76V-GFP was used. (394) The transgenic mouse has a N-terminal ubiquitin mutation (UbG76V) fused with a green fluorescent protein (GFP), expressed widely and at high levels by a chimeric cytomegalovirus immediate early (CMV-IE) enhancer and a chicken β-actin promoter (394). Lindsten and colleagues showed that UbG76V-GFP transcripts were expressed in different tissues, with predominant expression in skeletal muscle, heart, testis and cerebellum (394). The N-terminallinked ubiquitin molecule serves as an acceptor for polyubiquitin chains, through the canonical Lysine 48 and the less common Lysine 29. The G76V substitution prevents the removal of GFP alone from the fusion protein by cellular ubiquitin C-terminal hydrolases, leading to efficient ubiquitination and proteasomal degradation of the UbG76V-GFP fusion protein. As a result, no GFP-fluorescence was observed in any cryosections of tissue obtained from adult UbG76V-GFP mice under normal conditions. However, when UPS is impaired or saturated or pharmacologically inhibited with different proteasome inhibitors, it results in the accumulation of the UbG76V-GFP reporter. This was observed in primary fibroblasts and neonatal cardiomyocytes. There was detectable GPF fluorescence in liver, small intestine, pancreas, kidney and to a lower extent in the lung and spleen of mice with intraperitoneal (i.p.) injection of the proteasome inhibitor MG262 (5 μmol/kg). However, no fluorescent cells were observed in the brain, heart and skeletal muscles (394).

5.1.3 Myosin Binding Protein C 3 (MYBPC3)

Mutation in the gene *MYBPC3* encoding encodes cardiac myosin binding protein C (cMYBPC) are one of the most common cause HCM (395). So far over 350 individual mutations have been identified which represent approximately 40% of all HCM causing mutation, making it, along with *MHY7*, the most frequently mutated gene in HCM (113, 396, 397). Unlike mutations in *MHY7* which are mainly nonsynonymous single nucleotide e polymorphisms (nsSNPs), mutations in *MYBPC* are truncating mutations, causing disruption of reading frame by nonsense mutations, insertions or deletions, splicing or branch point mutations, leading to truncation in the protein. These mutations result in protein lacking myosin-binding and/or titin-binding sites and prevent the incorporation of the protein into the sarcomere (398, 399). Most HCM causing *MYBPC3* mutations are heterozygous with late disease onset.

cMyBPC is composed of eight immunoglobulin (Ig) domains, with three fibronectin domains towards terminal carboxyl group. The protein interacts with myosin S2 region and actin in the interfilamentous space. These interactions are regulated by phosphorylation state of cMyBP-C (400-402). The phosphorylation state of three serine residues (Ser273, 282 and 302) affects cMyBP-C's ability to regulate crossbridge cycling and dysregulation of these residues results in cardiomyopathy
(403, 404). A recent study has delineated the role of cMyBP-C as a ''molecular brake'' on myosin crossbridge cycling and in its dephosphorylated state it slows down actomyosin motor generation (405). The phosphorylation of these sites has identified to be regulated by a number of protein kinases including PKA (406, 407), Ca^{2+}/calmodulin-dependent kinase II (408), p90 ribosomal S6 kinase (409), PKD (410), and PKC (407).

Recent data suggest that accumulation of ubiquitinated proteins is a feature of HCM in humans and in a mouse model carrying c.772G>A cMyBPC point mutation (114). The c.772G>A *MYBPC3* transition is one of the most frequent HCM mutations (13% in a large Italian cohort) and is associated with a severe phenotype and poor prognosis in humans in the heterozygous state (395, 411-413). Homozygous KI mice exhibited left ventricular hypertrophy, increased heart weight/body weight ratio, lower fractional shortening and diastolic dysfunction (375, 414). Heterozygous unchallenged mice showed no major phenotype (415). The molecular phenotype of homozygous KI mice is characterized by 80% lower total Mybpc3 mRNA levels and 90% lower mutant cMyBPC protein levels. This reduction in cMyBPC was due to a combination of activation of nonsense-Mediated mRNA Decay and protein degradation via the ubiquitin-proteasome system (114).

Further studies with the mouse model highlighted accumulation of ubiquitinated proteins and greater proteasomal activities (416). One-year old KI mice, crossed with UbG76V mice, showed accumulation of the UPS substrate UbG76V-GFP protein, suggesting UPS impairment (416). These mice also expressed higher levels of autophagy related proteins including beclin-1, LC3-I, LC3-II and p62/SQSTM1, which suggested defective autophagy pathway (416). Though heterozygous KI mice failed to show a phenotype under normal conditions, adrenergic stress showed significant septal hypertrophy in KI/+ mice compared to WT. These KI/+, which mirror the genetics of affected HCM patients, also exhibited proteasome impairment (417). The findings from this mouse model support the concept that proteasome impairment contributes to the pathophysiology of HCM, at least in cases associated with *MYBPC3* gene mutations.

The aim of this chapter is to evaluate the expression of C58G mutant *in vitro* and to assess the pathways involved in regulation of expression of protein. Mutations in *MYBPC3*, show protein destabilization similar to MLP and are degraded by the two major proteolytic systems, autophagy pathway and ubiquitin proteasome system (UPS) (359, 360). These pathways have also been shown to contribute to cardiac disease pathology in mouse models. To monitor degradation and activity of the UPS, Csrp3 KI mice were crossed with transgenic mice that overexpress UbG76V-GFP, a mutant form of ubiquitin conjugated to GFP which accumulates in conditions of proteasomal overload (394). As described earlier in chapter 3, Csrp3 KI/+ mice showed no overt phenotype, even after ageing them to 12 months (data not shown).

MYBPC G772A heterozygous mice showed no phenotype under normal conditions (416). It was hypothesized that Csrp3 KI/+ have significantly increased UPS load. Since Mybpc3 G772A exhibited increased proteasomal load these mice were crossed with Csrp3 KI animals with the hypothesis that the presence of two mutations that increase overall proteasomal load in cardiomyocytes would lead to an overt cardiac phenotype.

5.2 Results

5.2.1 C58G MLP is destabilized *in vitro*

Mutatn MLP protein was found to be destabilized *in vitro.* HEK293 cells were transfected with GFP-tagged WT MLP and HA-tagged WT, C58G and L44P MLP. Western blot analysis highlighted reduced expression of HCM causing MLP mutations C58G and L44P, whereas no change was observed in GFP tagged WT MLP protein levels. These results not only show the destabilization of mutant protein but also that the mutant protein has no dominant negative effect as its presence and degradation does not affect WT protein.

These findings of are in line with the expression of MLP in Csrp3 KI animals (Fig. 3-2) where MLP is reduced by 50% in KI/+ mice, and by up to 80% in KI/KI animals.

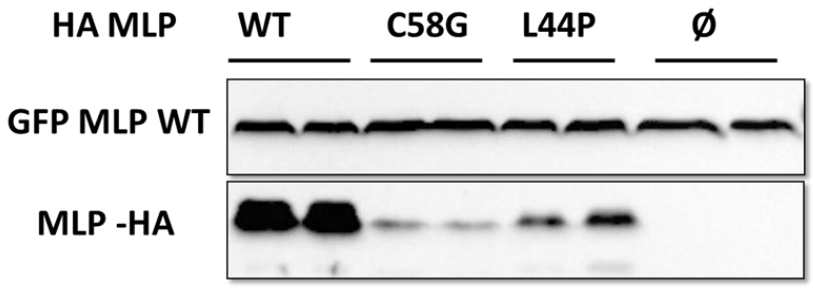


Figure 5-3: C58G MLP is destabilized *in vitro*- HEK293 cells were transfected with GFP tagged WT MLP and HA-tagged WT, C58G, L44P MLP and Ø vector. Mutant MLP showed reduced expression but had no dominant negative effect on the WT MLP.

5.2.2 The UPS is responsible for the protein depletion of HCM-associated MLP mutants

To identify which of the two major protein degradation pathways in eukaryotic cells, UPS or autophagy (359, 360) were involved in degradation of mutant MLP, HEK293

were transfected with mutant and WT MLP and treated with an inhibitor of UPS, MG132 (10uM for 8 hrs) (Fig, 5-4a). Similar to previous results MLP C58G was destabilized under control conditions, however, treatment with MG-132 increased MLP C58G expression to levels comparable to WT. K48 blot was performed on lysates from these cells to confirm inhibition of the proteasome pathways by showing the accumulation of UPS related ubiquitinated proteins.

To confirm the role of autophagy pathway in degradation HEK293 cells were silenced for key autophagy protein Atg5 using Atg5 siRNA (Fig, 5-4b). Silencing was confirmed by reduced Atg5 expression in these cells and the LC3 I/II ratio. Silencing of Atg5 failed to recover levels of mutant MLP to those of WT. Surprisingly, the expression of both WT and C58G recombinant protein was reduced after silencing of Atg5.

These experiments suggest that the UPS is responsible for the protein degradation of mutant MLPs.

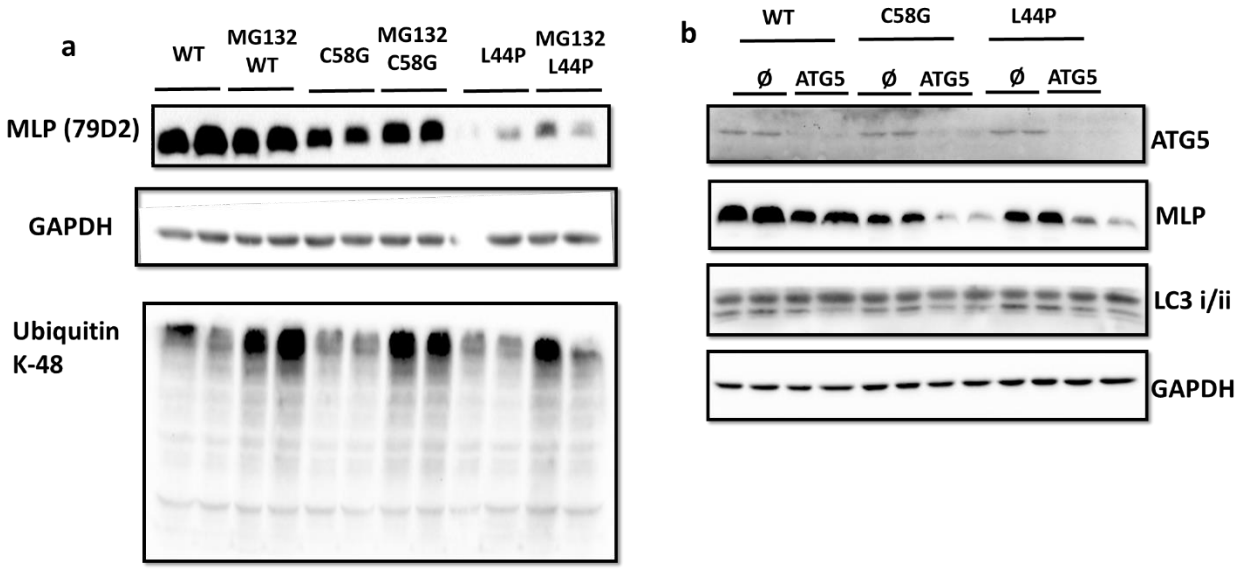


Figure 5-4: C58G MLP mutant protein is degraded by proteasomal pathway rather than autophagy lysosomal pathway. **a** – HEK293 cells were transfected with WT and C58G MLP. C58G had reduced expression under DMSO treated conditions but treatement with proteasomal inhibitor MG-132 (10 uM for 8 hrs) increased expression. GAPDH served as loading control and K-48 Ubiquitin served as indicatior for effective inhibition of proteasomal pathway. **b** – HEK 293 cells were transfected with scrambled siRNA or ATG5 siRNA and then transfected with WT and C58G MLP. Atg5 blot show succesful silencing of protein and affect on autophagy pathway was confirmed by LC3 blot. Under scrambled siRNA C58G showed reduced expression compared to WT but after Atg5 silencing these levels were further reduced for both WT and C58G protein. GAPDH served as loading control

5.2.3 Impairment of the ubiquitin-proteasome system In Csrp3 KI mice

To validate the role of the ubiquitin proteasomal system in degradation of C58G mutant protein *in vivo*, WT and Csrp3 knock-in mice were crossed with a transgenic ubiquitin G76V-GFP (Tg_Ub) mouse reporter line (see intro) (394). These transgenic mice allow monitoring of global UPS *in vitro* by ubiquitously expressing a fluorescent substrate of the UPS, which under normal conditions is degraded by the system. However, if the UPS is impaired/saturated or inhibited pharmacologically or genetically the UbG76VGFP substrate accumulates and can be detected by blotting for GFP.

Morphometric analysis of 6-month-old KI Tg_Ub mice showed similar results to knockin mice alone (Fig, 5-5a). This suggested that there was no effect of the transgenic line on the development of a cardiac phenotype in the mice. Csrp3 KI/KI Tg_Ub mice had significantly higher HW/BW ratio, whereas no difference was observed between Tg_Ub and KI/+ Tg_Ub mice. To evaluate accumulation of ubiquitin, the reporter heart tissue was blotted for GFP (Fig, 5-5b). There was significant accumulation of GFP-Ub in Csrp3 KI/KI Tg_Ub mice whereas levels of GFP-Ub were unremarkable between WT and KI/+ mice as confirmed by densitometry results (Fig, 5-5c). These results suggest overload of the UPS in KI/KI mice.

To evaluate the pathway responsible for increased ubiquitination in KI/KI mice ventricular protein was blotted for UPS specific K-48 ubiquitin (Fig, 5-5d) and autophagy specific K-63 ubiquitin (Fig, 5-5e). Surprisingly no changes were observed in either ubiquitin levels in any of the groups.

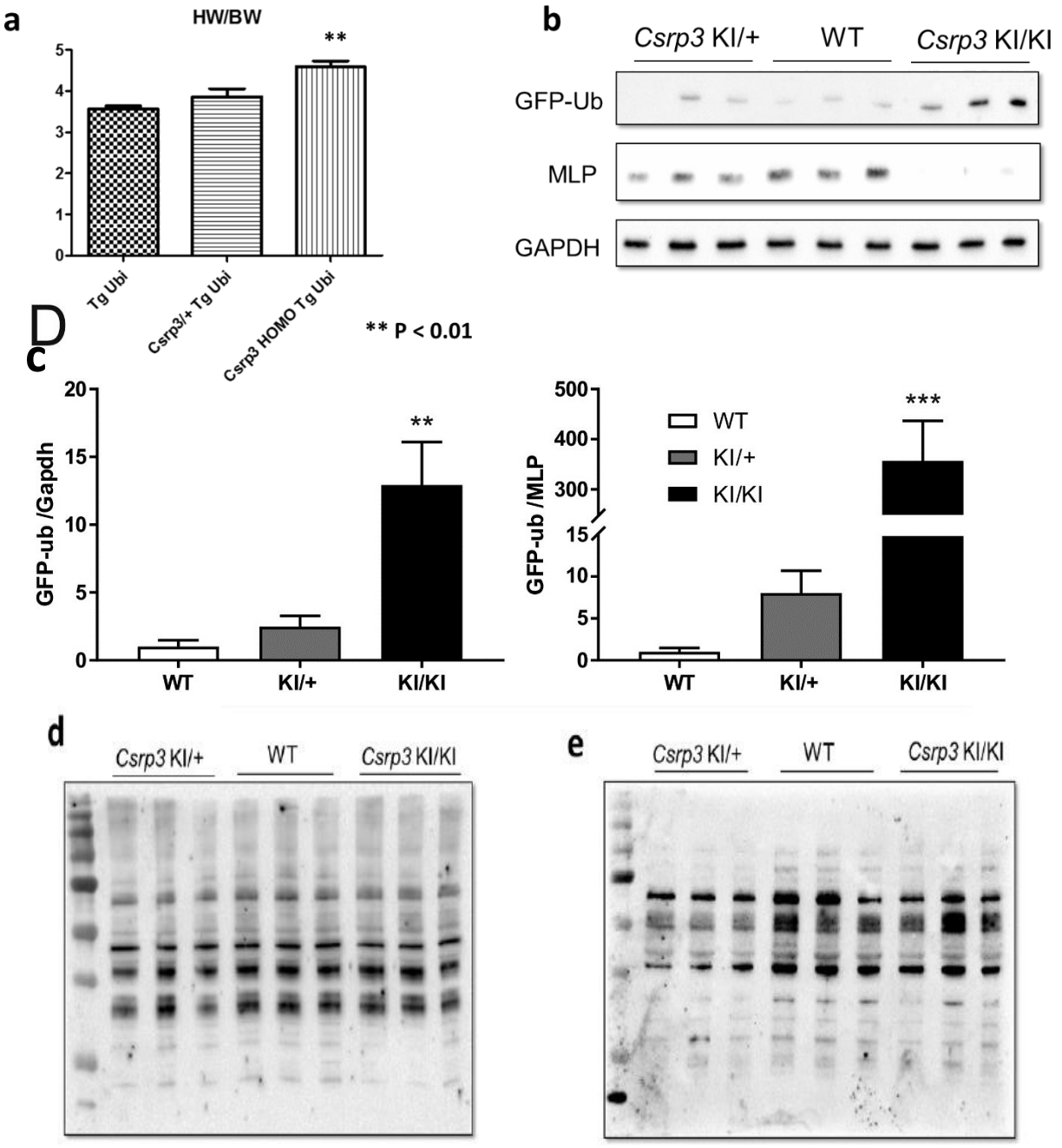


Figure 5-5 – **a)** Morphometric analysis of knock-in mice at different ages. Graphs represent the heart weight (HW) to Body Weight (BW) ratio (mg/g) for 6-month-old mice Data are expressed as mean ± SEM with **P < 0.01, two-way ANOVA **b)-** The ubiquitin G76V GFP reporter (GFP-Ub) was crossed onto WT, KI/+ and KI/KI mice of the three genotypes. Protein lysates from heart tissue of 6-month-old mice were prepared and blotted for total GFP. There was marked increased in the accumulation of GFP tagged ubiquitin (GFP-Ub) in KI/KI mice in comparison to WT and KI/+ mice, as confirmed by densitometry in **c)**. indicating proteasomal overload. MLP expression confirms genotype and GAPDH was used as loading control. Representative Western blots of ventricular protein from KI/-UbG76V-GFP and WT mice d**)** UPS associated ubiquitin anti-Ub (K48) antibody **e)** autophagy pathway associate ubiquitin, anti-Ub (K48). **p < 0.01, ***p < 0.001.

5.2.4 Assessment of Cardiac Function by Echocardiography

To evaluate any possible effect of transgenic ubiquitin on cardiac function and dimensions of KI mice cardiac echocardiographic studies were performed on these knock-in mice at the age of 6 months.

In accordance with previous findings in chapter 3 no statistical difference observed between KI/+ and WT mice in any of the parameters. However, KI/KI mice had significantly ($p<0.0001$) reduced ejection fraction (EF) (Fig, 5-6a), increased LV end systolic dimensions (LVESD) (Fig, 6b), and increased end diastolic anterior wall thickness (Fig, 5-6c).

Some of the parameters failed to show a difference. There was no statistical difference between homozygous KI/KI and WT in LV heart mass (Fig, 5-6d), however there was a trend towards increased LV mass in KI/KI. No difference was observed in LV end diastolic dimensions (LVEDD) (Fig, 5-6e), and end diastolic posterior wall thickness (Fig, 5-6f).

These findings highlight that the presence of the mutant ubiquitin GFP fusion protein does not affect cardiac function.

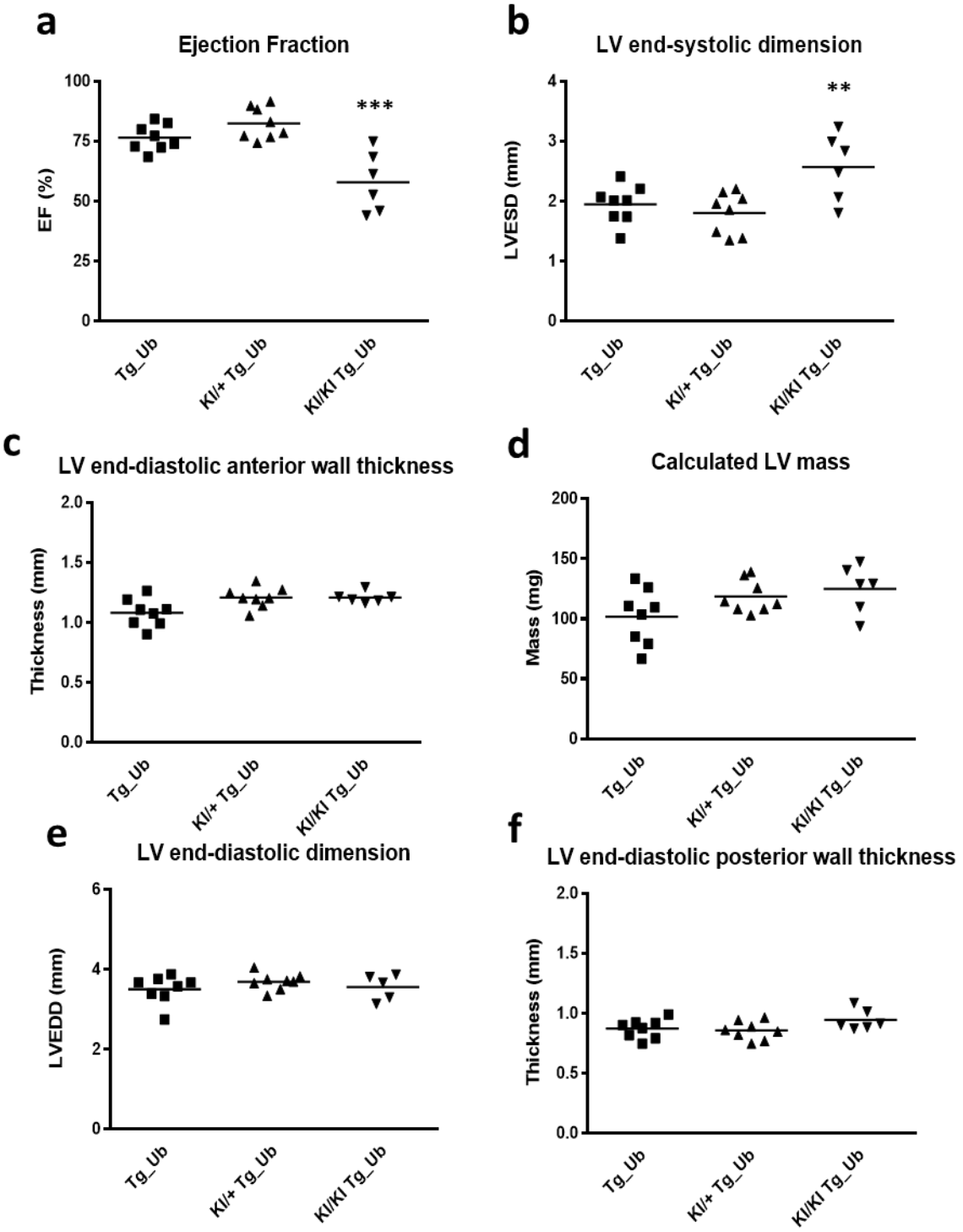


Figure 5-6.: Echocardiographic assessment to delineating the functional phenotype of MLP C58G mouse crossed with Transgenic UbG76V (Tg_Ub) mice at 6 months. KI/+ Tg_Ub animals showed no difference in phenotype when compared to WT animals in all parameters. KI/KI Tg_Ub animals demonstrated diminished systolic function as seen by (***a***) ejection fraction and **(b)** increased LVESSD. KI/KI Tg_Ub animals had slight increase in **(c)** anterior wall thickness **(f)** while no change in posterior wall thickness was observed. KI/KI Tg_Ub animals had no change in **(d)** LV mass or **(e)** LVEDD. ****P<0.0001 versus WT, **P<0.001 versus WT. Data acquisition and analysis were performed by Matt Kelly.

5.2.5 Proteasomal Activities in Csrp3 KI/KI mice

To evaluate which proteolytic component of the 26S proteasome was responsible for the increase in UPS activity, as measured in the UBG76V mouse model, proteasomal activities (chymotrypsin-like, trypsin-like and caspase-like activity) were determined in ventricular cytosolic protein extracts mouse ventricular cytosolic protein extracts.

Surprisingly, no statistical differences were observed between the WT and homozygous KI group in trypsin-like (Fig. 5-7a), caspase-like (Fig. 5-7b) or chymotrypsin-like (Fig. 5-7c) proteasome activities.

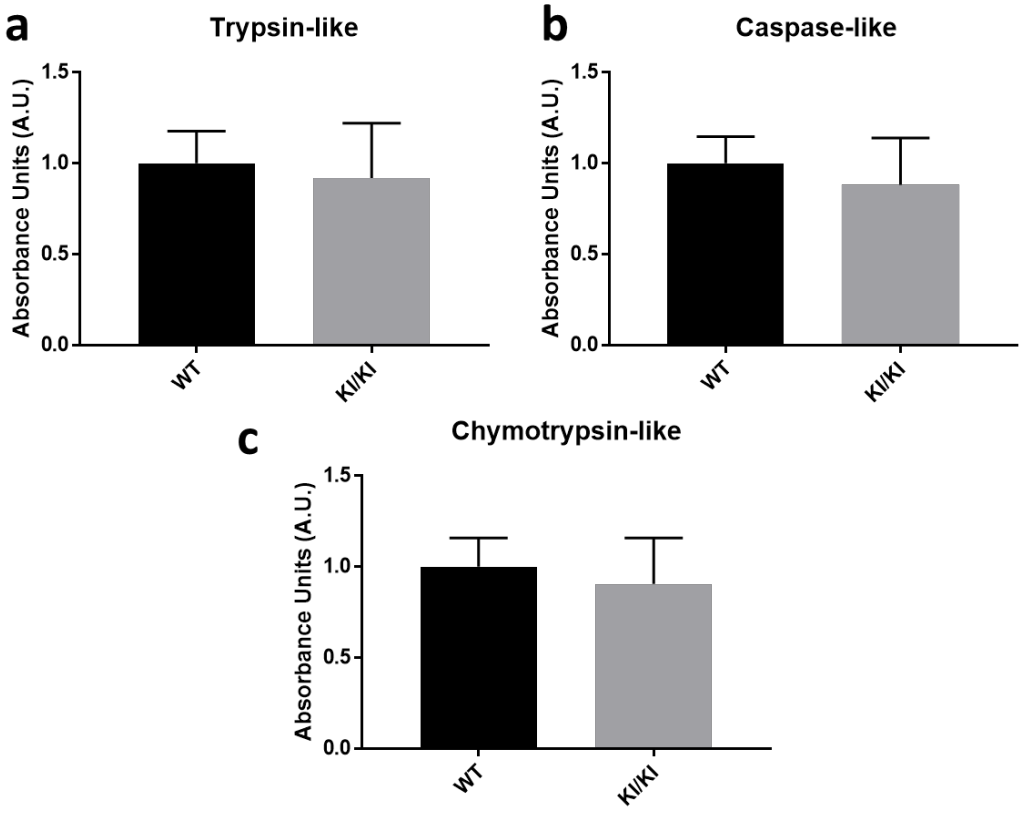


Figure 5-7. Proteasomal activities in WT and Crspr3 KI/KI mice. Analyses were performed in ventricular cytosolic protein extracts. Representative graphs of courses of a) trypsin-like activity, b) caspase-like activity and c) chymotrypsin-like activity of the proteasome in WT (black) and KI/KI (grey). Data are related to WT and expressed as mean ± SEM (*n* = 6 animals per group and age).

5.2.6 Csrp3 KI/+ Mybpc3 KI/+ mice do not develop cardiomyopathy

KI/+ showed no overt phenotype as indicated in chapter 3, and even after aging mice to 6 months, as also seen by data from the KI/+ Tg_Ub mice (Fig 5.6). Since UPS overload was identified in homozygous KI mice, heterozygous KI mice were crossed with Mybpc KI/+ mouse model where mutant protein has been shown to be degraded by UPS (114). The hypothesis was that UPS is a major contributor to the development of cardiomyopathy and therefore the combined presence of two mutant proteins, which are both degraded by UPS, would lead to sufficient impairment of UPS and result in an overt cardiac phenotype.

Csrp3 KI/+ mice were crossed with Mybpc3 knock-in (KI) mice, carrying the missense G772A mutation (415). Cardiac *in vivo* phenotyping and *ex vivo* analysis were performed on three group of animals; Mybc3/+ Csrp3 +/+ (heterozygous for Mybpc KI), Csrp3 KI/+ Mybpc3+/+ (heterozygous for Csrp3 KI), and Mybcp3/+ Csrp3 KI+ (heterozygous for both mutation) animals.

Morphometric analysis of 6-month-old mice showed no difference in HW/BW, HW/TL or BW/TL ratio between Csrp3 KI/+, Mybpc3 KI/+ and Csrp3 KI/+ Mybpc3 KI/+ (double het) (Fig. 5-8). To evaluate the cardiac function and dimensions in double heterozygous mice echocardiographic studies were performed. No statistical difference was observed in systolic function as assessed by calculating ejection fraction (EF) and Fractional Shortening (FS) (Fig. 5-9a), LV mass (Fig. 5-9b), LV end diastolic dimension (LVEDD) (Fig. 5-9c), end systolic dimensions (LVESD) (Fig. 5-9d), LV diastolic anterior (Fig. 5-9e) and posterior (Fig. 5-9f) wall thickness. In accordance with the morphometric analysis, no differences were observed between the three groups in cardiac dimensions.

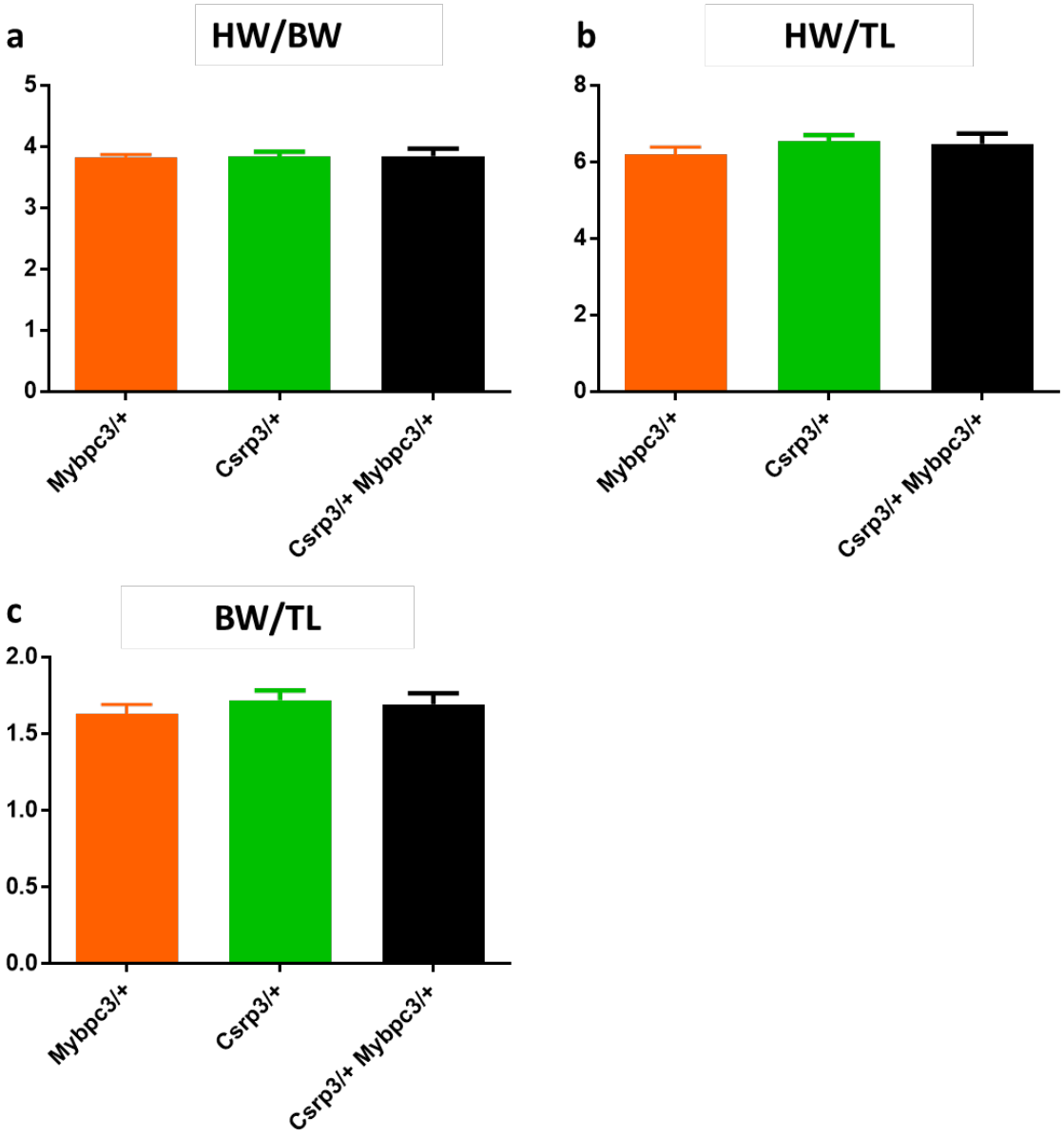


Figure 5-8: Morphometric analysis of knock-in mice. Graphs represent **a)** the heart weight (HW) to Body Weight (BW) ratio (mg/g) **b)** HW to Tibial length (TL) and **c)** BW to TL for 6-month-old mice. Data are expressed as mean ± SEM (n=7-8 per group).

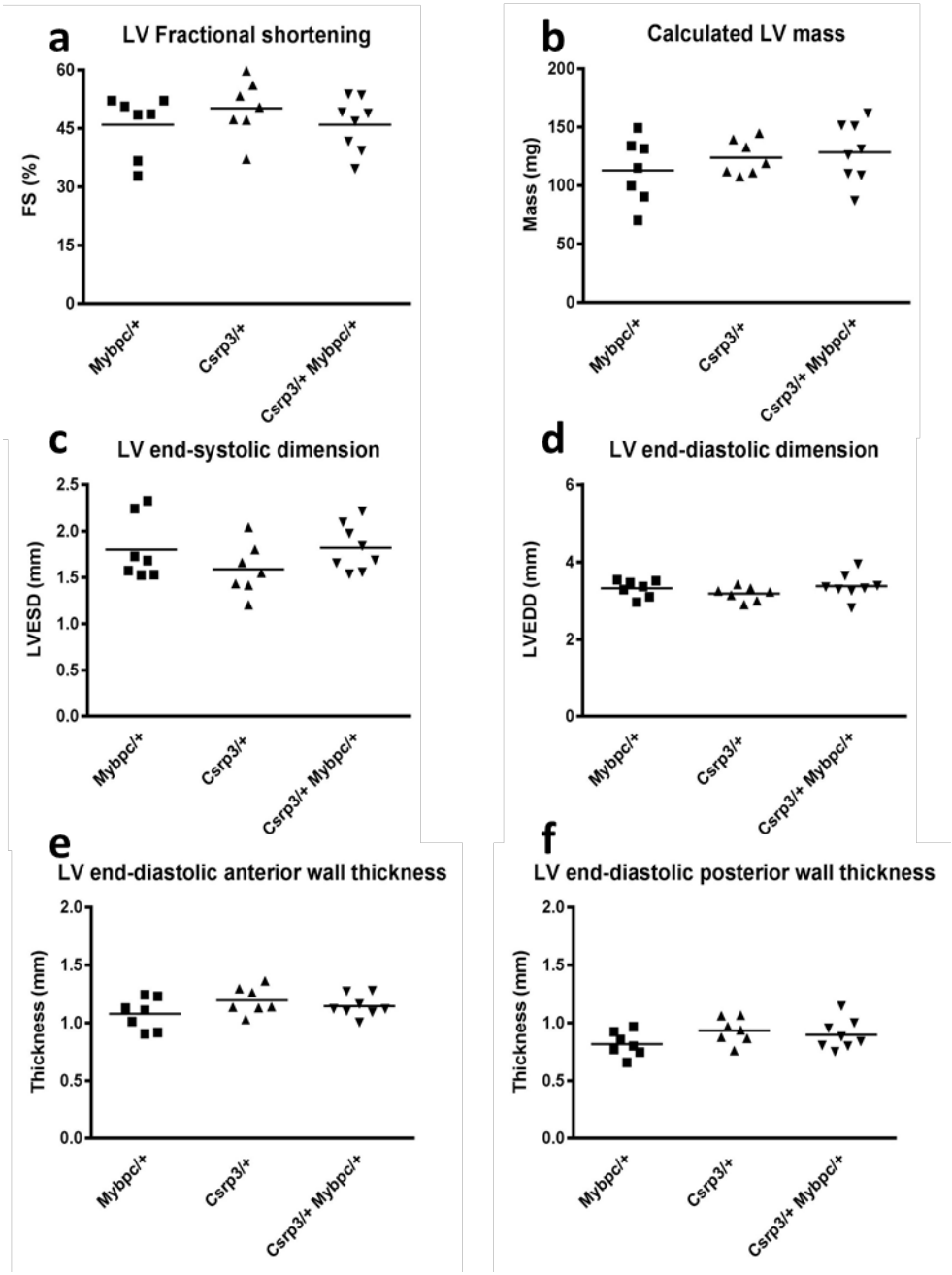


Figure 5-9. Echocardiographic assessment to delineating the functional phenotype of Csrp3 KI/+, Mybpc3 KI/+ and Csrp3 KI/+ Mybpc3 KI/+. The mice aged 6 months, in all three groups showed no difference in phenotype There was no change in **b)** LVfractional shortening **c)** LV calculated mass **d)** LV end-systolic dimension **e)** LV-end diastolic dimension, **f)** LV end-diastolic anterior wall thickness, **g)** LV end-diastolic posterior wall thickness. n=7-8 per group. Data acquisition and analysis for b,c,d were performed by Matt Kelly.

5.2.7 Assessment of Cardiac Function by Left Ventricular Haemodynamics

To further test the hypothesis that UPS is a major contributor to the development of cardiomyopathy cardiac function was assessed by left ventricular hemodynamics (Fig. 5-10)., which is a more sensitive method than cardiac echocardiography. Left ventricular pressures were measured as described in Section 2.8.2.

No differences were observed among all three groups in key parameters including the end systolic pressure (Fig. 5-10a), end diastolic pressure (Fig. 5-10b), mean pressure (Fig. 5-10c), cycle duration (Fig. 5-10d), minimal rate of pressure decrease during diastolic relaxation (dP/dt min) (Fig. 5-10e), maximal rate of pressure increase during systolic contraction (dP/dt max) (Fig. 5-10f), the time constant of left ventricular relaxation, tau (Fig. 5-10g) and left ventricular contractility index (Fig. 5-10h).

Dobutamine infusion (4 ng/g BW/minute &16 ng/g BW/minute) caused overall changes in Max dp/dt (increase), contractility index (increase), and Tau (decrease) but no significant change was observed within groups.

These findings suggest that crossing of these two mutant mice did not affect cardiac function in any significant way and there were no signs of cardiomyopathy.

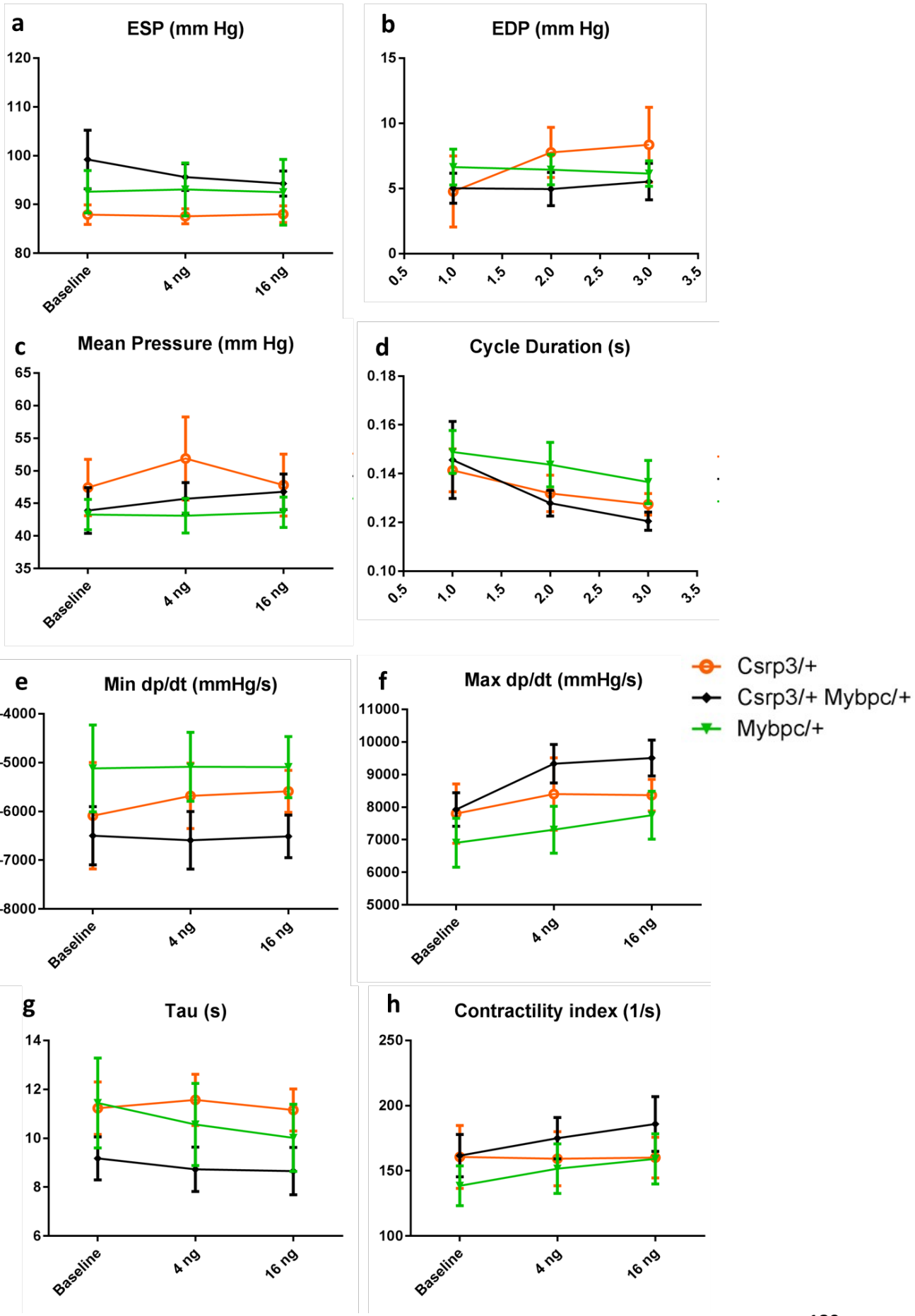

a
ESP (mm Hg)
120
110
100
90
80
Baseline
4 ng
16 ng
b
EDP (mm Hg)
15
10
5
0
0.5
1.0
1.5
2.0
2.5
3.0
3.5
c
Mean Pressure (mm Hg)
65
60
55
50
45
40
35
Baseline
4 ng
16 ng
d
Cycle Duration (s)
0.18
0.16
0.14
0.12
0.10
0.5
1.0
1.5
2.0
2.5
3.0
3.5
e
Min dp/dt (mmHg/s)
-4000
-5000
-6000
-7000
-8000
Baseline
4 ng
16 ng
f
Max dp/dt (mmHg/s)
11000
10000
9000
8000
7000
6000
5000
Baseline
4 ng
16 ng
Csrp3/+
Csrp3/+ Mybpc/+
Mybpc/+
g
Tau (s)
14
12
10
8
6
Baseline
4 ng
16 ng
h
Contractility index (1/s)
250
200
150
100
Baseline
4 ng
16 ng

Figure 5-10: Haemodynamic measurements in 6-month-old Csrp3 KI/+ (green), Mybpc3 KI/+ (orange) and Csrp3 KI/+ Mybpc3 KI/+ (black). Mice in all three KI/+ showed no difference in **a)** End Systolic Pressure (ESP) **b)** End Diastolic Pressure (EDP) **c)** Mean Pressure **d)** Cycle Duration **e)** Diastolic function (dP/dtmin**) f)** Systolic function (dP/dtmax) **g)** relaxation constant Tau, and **h)** Contractility Index. There were no significant following dobutamine infusion at both concentrations 4ng/g BW/minute and 16ng/g BW/minute either. N= 6-7 per group. Data acquisition was performed by Julia Beglov.

5.2.8 Molecular Characterization of Csrp3 KI/+ Mybpc3 KI/+ mice

Csrp3 KI/+ mice were crossed with Mybpc3 G772A mutant heterozygous (Mybpc3/+) mice to generate double heterozygous mutant mice.

No differences were observed Mybpc expression in the hearts of three groups (Fig. 511a). Csrp3 mutation carrying animals (Csrp3/+) showed reduced expression of MLP. Gapdh was used as loading control. Ventricular protein was blotted for K48 ubiquitinated proteins in these mice (Fig. 5-11b). K48 ubiquitinated proteins are degraded by proteasome and therefore would suggest if there was increased UPS degradation within these mice. No changes were observed in total K48 ubiquitinated proteins within any of the groups.

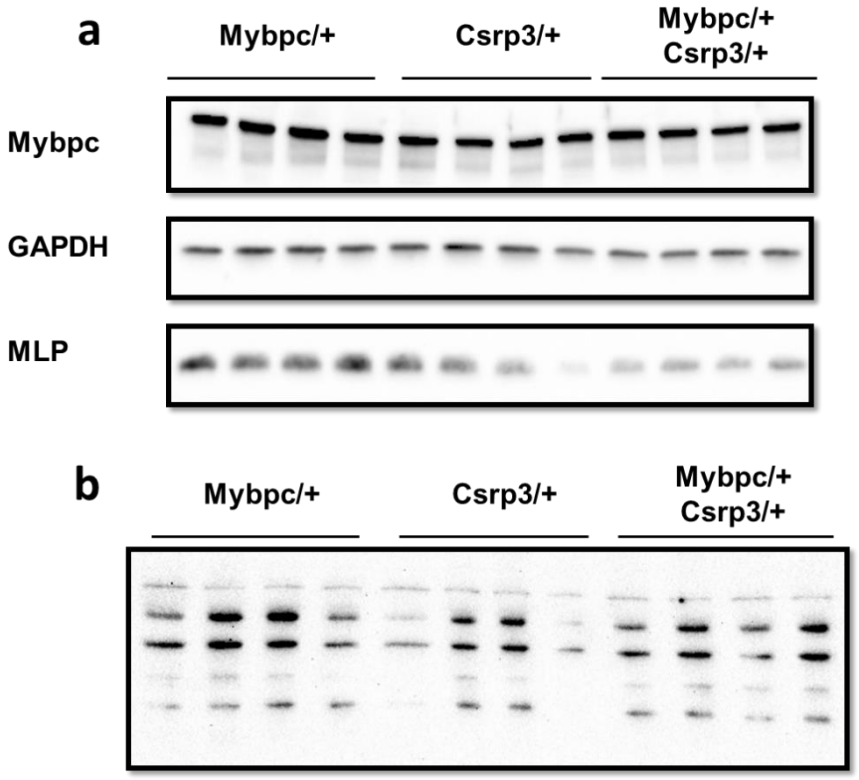


Figure 5-11. Molecular Characterization Csrp3 KI/+ Mybpc3 KI/+ mice. Representative western blot of ventricular protein from Mybpc3/+, Csrp3 KI/+ and Csrp3 KI/+ Mybpc3 KI/+ mice. (a) Mypbc3, and MLP protein levels were assessed. Mypbc3 showed no difference while MLP had lower expression in KI/+ mice compared to WT. GAPDH was used as loading control. (b) UPS associated ubiquitin anti-Ub (K48) antibody blot showed no difference in levels of K48 ubiquitinated proteins within the three groups.

5.3 Primary Conclusions of this Chapter:

1. The Csrp3 C58G and L44P mutation causes protein destabilization and increased degradation. No dominant negative effect of mutant on WT MLP was observed.
2. The C58G and L44P MLP mutant proteins are degraded by the UPS rather than autophagy lysosomal pathway.
3. Csrp3 KI/KI mice show UPS overload and impairment as indicated by the elevated protein levels of UBG76V-GFP fusion protein reporter *in vivo*.
4. Csrp3 KI/+ mice crossed with Mybpc3 KI/+ showed no overt cardiac phenotype as measured by morphometric analysis, echocardiography and left ventricular hemodynamics.

5.4 Discussion

The findings of MLP destabilization *in vitro*, and reduced expression in both heterozygous and homozygous Csrp3 knock-in mice are in line with previous work that showed heart tissue from a patient heterozygous for Csrp3 C58G exhibited diminished MLP expression (231). This protein depletion is observed in other HCM causing MLP mutations (L44P, S54R/E55G, data not shown). To evaluate whether the presence of the mutant copy also affects degradation of WT MLP, WT and mutant MLP with different tags were co-transfected. The results highlighted that degradation of C58G MLP is independent of WT MLP suggesting that presence of one mutant copy of the gene might not affect function of the normal copy. This was also confirmed in AV transduced neonatal rat cardiomyocytes (NRCs) (209).

Eukaryotic cells degrade proteins via two major pathways, the UPS and the autophagy pathway (359, 360). Use of MG-132, a known proteasome inhibitor (383), recovered expression of MLP mutant protein to levels comparable to WT protein (Fig. 4a) suggesting that the two mutant MLP proteins are mainly degraded by the UPS. Degradation by autophagic pathways was ruled out as MLP WT and C58G expression was unaffected by silencing of Atg5, an integral component of the autophagy pathway (418). Surprisingly, knock down of Atg5 caused reduction in expression of both WT and mutant protein, which may indicate general toxicity within the cell. Together these findings highlight that UPS is involved in degradation of MLP mutant protein and autophagy does not play a direct role.

Mutant or misfolded proteins are largely degraded by the UPS. However, it was important to rule out autophagy as it is part of the cell's response to proteotoxic stress. When misfolded proteins escaped from the UPS surveillance, they tend to form aggregates which are inaccessible to the proteasome, activate autophagy and are

thereby degraded by the lysosome (419, 420). Further, a study by Sarikas and colleagues highlighted that treatment of the NRCs with bafilomycin A1 (50nM, 6 h), an inhibitor of autophagy, increased the expression of one of the mutant truncated cMyBPC3, while the other remain unaffected (421). These results are in line with findings from a recent study by Singh and colleagues showing that autophagy is impaired in Mybpc3 knockin mice, and the activation of autophagy by rapamycin and caloric restriction reduced cardiac hypertrophy in the mouse model.

UPS activity is dysregulated in several human cardiac disease and mouse models (383, 420, 422). Cardiac hypertrophy, whether physiological or pathological, also results in considerable remodelling of the cardiac muscle (423). The hypertrophy of cardiomyocytes is due to cell enlargement which requires an increase in total protein content which is achieved by increase in protein synthesis. During physiological hypertrophy, brought upon by exercise or pregnancy, there is an increase in protein degradation rate as a co-translational protein quality control mechanism to ensure that proteins synthesised abnormally are degraded. On the contrary the exact mechanism of how UPS is involved in maladaptive cardiac hypertrophy is unclear However, data from human cardiac biopsies suggest accumulation of ubiquitinated protein and ubiquitinated aggregates in heart failure patients and that the defective protein degradation contributes to heart failure (424-427).

Though the results of this thesis might suggest that MLP degradation is not carried out by autophagy pathway, the role of autophagy in development of disease phenotype cannot be completely overruled as there is some interplay between these two pathways. As mentioned earlier UPS and autophagy may work together to degrade certain proteins (419, 428). UPS impairment has also been shown to induce autophagy

in order to reduce proteotoxicity as shown in rat cardiomyocytes, where inhibition of proteasome with MG132 induced autophagy (429, 430). UPS impairment can also affect autophagy mediated degradation as observed in mouse model of Mybpc3 G772A. The mouse model had increased expression of autophagy pathway related proteins, however there was an absence of transcriptional activation of autophagy genes suggesting a blockade in autophagy mediated proteolysis (417) .

Though there is increase in ubiquitinated proteins there is no consensus whether this increase is due to UPS impairment. There are reports that show that UPS levels and activity remains unaffected in failing human hearts (427), whereas some have reported that UPS is impaired in failing hearts, possibly as a result of oxidative modifications on proteasome subunits (426). Contrasting results are reported in experimental mouse models of heart failure, induced by transverse aortic constriction (TAC), where proteasomal activity is either increased (431) or decreased (425). In the latter study it also appears that the decrease in proteasome activity precedes cardiac dysfunction.

Mutations in the cardiac myosin-binding protein C, *MYBPC3*, are the most common cause of HCM, accounting for about half of the identified mutations (90). HCM mutations are frequently frameshifts resulting in production of C-terminally truncated cMyBPC. Though researchers were able to detect nonsense mRNA in patients carrying these frameshift mutations, they were unable to detect the presence of truncated c-MYBPC protein (432-435). Similar results were seen in transgenic mouse models of these mutations and experiments where mutated genes were transferred to the myocardium by gene delivery (436-438). These truncated proteins have been shown to be degraded by UPS, as inhibition of the system increased expression of mutant

protein. The expression and subsequent degradation of these proteins leads to UPS overload and impaired proteasomal activity (436, 439).

These findings suggest that the clinical hypertrophic phenotype in patients and mouse models carrying these mutations may be partly due to absence of required protein levels to maintain sarcomeric integrity and in part due to UPS overload. Recent work on other HCM causing mutations support the concept that UPS dysfunction can lead to clinical phenotype. One such study showed that *MYBPC3* missense E344K mutation causes protein destabilization, leading to UPS impairment and subsequent LV dilation and dysfunction (439). Another study revealed that loss of function mutation in the gene TRIM63 encoding Muscle RING Finger 1 (MuRF1) can cause HCM. MuRF1 is an E3 ubiquitin ligase which ubiquitinates sarcomeric proteins, resulting in their degradation by UPS. These loss of function mutations lead to impairment of UPS contributing to development of HCM, supporting the hypothesis that impaired UPS leads to cardiac dysfunction (440).

MLP C58G mutant, similar to *MYBPC3* mutants, is destabilized and the results of this chapter highlight that it is degraded by the UPS, rather than by autophagy. To evaluate global function of UPS in Csrp3 knock-in mouse, KI mice were crossed with transgenic mice expressing UbG76V-GFP reporter fusion protein. The UbG76V-GFP protein is a specific substrate of the UPS rather than general ubiquitin levels and represents the balance between ubiquitination and deubiquitination (394). There was no change observed in the morphometric analysis after knock-in mice were crossed with the UbG76V-GFP transgenic mice, suggesting the lack of aberrant effect of the transgenic reporter on the cardiac function of knock-in mice. The UbG76V-GFP protein levels were significantly higher in KI/KI mice compared to KI/+ and WT animals crossed with the transgenic. These results highlight KI/KI mice have UPS overload and subsequent

impairment which, which contributes to development of an overt cardiac phenotype in these animals.

Similar to the MLP C58G model, UPS impairment has been reported in a number of mouse models of HCM and heart failure (417, 441, 442) which lead to the suggestion that UPS regulation is an important adaptations in cardiac disease. These results suggested that the use of proteasome inhibitors might inhibit or reduce hypertrophy thereby rescuing or improving cardiac function. Proteasomal inhibition in experimental mouse models of cardiac hypertrophy, induced by isoprenaline (443), and TAC (444), showed improved cardiac function and reduced hypertrophy. However, proteasome inhibition with epoxomicin in *MYPBC* genetic mutant mouse models showed no reduction in pre-existing cardiac hypertrophy or changes in morphometric data such as HW/BW (445). No changes in mRNA levels of hypertrophy markers were observed either. The contradictory results between these models might be due the difference in mechanisms of development of disease.

Specific proteasomal activities (chymotrypsin-like, trypsin-like and caspase-like) were evaluated using fluorogenic substrates in KI/KI mice *ex-vivo* and surprisingly no significant changes were observed between WT and homozygous KI/KI group. These data conflict the findings from the UPS reporter mouse where the higher levels of UbGFP suggested proteasomal impairment. These differences in data might be explained by the different preparation/purification modes or techniques for proteolytic analysis. The *ex vivo* studies depend on the isolating the enzymes from protein lysates of frozen samples. It has been suggested that isolation and purification processes lead to activation of the enzyme as well as to structural changes (446, 447).The experiment was carried out on the soluble fraction of crude tissue homogenates and both endogenous activating and inhibiting factors of the proteasome were isolated (446,

448), however it failed to recapitulate the findings of the *in vivo* experiment. Another reason for lack of elevation of the proteolytic activities could be that the 20S proteasome is not able to compensate for increased demand. It should also be noted that the proteasome activity declines with age due to decreased overall proteasome content, alterations and/or replacement of proteasome subunits and formation of inhibitory cross-linked proteins (449). However, this cannot be the reason here as studies highlighting decline of activity look at mice well over the age of 12 months (449), whereas these studies were performed with 6 month old mice.

Csrp3 KI/+ mice failed to recapitulate a disease phenotype, in contrast to WT mice, even after aging mice to 12 months (data not shown). Since UPS overload was identified as a contributor to development of heart failure in homozygous knock-in mice, KI/+ were crossed with Mybpc3 knock-in (KI) mice, with a missense G772A mutation, which is one of the most frequent HCM mutations. The Mybc3 G772A KI/+ mice are indistinguishable from WT littermate controls but develop septal hypertrophy upon chronic stress, induced by isoprenaline/phenylephrine treatment for 1 week (416). The hypothesis was that the presence of two mutant proteins, which are both degraded by UPS, would lead to UPS overload and impairment resulting in an overt cardiac phenotype. However, there was no difference observed in morphometric analysis, or cardiac function by transthoracic echocardiography or left ventricular hemodynamics within the three groups Mybpc KI/+, Csrp3 KI/+ and Csrp3 KI/+ Mybpc KI/+. No change was observed in left ventricular function under baseline conditions or after infusion of dobutamine at two different concentrations.

There are a few reasons why this model failed to show an overt phenotype. The proteasomal load of the two mutation together might not have been enough to cause

impairment or the stress on UPS by mutant MLP degradation was not as much as the adrenergic stress induced in previous studies (417). The mutant proteins might either directly inhibit different subunits of the proteasome or indirectly, through feedback mechanisms or affect different processes in the UPS. Since abundance of MLP is lower than Mybpc3 (450, 451)the combined load of these mutant proteins on the UPS may not be sufficient to trigger cardiac maladaptation by UPS impairment (452).

Mybpc protein levels in Mybpc KI/+ mice and double heterozygous KI mice were comparable to WT controls. This was surprising as expression was expected to be reduced, as the mutant protein is a target for degradation. Perhaps this was due to some compensatory signalling within the knock-in hearts. RNA levels need to be assessed to evaluate if the heart in these mice is compensating the lack of expression by increasing the level of transcription of Mybpc in these mice.

The findings of this chapter highlight UPS impairment as a key contributor to the development of cardiomyopathy phenotype in KI/KI animals. Further work is required to understand the mechanism of how mutant protein causes this impairment. One probable mechanism, as mentioned, is the overloading of the proteasome system. These mutant proteins might potentially block the proteasome for other proteins to be degraded, as observed in a study where c-Mybpc formed aggregates blocking the degradation of other proteasome substrates (436). This is a well-known feature of neurodegenerative disorders, where misfolded proteins and aggregates have been suggested to overload the proteasome and/or block the pore (453). For example, in Alzheimer's disease aggregated tau protein, tagged with ubiquitin, blocks the gate the 19S catalytic particle by binding to its recognition site, causing proteasomal impairment (454). Other potential mechanisms leading to UPS impairment might be due to the

direct effect of changes in calcium signalling pathways as a consequence of heart failure. For example, the calcium binding protein, Calmodulin, has been shown to interact with subunits of the 26S proteasome. Aberrant signalling changes could disrupt these interactions leading to changes in activity of UPS (455). Another potential mechanism of calcium mediated proteasome impairment is highlighted by studies where increased calcium concentrations induce mitochondrial dysfunction which lead to increase in reactive oxygen species (ROS). These ROS interact with proteasome to cause impairment (456-458).

It is also important to study what pathways within the UPS are responsible for the degradation of MLP. Recent work has highlighted that mutant C58G MLP interacts with co-chaperone BCL-2 associated athanogene3 (Bag3), which plays an important role in protein quality control [23] in the heart and has a crucial role in the maintenance of cardiac homeostasis. Csrp3 KI/KI mice exhibited a significant increase in expression of Bag3 and its associated heat shock proteins (Hsp), Hsp 70 and Hsc70. Overexpression of Bag3 in a mouse model activates cardiac hypertrophy so it can be hypothesized that the induction of Bag3 contributes to the pathogenic hypetrophic signalling in the Csrp3 KI/KI mice.

The findings of this chapter highlight the protein degradation and resulting proteasomal overload play key roles in development and progression of cardiomyopathy phenotype in *Csrp3* KI mouse model. These findings, along with other published *in vitro* work from the group (209), suggest that this might be a common mechanism for HCM-causing CSRP3 mutations that result in low protein expression of MLP.

Chapter 6. General Discussion

In terms of genetic etiologies HCM and DCM are the most well understood cardiomyopathies (90, 459). Most of the disease-causing mutations are inherited in an autosomal dominant manner (90). Though these diseases manifest themselves differently in terms of phenotypes there is a significant overlap in the molecular pathways governing them. HCM and DCM both exhibit cellular hypertrophy of cardiomyocytes (460), fibrosis driven by fibroblast activation and collagen deposition (461, 462).

Genome wide linkage analysis in large families has led to the identification of disease specific gene loci which have enhanced our understanding of cardiomyopathies (463465). As the pathogenic variants attributed to HCM all belonged to genes encoding sarcomeric components, including *MYH7*, *TPM1*, *TNNT2* and *MYBPC3*, HCM was theorized to be a “disease of the sarcomere” (90, 107, 464, 466). In contrast to HCM, DCM can be of both genetic and acquired origin. Mutations causing DCM are not limited to those in sarcomeric proteins but also include cytoskeletal, nuclear envelope, desmosomal, ion channels and Z-disc proteins. Acquired causes of DCM include infectious agents, drugs and toxins, and endocrine disturbances (467).

Mutations in the gene *CSRP3* encoding for Muscle Lim Protein (MLP) have been shown to cause hypertrophic and dilated cardiomyopathy (188, 215, 216). These mutations are particularly interesting to study as MLP is one of the few non-sarcomeric proteins that lead to autosomal HCM (182, 216, 234, 468). The accessibility of next generation sequencing data has helped to validate previously published pathogenic variants. One such variant, *CSRP3* p. W4R, described initially as a DCM-causing pathogenic variant (469), has been re-classified as a benign polymorphism (182, 216).

Linkage analysis in a large German HCM pedigree led to identification of the C58G missense pathogenic variant in *CSRP3* (216). The MLP C58G mutant protein, when compared to MLP wildtype, was shown to be more susceptible to degradation *in vitro*. This supported findings that MLP levels in a cardiac biopsy were significantly reduced, up to 40% in a patient with a heterozygous MLP C58G pathogenic variant (215).

Several studies on MLP have been published since its initial identification by Arber and colleagues (189, 470), including development of MLP KO mouse model, however, the exact mechanisms by which MLP loss affects cardiac function is still unclear. This thesis focused on understanding the underlying mechanisms governing nonsarcomeric HCM caused by the best characterized human MLP mutation, C58G. The aim was to evaluate the phenotype of a C58G mouse model, highlight perturbations in signaling pathways through biochemical techniques and validate findings using other mouse models of disease.

The Csrp3 KI homozygous (KI/KI) mice exhibited features of human cardiomyopathy, whereas the heterozygous mouse (Csrp3 KI/+) failed to show a significant difference when compared to WT littermate controls. The KI/KI mice showed impairment in both diastolic and systolic function, increased left ventricular mass and chamber dimensions and reduced contractile reserve. These findings highlight a DCM phenotype along with compensatory hypertrophy. No significant fibrosis, which usually accompanies hypertrophy, was observed by hydroxyproline assay, western lot for collagen and histological analysis. However, qPCR and RNASeq results showed increase expression of fibrosis related genes. Further, the phenotype of KI/KI was similar to MLP KO mice (189).

KI/+ mice failed to develop a pathological phenotype and were comparable to WT littermate controls in most parameters. Though this result was contradictory to our initial hypothesis that heterozygous mutant mice will develop a cardiomyopathy phenotype, it is in line with the study of MLP heterozygous KO mice (MLP +/−) which showed no overt phenotype under normal conditions. MLP +/- mice however presented with increased left ventricular dilation and systolic dysfunction and decreased survival after induction of myocardial infarction. These findings were associated with a suppressed pro-hypertrophic Calcineurin-Nuclear Factor of Activated T-cells (NFAT) signaling pathway (208). To uncover any phenotype, aortic banding was performed on KI/+, however these mice failed to show any differences compared to WT controls (209). These results are contrary to the mechanosensing function of MLP and more studies need to be conducted to clarify the role of MLP in regulation of heart function. The results of KI/+ mice are also similar to HCM mouse models of other genes such as myosin binding protein C and myosin heavy chain where heterozygous mice showed no significant difference in phenotype to their littermate controls (114, 254, 267). Further, MLP C58G mutation-linked cardiac hypertrophy has been shown to be late onset, suggesting that the phenotype of KI/+ mice should have been evaluated in older mice, to observe any significant changes compared to WT mice. However, the KI/+ mice were observed for a year, and they failed to show any significant changes in cardiac function.

Though mice serve as good model organisms for studying most disease mechanisms for cardiomyopathies, they also have fundamental differences in cardiac physiology compared to humans, which may affect the development phenotype in mice compared to humans. These include significant differences in heart rate and electrical conduction as well as different composition of cardiac specific protein isoforms (471, 472). Further,

recapitulation of human disease is also difficult in some cases due to the difference in lifestyle between mice and humans, where mice have a far more sedentary lifestyle.

To better understand the signaling pathways leading to the overt phenotype in MLP KI/KI mice, RNASeq was used to evaluate the transcriptomic profile of these mice. The transcriptomics results highlighted hallmarks of hypertrophic pathways such as increased expression of *Nppa, Nppb, Acta1, Myh7* and increased expression of genes involved in fibrosis such as *Tgfb, Col9a2, Fgf6*. These results were in agreement with other results from the lab where qPCR was conducted to the heart tissue from these animals (209). Further bioinformatic analysis using GOrilla and KEGG pathway enrichment highlighted pathways including in accordance with the phenotype. The most enriched GO cellular components was the “sarcomere” and other cellular components included “extracellular matrix”, “proteinaceous extra cellular region” and “extracellular region”. The most enriched GO biological process was “regulation of heart rate” and other significant processes included “regulation of cell proliferation”, “development process”, “anatomical structure development” and “negative regulation of biological process”. All these processes highlight a phenotype representative of heart failure. RNASeq of another DCM mouse model that expresses a missense mutation (p.Arg9Cys) in phospholamban ($PLN^{R9C/+}$) showed similar GO compartments and the pathways highlighted in Csrp3 KI/KI mice. The $PLN^{R9C/+}$ mice, however, exhibited more metabolic dysregulation than the Csrp3 KI mouse model (316). KI/+ mice were not used for transcriptomic studies as they had failed to show any overt phenotype or significant differences in qPCR results.

RNASeq analysis was also conducted on MLP KO mice to compare their transcriptome with that of KI/KI mice. The two mouse models had an overlap in the genes which were upregulated and downregulated but also exhibited some difference.

GO pathway analysis showed a similar profile for both these mouse models. The similarity in underlying transcriptome of these two mouse models suggests that the development of disease in both mouse models is similar. Though the expression of number of genes highlighted in these two mouse models were expected with a murine model of cardiomyopathy, there were quite a few genes, such as *Syndig1, Chodl, Frem1 and Tmem200a*, which are usually not associated with cardiomyopathies.

Surprisingly, RNASeq failed to detect changes in expression of genes related to the UPS. This might be due to the proteasome assembly/disassembly being a mode of regulation of UPS rather than changes in transcription level of the components in UPS pathway.

MLP protein expression levels were reduced in both KI/+ and KI/KI mouse models. The reduced levels were attributed to destabilization of protein along with increased degradation of mutant protein. The degradation did not affect the levels of WT MLP. The results highlighted that mutant protein was degraded by the UPS rather than autophagy lysosomal pathway. These results were supported by findings of proteasome overload and impairment in mice which were generated by breeding knock-in mice with transgenic mouse expressing mutant UBG76V-GFP reporter protein. The findings of this thesis were similar to studies conducted by Carrier and colleagues on a mutant Mybpc knock-in mouse (416). The findings from Csrp3 KI/KI mouse model highlight that the HCM phenotype in these mice is driven by the lack of functional MLP protein and the proteasomal overload.

We crossed Csrp3 KI/+ mice crossed with Mybpc3 KI/+ with the hypothesis that the increase in proteasome activity due to these two mutations would cause overload of the UPS and lead to an overt phenotype. However, these double mutant mice showed

no overt cardiac phenotype as measured by morphometric analysis, echocardiography and left ventricular hemodynamics. These results could be attributed to the relative size of the proteins and their relative expression within the cardiomyocytes as the overload caused by the heavier and highly expressed mutant Mybpc protein may be greater than that caused by mutant MLP protein. A recent study published by Jiyayang and colleague has shed some light on these experiments. The authors generated a mouse model lacking both MLP and cMYBPC (473). Their hypothesis was that the hypercontractility of MYBPC KO mice would compensate for the DCM phenotype of MLP KO mice. The results supported their hypothesis as double KO (dKO) mice exhibited reduced hypertrophy, improved ejection fraction and rate of pressure development compared with MLP KO mice. The improved systolic function in MLP KO mice was attributed to improved calcium sensitivity of force generation, and significantly accelerated rate of cross-bridge detachment (473). We had not taken into account the compensatory mechanisms of disease while generating the double mutant mice and perhaps the increase in proteasome activity that might have resulted from two different mutations was offset by the different cardiac regulatory mechanisms in the different mouse models. It should be noted, however, that the we used mutant mice with at least one functional copy of genes for both *Mlp* and *Mybpc* which might have reduced the effect of these compensatory mechanism, especially considering both these mutations do not recapitulate the human disease in heterozygous state. Surprisingly western blot analysis of the Mybpc/+ mice showed no changes in expression of total Mybpc in heart tissue (Figure 5-11). It was expected the protein levels would be lower than WT littermate control. This might suggest some form of compensation in these mice causing increase in protein expression driven by the one functional copy of Mybpc.

We have been able to generate a murine model that recapitulates the human DCM phenotype. Barring traditional caveats associated with murine models of human disease, the pathomechanisms described in previous chapters are of direct relevance to patients with cardiomyopathies resulting from mutations in MLP. However, mutations in MLP genes are very rare, potentially limiting the clinical impact of the mechanisms described. Nevertheless, similarities between *CSRP3* and *MYBPC3* associated cardiomyopathies and the broader families of HCM and DCM suggest that shared mechanisms of disease progression may exist. If these associations are correct, treatments targeting mechanisms underlying MLP related cardiomyopathy may be effective for HCM and DCM and may have broader implications for acquired cardiac conditions.

6.1 Further Studies and Therapeutic Implications:

The goal of understanding the cellular and molecular mechanisms driving pathogenesis of disease is to allow us to develop novel therapeutics, in the hope of improving the outcomes and improving the quality of life for patients suffering from these diseases. The findings of this thesis have highlighted a unique pathway driving pathogenesis of heart failure associated with a rare mutation in a non-sarcomeric protein, MLP. These results along with other findings from the literature highlight the similarities in pathophysiological mechanisms of HCM and DCM caused by mutations in different genes. The conclusions therefore can be applied more broadly to other models of disease and therefore may provide opportunities for disease prevention or reversion.

Several studies have highlighted the role of ubiquitin proteasome system in development of cardiac disease (443, 444). Inhibition of the proteasome has been

shown to reduce hypertrophy and improve cardiac function in experimental models of disease (26). To identify which factor, UPS impairment or the lack of MLP protein, contributes to development of disease a study could be designed where UPS is inhibited. The inhibition would lead to increase protein expression of MLP and reduced stress on the cell caused by increased UPS activity. Though the protein would still be affected by the mutation, MLP might still be able to perform some of its functions. A similar study was conducted by Schlossarek and colleagues on the genetically modified mouse model of Mybpc (416). One-week treatment with epoxomicin showed a slight, yet significant, improvement in cardiac function of the knockin mouse model but showed no significant change in hypertrophy (474). Targeting the UPS for therapy is challenging as it plays a crucial role in many fundamental biological processes. However, there is some evidence in the literature that is contrary to the findings presented by Schlossarek and colleagues when proteasome inhibitors are used chronically (475). Further, though bortezomib (reversible proteasome inhibitor) is well tolerated in multiple myeloma cancer patients, it has been linked with increased cardiac complications in elderly patients and patients with pre-existing heart conditions (476-478). (29-31). Though chronic UPS suppression may lead to complications, acute treatment with UPS inhibitors might be a therapeutic option to improve cardiac function.

Though the results in this thesis were able to show that MLP degradation takes place by UPS rather than autophagy lysosomal pathway further experiments need to be conducted to identify which proteins and pathways within the UPS are responsible for degradation of MLP and which of these can be potential therapeutic targets for treatment of disease. Recent study by our group has highlighted that the co-chaperone protein BCL-2 associated athanogene3 (Bag3) interacts with MLP C58G in KI/KI hearts. Further both transcript and protein expression of the Bag3 protein were

significantly increased in hearts of Csrp3 KI/KI animals (479). Bag3 serves an important role in maintain protein quality within the cell and loss of function mutations in the protein result in DCM phenotype, in murine experimental model and humans (480). These findings suggest that the Bag3 signaling axis might contribute to the pathomechanisms driving hypertrophic signaling in Csrp3 KI/KI mice. More *in vitro* and *in vivo* experiments need to be conducted to investigate whether the increase in Bag3 levels in MLP KI/KI mice are contribute to disease progression or are increased as a compensation to reduced cardiac function.

Further experiments are required to investigate whether these genes are potential biomarkers of disease and play a causal role in development of disease or whether they are dysregulated as a consequence to the heart failure phenotype. One method would be to profile the transcriptome of these mice before development of heart failure and post heart failure. This would allow us to differentiate between the genes that affect development of disease compared with those dysregulated due to the disease. The outcomes of these analysis also need to be compared with results from other murine mouse models of cardiomyopathy to understand the difference in disease causation and progression towards heart failure due to different sarcomeric and nonsarcomeric genes. One of the challenges of conducting such studies is the different mouse backgrounds that laboratories use. Further results are also affected by the different methods of data analysis and isolation of RNA for analysis. Finally, though the transcriptome offers insight into the pathways affected within the cells, proteomic studies need to be conducted as some changes in RNA may not translate into meaningful protein and signaling changes. This was evident with the upregulation of profibrotic genes in these mice, however, no significant fibrosis was observed in these mice at the protein level.

Recent findings from our lab highlight the role of aberrant PKCα signaling in development of heart failure phenotype in MLP KO mice. MLP inhibits activity PKCα activity and the absence of MLP results in persistent long-term activation of PKCα which contributes to the heart failure phenotype (258). It was observed that MLP is a substrate for PKCα and the phosphorylation of MLP was dependent on the mutation and eventual disease state. *In vitro* experiments showed that MLP mutants that caused DCM were hyper-phosphorylated by PKCα whereas MLP mutants that were associated with the development of HCM were hypo-phosphorylated. These findings show that the state of phosphorylation of MLP might affect its function and interacting partners. Further, it is unclear at present whether MLP phosphorylation and other posttranslational modifications (PTM) affect its oligomerization which in turn affects its localization within the cell (199, 481). To better understand MLP's function, proteomic analyses focusing on PTMs needs to be performed on protein isolated from different experimental models of heart disease and at different stages.

Other potential therapies include delivery of adeno-associated virus encoding for MLP. Similar strategy delivering *Mybpc-3* prevented development of HCM in a mouse model (482). Another exciting treatment undergoing clinical trials is the orally administered small molecule MYK-461. MYK-461 allosterically inhibits myosin ATPase activity, diminishes myocyte force production, and has been shown to suppress development of cardiac hypertrophy, myocyte disarray, and fibrosis in a mouse model of HCM (483). Considering its mode of action MYK-461 could be used a therapeutic option for MLP patients but more studies need to be conducted, starting with treatment of drug on MLP animal models.

This thesis investigated the pathophysiology of cardiomyopathy caused by MLP C58G protein to study the molecular mechanism of HCM in a genomic context as close as possible to the human condition. The mutation was chosen as a known pathogenic variant. The mouse model of *CSRP3* C58G exhibited a DCM phenotype with compensatory hypertrophy in the homozygous setting. This systolic and diastolic dysfunction was associated with reduced MLP protein expression owing to increased turnover by the UPS. Heterozygous mice failed to show an overt phenotype which could be explained by the fact that *CSRP3* mutations caused HCM is often characterized by late on-set in humans and that there are fundamental differences in physiology between the heart of a human and that of a mouse. The mouse model helped shed light on the underlying pathomechanisms of cardiomyopathy caused due to mutations in nonsarcomeric proteins.

References

1. Avraham R. The circulatory system. Philadelphia, PA: Chelsea House Publishers; 2000.

2. Klabunde RE. Cardiovascular Physiology Concepts. 2nd ed. Lippincott Williams and Wilkins; 2011.

3. Parker KK, Ingber DE. Extracellular matrix, mechanotransduction and structural hierarchies in heart tissue engineering. Philos Trans R Soc Lond , B, Biol Sci. 2007 Aug 29,;362(1484):1267-79.

4. Vliegen HW, van der Laarse A, Cornelisse CJ, Eulderink F. Myocardial changes in pressure overload-induced left ventricular hypertrophy. A study on tissue composition, polyploidization and multinucleation. Eur Heart J. 1991 Apr;12(4):48894.

5. Severs NJ. Intercellular junctions and the cardiac intercalated disk. Adv Myocardiol. 1985;5:223-42.

6. Bernstein SA, Morley GE. Gap junctions and propagation of the cardiac action potential. Adv Cardiol. 2006;42:71-85.

7. Luther PK. The vertebrate muscle Z-disc: sarcomere anchor for structure and signalling. J Muscle Res Cell Motil. 2009;30(5-6):171-85.

8. Huxley H, Hanson J. Changes in the cross-striations of muscle during contraction and stretch and their structural interpretation. Nature. 1954 May 22,;173(4412):9736.

9. Huxley AF, Niedergerke R. Measurement of muscle striations in stretch and contraction. J Physiol (Lond). 1954 May 28,;124(2):47P.

10. Reisler E. Actin molecular structure and function. Curr Opin Cell Biol. 1993 Feb;5(1):41-7.

11. Halliburton WD. On Muscle-Plasma. J Physiol (Lond). 1887 Aug;8(3-4):133-202.

12. Tobacman LS. Thin filament-mediated regulation of cardiac contraction. Annu Rev Physiol. 1996;58:447-81.

13. Pardee JD, Spudich JA. Purification of muscle actin. Meth Enzymol. 1982;85 Pt B:164-81.

14. Pollard TD. Regulation of actin filament assembly by Arp2/3 complex and formins. Annu Rev Biophys Biomol Struct. 2007;36:451-77.
15. Otterbein LR, Graceffa P, Dominguez R. The crystal structure of uncomplexed actin in the ADP state. Science. 2001 Jul 27,;293(5530):708-11.

16. Wegner A. Head to tail polymerization of actin. J Mol Biol. 1976 Nov;108(1):139-50.

17. Korn ED, Carlier MF, Pantaloni D. Actin polymerization and ATP hydrolysis. Science. 1987 Oct 30,;238(4827):638-44.

18. Dominguez R, Holmes KC. Actin structure and function. Annu Rev Biophys. 2011;40:169-86.

19. Gordon AM, Regnier M, Homsher E. Skeletal and cardiac muscle contractile activation: tropomyosin "rocks and rolls". News Physiol Sci. 2001 Apr;16:49-55.

20. Solaro RJ, Rarick HM. Troponin and tropomyosin: proteins that switch on and tune in the activity of cardiac myofilaments. Circ Res. 1998 Sep 07,;83(5):471-80.

21. Xu C, Craig R, Tobacman L, Horowitz R, Lehman W. Tropomyosin positions in regulated thin filaments revealed by cryoelectron microscopy. Biophys J. 1999 Aug;77(2):985-92.

22. Katrukha IA. Human cardiac troponin complex. Structure and functions. Biochemistry Mosc. 2013 Dec;78(13):1447-65.

23. Filatov VL, Katrukha AG, Bulargina TV, Gusev NB. Troponin: structure, properties, and mechanism of functioning. Biochemistry Mosc. 1999 Sep;64(9):96985.

24. Sundaralingam M, Bergstrom R, Strasburg G, Rao ST, Roychowdhury P, Greaser M, et al. Molecular structure of troponin C from chicken skeletal muscle at 3angstrom resolution. Science. 1985 Feb 22,;227(4689):945-8.

25. Houdusse A, Love ML, Dominguez R, Grabarek Z, Cohen C. Structures of four Ca2+-bound troponin C at 2.0 A resolution: further insights into the Ca2+-switch in the calmodulin superfamily. Structure. 1997 Dec 15,;5(12):1695-711.

26. Zot HG, Potter JD. A structural role for the Ca2+-Mg2+ sites on troponin C in the regulation of muscle contraction. Preparation and properties of troponin C depleted myofibrils. J Biol Chem. 1982 Jul 10,;257(13):7678-83.

27. Potter JD, Gergely J. Troponin, tropomyosin, and actin interactions in the Ca2+ regulation of muscle contraction. Biochemistry. 1974 Jun 18,;13(13):2697-703.

28. Lakowicz JR, Gryczynski I, Cheung HC, Wang CK, Johnson ML, Joshi N. Distance distributions in proteins recovered by using frequency-domain fluorometry. Applications to troponin I and its complex with troponin C. Biochemistry. 1988 Dec 27,;27(26):9149-60.

29. Wang CK, Cheung HC. Proximity relationship in the binary complex formed between troponin I and troponin C. J Mol Biol. 1986 Oct 05,;191(3):509-21.

30. Shave R, Ross P, Low D, George K, Gaze D. Cardiac troponin I is released following high-intensity short-duration exercise in healthy humans. Int J Cardiol. 2010 Nov 19,;145(2):337-9.

31. Metzger JM, Westfall MV. Covalent and noncovalent modification of thin filament action: the essential role of troponin in cardiac muscle regulation. Circ Res. 2004 Feb 06,;94(2):146-58.

32. Burkart EM, Sumandea MP, Kobayashi T, Nili M, Martin AF, Homsher E, et al. Phosphorylation or glutamic acid substitution at protein kinase C sites on cardiac troponin I differentially depress myofilament tension and shortening velocity. J Biol Chem. 2003 Mar 28,;278(13):11265-72.

33. Buscemi N, Foster DB, Neverova I, Van Eyk JE. p21-activated kinase increases the calcium sensitivity of rat triton-skinned cardiac muscle fiber bundles via a mechanism potentially involving novel phosphorylation of troponin I. Circ Res. 2002 Sep 20,;91(6):509-16.

34. Kentish JC, McCloskey DT, Layland J, Palmer S, Leiden JM, Martin AF, et al. Phosphorylation of troponin I by protein kinase A accelerates relaxation and crossbridge cycle kinetics in mouse ventricular muscle. Circ Res. 2001 May 25,;88(10):1059-65.

35. Knott A, Purcell I, Marston S. In vitro motility analysis of thin filaments from failing and non-failing human heart: troponin from failing human hearts induces slower filament sliding and higher Ca(2+) sensitivity. J Mol Cell Cardiol. 2002 Apr;34(4):46982.

36. Bodor GS, Oakeley AE, Allen PD, Crimmins DL, Ladenson JH, Anderson PA. Troponin I phosphorylation in the normal and failing adult human heart. Circulation. 1997 Sep 02,;96(5):1495-500.

37. Perry SV. Troponin T: genetics, properties and function. J Muscle Res Cell Motil. 1998 Aug;19(6):575-602.

38. Anderson PA, Malouf NN, Oakeley AE, Pagani ED, Allen PD. Troponin T isoform expression in humans. A comparison among normal and failing adult heart, fetal heart, and adult and fetal skeletal muscle. Circ Res. 1991 Nov;69(5):1226-33.

39. Li MX, Wang X, Sykes BD. Structural based insights into the role of troponin in cardiac muscle pathophysiology. J Muscle Res Cell Motil. 2004;25(7):559-79.

40. Vicente-Manzanares M, Ma X, Adelstein RS, Horwitz AR. Non-muscle myosin II takes centre stage in cell adhesion and migration. Nat Rev Mol Cell Biol. 2009 Nov;10(11):778-90.

41. Szczesna D, Zhao J, Jones M, Zhi G, Stull J, Potter JD. Phosphorylation of the regulatory light chains of myosin affects Ca2+ sensitivity of skeletal muscle contraction. J Appl Physiol. 2002 Apr;92(4):1661-70.

42. Rayment I, Holden HM, Whittaker M, Yohn CB, Lorenz M, Holmes KC, et al. Structure of the actin-myosin complex and its implications for muscle contraction. Science. 1993 Jul 02,;261(5117):58-65.

43. Lowey S, Waller GS, Trybus KM. Skeletal muscle myosin light chains are essential for physiological speeds of shortening. Nature. 1993 Sep 30,;365(6445):454-6.

44. Hernandez OM, Jones M, Guzman G, Szczesna-Cordary D. Myosin essential light chain in health and disease. Am J Physiol Heart Circ Physiol. 2007 Apr;292(4):1643.

45. Trayer IP, Trayer HR, Levine BA. Evidence that the N-terminal region of A1-light chain of myosin interacts directly with the C-terminal region of actin. A proton magnetic resonance study. Eur J Biochem. 1987 Apr 01,;164(1):259-66.

46. Schaub MC, Hefti MA, Zuellig RA, Morano I. Modulation of contractility in human cardiac hypertrophy by myosin essential light chain isoforms. Cardiovasc Res. 1998 Feb;37(2):381-404.

47. Timson DJ, Trayer HR, Smith KJ, Trayer IP. Size and charge requirements for kinetic modulation and actin binding by alkali 1-type myosin essential light chains. J Biol Chem. 1999 Jun 25,;274(26):18271-7.

48. Griffith LM, Downs SM, Spudich JA. Myosin light chain kinase and myosin light chain phosphatase from Dictyostelium: effects of reversible phosphorylation on myosin structure and function. J Cell Biol. 1987 May;104(5):1309-23.

49. Sweeney HL, Bowman BF, Stull JT. Myosin light chain phosphorylation in vertebrate striated muscle: regulation and function. Am J Physiol. 1993 May;264(5 Pt 1):1085.

50. Margossian SS. Reversible dissociation of dog cardiac myosin regulatory light chain 2 and its influence on ATP hydrolysis. J Biol Chem. 1985 Nov 05,;260(25):13747-54.

51. Levine RJ, Yang Z, Epstein ND, Fananapazir L, Stull JT, Sweeney HL. Structural and functional responses of mammalian thick filaments to alterations in myosin regulatory light chains. J Struct Biol. 1998;122(1-2):149-61.

52. Pfuhl M, Gautel M. Structure, interactions and function of the N-terminus of cardiac myosin binding protein C (MyBP-C): who does what, with what, and to whom? J Muscle Res Cell Motil. 2012 May;33(1):83-94.

53. Harris SP, Bartley CR, Hacker TA, McDonald KS, Douglas PS, Greaser ML, et al. Hypertrophic cardiomyopathy in cardiac myosin binding protein-C knockout mice. Circ Res. 2002 Mar 22,;90(5):594-601.

54. Freiburg A, Gautel M. A molecular map of the interactions between titin and myosin-binding protein C. Implications for sarcomeric assembly in familial hypertrophic cardiomyopathy. Eur J Biochem. 1996 Jan 15,;235(1-2):317-23.

55. Okagaki T, Weber FE, Fischman DA, Vaughan KT, Mikawa T, Reinach FC. The major myosin-binding domain of skeletal muscle MyBP-C (C protein) resides in the COOH-terminal, immunoglobulin C2 motif. J Cell Biol. 1993 Nov;123(3):619-26.

56. Sadayappan S, Gulick J, Osinska H, Martin LA, Hahn HS, Dorn GW, II, et al. Cardiac Myosin-Binding Protein-C Phosphorylation and Cardiac Function. Circulation Research. 2005 Nov 25,;97(11):1156-63.

57. Gruen M, Gautel M. Mutations in beta-myosin S2 that cause familial hypertrophic cardiomyopathy (FHC) abolish the interaction with the regulatory domain of myosinbinding protein-C. J Mol Biol. 1999 Feb 26,;286(3):933-49.

58. Weisberg A, Winegrad S. Alteration of myosin cross bridges by phosphorylation of myosin-binding protein C in cardiac muscle. Proc Natl Acad Sci U S A. 1996 Aug 20,;93(17):8999-9003.

59. Trinick J, Knight P, Whiting A. Purification and properties of native titin. J Mol Biol. 1984 Dec 05,;180(2):331-56.

60. Guo W, Bharmal SJ, Esbona K, Greaser ML. Titin diversity--alternative splicing gone wild. J Biomed Biotechnol. 2010;2010:753675.

61. Ehler E, Gautel M. The sarcomere and sarcomerogenesis. Adv Exp Med Biol. 2008;642:1-14.

62. Linke WA. Sense and stretchability: the role of titin and titin-associated proteins in myocardial stress-sensing and mechanical dysfunction. Cardiovasc Res. 2008 Mar 01,;77(4):637-48.

63. Tskhovrebova L, Trinick J. Titin: properties and family relationships. Nat Rev Mol Cell Biol. 2003 Sep;4(9):679-89.

64. Whiting A, Wardale J, Trinick J. Does titin regulate the length of muscle thick filaments? J Mol Biol. 1989 Jan 05,;205(1):263-8.

65. Radke MH, Polack C, Methawasin M, Fink C, Granzier HL, Gotthardt M. Deleting
Full Length Titin Versus the Titin M-Band Region Leads to Differential Mechanosignaling and Cardiac Phenotypes. Circulation. 2019 Apr 09,;139(15):181327.

66. Linke WA. Titin Gene and Protein Functions in Passive and Active Muscle. Annu Rev Physiol. 2018 02 10,;80:389-411.

67. Trombitás K, Redkar A, Centner T, Wu Y, Labeit S, Granzier H. Extensibility of isoforms of cardiac titin: variation in contour length of molecular subsegments provides a basis for cellular passive stiffness diversity. Biophys J. 2000 Dec;79(6):3226-34.

68. Lalande S, Mueller PJ, Chung CS. The link between exercise and titin passive stiffness. Exp Physiol. 2017 09 01,;102(9):1055-66.

69. Labeit S, Kolmerer B. Titins: giant proteins in charge of muscle ultrastructure and elasticity. Science. 1995 Oct 13,;270(5234):293-6.

70. Gigli M, Begay RL, Morea G, Graw SL, Sinagra G, Taylor MRG, et al. A Review of the Giant Protein Titin in Clinical Molecular Diagnostics of Cardiomyopathies. Front Cardiovasc Med. 2016;3:21.

71. Sorimachi H, Ishiura S, Suzuki K. Structure and physiological function of calpains. Biochem J. 1997 Dec 15,;328 (Pt 3):721-32.

72. Lange S, Xiang F, Yakovenko A, Vihola A, Hackman P, Rostkova E, et al. The kinase domain of titin controls muscle gene expression and protein turnover. Science. 2005 Jun 10,;308(5728):1599-603.

73. Wu Y, Cazorla O, Labeit D, Labeit S, Granzier H. Changes in titin and collagen underlie diastolic stiffness diversity of cardiac muscle. J Mol Cell Cardiol. 2000 Dec;32(12):2151-62.

74. Tskhovrebova L, Trinick J. Titin: properties and family relationships. Nat Rev Mol Cell Biol. 2003 Sep;4(9):679-89.

75. Linke WA. Sense and stretchability: the role of titin and titin-associated proteins in myocardial stress-sensing and mechanical dysfunction. Cardiovasc Res. 2008 Mar 01,;77(4):637-48.

76. Hanson J, Huxley HE. Structural basis of the cross-striations in muscle. Nature. 1953 Sep 19,;172(4377):530-2.

77. Huxley HE. The double array of filaments in cross-striated muscle. J Biophys Biochem Cytol. 1957 Sep 25,;3(5):631-48.

78. Geeves MA, Holmes KC. The molecular mechanism of muscle contraction. Adv Protein Chem. 2005;71:161-93.

79. McKillop D, Boyle GW, Cockshott ID, Jones DC, Phillips PJ, Yates RA. Metabolism and enantioselective pharmacokinetics of Casodex in man. Xenobiotica. 1993 Nov;23(11):1241-53.

80. Stanfield CL, Wilson-Ashworth H. Principles of human physiology. 4th ed. Harlow: Pearson Education; 2011.

81. Savarese G, Lund LH. Global Public Health Burden of Heart Failure. Cardiac failure review. 2017 Apr;3(1):7.

82. John E. A. Blair, Mark Huffman, Sanjiv J. Shah. Heart Failure in North America. Current Cardiology Reviews. 2013 May;9(2):128-46.

83. Robertson J, McElduff P, Pearson S, Henry DA, Inder KJ, Attia JR. The health services burden of heart failure: an analysis using linked population health data-sets. BMC Health Serv Res. 2012 Apr 25,;12:103.

84. Guo Y, Lip GYH, Banerjee A. Heart failure in East Asia. Curr Cardiol Rev. 2013 May;9(2):112-22.

85. Al-Shamiri MQ. Heart Failure in the Middle East. Curr Cardiol Rev. 2013 5;9(2):174-8.

86. Heidenreich PA, Albert NM, Allen LA, Bluemke DA, Butler J, Fonarow GC, et al. Forecasting the Impact of Heart Failure in the United States. Circ Heart Fail. 2013 5;6(3):606-19.

87. Ziaeian B, Fonarow GC. Epidemiology and aetiology of heart failure. Nature reviews. Cardiology. 2016 Jun;13(6):368-78.

88. Metra M, Teerlink JR. Heart failure. The Lancet. 2017 /10/28;390(10106):1981-95.

89. Federmann M, Hess OM. Differentiation between systolic and diastolic dysfunction. Eur Heart J. 1994 Dec;15 Suppl D:2-6.

90. Watkins H, Ashrafian H, Redwood C. Inherited cardiomyopathies. N Engl J Med. 2011 Apr 28,;364(17):1643-56.

91. Elliott P, Andersson B, Arbustini E, Bilinska Z, Cecchi F, Charron P, et al. Classification of the cardiomyopathies: a position statement from the European Society Of Cardiology Working Group on Myocardial and Pericardial Diseases. Eur Heart J. 2008 Jan;29(2):270-6.

92. Kamisago M, Sharma SD, DePalma SR, Solomon S, Sharma P, McDonough B, et al. Mutations in sarcomere protein genes as a cause of dilated cardiomyopathy. N Engl J Med. 2000 Dec 07,;343(23):1688-96.

93. Maron BJ. Hypertrophic cardiomyopathy: a systematic review. JAMA. 2002 Mar 13,;287(10):1308-20.

94. Maron BJ, Doerer JJ, Haas TS, Tierney DM, Mueller FO. Sudden deaths in young competitive athletes: analysis of 1866 deaths in the United States, 1980-2006.
Circulation. 2009 Mar 03,;119(8):1085-92.

95. Sen-Chowdhry S, Jacoby D, Moon JC, McKenna WJ. Update on hypertrophic cardiomyopathy and a guide to the guidelines. Nat Rev Cardiol. 2016 11;13(11):65175.

96. Elliott PM, Anastasakis A, Borger MA, Borggrefe M, Cecchi F, Charron P, et al. 2014 ESC Guidelines on diagnosis and management of hypertrophic cardiomyopathy: the Task Force for the Diagnosis and Management of Hypertrophic Cardiomyopathy of the European Society of Cardiology (ESC). Eur Heart J. 2014 Oct 14,;35(39):2733-79.

97. Maron BJ. The electrocardiogram as a diagnostic tool for hypertrophic cardiomyopathy: revisited. Ann Noninvasive Electrocardiol. 2001 Oct;6(4):277-9.

98. Maron BJ, Olivotto I, Spirito P, Casey SA, Bellone P, Gohman TE, et al. Epidemiology of hypertrophic cardiomyopathy-related death: revisited in a large nonreferral-based patient population. Circulation. 2000 Aug 22,;102(8):858-64.

99. Spirito P, Seidman CE, McKenna WJ, Maron BJ. The management of hypertrophic cardiomyopathy. N Engl J Med. 1997 Mar 13,;336(11):775-85.

100. Katritsis DG, Gersh BJ, Camm AJ. A Clinical Perspective on Sudden Cardiac Death. Arrhythmia & electrophysiology review. 2016;5(3):177.

101. Priori SG. Genetic testing to predict sudden cardiac death: current perspectives and future goals. Indian Heart J. 2014 -1;66(Suppl 1):S60.

102. Bezzina CR, Lahrouchi N, Priori SG. Genetics of sudden cardiac death. Circ Res. 2015 Jun 05,;116(12):1919-36.

103. Deo R, Albert CM. Epidemiology and Genetics of Sudden Cardiac Death. Circulation. 2012 -1-31;125(4):620-37.

104. Shirani J, Pick R, Roberts WC, Maron BJ. Morphology and significance of the left ventricular collagen network in young patients with hypertrophic cardiomyopathy and sudden cardiac death. J Am Coll Cardiol. 2000 JAN;35(1):36-44.

105. Liew AC, Vassiliou VS, Cooper R, Raphael CE. Hypertrophic CardiomyopathyPast, Present and Future. Journal of clinical medicine. 2017 Dec 12,;6(12):118.

106. Maron BJ, Rowin EJ, Casey SA, Maron MS. How Hypertrophic Cardiomyopathy Became a Contemporary Treatable Genetic Disease With Low Mortality: Shaped by 50 Years of Clinical Research and Practice. JAMA Cardiology. 2016 Apr 1,;1(1):98105.

107. Geisterfer-Lowrance AA, Kass S, Tanigawa G, Vosberg HP, McKenna W, Seidman CE, et al. A molecular basis for familial hypertrophic cardiomyopathy: a beta cardiac myosin heavy chain gene missense mutation. Cell. 1990 Sep 07,;62(5):999-1006.

108. Marian AJ, Braunwald E. Hypertrophic Cardiomyopathy: Genetics, Pathogenesis, Clinical Manifestations, Diagnosis, and Therapy. Circ Res. 2017 Sep 15,;121(7):749-70.

109. Braunwald E, MD. Heart Failure. JACC: Heart Failure. 2013;1(1):1-20.

110. Richard P, Charron P, Carrier L, Ledeuil C, Cheav T, Pichereau C, et al. Hypertrophic cardiomyopathy: distribution of disease genes, spectrum of mutations, and implications for a molecular diagnosis strategy. Circulation. 2003 May 06,;107(17):2227-32.

111. Millat G, Bouvagnet P, Chevalier P, Dauphin C, Jouk PS, Da Costa A, et al. Prevalence and spectrum of mutations in a cohort of 192 unrelated patients with hypertrophic cardiomyopathy. Eur J Med Genet. 2010 Sep-Oct;53(5):261-7.

112. Erdmann J, Daehmlow S, Wischke S, Senyuva M, Werner U, Raible J, et al. Mutation spectrum in a large cohort of unrelated consecutive patients with hypertrophic cardiomyopathy. Clin Genet. 2003 Oct;64(4):339-49.

113. Richard P, Charron P, Carrier L, Ledeuil C, Cheav T, Pichereau C, et al. Hypertrophic cardiomyopathy: distribution of disease genes, spectrum of mutations, and implications for a molecular diagnosis strategy. Circulation. 2003 May 06,;107(17):2227-32.

114. Vignier N, Schlossarek S, Fraysse B, Mearini G, Krämer E, Pointu H, et al. Nonsense-mediated mRNA decay and ubiquitin-proteasome system regulate cardiac myosin-binding protein C mutant levels in cardiomyopathic mice. Circ Res. 2009 Jul 31,;105(3):239-48.

115. Mearini G, Schlossarek S, Willis MS, Carrier L. The ubiquitin-proteasome system in cardiac dysfunction. Biochim Biophys Acta. 2008 Dec;1782(12):749-63.

116. Vasudevan S, Peltz SW, Wilusz CJ. Non-stop decay--a new mRNA surveillance pathway. Bioessays. 2002 Sep;24(9):785-8.

117. Frischmeyer PA, van Hoof A, O'Donnell K, Guerrerio AL, Parker R, Dietz HC. An mRNA surveillance mechanism that eliminates transcripts lacking termination codons. Science. 2002 Mar 22,;295(5563):2258-61.

118. Wolny M, Colegrave M, Colman L, White E, Knight PJ, Peckham M. Cardiomyopathy mutations in the tail of β-cardiac myosin modify the coiled-coil structure and affect integration into thick filaments in muscle sarcomeres in adult cardiomyocytes. J Biol Chem. 2013 Nov 01,;288(44):31952-62.

119. Robinson P, Liu X, Sparrow A, Patel S, Zhang Y, Casadei B, et al. Hypertrophic cardiomyopathy mutations increase myofilament Ca2+ buffering, alter intracellular Ca2+ handling, and stimulate Ca2+-dependent signaling. J Biol Chem. 2018 07 06,;293(27):10487-99.

120. Seidman JG, Seidman C. The genetic basis for cardiomyopathy: from mutation identification to mechanistic paradigms. Cell. 2001 Feb 23,;104(4):557-67.

121. Ashrafian H, Watkins H. Reviews of translational medicine and genomics in cardiovascular disease: new disease taxonomy and therapeutic implications cardiomyopathies: therapeutics based on molecular phenotype. J Am Coll Cardiol. 2007 Mar 27,;49(12):1251-64.

122. Ashrafian H, Redwood C, Blair E, Watkins H. Hypertrophic cardiomyopathy:a paradigm for myocardial energy depletion. Trends Genet. 2003 May;19(5):263-8.

123. Spindler M, Saupe KW, Christe ME, Sweeney HL, Seidman CE, Seidman JG, et al. Diastolic dysfunction and altered energetics in the alphaMHC403/+ mouse model of familial hypertrophic cardiomyopathy. J Clin Invest. 1998 Apr 15,;101(8):1775-83.

124. Crilley JG, Boehm EA, Blair E, Rajagopalan B, Blamire AM, Styles P, et al. Hypertrophic cardiomyopathy due to sarcomeric gene mutations is characterized by impaired energy metabolism irrespective of the degree of hypertrophy. J Am Coll Cardiol. 2003 May 21,;41(10):1776-82.

125. Marian AJ. Pathogenesis of diverse clinical and pathological phenotypes in hypertrophic cardiomyopathy. Lancet. 2000 Jan 01,;355(9197):58-60.

126. Lan F, Lee AS, Liang P, Sanchez-Freire V, Nguyen PK, Wang L, et al. Abnormal calcium handling properties underlie familial hypertrophic cardiomyopathy pathology in patient-specific induced pluripotent stem cells. Cell Stem Cell. 2013 Jan 03,;12(1):101-13.

127. Davies MJ, McKenna WJ. Hypertrophic cardiomyopathy--pathology and pathogenesis. Histopathology. 1995 Jun;26(6):493-500.

128. Evans W. Familial cardiomegaly. Br Heart J. 1949 Jan;11(1):68-82.

129. Davies MJ. The cardiomyopathies: an overview. Heart (British Cardiac Society). 2000 Apr;83(4):469.

130. Sweet M, Taylor MRG, Mestroni L. Diagnosis, prevalence, and screening of familial dilated cardiomyopathy. Expert opinion on orphan drugs. 2015;3(8):869-76.

131. Dec GW, Fuster V. Idiopathic dilated cardiomyopathy. N Engl J Med. 1994 Dec 08,;331(23):1564-75.

132. Nugent AW, Daubeney PEF, Chondros P, Carlin JB, Cheung M, Wilkinson LC, et al. The epidemiology of childhood cardiomyopathy in Australia. N Engl J Med. 2003 Apr 24,;348(17):1639-46.

133. Opie LH, Commerford PJ, Gersh BJ, Pfeffer MA. Controversies in ventricular remodelling. Lancet. 2006 Jan 28,;367(9507):356-67.
134. Alter P, Rupp H, Stoll F, Adams P, Figiel JH, Klose KJ, et al. Increased end diastolic wall stress precedes left ventricular hypertrophy in dilative heart failure--use of the volume-based wall stress index. Int J Cardiol. 2012 May 31,;157(2):233-8.

135. Mathew T, Williams L, Navaratnam G, Rana B, Wheeler R, Collins K, et al. Diagnosis and assessment of dilated cardiomyopathy: a guideline protocol from the British Society of Echocardiography. Echo Res Pract. 2017 -3-23;4(2):G13.

136. McMurray JJV, Adamopoulos S, Anker SD, Auricchio A, Böhm M, Dickstein K, et al. ESC Guidelines for the diagnosis and treatment of acute and chronic heart failure 2012: The Task Force for the Diagnosis and Treatment of Acute and Chronic Heart Failure 2012 of the European Society of Cardiology. Developed in collaboration with the Heart Failure Association (HFA) of the ESC. Eur Heart J. 2012 Jul;33(14):1787-847.

137. Yancy CW, Jessup M, Bozkurt B, Butler J, Casey DE, Colvin MM, et al. 2017 ACC/AHA/HFSA Focused Update of the 2013 ACCF/AHA Guideline for the Management of Heart Failure: A Report of the American College of Cardiology/American Heart Association Task Force on Clinical Practice Guidelines and the Heart Failure Society of America. Circulation. 2017 Aug 08,;136(6):e161.

138. Atherton JJ, Sindone A, De Pasquale CG, Driscoll A, MacDonald PS, Hopper I, et al. National Heart Foundation of Australia and Cardiac Society of Australia and New Zealand: Guidelines for the Prevention, Detection, and Management of Heart Failure in Australia 2018. Heart Lung Circ. 2018 Oct;27(10):1123-208.

139. Køber L, Thune JJ, Nielsen JC, Haarbo J, Videbæk L, Korup E, et al. Defibrillator Implantation in Patients with Nonischemic Systolic Heart Failure. N Engl J Med. 2016 09 29,;375(13):1221-30.

140. Dipchand AI, Rossano JW, Edwards LB, Kucheryavaya AY, Benden C, Goldfarb S, et al. The Registry of the International Society for Heart and Lung Transplantation: Eighteenth Official Pediatric Heart Transplantation Report--2015; Focus Theme: Early Graft Failure. J Heart Lung Transplant. 2015 Oct;34(10):123343.

141. Lund LH, Edwards LB, Kucheryavaya AY, Benden C, Dipchand AI, Goldfarb S, et al. The Registry of the International Society for Heart and Lung Transplantation: Thirty-second Official Adult Heart Transplantation Report--2015; Focus Theme: Early Graft Failure. J Heart Lung Transplant. 2015 Oct;34(10):1244-54.

142. Michels VV, Moll PP, Miller FA, Tajik AJ, Chu JS, Driscoll DJ, et al. The frequency of familial dilated cardiomyopathy in a series of patients with idiopathic dilated cardiomyopathy. N Engl J Med. 1992 Jan 09,;326(2):77-82.

143. Grünig E, Tasman JA, Kücherer H, Franz W, Kübler W, Katus HA. Frequency and phenotypes of familial dilated cardiomyopathy. J Am Coll Cardiol. 1998 Jan;31(1):186-94.

144. Seidman JG, Seidman C. The genetic basis for cardiomyopathy: from mutation identification to mechanistic paradigms. Cell. 2001 Feb 23,;104(4):557-67.

145. McNally EM, Golbus JR, Puckelwartz MJ. Genetic mutations and mechanisms in dilated cardiomyopathy. J Clin Invest. 2013 Jan;123(1):19-26.

146. Feng J, Yan J, Buzin CH, Towbin JA, Sommer SS. Mutations in the dystrophin gene are associated with sporadic dilated cardiomyopathy. Mol Genet Metab. 2002 Sep-Oct;77(1-2):119-26.

147. Jefferies JL, Eidem BW, Belmont JW, Craigen WJ, Ware SM, Fernbach SD, et al. Genetic predictors and remodeling of dilated cardiomyopathy in muscular dystrophy. Circulation. 2005 Nov 01,;112(18):2799-804.

148. Ortiz-Lopez R, Li H, Su J, Goytia V, Towbin JA. Evidence for a dystrophin missense mutation as a cause of X-linked dilated cardiomyopathy. Circulation. 1997 May 20,;95(10):2434-40.

149. Franz WM, Müller M, Müller OJ, Herrmann R, Rothmann T, Cremer M, et al. Association of nonsense mutation of dystrophin gene with disruption of sarcoglycan complex in X-linked dilated cardiomyopathy. Lancet. 2000 May 20,;355(9217):1781-
5.

150. Tsubata S, Bowles KR, Vatta M, Zintz C, Titus J, Muhonen L, et al. Mutations in the human delta-sarcoglycan gene in familial and sporadic dilated cardiomyopathy. J Clin Invest. 2000 Sep;106(5):655-62.

151. McNally EM. New approaches in the therapy of cardiomyopathy in muscular dystrophy. Annu Rev Med. 2007;58:75-88.

152. Haas M, Vlcek V, Balabanov P, Salmonson T, Bakchine S, Markey G, et al. European Medicines Agency review of ataluren for the treatment of ambulant patients aged 5 years and older with Duchenne muscular dystrophy resulting from a nonsense mutation in the dystrophin gene. Neuromuscul Disord. 2015 Jan;25(1):513.

153. Niks EH, Aartsma-Rus A. Exon skipping: a first in class strategy for Duchenne muscular dystrophy. Expert Opin Biol Ther. 2017 02;17(2):225-36.

154. Carboni N, Marrosu G, Porcu M, Mateddu A, Solla E, Cocco E, et al. Dilated cardiomyopathy with conduction defects in a patient with partial merosin deficiency due to mutations in the laminin-α2-chain gene: a chance association or a novel phenotype? Muscle Nerve. 2011 Nov;44(5):826-8.

155. Tsubata S, Bowles KR, Vatta M, Zintz C, Titus J, Muhonen L, et al. Mutations in the human delta-sarcoglycan gene in familial and sporadic dilated cardiomyopathy. The Journal of clinical investigation. 2000 Sep;106(5):655-62.

156. Cox GF, Kunkel LM. Dystrophies and heart disease. Curr Opin Cardiol. 1997 May;12(3):329-43.

157. Begay RL, Graw SL, Sinagra G, Asimaki A, Rowland TJ, Slavov DB, et al. Filamin C Truncation Mutations Are Associated With Arrhythmogenic Dilated Cardiomyopathy and Changes in the Cell-Cell Adhesion Structures. JACC Clin Electrophysiol. 2018 Apr;4(4):504-14.

158. Fürst DO, Goldfarb LG, Kley RA, Vorgerd M, Olivé M, van der Ven, Peter F. M. Filamin C-related myopathies: pathology and mechanisms. Acta Neuropathol. 2013 Jan;125(1):33-46.

159. Bains S, Tester DJ, Asirvatham SJ, Noseworthy PA, Ackerman MJ, Giudicessi JR. A Novel Truncating Variant in FLNC-Encoded Filamin C May Serve as a Proarrhythmic Genetic Substrate for Arrhythmogenic Bileaflet Mitral Valve Prolapse Syndrome. Mayo Clin Proc. 2019 May;94(5):906-13.

160. Milner DJ, Weitzer G, Tran D, Bradley A, Capetanaki Y. Disruption of muscle architecture and myocardial degeneration in mice lacking desmin. J Cell Biol. 1996 Sep;134(5):1255-70.

161. Olson TM, Illenberger S, Kishimoto NY, Huttelmaier S, Keating MT, Jockusch BM. Metavinculin mutations alter actin interaction in dilated cardiomyopathy. Circulation. 2002 Jan 29,;105(4):431-7.

162. Maeda M, Holder E, Lowes B, Valent S, Bies RD. Dilated cardiomyopathy associated with deficiency of the cytoskeletal protein metavinculin. Circulation. 1997 Jan 07,;95(1):17-20.

163. LeWinter MM, Granzier HL. Cardiac titin and heart disease. J Cardiovasc Pharmacol. 2014 Mar;63(3):207-12.

164. Nagueh SF, Shah G, Wu Y, Torre-Amione G, King NMP, Lahmers S, et al. Altered titin expression, myocardial stiffness, and left ventricular function in patients with dilated cardiomyopathy. Circulation. 2004 Jul 13,;110(2):155-62.

165. Roberts AM, Ware JS, Herman DS, Schafer S, Baksi J, Bick AG, et al. Integrated allelic, transcriptional, and phenomic dissection of the cardiac effects of titin truncations in health and disease. Sci Transl Med. 2015 Jan 14,;7(270):270ra6.

166. Hinson JT, Chopra A, Nafissi N, Polacheck WJ, Benson CC, Swist S, et al. HEART DISEASE. Titin mutations in iPS cells define sarcomere insufficiency as a cause of dilated cardiomyopathy. Science. 2015 Aug 28,;349(6251):982-6.

167. Norton N, Li D, Rampersaud E, Morales A, Martin ER, Zuchner S, et al. Exome sequencing and genome-wide linkage analysis in 17 families illustrate the complex contribution of TTN truncating variants to dilated cardiomyopathy. Circ Cardiovasc Genet. 2013 Apr;6(2):144-53.

168. Gerull B, Gramlich M, Atherton J, McNabb M, Trombitás K, Sasse-Klaassen S, et al. Mutations of TTN, encoding the giant muscle filament titin, cause familial dilated cardiomyopathy. Nat Genet. 2002 Feb;30(2):201-4.

169. Begay RL, Graw S, Sinagra G, Merlo M, Slavov D, Gowan K, et al. Role of Titin Missense Variants in Dilated Cardiomyopathy. J Am Heart Assoc. 2015 Nov 13,;4(11).

170. Gigli M, Begay RL, Morea G, Graw SL, Sinagra G, Taylor MRG, et al. A Review of the Giant Protein Titin in Clinical Molecular Diagnostics of Cardiomyopathies. Front Cardiovasc Med. 2016;3:21.

171. Akinrinade O, Ollila L, Vattulainen S, Tallila J, Gentile M, Salmenperä P, et al. Genetics and genotype-phenotype correlations in Finnish patients with dilated cardiomyopathy. European heart journal. 2015 Sep 7,;36(34):2327-37.

172. Olson TM, Michels VV, Thibodeau SN, Tai YS, Keating MT. Actin mutations in dilated cardiomyopathy, a heritable form of heart failure. Science. 1998 May 01,;280(5364):750-2.

173. Daehmlow S, Erdmann J, Knueppel T, Gille C, Froemmel C, Hummel M, et al. Novel mutations in sarcomeric protein genes in dilated cardiomyopathy. Biochem Biophys Res Commun. 2002 Oct 18,;298(1):116-20.

174. Villard E, Duboscq-Bidot L, Charron P, Benaiche A, Conraads V, Sylvius N, et al. Mutation screening in dilated cardiomyopathy: prominent role of the beta myosin heavy chain gene. Eur Heart J. 2005 Apr;26(8):794-803.

175. Frey N, Luedde M, Katus HA. Mechanisms of disease: hypertrophic cardiomyopathy. Nat Rev Cardiol. 2011 Oct 25,;9(2):91-100.

176. Kamisago M, Sharma SD, DePalma SR, Solomon S, Sharma P, McDonough B, et al. Mutations in sarcomere protein genes as a cause of dilated cardiomyopathy. N Engl J Med. 2000 Dec 07,;343(23):1688-96.

177. Hanson EL, Jakobs PM, Keegan H, Coates K, Bousman S, Dienel NH, et al. Cardiac troponin T lysine 210 deletion in a family with dilated cardiomyopathy. J Card Fail. 2002 Feb;8(1):28-32.

178. Li D, Czernuszewicz GZ, Gonzalez O, Tapscott T, Karibe A, Durand JB, et al. Novel cardiac troponin T mutation as a cause of familial dilated cardiomyopathy. Circulation. 2001 Oct 30,;104(18):2188-93.

179. Mogensen J, Murphy RT, Shaw T, Bahl A, Redwood C, Watkins H, et al. Severe disease expression of cardiac troponin C and T mutations in patients with idiopathic dilated cardiomyopathy. J Am Coll Cardiol. 2004 Nov 16,;44(10):2033-40.

180. Stefanelli CB, Rosenthal A, Borisov AB, Ensing GJ, Russell MW. Novel troponin T mutation in familial dilated cardiomyopathy with gender-dependant severity. Mol Genet Metab. 2004 Sep-Oct;83(1-2):188-96.

181. Fung YW, Wang RX, Heng HH, Liew CC. Mapping of a human LIM protein (CLP) to human chromosome 11p15.1 by fluorescence in situ hybridization. Genomics. 1995 Aug 10,;28(3):602-3.

182. Bos JM, Poley RN, Ny M, Tester DJ, Xu X, Vatta M, et al. Genotype-phenotype relationships involving hypertrophic cardiomyopathy-associated mutations in titin, muscle LIM protein, and telethonin. Mol Genet Metab. 2006 May;88(1):78-85.

183. Geier C, Perrot A, Ozcelik C, Binner P, Counsell D, Hoffmann K, et al. Mutations in the human muscle LIM protein gene in families with hypertrophic cardiomyopathy. Circulation. 2003 Mar 18,;107(10):1390-5.

184. Buyandelger B, Ng K, Miocic S, Piotrowska I, Gunkel S, Ku C, et al. MLP (muscle LIM protein) as a stress sensor in the heart. Pflugers Arch - Eur J Physiol. 2011 Jul;462(1):135-42.

185. Mohapatra B, Jimenez S, Lin JH, Bowles KR, Coveler KJ, Marx JG, et al. Mutations in the muscle LIM protein and alpha-actinin-2 genes in dilated cardiomyopathy and endocardial fibroelastosis. Mol Genet Metab. 2003 SepOct;80(1-2):207-15.

186. Hershberger RE, Parks SB, Kushner JD, Li D, Ludwigsen S, Jakobs P, et al. Coding Sequence Mutations Identified in MYH7, TNNT2, SCN5A, CSRP3, LBD3, and TCAP from 313 Patients with Familial or Idiopathic Dilated Cardiomyopathy. Clinical and Translational Science. 2008 May;1(1):21-6.

187. Knöll R, Hoshijima M, Chien KR. Muscle LIM protein in heart failure. Exp Clin Cardiol. 2002;7(2-3):104-5.

188. Gehmlich K, Geier C, Milting H, Fürst D, Ehler E. Back to square one: what do we know about the functions of Muscle LIM Protein in the heart? J Muscle Res Cell Motil. 2008 Dec;29(6):155-8.

189. Arber S, Hunter JJ, Ross J, Hongo M, Sansig G, Borg J, et al. MLP-deficient mice exhibit a disruption of cardiac cytoarchitectural organization, dilated cardiomyopathy, and heart failure. Cell. 1997 Feb 07,;88(3):393-403.

190. Arber S, Halder G, Caroni P. Muscle LIM protein, a novel essential regulator of myogenesis, promotes myogenic differentiation. Cell. 1994 Oct 21,;79(2):221-31.

191. Kadrmas JL, Beckerle MC. The LIM domain: from the cytoskeleton to the nucleus. Nat Rev Mol Cell Biol. 2004 Nov;5(11):920-31.

192. HX2CX2CX2CX16_21CX2-3(C/H/D) S. Molecular Dissection of a LIM Domain. Mol Biol Cell. 1997 -2;8:219-30.

193. Michelsen JW, Schmeichel KL, Beckerle MC, Winge DR. The LIM motif defines a specific zinc-binding protein domain. Proc Natl Acad Sci U S A. 1993 May 15,;90(10):4404-8.

194. Kosa JL, Michelsen JW, Louis HA, Olsen JI, Davis DR, Beckerle MC, et al. Common metal ion coordination in LIM domain proteins. Biochemistry. 1994 Jan 18,;33(2):468-77.

195. Archer VE, Breton J, Sanchez-Garcia I, Osada H, Forster A, Thomson AJ, et al. Cysteine-rich LIM domains of LIM-homeodomain and LIM-only proteins contain zinc but not iron. Proc Natl Acad Sci U S A. 1994 Jan 04,;91(1):316-20.

196. Arber S, Caroni P. Specificity of single LIM motifs in targeting and LIM/LIM interactions in situ. Genes Dev. 1996 02/01/;10(3):289-300.

197. Weiskirchen R, Günther K. The CRP/MLP/TLP family of LIM domain proteins: acting by connecting. Bioessays. 2003 Feb;25(2):152-62.

198. Schallus T, Fehér K, Ulrich AS, Stier G, Muhle-Goll C. Structure and dynamics of the human muscle LIM protein. FEBS Lett. 2009 Mar 18,;583(6):1017-22.

199. Boateng SY, Belin RJ, Geenen DL, Margulies KB, Martin JL, Hoshijima M, et al. Cardiac dysfunction and heart failure are associated with abnormalities in the subcellular distribution and amounts of oligomeric muscle LIM protein. Am J Physiol Heart Circ Physiol. 2007 Jan;292(1):259.

200. Boateng SY, Senyo SE, Qi L, Goldspink PH, Russell B. Myocyte remodeling in response to hypertrophic stimuli requires nucleocytoplasmic shuttling of muscle LIM protein. J Mol Cell Cardiol. 2009 Oct;47(4):426-35.

201. Lange S, Gehmlich K, Lun AS, Blondelle J, Hooper C, Dalton ND, et al. MLP and CARP are linked to chronic PKCα signalling in dilated cardiomyopathy. Nature communications. 2016 Jun 29,;7:12120.

202. Mahesh P. Gupta, Sadhana A. Samant, Stephen H. Smith, Sanjeev G. Shroff. HDAC4 and PCAF Bind to Cardiac Sarcomeres and Play a Role in Regulating Myofilament Contractile Activity. Journal of Biological Chemistry. 2008 Apr 11,;283(15):10135-46.

203. Fung YW, Wang R, Liew CC. Characterization of a human cardiac gene which encodes for a LIM domain protein and is developmentally expressed in myocardial development. J Mol Cell Cardiol. 1997 Jan;29(1):426-7.

204. Knöll R, Hoshijima M, Chien KR. Muscle LIM protein in heart failure. Experimental and clinical cardiology. 2002;7(2-3):104.

205. Louis HA, Pino JD, Schmeichel KL, Pomiès P, Beckerle MC. Comparison of three members of the cysteine-rich protein family reveals functional conservation and divergent patterns of gene expression. J Biol Chem. 1997 Oct 24,;272(43):27484-91.

206. Gehmlich K, Geier C, Osterziel KJ, Van der Ven, Peter F. M., Fürst DO. Decreased interactions of mutant muscle LIM protein (MLP) with N-RAP and alphaactinin and their implication for hypertrophic cardiomyopathy. Cell Tissue Res. 2004 Aug;317(2):129-36.

207. Papalouka V, Arvanitis DA, Vafiadaki E, Mavroidis M, Papadodima SA, Spiliopoulou CA, et al. Muscle LIM protein interacts with cofilin 2 and regulates Factin dynamics in cardiac and skeletal muscle. Mol Cell Biol. 2009 Nov;29(22):604658.

208. Heineke J, Ruetten H, Willenbockel C, Gross SC, Naguib M, Schaefer A, et al. Attenuation of cardiac remodeling after myocardial infarction by muscle LIM proteincalcineurin signaling at the sarcomeric Z-disc. Proc Natl Acad Sci U S A. 2005 Feb 01,;102(5):1655-60.

209. Zolk O, Caroni P, Böhm M. Decreased expression of the cardiac LIM domain protein MLP in chronic human heart failure. Circulation. 2000 Jun 13,;101(23):26747.

210. Flick MJ, Konieczny SF. The muscle regulatory and structural protein MLP is a cytoskeletal binding partner of betaI-spectrin. J Cell Sci. 2000 May;113 (Pt 9):155364.

211. Elisabeth Ehler, Robert Horowits, Christian Zuppinger, Robert L. Price, Evelyne Perriard, Martin Leu, et al. Alterations at the Intercalated Disk Associated with the Absence of Muscle LIM Protein. The Journal of Cell Biology. 2001 May 14,;153(4):763-72.

212. Kong Y, Flick MJ, Kudla AJ, Konieczny SF. Muscle LIM protein promotes myogenesis by enhancing the activity of MyoD. Mol Cell Biol. 1997 Aug;17(8):475060.

213. Boateng SY, Belin RJ, Geenen DL, Margulies KB, Martin JL, Hoshijima M, et al. Cardiac dysfunction and heart failure are associated with abnormalities in the subcellular distribution and amounts of oligomeric muscle LIM protein. Am J Physiol Heart Circ Physiol. 2007 Jan;292(1):259.

214. Vafiadaki E, Arvanitis DA, Sanoudou D. Muscle LIM Protein: Master regulator of cardiac and skeletal muscle functions. Gene. 2015 July 15,;566(1):1-7.

215. Geier C, Gehmlich K, Ehler E, Hassfeld S, Perrot A, Hayess K, et al. Beyond the sarcomere: CSRP3 mutations cause hypertrophic cardiomyopathy. Hum Mol Genet. 2008 Sep 15,;17(18):2753-65.

216. Geier C, Perrot A, Ozcelik C, Binner P, Counsell D, Hoffmann K, et al. Mutations in the human muscle LIM protein gene in families with hypertrophic cardiomyopathy. Circulation. 2003 Mar 18,;107(10):1390-5.

217. Buyandelger B, Ng K, Miocic S, Gunkel S, Piotrowska I, Ku C, et al. Genetics of mechanosensation in the heart. J Cardiovasc Transl Res. 2011 Jun;4(3):238-44.

218. Su Z, Yao A, Zubair I, Sugishita K, Ritter M, Li F, et al. Effects of deletion of muscle LIM protein on myocyte function. Am J Physiol Heart Circ Physiol. 2001 Jun;280(6):2665.

219. Esposito G, Santana LF, Dilly K, Cruz JD, Mao L, Lederer WJ, et al. Cellular and functional defects in a mouse model of heart failure. Am J Physiol Heart Circ Physiol. 2000 Dec;279(6):3101.

220. Kemecsei P, Miklós Z, Bíró T, Marincsák R, Tóth BI, Komlódi-Pásztor E, et al. Hearts of surviving MLP-KO mice show transient changes of intracellular calcium handling. Mol Cell Biochem. 2010 Sep;342(1-2):251-60.

221. Antoons G, Vangheluwe P, Volders PGA, Bito V, Holemans P, Ceci M, et al. Increased phospholamban phosphorylation limits the force–frequency response in the MLP–/– mouse with heart failure. Journal of Molecular and Cellular Cardiology. 2006 March 1,;40(3):350-60.

222. Hagemann D, Xiao R. Dual site phospholamban phosphorylation and its physiological relevance in the heart. Trends Cardiovasc Med. 2002 Feb;12(2):51-6.

223. Minamisawa S, Hoshijima M, Chu G, Ward CA, Frank K, Gu Y, et al. Chronic phospholamban-sarcoplasmic reticulum calcium ATPase interaction is the critical calcium cycling defect in dilated cardiomyopathy. Cell. 1999 Oct 29,;99(3):313-22.

224. Minamisawa S, Hoshijima M, Chu G, Ward CA, Frank K, Gu Y, et al. Chronic phospholamban-sarcoplasmic reticulum calcium ATPase interaction is the critical calcium cycling defect in dilated cardiomyopathy. Cell. 1999 Oct 29,;99(3):313-22.

225. Fajardo G, Zhao M, Urashima T, Farahani S, Hu D, Reddy S, et al. Deletion of the β2-adrenergic receptor prevents the development of cardiomyopathy in mice. Journal of Molecular and Cellular Cardiology. 2013 October 1,;63:155-64.

226. Heineke, Joerg|Wollert, Kai C.|Osinska, Hanna|Sargent, Michelle A.|York, Allen J.|Robbins, Jeffrey|Molkentin, Jeffery D. Calcineurin protects the heart in a

murine model of dilated cardiomyopathy. Journal of Molecular and Cellular Cardiology. 2009;48(6):1080-7.

227. Kuhn C, Frank D, Dierck F, Oehl U, Krebs J, Will R, et al. Cardiac remodeling is not modulated by overexpression of muscle LIM protein (MLP). Basic Res Cardiol. 2012 May;107(3):262.

228. Omens JH, Usyk TP, Li Z, McCulloch AD. Muscle LIM protein deficiency leads to alterations in passive ventricular mechanics. Am J Physiol Heart Circ Physiol. 2002 Feb;282(2):680.

229. Heineke J, Ruetten H, Willenbockel C, Gross SC, Naguib M, Schaefer A, et al. Attenuation of cardiac remodeling after myocardial infarction by muscle LIM proteincalcineurin signaling at the sarcomeric Z-disc. Proc Natl Acad Sci U S A. 2005 Feb 01,;102(5):1655-60.

230. Kuhn C, Frank D, Dierck F, Oehl U, Krebs J, Will R, et al. Cardiac remodeling is not modulated by overexpression of muscle LIM protein (MLP). Basic Res Cardiol.
2012 May;107(3):1-14.
231. Geier C, Gehmlich K, Ehler E, Hassfeld S, Perrot A, Hayess K, et al. Beyond the sarcomere: CSRP3 mutations cause hypertrophic cardiomyopathy. Hum Mol Genet. 2008 September 15;17(18):2753-65.

232. Ehsan M, Kelly M, Hooper C, Yavari A, Beglov J, Bellahcene M, et al. Mutant Muscle LIM Protein C58G causes cardiomyopathy through protein depletion. J Mol Cell Cardiol. 2018 Aug;121:287-96.

233. Bos JM, Poley RN, Ny M, Tester DJ, Xu X, Vatta M, et al. Genotype-phenotype relationships involving hypertrophic cardiomyopathy-associated mutations in titin, muscle LIM protein, and telethonin. Mol Genet Metab. 2006 May;88(1):78-85.

234. Hershberger RE, Parks SB, Kushner JD, Li D, Ludwigsen S, Jakobs P, et al. Coding Sequence Mutations Identified in MYH7, TNNT2, SCN5A, CSRP3, LBD3, and TCAP from 313 Patients with Familial or Idiopathic Dilated Cardiomyopathy. Clinical and Translational Science. 2008 May;1(1):21-6.

235. Yin FC, Spurgeon HA, Rakusan K, Weisfeldt ML, Lakatta EG. Use of tibial length to quantify cardiac hypertrophy: application in the aging rat. Am J Physiol. 1982 Dec;243(6):941.

236. Derchi G, Bellone P, Chiarella F, Randazzo M, Zino V, Vecchio C. Plasma levels of atrial natriuretic peptide in hypertrophic cardiomyopathy. The American Journal of Cardiology. 1992 December 1,;70(18):1502-4.

237. Fahy GJ, McCreery CJ, O'Sullivan F, Keenan AK, Quigley PJ, Maurer BJ. Plasma atrial natriuretic peptide is elevated in patients with hypertrophic cardiomyopathy. Int J Cardiol. 1996 Jul 26,;55(2):149-55.

238. Hasegawa K, Fujiwara H, Doyama K, Miyamae M, Fujiwara T, Suga S, et al. Ventricular expression of brain natriuretic peptide in hypertrophic cardiomyopathy. Circulation. 1993 Aug;88(2):372-80.

239. Yoshibayashi M, Kamiya T, Saito Y, Matsuo H. Increased plasma levels of brain natriuretic peptide in hypertrophic cardiomyopathy. N Engl J Med. 1993 Aug 05,;329(6):433-4.

240. Brito D, Matias JS, Sargento L, Cabral MJ, Madeira HC. Plasma N-terminal probrain natriuretic peptide: a marker of left ventricular hypertrophy in hypertrophic cardiomyopathy. Rev Port Cardiol. 2004 Dec;23(12):1557-82.

241. Motwani JG, McAlpine H, Kennedy N, Struthers AD. Plasma brain natriuretic peptide as an indicator for angiotensin-converting-enzyme inhibition after myocardial infarction. Lancet. 1993 May 01,;341(8853):1109-13.

242. Lim SD, Roberts R, Marian AJ. Expression profiling of cardiac genes in human hypertrophic cardiomyopathy: insight into the pathogenesis of phenotypes. ACC Current Journal Review. 2002;11(2):48-9.

243. Friedrich FW, Wilding BR, Reischmann S, Crocini C, Lang P, Charron P, et al. Evidence for FHL1 as a novel disease gene for isolated hypertrophic cardiomyopathy. Hum Mol Genet. 2012 Jul 15,;21(14):3237-54.

244. Friedrich FW, Reischmann S, Schwalm A, Unger A, Ramanujam D, Münch J, et al. FHL2 expression and variants in hypertrophic cardiomyopathy. Basic Res Cardiol. 2014;109(6):451.

245. Zolk O, Frohme M, Maurer A, Kluxen F, Hentsch B, Zubakov D, et al. Cardiac ankyrin repeat protein, a negative regulator of cardiac gene expression, is augmented in human heart failure. Biochem Biophys Res Commun. 2002 May 24,;293(5):1377-82.

246. Basso C, Thiene G, Corrado D, Buja G, Melacini P, Nava A. Hypertrophic cardiomyopathy and sudden death in the young: Pathologic evidence of myocardial ischemia. Hum Pathol. 2000 AUG;31(8):988-98.

247. Varnava AM, Elliott PM, Sharma S, McKenna WJ, Davies MJ. Hypertrophic cardiomyopathy: the interrelation of disarray, fibrosis, and small vessel disease. Heart. 2000 NOV;84(5):476-82.

248. Varnava AM, Elliott PM, Mahon N, Davies MJ, McKenna WJ. Relation between myocyte disarray and outcome in hypertrophic cardiomyopathy. Am J Cardiol. 2001 AUG 1;88(3):275-9.

249. Choudhury L, Mahrholdt H, Wagner A, Choi KM, Elliott MD, Klocke FJ, et al. Myocardial scarring in asymptomatic or mildly symptomatic patients with hypertrophic cardiomyopathy. J Am Coll Cardiol. 2002 DEC 18;40(12):2156-64.

250. Crilley JG, Boehm EA, Blair E, Rajagopalan B, Blamire AM, Styles P, et al. Hypertrophic cardiomyopathy due to sarcomeric gene mutations is characterized by impaired energy metabolism irrespective of the degree of hypertrophy. J Am Coll Cardiol. 2003 MAY 21;41(10):1776-82.

251. Debold EP, Schmitt JP, Patlak JB, Beck SE, Moore JR, Seidman JG, et al. Hypertrophic and dilated cardiomyopathy mutations differentially affect the molecular force generation of mouse alpha-cardiac myosin in the laser trap assay. Am J Physiol -Heart Circul Physiol. 2007 JUL;293(1):H291.

252. Lombardi R, Rodriguez G, Chen SN, Ripplinger CM, Li W, Chen J, et al. Resolution of Established Cardiac Hypertrophy and Fibrosis and Prevention of Systolic Dysfunction in a Transgenic Rabbit Model of Human Cardiomyopathy Through Thiol-Sensitive Mechanisms. Circulation. 2009 MAR 17;119(10):U88.

253. Tardiff JC. Sarcomeric proteins and familial hypertrophic cardiomyopathy: Linking mutations in structural proteins to complex cardiovascular phenotypes. Heart Fail Rev. 2005 SEP;10(3):237-48.

254. Geisterfer-Lowrance AA, Christe M, Conner DA, Ingwall JS, Schoen FJ, Seidman CE, et al. A mouse model of familial hypertrophic cardiomyopathy. Science. 1996 May 03,;272(5262):731-4.

255. Kim JB, Porreca GJ, Song L, Greenway SC, Gorham JM, Church GM, et al. Polony multiplex analysis of gene expression (PMAGE) in mouse hypertrophic cardiomyopathy. Science. 2007 JUN 8;316(5830):1481-4.

256. Kliment CR, Englert JM, Crum LP, Oury TD. A novel method for accurate collagen and biochemical assessment of pulmonary tissue utilizing one animal. Int J Clin Exp Pathol. 2011 -4-30;4(4):349-55.

257. Hulmes DJS. Collagen Diversity, Synthesis and Assembly. In: Collagen. Springer, Boston, MA; 2008. p. 15-47.

258. Lange S, Gehmlich K, Lun AS, Blondelle J, Hooper C, Dalton ND, et al. MLP and CARP are linked to chronic PKCα signalling in dilated cardiomyopathy. Nature communications. 2016;7:12120.

259. Walkin L, Herrick SE, Summers A, Brenchley PE, Hoff CM, Korstanje R, et al. The role of mouse strain differences in the susceptibility to fibrosis: a systematic review. Fibrogenesis Tissue Repair. 2013 -9-25;6:18.

260. Faulx MD, Ernsberger P, Vatner D, Hoffman RD, Lewis W, Strachan R, et al. Strain-dependent beta-adrenergic receptor function influences myocardial

responses to isoproterenol stimulation in mice. Am J Physiol Heart Circ Physiol. 2005 Jul;289(1):30.

261. Leelahavanichkul A, Yan Q, Hu X, Eisner C, Huang Y, Chen R, et al. Angiotensin II overcomes strain-dependent resistance of rapid CKD progression in a new remnant kidney mouse model. Kidney Int. 2010 Dec;78(11):1136-53.

262. Nerbonne JM, Nichols CG, Schwarz TL, Escande D. Genetic manipulation of cardiac K(+) channel function in mice: what have we learned, and where do we go from here? Circ Res. 2001 Nov 23,;89(11):944-56.

263. Miyata S, Minobe W, Bristow MR, Leinwand LA. Myosin heavy chain isoform expression in the failing and nonfailing human heart. Circ Res. 2000 Mar 03,;86(4):386-90.

264. Lompré AM, Nadal-Ginard B, Mahdavi V. Expression of the cardiac ventricular alpha- and beta-myosin heavy chain genes is developmentally and hormonally regulated. J Biol Chem. 1984 May 25,;259(10):6437-46.

265. Schwartz K, Lecarpentier Y, Martin JL, Lompré AM, Mercadier JJ, Swynghedauw B. Myosin isoenzymic distribution correlates with speed of myocardial contraction. J Mol Cell Cardiol. 1981 Dec;13(12):1071-5.

266. Litten RZ, Martin BJ, Low RB, Alpert NR. Altered myosin isozyme patterns from pressure-overloaded and thyrotoxic hypertrophied rabbit hearts. Circ Res. 1982 Jun;50(6):856-64.

267. Blankenburg R, Hackert K, Wurster S, Deenen R, Seidman JG, Seidman CE, et al. β-Myosin heavy chain variant Val606Met causes very mild hypertrophic cardiomyopathy in mice, but exacerbates HCM phenotypes in mice carrying other HCM mutations. Circ Res. 2014 Jul 07,;115(2):227-37.

268. Hao Y, Tsuruda T, Sekita-Hatakeyama Y, Kurogi S, Kubo K, Sakamoto S, et al. Cardiac hypertrophy is exacerbated in aged mice lacking the osteoprotegerin gene. Cardiovasc Res. 2016 May 01,;110(1):62-72.

269. Bueno OF, van Rooij E, Molkentin JD, Doevendans PA, De Windt LJ. Calcineurin and hypertrophic heart disease: novel insights and remaining questions. Cardiovasc Res. 2002 Mar;53(4):806-21.

270. Lim HW, Molkentin JD. Calcineurin and human heart failure. Nat Med. 1999 Mar;5(3):246-7.

271. Haq S, Choukroun G, Lim H, Tymitz KM, del Monte F, Gwathmey J, et al. Differential activation of signal transduction pathways in human hearts with hypertrophy versus advanced heart failure. Circulation. 2001 Feb 06,;103(5):670-7.

272. Bueno OF, Wilkins BJ, Tymitz KM, Glascock BJ, Kimball TF, Lorenz JN, et al. Impaired cardiac hypertrophic response in Calcineurin Abeta -deficient mice. Proc Natl Acad Sci U S A. 2002 Apr 02,;99(7):4586-91.

273. Torac E, Gaman L, Atanasiu V. The regulator of calcineurin (RCAN1) an important factor involved in atherosclerosis and cardiovascular diseases development. Journal of medicine and life. 2014 Oct;7(4):481.

274. Fuentes JJ, Genescà L, Kingsbury TJ, Cunningham KW, Pérez-Riba M, Estivill X, et al. DSCR1, overexpressed in Down syndrome, is an inhibitor of calcineurinmediated signaling pathways. Hum Mol Genet. 2000 Jul 01,;9(11):1681-90.

275. Hai Wu, Shih-chu Kao, Tomasa Barrientos, Scott H. Baldwin, Eric N. Olson, Gerald R. Crabtree, et al. Down Syndrome Critical Region-1 Is a Transcriptional Target of Nuclear Factor of Activated T Cells-c1 within the Endocardium during Heart Development. Journal of Biological Chemistry. 2007 Oct 19,;282(42):30673-9.

276. Snyder M, Wang Z, Gerstein M. RNA-Seq: a revolutionary tool for transcriptomics. Nature Reviews Genetics. 2009 Jan;10(1):57-63.

277. DeRisi JL, Iyer VR, Brown PO. Exploring the metabolic and genetic control of gene expression on a genomic scale. Science. 1997 Oct 24,;278(5338):680-6.

278. Fodor SP, Rava RP, Huang XC, Pease AC, Holmes CP, Adams CL. Multiplexed biochemical assays with biological chips. Nature. 1993 Aug 05,;364(6437):555-6.

279. Cheng J, Kapranov P, Drenkow J, Dike S, Brubaker S, Patel S, et al. Transcriptional maps of 10 human chromosomes at 5-nucleotide resolution. Science. 2005 May 20,;308(5725):1149-54.

280. Bertone P, Stolc V, Royce TE, Rozowsky JS, Urban AE, Zhu X, et al. Global identification of human transcribed sequences with genome tiling arrays. Science. 2004 Dec 24,;306(5705):2242-6.

281. David L, Huber W, Granovskaia M, Toedling J, Palm CJ, Bofkin L, et al. A highresolution map of transcription in the yeast genome. Proc Natl Acad Sci U S A. 2006 Apr 04,;103(14):5320-5.

282. Okoniewski MJ, Miller CJ. Hybridization interactions between probesets in short oligo microarrays lead to spurious correlations. BMC Bioinformatics. 2006 Jun 02,;7:276.

283. Royce TE, Rozowsky JS, Gerstein MB. Toward a universal microarray: prediction of gene expression through nearest-neighbor probe sequence identification. Nucleic Acids Res. 2007;35(15):e99.

284. Freyhult E, Landfors M, Önskog J, Hvidsten TR, Rydén P. Challenges in microarray class discovery: a comprehensive examination of normalization, gene selection and clustering. BMC Bioinformatics. 2010 Oct 11,;11:503.

285. Bentley DR, Balasubramanian S, Swerdlow HP, Smith GP, Milton J, Brown CG, et al. Accurate whole human genome sequencing using reversible terminator chemistry. Nature. 2008 Nov 06,;456(7218):53-9.

286. Lister R, O'Malley RC, Tonti-Filippini J, Gregory BD, Berry CC, Millar AH, et al. Highly integrated single-base resolution maps of the epigenome in Arabidopsis. Cell. 2008 May 02,;133(3):523-36.

287. Mortazavi A, Williams BA, McCue K, Schaeffer L, Wold B. Mapping and quantifying mammalian transcriptomes by RNA-Seq. Nat Methods. 2008 Jul;5(7):621-8.

288. Nagalakshmi U, Wang Z, Waern K, Shou C, Raha D, Gerstein M, et al. The transcriptional landscape of the yeast genome defined by RNA sequencing. Science. 2008 Jun 06,;320(5881):1344-9.

289. Wilhelm BT, Marguerat S, Watt S, Schubert F, Wood V, Goodhead I, et al. Dynamic repertoire of a eukaryotic transcriptome surveyed at single-nucleotide resolution. Nature. 2008 Jun 26,;453(7199):1239-43.

290. Cloonan N, Forrest ARR, Kolle G, Gardiner BBA, Faulkner GJ, Brown MK, et al. Stem cell transcriptome profiling via massive-scale mRNA sequencing. Nat Methods. 2008 Jul;5(7):613-9.

291. Marioni JC, Mason CE, Mane SM, Stephens M, Gilad Y. RNA-seq: an assessment of technical reproducibility and comparison with gene expression arrays. Genome Res. 2008 Sep;18(9):1509-17.

292. Morin R, Bainbridge M, Fejes A, Hirst M, Krzywinski M, Pugh T, et al. Profiling the HeLa S3 transcriptome using randomly primed cDNA and massively parallel short-read sequencing. BioTechniques. 2008 Jul;45(1):81-94.

293. Wilhelm BT, Landry J. RNA-Seq-quantitative measurement of expression through massively parallel RNA-sequencing. Methods. 2009 Jul;48(3):249-57.

294. Pastinen T. Genome-wide allele-specific analysis: insights into regulatory variation. Nat Rev Genet. 2010 Aug;11(8):533-8.

295. Dohm JC, Lottaz C, Borodina T, Himmelbauer H. Substantial biases in ultrashort read data sets from high-throughput DNA sequencing. Nucleic Acids Res. 2008 Sep;36(16):e105.

296. Risso D, Schwartz K, Sherlock G, Dudoit S. GC-content normalization for RNASeq data. BMC Bioinformatics. 2011 Dec 17,;12:480.

297. Hansen KD, Brenner SE, Dudoit S. Biases in Illumina transcriptome sequencing caused by random hexamer priming. Nucleic Acids Res. 2010 Jul;38(12):e131.

298. Jones DC, Ruzzo WL, Peng X, Katze MG. A new approach to bias correction in RNA-Seq. Bioinformatics. 2012 Apr 01,;28(7):921-8.

299. Young MD, Wakefield MJ, Smyth GK, Oshlack A. Gene ontology analysis for RNA-seq: accounting for selection bias. Genome Biol. 2010;11(2):R14.

300. Oshlack A, Wakefield MJ. Transcript length bias in RNA-seq data confounds systems biology. Biol Direct. 2009 Apr 16,;4:14.

301. Schuierer S, Carbone W, Knehr J, Petitjean V, Fernandez A, Sultan M, et al. A comprehensive assessment of RNA-seq protocols for degraded and low-quantity samples. BMC Genomics. 2017 06 05,;18(1):442.

302. Martin JA, Wang Z. Next-generation transcriptome assembly. Nature Reviews Genetics. 2011 -10;12(10):671-82.

303. Sultan M, Schulz MH, Richard H, Magen A, Klingenhoff A, Scherf M, et al. A global view of gene activity and alternative splicing by deep sequencing of the human transcriptome. Science. 2008 Aug 15,;321(5891):956-60.

304. Bullard JH, Purdom E, Hansen KD, Dudoit S. Evaluation of statistical methods for normalization and differential expression in mRNA-Seq experiments. BMC Bioinformatics. 2010 Feb 18,;11:94.

305. Anders S, Huber W. Differential expression analysis for sequence count data. Genome Biol. 2010;11(10):R106.

306. Langmead B, Hansen KD, Leek JT. Cloud-scale RNA-sequencing differential expression analysis with Myrna. Genome Biol. 2010;11(8):R83.

307. Robinson MD, Oshlack A. A scaling normalization method for differential expression analysis of RNA-seq data. Genome Biol. 2010;11(3):R25.

308. Li J, Jiang H, Wong WH. Modeling non-uniformity in short-read rates in RNASeq data. Genome Biol. 2010;11(5):R50.

309. Love MI, Huber W, Anders S. Moderated estimation of fold change and dispersion for RNA-seq data with DESeq2. Genome Biol. 2014;15(12):550.

310. Robinson MD, McCarthy DJ, Smyth GK. edgeR: a Bioconductor package for differential expression analysis of digital gene expression data. Bioinformatics. 2010 Jan 01,;26(1):139-40.

311. Eden E, Navon R, Steinfeld I, Lipson D, Yakhini Z. GOrilla: a tool for discovery and visualization of enriched GO terms in ranked gene lists. BMC bioinformatics. 2009 Feb 3,;10(1):48.

312. Eden E, Navon R, Steinfeld I, Lipson D, Yakhini Z. GOrilla: a tool for discovery and visualization of enriched GO terms in ranked gene lists. BMC Bioinformatics. 2009 Feb 03,;10:48.

313. Conesa A, Madrigal P, Tarazona S, Gomez-Cabrero D, Cervera A, McPherson A, et al. A survey of best practices for RNA-seq data analysis. Genome Biol. 2016 Jan 26,;17:13.

314. Oshlack A, Robinson MD, Young MD. From RNA-seq reads to differential expression results. Genome Biol. 2010;11(12):220.

315. Heinig M, Adriaens ME, Schafer S, van Deutekom, Hanneke W M, Lodder EM, Ware JS, et al. Natural genetic variation of the cardiac transcriptome in non-diseased donors and patients with dilated cardiomyopathy. Genome Biol. 2017 09 14,;18(1):170.

316. Burke MA, Chang S, Wakimoto H, Gorham JM, Conner DA, Christodoulou DC, et al. Molecular profiling of dilated cardiomyopathy that progresses to heart failure. JCI Insight. 2016 May 05,;1(6).

317. Christodoulou DC, Wakimoto H, Onoue K, Eminaga S, Gorham JM, DePalma SR, et al. 5'RNA-Seq identifies Fhl1 as a genetic modifier in cardiomyopathy. J Clin Invest. 2014 Mar;124(3):1364-70.

318. Song HK, Hong S, Kim T, Kim DH. Deep RNA sequencing reveals novel cardiac transcriptomic signatures for physiological and pathological hypertrophy. PLoS ONE. 2012;7(4):e35552.

319. Yang K, Yamada KA, Patel AY, Topkara VK, George I, Cheema FH, et al. Deep RNA sequencing reveals dynamic regulation of myocardial noncoding RNAs in failing human heart and remodeling with mechanical circulatory support. Circulation. 2014 Mar 04,;129(9):1009-21.

320. Liu Y, Morley M, Brandimarto J, Hannenhalli S, Hu Y, Ashley EA, et al. RNASeq identifies novel myocardial gene expression signatures of heart failure. Genomics. 2015 February 1,;105(2):83-9.

321. Ren C, Liu J, Li J, Li J, Dai J, Lai Y. RNA-seq profiling of mRNA associated with hypertrophic cardiomyopathy. Mol Med Rep. 2016 Dec;14(6):5573-86.

322. Li W, Li L, Zhang S, Zhang C, Huang H, Li Y, et al. Identification of potential genes for human ischemic cardiomyopathy based on RNA-Seq data. Oncotarget. 2016 Dec 13,;7(50):82063.

323. Ortega A, Gil-Cayuela C, Tarazón E, García-Manzanares M, Montero JA, Cinca J, et al. New Cell Adhesion Molecules in Human Ischemic Cardiomyopathy. PCDHGA3 Implications in Decreased Stroke Volume and Ventricular Dysfunction. PLoS ONE. 2016;11(7):e0160168.

324. Prunotto A, Stevenson BJ, Berthonneche C, Schüpfer F, Beckmann JS, Maurer F, et al. RNAseq analysis of heart tissue from mice treated with atenolol and isoproterenol reveals a reciprocal transcriptional response. BMC Genomics. 2016 09 07,;17:717.

325. Schiano C, Costa V, Aprile M, Grimaldi V, Maiello C, Esposito R, et al. Heart failure: Pilot transcriptomic analysis of cardiac tissue by RNA-sequencing. Cardiol J. 2017;24(5):539-53.

326. Rindler TN, Hinton RB, Salomonis N, Ware SM. Molecular Characterization of Pediatric Restrictive Cardiomyopathy from Integrative Genomics. Scientific reports. 2017 Jan 18,;7:39276.

327. Gil-Cayuela C, Ortega A, Tarazón E, Martínez-Dolz L, Cinca J, GonzálezJuanatey JR, et al. Myocardium of patients with dilated cardiomyopathy presents altered expression of genes involved in thyroid hormone biosynthesis. PLoS ONE. 2018;13(1):e0190987.

328. Kim D, Langmead B, Salzberg SL. HISAT: a fast spliced aligner with low memory requirements. Nat Methods. 2015 Apr;12(4):357-60.

329. Li H, Handsaker B, Wysoker A, Fennell T, Ruan J, Homer N, et al. The Sequence Alignment/Map format and SAMtools. Bioinformatics. 2009 Aug 15,;25(16):2078-9.

330. Subramanian A, Tamayo P, Mootha VK, Mukherjee S, Ebert BL, Gillette MA, et al. Gene set enrichment analysis: a knowledge-based approach for interpreting genome-wide expression profiles. Proc Natl Acad Sci U S A. 2005 Oct 25,;102(43):15545-50.

331. Krämer A, Green J, Pollard J, Tugendreich S. Causal analysis approaches in Ingenuity Pathway Analysis. Bioinformatics. 2014 Feb 15,;30(4):523-30.

332. Schmitt JP, Kamisago M, Asahi M, Li GH, Ahmad F, Mende U, et al. Dilated cardiomyopathy and heart failure caused by a mutation in phospholamban. Science. 2003 Feb 28,;299(5611):1410-3.

333. Davis AP, Sherlock G, Botstein D, Eppig JT, Matese JC, Harris MA, et al. Gene Ontology: tool for the unification of biology. Nature Genetics. 2000 May;25(1):25-9.

334. Tomczak A, Mortensen JM, Winnenburg R, Liu C, Alessi DT, Swamy V, et al. Interpretation of biological experiments changes with evolution of the Gene Ontology and its annotations. Sci Rep. 2018 Mar 23,;8(1):5115.

335. Bonnans C, Chou J, Werb Z. Remodelling the extracellular matrix in development and disease. Nat Rev Mol Cell Biol. 2014 -12;15(12):786-801.

336. Louzao-Martinez L, Vink A, Harakalova M, Asselbergs FW, Verhaar MC, Cheng C. Characteristic adaptations of the extracellular matrix in dilated cardiomyopathy. Int J Cardiol. 2016 Oct 01,;220:634-46.

337. Tham YK, Bernardo BC, Ooi JYY, Weeks KL, McMullen JR. Pathophysiology of cardiac hypertrophy and heart failure: signaling pathways and novel therapeutic targets. Arch Toxicol. 2015 Sep;89(9):1401-38.

338. Hunter JJ, Chien KR. Signaling pathways for cardiac hypertrophy and failure. N Engl J Med. 1999 Oct 21,;341(17):1276-83.

339. Mary P Lee, Katherine E Yutzey. Twist1 Directly Regulates Genes That Promote Cell Proliferation and Migration in Developing Heart Valves. PLoS One. 2011 Dec 1,;6(12):e29758.

340. Baumgarten A, Bang C, Tschirner A, Engelmann A, Adams V, von Haehling S, et al. TWIST1 regulates the activity of ubiquitin proteasome system via the miR199/214 cluster in human end-stage dilated cardiomyopathy. Int J Cardiol. 2013 Sep 30,;168(2):1447-52.

341. Baumgarten A, Bang C, Tschirner A, Engelmann A, Adams V, von Haehling S, et al. TWIST1 regulates the activity of ubiquitin proteasome system via the miR199/214 cluster in human end-stage dilated cardiomyopathy. Int J Cardiol. 2013 Sep 30,;168(2):1447-52.

342. Raaz U, Schellinger IN, Chernogubova E, Warnecke C, Kayama Y, Penov K, et al. Transcription Factor Runx2 Promotes Aortic Fibrosis and Stiffness in Type 2 Diabetes Mellitus. Circ Res. 2015 Aug 28,;117(6):513-24.

343. Franco D, Sedmera D, Lozano-Velasco E. Multiple Roles of Pitx2 in Cardiac Development and Disease. Journal of cardiovascular development and disease. 2017 Oct 11,;4(4):16.

344. Schachterle W. Transcriptional regulation of Gata4 in the developing heart [dissertation]. ProQuest Dissertations Publishing; 2011.

345. Sadam H, Liivas U, Kazantseva A, Pruunsild P, Kazantseva J, Timmusk T, et al. GLI2 cell-specific activity is controlled at the level of transcription and RNA processing: Consequences to cancer metastasis. Biochim Biophys Acta. 2016 Jan;1862(1):46-55.

346. Sun B, Huo R, Sheng Y, Li Y, Xie X, Chen C, et al. Bone morphogenetic protein-4 mediates cardiac hypertrophy, apoptosis, and fibrosis in experimentally pathological cardiac hypertrophy. Hypertension. 2013 Feb;61(2):352-60.

347. Wang Y, Morimoto S, Du C, Lu Q, Zhan D, Tsutsumi T, et al. Up-regulation of type 2 iodothyronine deiodinase in dilated cardiomyopathy. Cardiovasc Res. 2010 Sep 01,;87(4):636-46.

348. Altara R, Mallat Z, Booz GW, Zouein FA. The CXCL10/CXCR3 Axis and Cardiac Inflammation: Implications for Immunotherapy to Treat Infectious and Noninfectious Diseases of the Heart. J Immunol Res. 2016;2016.

349. Latif N, Khan MA, Birks E, O'Farrell A, Westbrook J, Dunn MJ, et al. Upregulation of the Bcl-2 family of proteins in end stage heart failure. J Am Coll Cardiol. 2000 Jun;35(7):1769-77.

350. Bangert A, Andrassy M, Müller A, Bockstahler M, Fischer A, Volz CH, et al. Critical role of RAGE and HMGB1 in inflammatory heart disease. PNAS. 2016 -01-12 00:00:00;113(2):E164.

351. Interaction of β1-adrenoceptor with RAGE mediates cardiomyopathy via CaMKII signaling [Internet].: American Society for Clinical Investigation; 2016 [updated -01-21; cited Jul 9, 2018]. Available from: https://insight.jci.org/articles/view/84969/version/1/pdf/render.

352. Li D, Wu J, Bai Y, Zhao X, Liu L. Isolation and Culture of Adult Mouse Cardiomyocytes for Cell Signaling and in vitro Cardiac Hypertrophy. Journal of Visualized Experiments. 2014(87).

353. Wolska BM, Solaro RJ. Method for isolation of adult mouse cardiac myocytes for studies of contraction and microfluorimetry. Am J Physiol. 1996 Sep;271(3 Pt 2):1250.

354. Katz Y, Wang ET, Airoldi EM, Burge CB. Analysis and design of RNA sequencing experiments for identifying isoform regulation. Nat Methods. 2010 Dec;7(12):1009-15.

355. Garber M, Grabherr MG, Guttman M, Trapnell C. Computational methods for transcriptome annotation and quantification using RNA-seq. Nat Methods. 2011 Jun;8(6):469-77.

356. Sims D, Sudbery I, Ilott NE, Heger A, Ponting CP. Sequencing depth and coverage: key considerations in genomic analyses. Nat Rev Genet. 2014 Feb;15(2):121-32.

357. Łabaj PP, Leparc GG, Linggi BE, Markillie LM, Wiley HS, Kreil DP. Characterization and improvement of RNA-Seq precision in quantitative transcript expression profiling. Bioinformatics. 2011 Jul 01,;27(13):383.

358. Tragante V, Gho, Johannes M. I. H., Felix JF, Vasan RS, Smith NL, Voight BF, et al. Gene Set Enrichment Analyses: lessons learned from the heart failure phenotype. BioData Min. 2017 -5-26;10.

359. Levine B, Kroemer G. Autophagy in the pathogenesis of disease. Cell. 2008 January 11;132(1):27-42.

360. Zolk O, Schenke C, Sarikas A. The ubiquitin–proteasome system: Focus on the heart. Cardiovasc Res. 2006 /06/01;70(3):410-21.

361. Kirkin V, McEwan DG, Novak I, Dikic I. A role for ubiquitin in selective autophagy. Mol Cell. 2009 May 15;34(3):259-69.

362. Tanida I. Autophagosome formation and molecular mechanism of autophagy. Antioxid Redox Signal. 2011 June 01;14(11):2201-14.

363. Gottlieb RA, Mentzer RM. Autophagy during cardiac stress: joys and frustrations of autophagy. Annu Rev Physiol. 2010;72:45-59.

364. Ivan Dikic, Zvulun Elazar. Mechanism and medical implications of mammalian autophagy. Nature Reviews. Molecular Cell Biology. 2018 Jun 1,;19(6):349-64.

365. Arias E, Cuervo AM. Chaperone-mediated autophagy in protein quality control. Curr Opin Cell Biol. 2011 Apr;23(2):184-9.

366. Gatica D, Chiong M, Lavandero S, Klionsky DJ. Molecular mechanisms of autophagy in the cardiovascular system. Circ Res. 2015 Jan 30,;116(3):456-67.

367. Yang Z, Klionsky DJ. Mammalian autophagy: core molecular machinery and signaling regulation. Curr Opin Cell Biol. 2010 Apr;22(2):124-31.

368. Ravikumar B, Sarkar S, Davies JE, Futter M, Garcia-Arencibia M, GreenThompson ZW, et al. Regulation of mammalian autophagy in physiology and pathophysiology. Physiol Rev. 2010 Oct;90(4):1383-435.

369. Klionsky DJ, Abeliovich H, Agostinis P, Agrawal DK, Aliev G, Askew DS, et al. Guidelines for the use and interpretation of assays for monitoring autophagy in higher eukaryotes. Autophagy. 2008 Feb;4(2):151-75.

370. Yang Z, Klionsky DJ. Mammalian autophagy: core molecular machinery and signaling regulation. Curr Opin Cell Biol. 2010 Apr;22(2):124-31.

371. Jasvinder Kaur, Jayanta Debnath. Autophagy at the crossroads of catabolism and anabolism. Nature Reviews. Molecular Cell Biology. 2015 Aug 1,;16(8):461-72.

372. Predmore JM, Wang P, Davis F, Bartolone S, Westfall MV, Dyke DB, et al. Ubiquitin proteasome dysfunction in human hypertrophic and dilated cardiomyopathies. Circulation. 2010 March 02;121(8):997-1004.

373. Wilkinson KD. DUBs at a glance. J Cell Sci. 2009 -7-15;122(14):2325-9.

374. Ciechanover A, Brundin P. The ubiquitin proteasome system in neurodegenerative diseases: sometimes the chicken, sometimes the egg. Neuron. 2003 Oct 09,;40(2):427-46.

375. Mearini G, Stimpel D, Krämer E, Geertz B, Braren I, Gedicke-Hornung C, et al.

Repair of Mybpc3 mRNA by 5′-trans-splicing in a Mouse Model of Hypertrophic Cardiomyopathy. Molecular Therapy - Nucleic Acids. 2013;2:e102.

376. Lilienbaum A. Relationship between the proteasomal system and autophagy. International journal of biochemistry and molecular biology. 2013;4(1):1.

377. Nagy V, Dikic I. Ubiquitin ligase complexes: from substrate selectivity to conjugational specificity. Biol Chem. 2010 Feb-Mar;391(2-3):163-9.

378. Wang C, Wang X. The interplay between autophagy and the ubiquitinproteasome system in cardiac proteotoxicity. Biochimica et biophysica acta. 2015 Feb;1852(2):188.

379. Wang X, Terpstra EJM. Ubiquitin receptors and protein quality control. J Mol Cell Cardiol. 2013 Feb;55:73-84.

380. David Vilchez, Isabel Saez, Andrew Dillin. The role of protein clearance mechanisms in organismal ageing and age-related diseases. Nature Communications. 2014 Dec 1,;5(1):5659.

381. Herrmann J, Ciechanover A, Lerman LO, Lerman A. The ubiquitin-proteasome system in cardiovascular diseases-a hypothesis extended. Cardiovasc Res. 2004 Jan 01,;61(1):11-21.

382. Hedhli N, Depre C. Proteasome inhibitors and cardiac cell growth. Cardiovascular Research. 2010 Jan 15,;85(2):321-9.

383. Mearini G, Schlossarek S, Willis MS, Carrier L. The ubiquitin–proteasome system in cardiac dysfunction. Biochimica et Biophysica Acta (BBA) - Molecular Basis of Disease. 2008 December 1,;1782(12):749-63.

384. Hochstrasser M. Ubiquitin, proteasomes, and the regulation of intracellular protein degradation. Curr Opin Cell Biol. 1995 Apr;7(2):215-23.

385. Yoshimori T. Autophagy: a regulated bulk degradation process inside cells. Biochem Biophys Res Commun. 2004 Jan 09,;313(2):453-8.

386. Webb JL, Ravikumar B, Atkins J, Skepper JN, Rubinsztein DC. Alpha-Synuclein is degraded by both autophagy and the proteasome. J Biol Chem. 2003 Jul 04,;278(27):25009-13.

387. Cuervo AM, Stefanis L, Fredenburg R, Lansbury PT, Sulzer D. Impaired degradation of mutant alpha-synuclein by chaperone-mediated autophagy. Science. 2004 Aug 27,;305(5688):1292-5.

388. Ravikumar B, Duden R, Rubinsztein DC. Aggregate-prone proteins with polyglutamine and polyalanine expansions are degraded by autophagy. Hum Mol Genet. 2002 May 01,;11(9):1107-17.

389. Ding W, Yin X. Sorting, recognition and activation of the misfolded protein degradation pathways through macroautophagy and the proteasome. Autophagy. 2008 Feb;4(2):141-50.

390. Ikeda F, Crosetto N, Dikic I. What determines the specificity and outcomes of ubiquitin signaling? Cell. 2010 Nov 24,;143(5):677-81.

391. Baboshina OV, Haas AL. Novel multiubiquitin chain linkages catalyzed by the conjugating enzymes E2EPF and RAD6 are recognized by 26 S proteasome subunit 5. J Biol Chem. 1996 Feb 02,;271(5):2823-31.

392. Kim PK, Hailey DW, Mullen RT, Lippincott-Schwartz J. Ubiquitin signals autophagic degradation of cytosolic proteins and peroxisomes. Proc Natl Acad Sci U S A. 2008 Dec 30,;105(52):20567-74.

393. Tan JMM, Wong ESP, Kirkpatrick DS, Pletnikova O, Ko HS, Tay S, et al. Lysine 63-linked ubiquitination promotes the formation and autophagic clearance of protein inclusions associated with neurodegenerative diseases. Hum Mol Genet. 2008 Feb 01,;17(3):431-9.

394. Lindsten K, Menendez-Benito V, Masucci MG, Dantuma NP. A transgenic mouse model of the ubiquitin/proteasome system. Nat Biotechnol. 2003 August 01;21(8):897-902.

395. Richard P, Charron P, Carrier L, Ledeuil C, Cheav T, Pichereau C, et al. Hypertrophic cardiomyopathy: distribution of disease genes, spectrum of mutations, and implications for a molecular diagnosis strategy. Circulation. 2003 May 06,;107(17):2227-32.

396. Schlossarek S, Mearini G, Carrier L. Cardiac myosin-binding protein C in hypertrophic cardiomyopathy: mechanisms and therapeutic opportunities. J Mol Cell Cardiol. 2011 Apr;50(4):613-20.

397. Olivotto I, Girolami F, Ackerman MJ, Nistri S, Bos JM, Zachara E, et al. Myofilament Protein Gene Mutation Screening and Outcome of Patients With Hypertrophic Cardiomyopathy. Mayo Clinic Proceedings. 2008 June 1,;83(6):630-8.

398. Carrier L, Bonne G, Bährend E, Yu B, Richard P, Niel F, et al. Organization and sequence of human cardiac myosin binding protein C gene (MYBPC3) and identification of mutations predicted to produce truncated proteins in familial hypertrophic cardiomyopathy. Circ Res. 1997 Mar;80(3):427-34.

399. Freiburg A, Gautel M. A molecular map of the interactions between titin and myosin-binding protein C. Implications for sarcomeric assembly in familial hypertrophic cardiomyopathy. Eur J Biochem. 1996 Jan 15,;235(1-2):317-23.

400. Kunst G, Kress KR, Gruen M, Uttenweiler D, Gautel M, Fink RH. Myosin binding protein C, a phosphorylation-dependent force regulator in muscle that controls

the attachment of myosin heads by its interaction with myosin S2. Circ Res. 2000 Jan 7-21;86(1):51-8.

401. Barefield D, Sadayappan S. Phosphorylation and function of cardiac myosin binding protein-C in health and disease. J Mol Cell Cardiol. 2010 May;48(5):866-75.

402. Bezold KL, Shaffer JF, Khosa JK, Hoye ER, Harris SP. A gain-of-function mutation in the M-domain of cardiac myosin-binding protein-C increases binding to actin. J Biol Chem. 2013 Jul 26,;288(30):21496-505.

403. Sadayappan S, Osinska H, Klevitsky R, Lorenz JN, Sargent M, Molkentin JD, et al. Cardiac myosin binding protein c phosphorylation is cardioprotective. PNAS. 2006 -11-07 00:00:00;103(45):16918-23.

404. Sadayappan S, Gulick J, Osinska H, Martin LA, Hahn HS, Dorn GW, et al. Cardiac myosin-binding protein-C phosphorylation and cardiac function. Circ Res. 2005 Nov 25,;97(11):1156-63.

405. Previs MJ, Beck Previs S, Gulick J, Robbins J, Warshaw DM. Molecular mechanics of cardiac myosin-binding protein C in native thick filaments. Science. 2012 Sep 07,;337(6099):1215-8.

406. Gautel M, Zuffardi O, Freiburg P, Labeit S. Phosphorylation switches specific for the cardiac isoform of myosin binding protein-C: A modulator of cardiac contraction? EMBO Journal. 1995;14(9):1952-60.

407. Mohamed AS, Dignam JD, Schlender KK. Cardiac myosin-binding protein C (MyBP-C): identification of protein kinase A and protein kinase C phosphorylation sites. Arch Biochem Biophys. 1998 Oct 15,;358(2):313-9.

408. Sadayappan S, Gulick J, Osinska H, Barefield D, Cuello F, Avkiran M, et al. A critical function for Ser-282 in cardiac Myosin binding protein-C phosphorylation and cardiac function. Circ Res. 2011 Jul 08,;109(2):141-50.

409. Cuello F, Bardswell SC, Haworth RS, Ehler E, Sadayappan S, Kentish JC, et al. Novel Role for p90 Ribosomal S6 Kinase in the Regulation of Cardiac Myofilament Phosphorylation. J Biol Chem. 2011 02/18/;286(7):5300-10.

410. Bardswell SC, Cuello F, Rowland AJ, Sadayappan S, Robbins J, Gautel M, et al. Distinct sarcomeric substrates are responsible for protein kinase D-mediated regulation of cardiac myofilament Ca2+ sensitivity and cross-bridge cycling. J Biol Chem. 2010 Feb 19,;285(8):5674-82.

411. Niimura H, Bachinski LL, Sangwatanaroj S, Watkins H, Chudley AE, McKenna W, et al. Mutations in the Gene for Cardiac Myosin-Binding Protein C and LateOnset Familial Hypertrophic Cardiomyopathy. The New England Journal of Medicine. 1998 Apr 30,;338(18):1248-57.

412. Marston S, Copeland O, Jacques A, Livesey K, Tsang V, McKenna WJ, et al. Evidence from human myectomy samples that MYBPC3 mutations cause hypertrophic cardiomyopathy through haploinsufficiency. Circ Res. 2009 Jul 31,;105(3):219-22.

413. Nanni L, Pieroni M, Chimenti C, Simionati B, Zimbello R, Maseri A, et al. Hypertrophic cardiomyopathy: two homozygous cases with “typical” hypertrophic cardiomyopathy and three new mutations in cases with progression to dilated cardiomyopathy. Biochemical and Biophysical Research Communications. 2003 September 19,;309(2):391-8.

414. Gedicke-Hornung C, Behrens-Gawlik V, Reischmann S, Geertz B, Stimpel D, Weinberger F, et al. Rescue of cardiomyopathy through U7snRNA-mediated exon skipping in Mybpc3-targeted knock-in mice. EMBO Molecular Medicine. 2013 Jul;5(7):1128-45.

415. Barefield D, Kumar M, de Tombe PP, Sadayappan S. Contractile dysfunction in a mouse model expressing a heterozygous MYBPC3 mutation associated with hypertrophic cardiomyopathy. Am J Physiol Heart Circ Physiol. 2014 - 315;306(6):H815.

416. Schlossarek S, Englmann D, Sultan K, Sauer M, Eschenhagen T, Carrier L. Defective proteolytic systems in Mybpc3-targeted mice with cardiac hypertrophy. Basic Res Cardiol. 2012 Jan;107(1):1-13.

417. Schlossarek S, Schuermann F, Geertz B, Mearini G, Eschenhagen T, Carrier L. Adrenergic stress reveals septal hypertrophy and proteasome impairment in heterozygous Mybpc3-targeted knock-in mice. J Muscle Res Cell Motil. 2012 May;33(1):5-15.

418. Otomo C, Metlagel Z, Takaesu G, Otomo T. Structure of the human ATG12ATG5 conjugate required for LC3 lipidation in autophagy. United States: FOREIGNNIH; 2013 Mar 4,. Report No.: 20.

419. Zheng Q, Su H, Tian Z, Wang X. Proteasome malfunction activates macroautophagy in the heart. American journal of cardiovascular disease. 2011;1(3):214.

420. Zheng Q, Wang X. Autophagy and the ubiquitin-proteasome system in cardiac dysfunction. Panminerva medica. 2010 Mar;52(1):9.

421. Sarikas A, Carrier L, Schenke C, Doll D, Flavigny J, Lindenberg KS, et al. Impairment of the ubiquitin–proteasome system by truncated cardiac myosin binding protein C mutants. Cardiovasc Res. 2005 /04/01;66(1):33-44.

422. De Meyer, Guido R Y, Martinet W. Autophagy in the cardiovascular system. Biochimica et Biophysica Acta (BBA) - Molecular Cell Research. 2009 September 1,;1793(9):1485-95.

423. Grossman W, Jones D, McLaurin LP. Wall stress and patterns of hypertrophy in the human left ventricle. J Clin Invest. 1975 Jul;56(1):56-64.

424. Birks EJ, Latif N, Enesa K, Folkvang T, Luong LA, Sarathchandra P, et al. Elevated p53 expression is associated with dysregulation of the ubiquitinproteasome system in dilated cardiomyopathy. Cardiovasc Res. 2008 /08/01;79(3):472-80.

425. Tsukamoto O, Minamino T, Okada K, Shintani Y, Takashima S, Kato H, et al. Depression of proteasome activities during the progression of cardiac dysfunction in pressure-overloaded heart of mice. Biochem Biophys Res Commun. 2006 February 24;340(4):1125-33.

426. Predmore JM, Wang P, Davis F, Bartolone S, Westfall MV, Dyke DB, et al. Ubiquitin proteasome dysfunction in human hypertrophic and dilated cardiomyopathies. Circulation. 2010 March 02;121(8):997-1004.

427. Kostin S, Pool L, Elsasser A, Hein S, Drexler HC, Arnon E, et al. Myocytes die by multiple mechanisms in failing human hearts. Circ Res. 2003 April 18;92(7):71524.

428. Zheng Q, Wang X. Autophagy and the ubiquitin-proteasome system in cardiac dysfunction. Panminerva medica. 2010 Mar;52(1):9.

429. Tannous P, Zhu H, Nemchenko A, Berry JM, Johnstone JL, Shelton JM, et al. Intracellular protein aggregation is a proximal trigger of cardiomyocyte autophagy. Circulation. 2008 Jun 17,;117(24):3070-8.

430. Ding W, Ni H, Gao W, Yoshimori T, Stolz DB, Ron D, et al. Linking of Autophagy to Ubiquitin-Proteasome System Is Important for the Regulation of Endoplasmic Reticulum Stress and Cell Viability. The American Journal of Pathology. 2007 August 1,;171(2):513-24.

431. Depre C, Wang Q, Yan L, Hedhli N, Peter P, Chen L, et al. Activation of the cardiac proteasome during pressure overload promotes ventricular hypertrophy. Circulation. 2006 October 24;114(17):1821-8.

432. Marston S, Copeland O, Jacques A, Livesey K, Tsang V, McKenna WJ, et al. Evidence from human myectomy samples that MYBPC3 mutations cause hypertrophic cardiomyopathy through haploinsufficiency. Circ Res. 2009 July 31;105(3):219-22.

433. Moolman JA, Reith S, Uhl K, Bailey S, Gautel M, Jeschke B, et al. A newly created splice donor site in exon 25 of the MyBP-C gene is responsible for inherited hypertrophic cardiomyopathy with incomplete disease penetrance. Circulation. 2000 March 28;101(12):1396-402.

434. W Rottbauer, M Gautel, J Zehelein, S Labeit, W M Franz, C Fischer, et al. Novel splice donor site mutation in the cardiac myosin-binding protein-C gene in familial hypertrophic cardiomyopathy. Characterization Of cardiac transcript and protein. The Journal of clinical investigation. 1997 Jul 15,;100(2):475-82.

435. van Dijk SJ, Dooijes D, dos Remedios C, Michels M, Lamers JM, Winegrad S, et al. Cardiac myosin-binding protein C mutations and hypertrophic cardiomyopathy: haploinsufficiency, deranged phosphorylation, and cardiomyocyte dysfunction. Circulation. 2009 March 24;119(11):1473-83.

436. Sarikas A, Carrier L, Schenke C, Doll D, Flavigny J, Lindenberg KS, et al. Impairment of the ubiquitin-proteasome system by truncated cardiac myosin binding protein C mutants. Cardiovasc Res. 2005 April 01;66(1):33-44.

437. Yang Q, Sanbe A, Osinska H, Hewett TE, Klevitsky R, Robbins J. In vivo modeling of myosin binding protein C familial hypertrophic cardiomyopathy. Circ Res. 1999 October 29;85(9):841-7.

438. Flavigny J, Souchet M, Sebillon P, Berrebi-Bertrand I, Hainque B, Mallet A, et al. COOH-terminal truncated cardiac myosin-binding protein C mutants resulting from familial hypertrophic cardiomyopathy mutations exhibit altered expression and/or incorporation in fetal rat cardiomyocytes. J Mol Biol. 1999 November 26;294(2):443-56.

439. Bahrudin U, Morisaki H, Morisaki T, Ninomiya H, Higaki K, Nanba E, et al. Ubiquitin-proteasome system impairment caused by a missense cardiac myosinbinding protein C mutation and associated with cardiac dysfunction in hypertrophic cardiomyopathy. J Mol Biol. 2008 December 26;384(4):896-907.

440. Pagan J, Seto T, Pagano M, Cittadini A. Role of the ubiquitin proteasome system in the heart. Circ Res. 2013 March 29;112(7):1046-58.

441. Depre C, Wang Q, Yan L, Hedhli N, Peter P, Chen L, et al. Activation of the cardiac proteasome during pressure overload promotes ventricular hypertrophy. Circulation. 2006 Oct 24,;114(17):1821-8.

442. Tsukamoto O, Minamino T, Okada K, Shintani Y, Takashima S, Kato H, et al. Depression of proteasome activities during the progression of cardiac dysfunction in pressure-overloaded heart of mice. Biochemical and Biophysical Research Communications. 2006 February 24,;340(4):1125-33.

443. Stansfield WE, Tang R, Moss NC, Baldwin AS, Willis MS, Selzman CH. Proteasome inhibition promotes regression of left ventricular hypertrophy. Am J Physiol Heart Circ Physiol. 2008 Feb;294(2):645.

444. Hedhli N, Lizano P, Hong C, Fritzky LF, Dhar SK, Liu H, et al. Proteasome inhibition decreases cardiac remodeling after initiation of pressure overload. Am J Physiol Heart Circ Physiol. 2008 Oct;295(4):1385.

445. Schlossarek S, Singh SR, Geertz B, Schulz H, Reischmann S, Hübner N, et al. Proteasome inhibition slightly improves cardiac function in mice with hypertrophic cardiomyopathy. Frontiers in physiology. 2014;5:484.

446. (Received for publication, November 21, 1991). Identification, Purification, and Characterizationf a Protein Activator (PA28)of the 20 S Proteasome (Macropain)". J Biol Chem. 1992 05/25/;267:10515-23.

447. Kopp F, Dahlmann B, Hendil KB. Evidence Indicating that the Human Proteasome is a Complex Dimer. Journal of Molecular Biology. 1993 January 5,;229(1):14-9.

448. Driscoll J, Frydman J, Goldberg AL. An ATP-stabilized inhibitor of the proteasome is a component of the 1500-kDa ubiquitin conjugate-degrading complex. PNAS. 1992 -06-01 00:00:00;89(11):4986-90.

449. Carrard G, Bulteau A, Petropoulos I, Friguet B. Impairment of proteasome structure and function in aging. The International Journal of Biochemistry & Cell Biology. 2002 November 1,;34(11):1461-74.

450. Uhlén M, Fagerberg L, Hallström BM, Lindskog C, Oksvold P, Mardinoglu A, et al. Proteomics. Tissue-based map of the human proteome. Science. 2015 Jan 23,;347(6220):1260419.

451. Lindskog C, Linné J, Fagerberg L, Hallström BM, Sundberg CJ, Lindholm M, et al. The human cardiac and skeletal muscle proteomes defined by transcriptomics and antibody-based profiling. BMC Genomics. 2015 Jun 25,;16:475.

452. Katayama T, Imaizumi K, Sato N, Miyoshi K, Kudo T, Hitomi J, et al. Presenilin1 mutations downregulate the signalling pathway of the unfolded-protein response. Nat Cell Biol. 1999 December 01;1(8):479-85.

453. Ciechanover A, Brundin P. The Ubiquitin Proteasome System in Neurodegenerative Diseases: Sometimes the Chicken, Sometimes the Egg. Neuron. 2003 October 9,;40(2):427-46.

454. Ciechanover A, Kwon YT. Degradation of misfolded proteins in neurodegenerative diseases: therapeutic targets and strategies. Experimental & molecular medicine. 2015 Mar 13,;47(3):e147.

455. Shen X, Valencia CA, Szostak JW, Szostak J, Dong B, Liu R. Scanning the human proteome for calmodulin-binding proteins. Proc Natl Acad Sci U S A. 2005 Apr 26,;102(17):5969-74.

456. Bianchi K, Rimessi A, Prandini A, Szabadkai G, Rizzuto R. Calcium and mitochondria: mechanisms and functions of a troubled relationship. Biochim Biophys Acta. 2004 Dec 06,;1742(1-3):119-31.

457. Celsi F, Pizzo P, Brini M, Leo S, Fotino C, Pinton P, et al. Mitochondria, calcium and cell death: a deadly triad in neurodegeneration. Biochim Biophys Acta. 2009 May;1787(5):335-44.

458. Peng T, Jou M. Oxidative stress caused by mitochondrial calcium overload. Ann N Y Acad Sci. 2010 Jul;1201:183-8.

459. McNally EM, Barefield DY, Puckelwartz MJ. The genetic landscape of cardiomyopathy and its role in heart failure. Cell Metab. 2015 Feb 03,;21(2):174-82.

460. Harvey PA, Leinwand LA. The cell biology of disease: cellular mechanisms of cardiomyopathy. J Cell Biol. 2011 Aug 08,;194(3):355-65.

461. Picard F, Brehm M, Fassbach M, Pelzer B, Scheuring S, Küry P, et al. Increased cardiac mRNA expression of matrix metalloproteinase-1 (MMP-1) and its inhibitor (TIMP-1) in DCM patients. Clin Res Cardiol. 2006 May;95(5):261-9.

462. Ho CY, López B, Coelho-Filho OR, Lakdawala NK, Cirino AL, Jarolim P, et al. Myocardial Fibrosis as an Early Manifestation of Hypertrophic Cardiomyopathy. The New England Journal of Medicine. 2010 Aug 5,;363(6):552-63.

463. Solomon SD, Geisterfer-Lowrance AA, Vosberg HP, Hiller G, Jarcho JA, Morton CC, et al. A locus for familial hypertrophic cardiomyopathy is closely linked to the cardiac myosin heavy chain genes, CRI-L436, and CRI-L329 on chromosome 14 at q11-q12. Am J Hum Genet. 1990 Sep;47(3):389-94.

464. Thierfelder L, MacRae C, Watkins H, Tomfohrde J, Williams M, McKenna W, et al. A familial hypertrophic cardiomyopathy locus maps to chromosome 15q2. Proc Natl Acad Sci U S A. 1993 Jul 01,;90(13):6270-4.

465. Watkins H, MacRae C, Thierfelder L, Chou YH, Frenneaux M, McKenna W, et al. A disease locus for familial hypertrophic cardiomyopathy maps to chromosome 1q3. Nat Genet. 1993 Apr;3(4):333-7.

466. Thierfelder L, Watkins H, MacRae C, Lamas R, McKenna W, Vosberg HP, et al. Alpha-tropomyosin and cardiac troponin T mutations cause familial hypertrophic cardiomyopathy: a disease of the sarcomere. Cell. 1994 Jun 03,;77(5):701-12.

467. McNally EM, Mestroni L. Dilated Cardiomyopathy: Genetic Determinants and Mechanisms. Circ Res. 2017 Sep 15,;121(7):731-48.

468. Mohapatra B, Jimenez S, Lin JH, Bowles KR, Coveler KJ, Marx JG, et al. Mutations in the muscle LIM protein and alpha-actinin-2 genes in dilated cardiomyopathy and endocardial fibroelastosis. Mol Genet Metab. 2003 SepOct;80(1-2):207-15.

469. Knöll R, Kostin S, Klede S, Savvatis K, Klinge L, Stehle I, et al. A common MLP (muscle LIM protein) variant is associated with cardiomyopathy. Circ Res. 2010 Mar 05,;106(4):695-704.

470. Arber S, Caroni P. Specificity of single LIM motifs in targeting and LIM/LIM interactions in situ. Genes Dev. 1996 Feb 01,;10(3):289-300.

471. Boukens BJ, Rivaud MR, Rentschler S, Coronel R. Misinterpretation of the mouse ECG: 'musing the waves of Mus musculus'. J Physiol (Lond). 2014 Nov 01,;592(21):4613-26.

472. Milani-Nejad N, Janssen PML. Small and large animal models in cardiac contraction research: advantages and disadvantages. Pharmacol Ther. 2014 Mar;141(3):235-49.

473. Li J, Gresham KS, Mamidi R, Doh CY, Wan X, Deschenes I, et al. Sarcomerebased genetic enhancement of systolic cardiac function in a murine model of dilated cardiomyopathy. Int J Cardiol. 2018 Dec 15,;273:168-76.

474. Schlossarek S, Singh SR, Geertz B, Schulz H, Reischmann S, Hübner N, et al. Proteasome inhibition slightly improves cardiac function in mice with hypertrophic cardiomyopathy. Front Physiol. 2014;5:484.

475. Herrmann J, Wohlert C, Saguner AM, Flores A, Nesbitt LL, Chade A, et al. Primary proteasome inhibition results in cardiac dysfunction. Eur J Heart Fail. 2013 Jun;15(6):614-23.

476. Enrico O, Gabriele B, Nadia C, Sara G, Daniele V, Giulia C, et al. Unexpected cardiotoxicity in haematological bortezomib treated patients. Br J Haematol. 2007 Aug;138(3):396-7.

477. Hacihanefioglu A, Tarkun P, Gonullu E. Acute severe cardiac failure in a myeloma patient due to proteasome inhibitor bortezomib. Int J Hematol. 2008 Sep;88(2):219-22.

478. Bockorny M, Chakravarty S, Schulman P, Bockorny B, Bona R. Severe heart failure after bortezomib treatment in a patient with multiple myeloma: a case report and review of the literature. Acta Haematol. 2012;128(4):244-7.

479. Behl C. Breaking BAG: The Co-Chaperone BAG3 in Health and Disease. Trends Pharmacol Sci. 2016 08;37(8):672-88.

480. Fang X, Bogomolovas J, Wu T, Zhang W, Liu C, Veevers J, et al. Loss-offunction mutations in co-chaperone BAG3 destabilize small HSPs and cause cardiomyopathy. J Clin Invest. 2017 Aug 01,;127(8):3189-200.

481. Hoffmann C, Moreau F, Moes M, Luthold C, Dieterle M, Goretti E, et al. Human muscle LIM protein dimerizes along the actin cytoskeleton and cross-links actin filaments. Mol Cell Biol. 2014 Aug;34(16):3053-65.

482. Mearini G, Stimpel D, Geertz B, Weinberger F, Krämer E, Schlossarek S, et al. Mybpc3 gene therapy for neonatal cardiomyopathy enables long-term disease prevention in mice. Nat Commun. 2014 Dec 02,;5:5515.

483. Green EM, Wakimoto H, Anderson RL, Evanchik MJ, Gorham JM, Harrison BC, et al. A small-molecule inhibitor of sarcomere contractility suppresses hypertrophic cardiomyopathy in mice. Science. 2016 Feb 05,;351(6273):617-21.